Ca^{2+} DEPENDENT REGULATION OF SINOATRIAL NODE PACEMAKING

Ph.D. thesis

Noémi Tóth, MD

Szeged

2022

Ca^{2+} dependent regulation of sinoatrial node pacemaking

Ph.D. thesis

Noémi Tóth, MD

Supervisor: Norbert Nagy, PhD

Department of Pharmacology and Pharmacotherapy,

Albert Szent-Györgyi Medical School,

Doctoral School of Multidisciplinary Medical Sciences,

University of Szeged

Szeged, Hungary

2022

TABLE OF CONTENTS

List of publications
Abbreviations
Abstract
1. INTRODUCTION 2
1.1 Sinoatrial node (SAN) as the primary pacemaker of the heart 2
1.2 „What keeps us ticking?" – Brief history of SAN pacemaking 3
1.3 Ca^{2+} homeostasis of the cardiomyocytes 4
1.4 Ca^{2+} dependent currents connecting Ca^{2+} handling and membrane potential 8
1.4.1 Ca^{2+}-current 8
1.4.2 Na^{+}/Ca^{2+} exchanger (NCX) 8
1.4.3 Small-conductance Ca^{2+} activated K^{+} channels 10
1.5 Recent concept for SAN pacemaking 11
1.6 SAN frequency induced changes in ventricular AP morphology 12
2. AIMS 14
3. MATERIALS AND METHODS 15
3.1 Animals 15
3.2 Tissue experiments on SAN 15
3.2.1 Conventional microelectrode technique on SAN 15
3.3 Tissue experiments on ventricular myocardium 16
3.3.1 Conventional microelectrode technique on canine papillary muscles 16
3.4 Cell experiments on SAN 17
3.4.1 Single SAN cell isolation 17
3.4.2 Measurement of NCX current with ramp protocol 17
3.4.3 Measurement of NCX current under SAN AP command 18
3.4.4 Measurement of $I_{K(Ca)}$ under SAN AP command 18
3.4.5 AP measurements in single SAN cells 18
3.4.6 Ca^{2+} transient measurements in SAN cells 19
3.5 Cell experiments in ventricular myocytes 20
3.5.1 Single left ventricular myocyte isolation 20
3.6 Statistical analysis 20
4. RESULTS 21
4.1 Investigation of forward NCX function and the NCX-I_f coupling in SAN pacemaking 21
4.1.1 NCX inhibition exerted CL prolongation on SAN tissue 21
4.1.2 NCX inhibition exerted larger CL lengthening effect when I_f was previously impaired 22
4.1.3 Repolarization inhibition induced bradycardia does not facilitate the CL lengthening effect of NCX inhibition 24
4.1.4 Reduction of $[Ca^{2+}]_i$ increases the CL lengthening effect of I_f inhibition 25
4.1.5 Subsequent inhibition of NCX and I_f increases the CL variability 27
4.2 Investigation of reverse NCX function in SAN pacemaking 28
4.2.1 Experimental validation of 2 mM and 8 mM $[Na^{+}]_{pip}$ groups in the measurement of reverse NCX current 29
4.2.2 Characterization of NCX current under the SAN AP 30
4.2.3 In the presence of active reverse NCX the CaT is larger 32
4.2.4 Reverse NCX activity enhances the SR Ca^{2+} content 33
4.2.5 Active reverse NCX enhances the spontaneous AP firing rate 34
4.3 $I_{K(Ca)}$ has no role in the spontaneous SAN pacemaking 36
4.4 Cardiac alternans show a restitution independent nature that is associated with enhanced frequency 38
5. DISCUSSION 41
5.1 Forward mode of the NCX has an important role in the spontaneous automaticity forming a strong functional coupling with I_f 41
5.2 Reverse mode of the NCX contributes to pacemaking by refilling the Ca^{2+} clock 43
5.3 $I_{(KCa)}$ has no role in the spontaneous automaticity in basal conditions 45
5.4 Ventricular alternans are independent from restitution 45
6. CONCLUSION 46
7. ACKNOWLEDGEMENT 47
8. FUNDING 47
9. REFERENCES 48

LIST OF PUBLICATIONS

The publications related to the subject of the Ph.D. thesis:

I.) Gergő Bitay, **Noémi Tóth**, Szilvia Déri, Jozefina Szlovák, Zsófia Kohajda, András Varró, Norbert Nagy. The Inhibition of the Small-Conductance Ca^{2+}-Activated Potassium Channels Decreases the Sinus Node Pacemaking during Beta-Adrenergic Activation. *Pharmaceuticals* 2022, https://doi.org/10.3390/ph15030313, (**IF**: 5.863, **Q1**)

II.) **Noémi Tóth**, Jozefina Szlovák, Zsófia Kohajda, Gergő Bitay, Roland Veress, Balázs Horváth, Julius Gy. Papp András Varró, Norbert Nagy. The development of L-type Ca^{2+} current mediated alternans does not depend on the restitution slope in canine ventricular myocardium. *Scientific Reports* 2021, DOI: 10.1038/s41598-021-95299-7 , (**IF**: 4.379, **D1**)

III.) Zsófia Kohajda*, **Noémi Tóth***, Jozefina Szlovák, Axel Loewe, Gergő Bitay, Péter Gazdag, János Prorok, Norbert Jost, Jouko Levijoki, Piero Pollesello, Julius Gy. Papp, András Varró, Norbert Nagy. Novel Na^{+}/Ca^{2+} Exchanger Inhibitor ORM-10962 Supports Coupled Function of Funny-Current and Na^{+}/Ca^{2+} Exchanger in Pacemaking of Rabbit Sinus Node Tissue. *Frontiers in Pharmacology 2020*, DOI: 10.3389/fphar.2019.01632 , (**IF**: 5.811, **Q1**)

+1.) **Noémi Tóth**, Axel Loewe, Jozefina Szlovák, Zsófia Kohajda, Gergő Bitay, Jouko Levijoki, Julius Gy. Papp, András Varró, Norbert Nagy. The reverse mode of the Na^{+}/Ca^{2+} exchanger contributes to the pacemaker mechanism in rabbit sinus node cells. *Scientific Reports, under major revision*

Related published abstracts of the "*The reverse mode of the Na^{+}/Ca^{2+} exchanger contributes to the pacemaker mechanism in rabbit sinus node cells*" study:

- Tóth, N; Loewe, A; Kohajda, Zs; Bitay, G; Levijoki, J; Papp, JGy; Varró, A; Nagy, N. Investigation of the reverse Na^{+}/Ca^{2+} exchanger function in the spontaneous automaticity of rabbit sinus node cells. SCRIPTA MEDICA 52 : Suppl.1 p. S16 (2021)
- Tóth, N; Szlovák, J; Loewe, A; Gazdag, P; Bitay, G; Levijoki, J; Papp, Gy; Varró, A; Nagy, N. A reverz Na^{+}/Ca^{2+} kicserélő szerepének vizsgálata a szinusz-csomó spontán automáciájában = The role of reverse Na^{+}/Ca^{2+} exchanger in the sinus node spontaneous automaticity. CARDIOLOGIA HUNGARICA 50 : Suppl. D pp. 168-168. , 1 p. (2020)

https://m2.mtmt.hu/gui2/?type=authors&mode=browse&sel=10068715

Impact factor of publications related to the subject of the Ph.D. thesis: 16.053

Other publications published under Ph.D. scholarship:

IV.) Zsófia Kohajda, László Virág, Tibor Hornyik, Zoltán Husti, Antia Sztojkov-Ivanov, Norbert Nagy, András Horváth, Richárd Varga, János Prorok, Jozefina Szlovák, **Noémi Tóth**, Péter Gazdag, Leila Topal, Muhammad Naveed, Tamás Árpádffy-Lovas, Bence Pászti, Tibor Magyar, István Koncz, Szilvia Déri, Vivien Demeter-Haludka, Zoltán Aigner, Balázs Ördög, Márta Patfalusi, László Tálosi, László Tiszlavicz, Imre Földesi, Norbert Jost, István Baczkó, András Varró. In vivo and cellular antiarrhythmic and cardiac electrophysiological effects of desethylamiodarone in dog cardiac preparations. *British Journal of Pharmacology* 2022, DOI: 10.1111/bph.15812 , (**IF**: 8.739, **D1**)

V.) István Koncz, Arie O. Verkerk, Michele Nicastro, Ronald Wilders, Tamás Árpádffy-Lovas, Tibor Magyar, **Noémi Tóth**, Norbert Nagy, Micah Madrid, Zexu Lin, Igor R. Efimov. Acetylcholine Reduces I_{Kr} and Prolongs Action Potentials in Human Ventricular Cardiomyocytes. *Biomedicines* 2022, DOI: 10.3390/biomedicines10020244 , (**IF**: 6.081, **Q1**)

VI.) Tibor Magyar, Tamás Árpádffy-Lovas, Bence Pászti, **Noémi Tóth**, Jozefina Szlovák, Péter Gazdag, Zsófia Kohajda, András Gyökeres, Balázs Györe, Zsolt Gurabi, Norbert Jost, László Virág, Juliu Gy. Papp, Norbert Nagy, István Koncz. Muscarinic agonists inhibit the ATP-dependent potassium current and suppress the ventricle-Purkinje action potential dispersion. *Canadian Journal of Physiology and Pharmacol*ogy 2021, DOI: 10.1139/cjpp-2020-0408 , **(IF:** 2.273**, Q3)**

VII.) Jozefina Szlovák*, Jakub Tomek*, Xin Zhou, **Noémi Tóth**, Roland Veress, Balázs Horváth, Norbert Szentandrássy, Jouko Levijoki, Julius Gy. Papp, Neil Herring, András Varró, David A. Eisner, Blanca Rodriguez, Norbert Nagy. Blockade of sodium-calcium exchanger via ORM-10962 attenuates cardiac alternans. *Journal of Molecular and. Cellular Cardiol*ogy 2021, DOI: 10.1016/j.yjmcc.2020.12.015 , (**IF**: 5.000, **Q1**)

VIII.) **Noémi Tóth**, Alexandra Soós, Alex Váradi, Péter Hegyi, Benedek Tinusz, Anna Vágvölgyi, Andrea Orosz, Margit Solymár, Alexandra Polyák, András Varró, Attila S. Farkas, Norbert Nagy. Effect of ivabradine in heart failure: a meta-analysis of heart failure patients with reduced versus preserved ejection fraction. *Canadian Journal of Physiology and Pharmacol*ogy 2021, DOI: 10.1139/cjpp-2020-0700 , (**IF**: 2.273, **Q3**)

IX.) Zsófia Kohajda, Axel Loewe, **Noémi Tóth**, András Varró, Norbert Nagy. The Cardiac Pacemaker Story-Fundamental Role of the Na^+/Ca^{2+} Exchanger in Spontaneous Automaticity. *Frontiers in Pharmacology 2020,* DOI: 10.3389/fphar.2020.00516 , (**IF**: 5.811, **Q1**)

X.) Axel Loewe, Yannick Lutz, Deborah Nairn, Alan Fabbri, Norbert Nagy, **Noemi Toth**, Xiaoling Ye, Doris H. Fuertinger, Simonetta Genovesi, Peter Kotanko, Jochen G. Raimann, Stefano Severi. Hypocalcemia-Induced Slowing of Human Sinus Node Pacemaking. *Biophysical Journal 2019*, DOI: 10.1016/j.bpj.2019.07.037 , (**IF**: 3.854, **D1**)

Impact factor of all publications: 50.084

ABBREVIATIONS

AP(s): action potential(s)

APD: action potential duration

APD_{25}: action potential duration at 25% of repolarization

APD_{50}: action potential duration at 50% of repolarization

APD_{90}: action potential duration at 90% of repolarization

AVN: atrioventricular node

BPM: beats per minute

DD: diastolic depolarization

DI: diastolic interval

DMSO: dimethyl sulfoxide

DOF: dofetilide

$[Ca^{2+}]_i$: intracellular Ca^{2+} concentration

CaT(s): Ca^{2+} transient(s)

CICR: Ca^{2+}-induced Ca^{2+}-release

CL(s): cycle length(s)

EC: extracellular

IC: intracellular

I_{CaL}: L-type Ca^{2+} current

I_{CaT}: T-type Ca^{2+} current

$I_{K(Ca)}$: Ca^{2+} activated K^+ current

I_{Kr}: rapid component of delayed rectifier K^+ current

I_{K1}: inward rectifier K^+ current

I_{Na}: fast Na^+ current

I_{NaL}: late Na^+ current

I_{to}: transient outward rectifier K^+ current

IVA: ivabradine

LCR(s): local Ca^{2+} release(s)

MDP: maximal diastolic potential

$[Na^+]_i$: intracellular Na^+ concentration

$[Na^+]_{pip}$: patch pipette Na^+ concentration

NCX: Na^+/Ca^{2+}-exchanger

ORM: ORM-10962

PLB: phospholamban

RYA: ryanodine

RyR: ryanodine receptor

SAN: sinoatrial node

SCD: sudden cardiac death

SEM: standard error of means

SERCA: sarcoplasmic-endoplasmic reticulum Ca^{2+}ATPase

SR: sarcoplasmic reticulum

STCLV: short-term cycle length variability

TOP: take off potential

ABSTRACT

Introduction: Normal heart rhythm depends on a precise and regular activity of the sinoatrial node (SAN) pacemaker cells. The exact electrophysiological mechanism of spontaneous cardiac pacemaking is not fully understood. Recent results suggest a tight cooperation between the intracellular Ca^{2+} handling ('Ca^{2+} clock') and surface membrane ion channels ('membrane clock') which is referred as the coupled clock mechanism. One of the suggested key players of this crosstalk is the Na^{+}/Ca^{2+}-exchanger (NCX), however direct evidence was unavailable so far, due to the lack of selective inhibitor.

Purpose: Our aim was to investigate the robustness and flexibility of SAN automaticity via analysing the role of different Ca^{2+} dependent currents such as NCX and Ca^{2+} activated K^{+} current ($I_{K(Ca)}$) in the mechanism of cardiac pacemaking. We also studied the effect of SAN frequency on the development of ventricular action potential (AP) and Ca^{2+} transient (CaT) alternans.

Methods: APs were measured from both SAN and ventricular papillary muscle preparations by conventional microelectrode technique. Ion currents combined with fluorescent Ca^{2+} tracking were recorded by whole cell and perforated configuration of patch clamp technique on isolated rabbit SAN cells and dog ventricular cardiomyocytes.

Results: The cycle length (CL) lengthening effect of NCX inhibition could be augmented when the funny current (I_f) was previously inhibited and vice-versa the effect of I_f reduction was facilitated when the Ca^{2+} handling was suppressed. Functioning reverse NCX resulted in larger Ca^{2+} transient amplitude with enhanced SR Ca^{2+} content. Spontaneous AP frequency increased as a consequence of active reverse NCX. Ca^{2+} activated K^{+} current had no role in SAN pacemaking. Ventricular action potential alternans showed strong rate-dependence having clear frequency threshold.

Conclusion: Our results provide the first pharmacological evidence regarding the role of both forward and reverse NCX current in pacemaker mechanism. Experimental and modelling data support a close cooperation between I_f and NCX establishing a "pacemaker reserve" mechanism. The reverse NCX activity may provide additional Ca^{2+} influx that could increase SR Ca^{2+} content providing a „Ca^{2+} reserve" mechanism. This „dual" function of NCX may provide a safety margin of pacemaking and largely increases the robustness (i.e. fail-safe) of spontaneous automaticity. Excessive SAN pacemaking induces ventricular AP and Ca^{2+} transient alternans as a result of mutual crosstalk of surface membrane ion channels and intracellular Ca^{2+}.

1. INTRODUCTION

1.1 Sinoatrial node (SAN) as the primary pacemaker of the heart

Normal heart rhythm depends on a precise and regular activity of the sinoatrial node that is located in the right atrium of the heart[1]. SAN serves as the primary center of the pacemaker system by initiating the heart beats. The electrical impulse generated in the SAN spreads towards to the atria and the atrioventricular node (AVN), which is also called the secondary pacemaker center of the heart[2]. Propagating through the bundle of His, right and left bundle branches, the impulse reaches the ventricular muscle[2]. At rest, the normal heart rate is generally considered as between 60 and 100 beats per minute (bpm), however it can vary greatly under pathophysiological conditions. Pacemaker cells that create the SAN possess the characteristic nature of automaticity, since they are able to ignite action potential (AP) in the absence of external stimuli. Spontaneous AP generation needs a unique cooperation of membrane ion channels and intracellular Ca^{2+} handling. One of the most important questions in the cardiac electrophysiology field is 'what is the main initiator mechanism that ignites the AP of the SAN cells to enable the spontaneous pacemaking of the heart'. Several theories was born to explain the mechanisms underlying the spontaneous rhythm generation, however the earliest ones were not able to fully support the phenomenon. With the development of electrophysiological protocols and the need to explore selective ion current blocking agents, the research on SAN accelerated providing new and modified hypotheses (see details in Chapter 1.2).

Normal function of the SAN is required to maintain the physiological cardiac output and ventricular function. Altered firing rate can upset the physiological cardiovascular balance and can lead to enhanced susceptibility of supraventricular or ventricular arrhythmias. Faster heart rate (tachycardia) could cause severe cardiovascular complications and frequency dependent rhythm disorders such as the development of cardiac alternans. Cardiac alternans are beat-to-beat oscillations of the action potential duration (APD) and the Ca^{2+} transient (CaT) amplitude[3].

Cardiac AP reflects the integrated behaviour of the ion currents and Ca^{2+} cycle.

The APs of SAN cells and AVN cells are different from the APs of the cells in the working myocardium[4,5]. Phase 0 depolarization is mediated by the openings of the T-type- then the L-type Ca^{2+} channels[5]. The activation of L-type Ca^{2+} channels is slower than the activation of Na^{+} channels in the ventricles, therefore the depolarization slope is less steep in pacemaker cells. Due to the lack of I_{to} activation, phase 1 repolarization is not present in SAN cells[5].

Upon repolarization (phase 3) only the rapid component of the delayed rectifier potassium current (I_{Kr}) is activated and hyperpolarizes the membrane to reach the maximal diastolic potential (MDP)[5]. The SAN AP shows a characteristic phase 4 depolarization, where the membrane potential onset is more depolarized (MDP is around -50 – -60 mV) and undergoes a slow diastolic depolarization (DD). DD ends at the take off potential (TOP), which is around -40 mV[5].

1.2 „What keeps us ticking?" – Brief history of SAN pacemaking

This question above was the title of a review study published in 2009 indicating that the basic mechanism of SAN pacemaking is still a matter of debate after more than 40 years of intensive research[6]. There is no doubt in the literature that the spontaneous activity of the pacemaker cells is controlled by the DD. However, our knowledge on the exact mechanism underlying this phenomenon is still incomplete, despite the intensive research work of different acknowledged laboratories.

The earliest theory of the pacemaking is originated from the 1950s, when Weidmann et al. attributed an important role to the decay of a K^+ current during the DD[7]. Two types of K^+-currents were distinguished: the time-independent, fast repolarizing current I_{K1}, and the time-dependent, slow current I_{K2} which is sensitive to adrenaline[7,8]. The proposed mechanism of pacemaking was the slow decay of the K^+-currents together with slow inward depolarizing currents (**Figure 1**)[8]. When K^+-currents are decayed, the inward background currents exceed the repolarizing currents and the membrane is slowly depolarized[8].

In 1979 Dario DiFrancesco discovered the so-called "funny current" (I_f) in Purkinje fibers[9]. "Funny current" got the name from its unconventional behaviour: the current carries depolarizing current (mix of Na^+ and K^+ ions) but it is activated upon hyperpolarization[9-11]. Additionally, it was found to be sensitive to adrenaline[9]. It was observed that I_f is able to cause spontaneous depolarizations in Purkinje fibers **(Figure 1)**[9]. An obvious question was emerged: are there two completely distinct mechanisms for the same function between two regions (SAN *vs.* Purkinje fibers) of the heart? A milestone of the SAN pacemaking research was when the I_{K2} was "reinterpreted" and it was demonstrated that I_{K2} is actually the same current as I_f **(Figure 1)**[10]**.** From 1982 to the beginning of the 2000's the "funny-concept" was the leading mechanism to explain SAN automaticity: hyperpolarization during repolarization activates I_f which depolarizes the membrane during the DD[10,11]. Additionally, I_f shows dual activation by voltage and cAMP, therefore it also transmits the changes of the autonomic nervous system[11].

With the discovery of I_f the spontaneous rhythm generation seemed to be explained for decades, however later the hypothesis was repeatedly challenged. Noma and Morad showed that complete block of I_f by caesium did not stop the spontaneous activity emphasizing other possible mechanisms than I_f[12].

In 1996, a new possible player in the SAN automaticity was suggested. Rigg and Terrar demonstrated that the inhibition of sarcoplasmic Ca^{2+} releases or refilling decreases the SAN frequency highlighting an important role of Ca^{2+} handling in pacemaking[13] **(Figure 1).**

In the beginning of the 2000's, Lakatta and his colleagues identified spontaneous, subsarcolemmal local Ca^{2+} releases (LCRs) that appear during the late DD[14-16]. It was claimed that LCRs produce an inward current by activating the forward Na^+/Ca^{2+} exchanger (NCX) and responsible for the ignition of SAN AP. This concept indicated that the primary mechanism of DD is the NCX mediated Na^+ influx and almost completely ignored the role I_f in SAN pacemaking. Later, this hypothesis was named as the *Ca^{2+} clock theory*, since the sarcoplasmic reticulum (SR) serves as the Ca^{2+} clock itself by generating rhythmic LCRs[17] **(Figure 1)**.

From that point an intensive debate emerged between the Ca^{2+} clock hypothesis and the „funny current" hypothesis[18,19]. The „funny-current" hypothesis was later extended to *membrane clock (M-clock) hypothesis* indicating that surface membrane ion channels have pivotal role in pacemaking. Intensive research in this field revealed that intracellular Ca^{2+} handling and surface membrane ion channels are tightly coupled during pacemaking[20]. This synergistic cooperation forms the latest concept of the so-called *coupled clock hypothesis*[20,21].

1.3 Ca^{2+} homeostasis of the cardiomyocytes

Ca^{2+} cycle is an important regulator of cardiomyocyte function, as it creates a close link between electrical signals of the heart and contractions of the myocytes **(Figure 2)**[22]. This paired mechanism that connects myocyte depolarization with mechanical contraction is the so-called excitation-contraction coupling[22]. Cardiac Ca^{2+} signaling essentially relies on important molecular players like ryanodine receptors, voltage-gated Ca^{2+} channels and active Ca^{2+} transport mechanisms **(Figure 2)**[23]. Excitation-contraction coupling is divided into four major mechanisms: (1) Ca^{2+} influx, (2) Ca^{2+} release, (3) Ca^{2+} reuptake and (4) Ca^{2+} efflux[22,24].

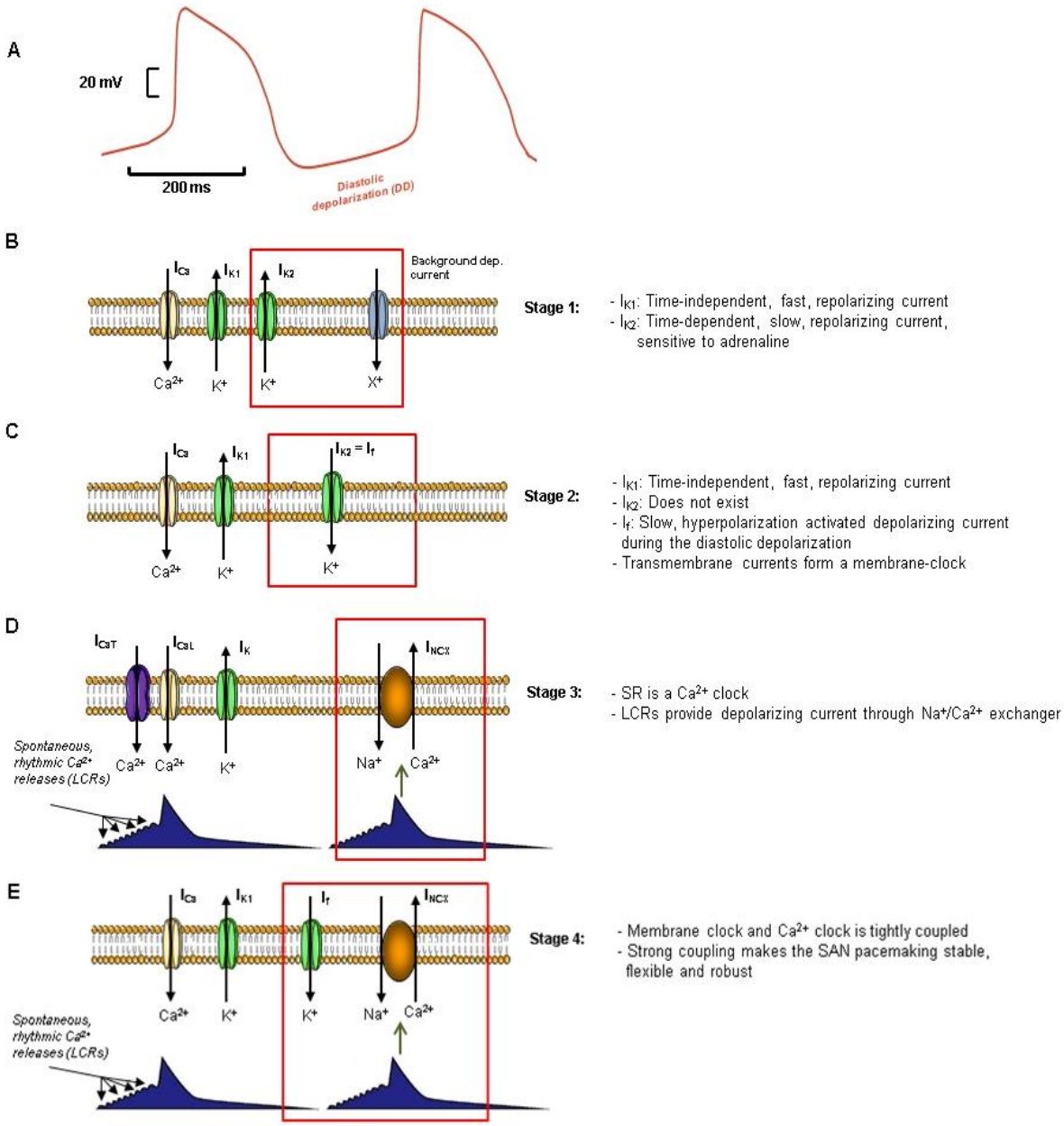

Figure 1: Early and modern concepts of SAN pacemaking

Panel A illustrates a representative SAN AP, while panel **B, C, D** and **E** represents the hypotheses born to explain the mechanism of SAN pacemaking with the corresponding ionic backgrounds. The proposed mechanisms were the following: **panel B**: slow decay of repolarizing K^+ currents and background depolarizing currents; **panel C**: activation of I_f; **panel D**: Ca^{2+} clock mediated activation of forward NCX current; **panel E:** activation of transmembrane depolarizing currents and local Ca^{2+} releases mediated activation of forward NCX. See the text for details (Chapter 1.2). *I_{CaL}: L-type Ca^{2+} current, I_{CaT}: T-type Ca^{2+} current, I_f: funny current, I_{Kr}: rapid component of delayed rectifier K^+ current, LCRs: local Ca^{2+} releases, SR: sarcoplasmic reticulum*

Upon depolarization, the positive membrane potential favors the opening of the L-type Ca^{2+} channels that enables Ca^{2+} to enter the cell reaching the restricted space between the SR and the sarcolemma[24,25]. The Ca^{2+} concentration of the restricted space varies between ~100 nM and ~10 μM during an action potential.

The elementary Ca^{2+} influx signal is mediated by the opening of the L-type Ca^{2+} channels, however a smaller portion of Ca^{2+} influx may result from the activation of T-type Ca^{2+} channels and reverse NCX **(Figure 2)**[22,24,26,27]. T-type Ca^{2+} channels are activated at more negative membrane potentials than L-type Ca^{2+} channels and show a sinoatrial specific expression[27,28]. Although T-type Ca^{2+} channels play an important role in the fast phase of depolarization in SAN cells, their role within ventricular cells is negligible[28].

The reverse mode of the NCX can also provide additional Ca^{2+} influx at positive membrane potential levels or with high intracellular Na^{+} concentration, however the contribution of the exchanger to the Ca^{2+} inflow is limited in ventricular cardiomyocytes under physiological conditions[24]. However, if the L-type Ca^{2+} channel function is impaired for some reason, the relative contribution of the reverse NCX current could increase and it could be able to initiate myocardial contraction on its own[22].

Ca^{2+} influx is further followed by Ca^{2+} release from the SR[22,29]. The entering Ca^{2+} induces the opening of the ryanodine receptors (RyR) on the SR via the Ca^{2+} induced Ca^{2+} release (CICR) mechanism **(Figure 2)**[22,24]. The activation of RyRs mobilizes Ca^{2+} from the SR, producing Ca^{2+} release termed as Ca^{2+} transient[22,24]. Spatial and temporal summation of the released Ca^{2+} produces an average global intracellular Ca^{2+} having systolic value of ~500 nM to ~1000 nM[29]. Ca^{2+} release is resulted in myocardial contraction, as Ca^{2+} sensitive troponin C binds the released Ca^{2+} ensuring cell shortening[22].

As cytoplasmic Ca^{2+} level decreases the cells return to the resting phase in preparation for the next depolarization. Fast and complete relaxation of the heart requires rapid dissociation of Ca^{2+} from troponin C, therefore during the relaxation period the sequestration of intracellular Ca^{2+} occurs[22,24]. Ca^{2+} extrusion from cytoplasmic space is driven by two main mechanisms: (1) Ca^{2+} reuptake and (2) Ca^{2+} efflux. Ca^{2+} reuptake to the SR is mediated by the sarcoplasmic-endoplasmic reticulum Ca^{2+} ATPase (SERCA) **(Figure 2)**[22]. The function of SERCA is regulated by the phosphorylation – dephosphorylation of phospholamban (PLB). Unphosphorylated PLB decreases the affinity of SERCA for Ca^{2+}, while phosphorylated monomers block the interaction with SERCA providing increased activity of the pump, therefore increased Ca^{2+} removal. The main Ca^{2+} efflux mechanism is the plasma membrane Na^{+}/Ca^{2+} exchanger **(Figure 2)**[22]. The forward operation mode of the NCX extrudes 1 Ca^{2+} ion to the extracellular space, while imports 3 Na^{+} ions to the cell, generating a depolarizing current[30]. The mitochondrial uniporter and the plasma membrane Ca^{2+} ATPase may also play a minor role in the Ca^{2+} efflux mechanism, however the involvement of these transport mechanisms is negligible in physiological conditions[22,24,31]. The relative contribution of the

main Ca^{2+} removal mechanism (i.e. SERCA and forward NCX) varies in a species-dependent manner. In mammalian ventricles that show similar AP pattern like human's, 70% of the cytoplasmic Ca^{2+} is removed by SERCA and around 28-30% is removed by forward NCX[31,32]. In contrast, in rat and mouse cardiomyocytes, the contribution of SERCA reuptake is around 92-94%, leaving only 5-7% for the Ca^{2+} extrusion by NCX[33]. It is important to note, that the rat ventricular action potential and Ca^{2+} handling characteristics show less similarity to human[33].

The excitation-contraction coupling is fundamentally controlled by $Ca^{2+,}$ therefore the mechanisms involved in Ca^{2+} cycle should provide a precise balance to maintain the normal cardiac function. Under physiological conditions the Ca^{2+} influx and Ca^{2+} efflux, the Ca^{2+} release and Ca^{2+} reuptake must be equal ensuring the optimal intracellular Ca^{2+} concentration[22].

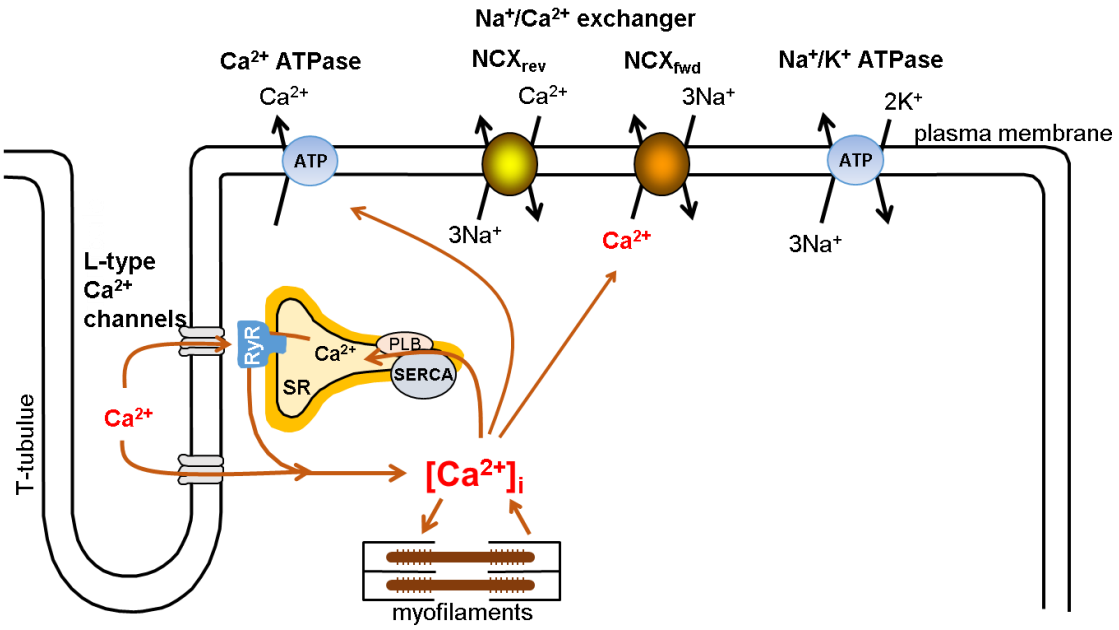

Figure 2: Schematic illustration of Ca^{2+} homeostasis

Main steps of the Ca^{2+} cycle and excitation-contraction coupling are illustrated. Ca^{2+} influx is mediated by the openings of the L-type Ca^{2+} channels. The inflowing Ca^{2+} induces Ca^{2+} release from SR via Ca^{2+} induced Ca^{2+} release (CICR). Ca^{2+} reuptake is ensured by SERCA, while Ca^{2+} extrusion is driven by mainly the forward operation of NCX, and in a lesser extent by the operation of plasma membrane Ca^{2+} ATPase. T-tubulues are present in ventricles, but missing in SAN cells.

NCX_{fwd}: forward mode of NCX, NCX_{rev}: reverse mode of NCX, PLB: phospholamban, RyR: ryanodine receptor, SERCA: sarcoplasmic-endoplasmic reticulum Ca^{2+} ATPase, SR: sarcoplasmic reticulum

1.4 Ca^{2+} dependent currents connecting Ca^{2+} handling and membrane potential

Since SAN pacemaking is based on mutual coupling between intracellular Ca^{2+} handling and membrane potential, Ca^{2+} dependent ionic currents have pivotal role in establishing connections between these systems.

1.4.1 Ca^{2+}-current

As shown, Ca^{2+} is the principal intracellular regulator of many cardiac molecular mechanisms (i.e. excitation-contraction coupling, spontaneous automaticity). Most of the inflowing Ca^{2+} enters the cell via the cardiac Ca^{2+} channels generating an inward depolarizing current[24]. Two types of Ca^{2+} channels are present in the cardiac myocytes: L-type- and T-type Ca^{2+} channels[27]. The presence of $I_{Ca,L}$ and $I_{Ca,T}$ varies among cardiac myocytes. High-voltage activated L-type Ca^{2+} channels ($Ca_v1.2$) are found in all region of the heart providing the main source of Ca^{2+} for the excitation-contraction coupling[27]. I_{CaL} via L-type Ca^{2+} channels shows a rapid activation at -40 mV, then this is followed by a slow inactivation that creates the plateau phase of the AP in the ventricles[27]. In contrast, low-voltage activated T-type Ca^{2+} channels ($Ca_v3.1$ and $Ca_v3.2$) are almost undetectable in ventricular myocytes, they are found primarily in the conduction system contributing to the depolarization of pacemaker cells[27,28]. However, in pathophysiological conditions, such as cardiac hypertrophy or heart failure I_{CaT} could be more prominent in ventricular cells compared to physiological circumstances[28].

1.4.2 Na^+/Ca^{2+} exchanger (NCX)

NCX is a member of the Ca^{2+}/cation antiporter (CaCA) superfamily, as the exchanger transports three Na^+ in exchange for one Ca^{2+} giving rise to an electrogenic transport through the membrane[30,34,35]. The electrogenic operation of NCX results in an ion current with one net charge in each transport cycle and influences the transmembrane voltage **(Figure 3)**[30,36,37]. The main role of the exchanger is the Ca^{2+} extrusion through the forward operation mode[24,36]. However, the direction of the ionic transport of the NCX is reversible and it can act in the reverse mode, when Ca^{2+} enters the cell **(Figure 3)**[24,36,38]. The direction of the ionic transport is markedly influenced by the actual membrane potential and the ionic gradients across the cell membrane. The operation mode is determined by the relationship of the membrane potential (V_m) and the NCX equilibrium potential (E_{NCX}), where E_{NCX} is calculated from transmembrane Na^+- and Ca^{2+} gradients ($E_{NCX}=3E_{Na}-2E_{Ca}$). Reverse mode (i.e. Ca^{2+} influx) is favored when V_m is more positive than the E_{NCX}, however when the difference

between V_m and E_{NCX} is negative, the exchanger acts in the forward mode (i.e. Ca^{2+} efflux)[22].

Considering the mode of action, NCX can depolarizes or repolarizes the cell membrane by generating inward or outward current, respectively **(Figure 3)**[22,39].

Several studies highlight the fundamental role of NCX in normal SAN automaticity[13,40-42]. Reduction in normal NCX function by low [Na^+] bath solution resulted in decreased spontaneous SAN cell firing rate in guinea pig SAN cells[43]. Severe bradycardia was present in partial atrial NCX1 knock out mouse model[44], while complete NCX knock out resulted in fully suppressed atrial depolarization appearing as ventricular escape rhythm on the ECG[45]. A non-selective NCX inhibitor, KB-R7943 also reduced the spontaneous beating rate in guinea pig SAN cells[43], however the parallel I_{CaL} inhibitory effect of KB-R7943 makes the interpretation difficult. As seen in the literature, several studies claim the essential role of NCX in the pacemaker mechanism of the SAN cells, however the supposed role of NCX could not be directly investigated because of the lack of properly selective NCX inhibitors.

Divalent (Ni^{2+}, Mg^{2+}, Co^{2+}, Sr^{2+}, Cd^{2+}, Ba^{2+}, Mn^{2+}) and trivalent (La^{3+}, Nd^{3+}, Tm^{3+}, Y^{3+}) cations inhibit the NCX current, but the inhibitory effect is nonspecific[46,47]. Benzyloxyphenyl derivatives such as KB-R7943 (2-[2-[4-(4-nitrobenzyl-oxy)phenyl]ethyl]isothio-urea-methanesulfonate, carbamidothioic acid) were the first promising novel NCX inhibitors, however experimental studies reported different blocking potency on the reverse and the forward mode[48]. Furthermore, experimental results revealed nonspecific effects on other transmembrane currents (I_{CaL}, I_{Na}, I_{Kr}), therefore the use of this agents for characterizing the NCX current in different conditions would be difficult to interpret[48]. SEA-0400 (2-(4-(2,5-difluorobenzyloxy)phenoxy)-5-ethoxy aniline) has improved selectivity compared to KB-R7943, however it still has nonspecific inhibitory effect on I_{CaL}[48-50]. Approximately 20% of I_{CaL} inhibition was shown[48]. Efforts were continuously made to explore selective inhibitors to investigate the NCX function in SAN pacemaking, Ca^{2+} handling, and other complex mechanisms such as cardiac arrhythmogenesis. Two novel NCX blockers were developed. The first one was ORM-10103, that has improved selectivity towards NCX, although it still has minor nonspecific effect by blocking I_{Kr} in the concentration of 3 μM[51]. ORM-1013 has quite similar EC_{50} values for the forward and reverse mode operation at 1 μM concentration (800 nM and 960 nM, respectively)[51]. The other compound is ORM-10962 (ORM), that turned out to be highly selective with high efficacy[52]. ORM-10962 is greatly NCX specific with no blocking effect on the I_{CaL}, I_{Na}, I_{NaL},

I_{NaK} and all the repolarizing currents (I_{Kr}, I_{Ks}, I_{to}, I_{K1})[52]. Therefore ORM is a suitable tool to study the existence and function of NCX in different cardiac mechanisms.

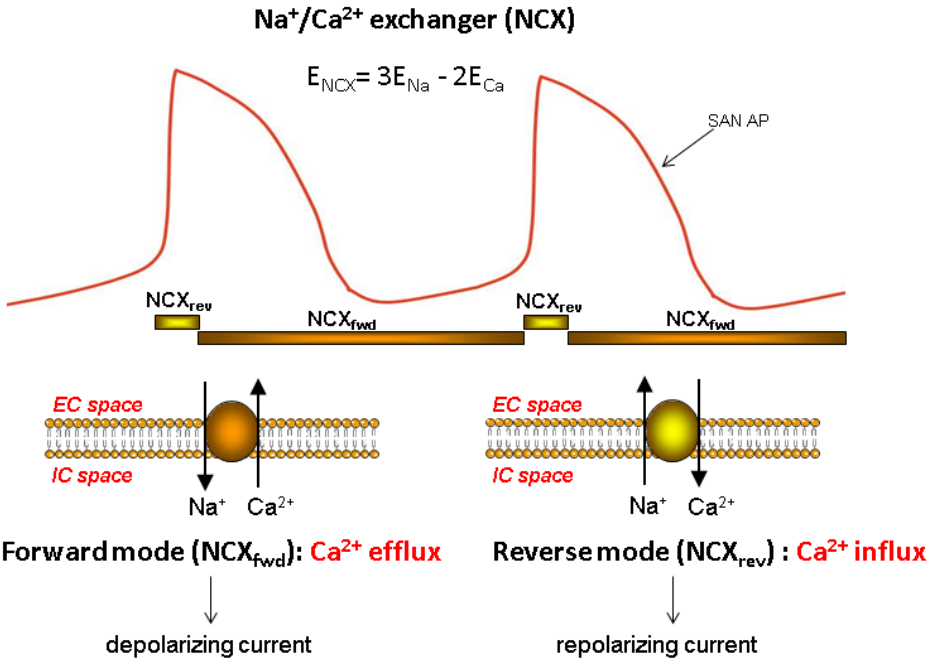

Figure 3: Schematic illustration of the NCX operation

Forward operation of NCX is illustrated with orange, while reverse mode is marked with yellow. Reverse NCX transports 3 Na^+ out of the cell with parallel Ca^{2+} import. In contrast, forward operation mode extrudes 1 Ca^{2+} and brings 3 Na^+ into the cell. Concentration gradients and thermodynamical properties favors mostly the forward NCX operation under the AP. Since the activity of NCX is electrogenic, one net charge in each cycle develops. Forward mode generates an inward depolarizing current, while reverse mode produces an outward repolarizing current.
NCX_{fwd}: forward mode of NCX, NCX_{rev}: reverse mode of NCX

1.4.3 Small-conductance Ca^{2+} activated K^+ channels

Theoretically, the Ca^{2+} activated K^+ channels could be also important players translating intracellular Ca^{2+} changes into membrane potential alterations. As a Ca^{2+} sensitive current, it could directly influence the repolarization kinetics improving the flexibility (i.e. adaptation) of pacemaking.

Early studies suggested that there is no active current in the ventricular myocytes that is activated by intracellular Ca^{2+} and carries exclusively K^+ ions[53]. However, later Xu et al. provided evidence of a notable small-conductance Ca^{2+} activated K^+ current ($I_{K(Ca)}$) in ventricular and atrial cardiomyocytes of mice and human[54]. In recent studies $I_{K(Ca)}$ is shown to have important role in several cardiovascular diseases such as atrial fibrillation, heart failure[55,56] or cardiac memory[57]. Under normal conditions no role was found in ventricular myocytes[58]. Ca^{2+}-driven nature of $I_{K(Ca)}$ suggests possible function in SAN pacemaking

providing functional connection between intracellular Ca^{2+} and the repolarization (**Figure 4**), however the role of $I_{K(Ca)}$ in SAN cells is poorly elucidated.

The bee venom toxin apamin in a concentration of 100 nM selectively blocks the Ca^{2+} activated K^+ channels[59], therefore a suitable tool to investigate the existence and role of $I_{K(Ca)}$ in SAN.

1.5 Recent concept for SAN pacemaking

NCX may have crucial importance in the clock-like oscillator system of SAN automaticity. Based on the recent concept of pacemaking (seen in Chapter 1.2) early LCR's activate the NCX during the DD independent of the I_{CaL} function **(Figure 4)**. The activation of the exchanger defines the „ignition" onset, while I_{CaT} and I_f also contribute to the slow depolarization to reach the threshold potential of I_{CaL}[60]. It is feasible that a low-voltage subtype of the L-type Ca^{2+} channels also involved in the process[60]. When membrane potential reaches the threshold of the I_{CaL} the opening of the channel provides large Ca^{2+} influx facilitating the Ca^{2+}-dependent LCRs and boosts the operation of the NCX[20]. I_{CaT} may have also important role in the diastolic Ca^{2+}-induced Ca^{2+}-release [60].

The coupled clock system is a synergistic mechanism: the Ca^{2+}-clock (LCR's) and the membrane clock (ensemble of surface membrane ion channels) operate together and neither of them is dominant[20,21] (**Figure 4**). It also implies that any perturbation in either clock will influence the other because of the tight coupling. It is assumed that close synchronization between clocks make the SAN automaticity more stable and safe: it largely reduces the beat-to-beat variability of the SAN pacemaking[20].

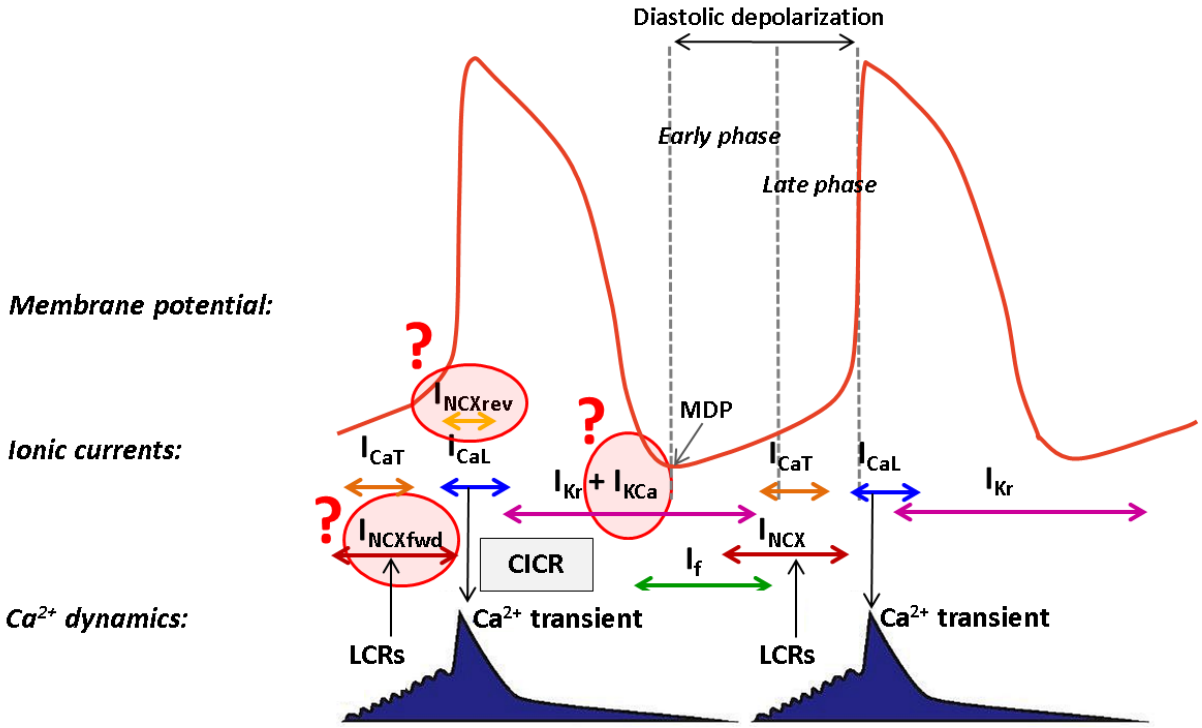

Figure 4: Coupled clock system of SAN pacemaking

Recent modeling and experimental results suggest that surface membrane ion channels and Ca^{2+} handling work tightly coupled since the membrane clock regulates the Ca^{2+} influx and efflux while the LCRs through the NCX also regulates the diastolic depolarization forming a coupled-clock system. The ionic background of coupled clock system is illustrated. The role of NCX and $I_{K(Ca)}$ in the spontaneous automaticity is suggested, however lacks the experimental evidence so far.

CICR: Ca^{2+} induced Ca^{2+} release, I_{CaL}: L-type Ca^{2+} current, I_{CaT}: T-type Ca^{2+} current, I_f: funny current, I_{KCa}: Ca^{2+} activated K^+ current, I_{NCXfwd}: forward NCX current, I_{NCXrev}: reverse NCX current, I_{Kr}: rapid component of delayed rectifier K^+ current, LCRs: local Ca^{2+} releases, MDP: maximal diastolic potential

1.6 SAN frequency induced changes in ventricular AP morphology

It has been known for a long time that actual frequency of SAN influences the ventricular AP morphology[61]. Accelerated SAN frequency appears with characteristic cycle length (CL) shortening **(Figure 5)**[61-64]. Diastolic interval (DI) is the most sensitive to any frequency alteration by influencing the recovery and refractory period of ionic currents, therefore slight CL shortening is mediated only by the shortening of DI. Moderate CL shortening can be caused by parallel shortening of the DI and APD, where APD is shortened but remains equal in each cycle **(Figure 5)**[64,65]. However, when frequency enhancement reaches a critical threshold, APD alternans occur when beat-to-beat oscillation of APD and parallel CaT alternans are present **(Figure 5)**[3,66,67]. Therefore, increased heart rate may promote the development of cardiac alternans[66,68]. The consequence of the cellular alterations is manifested on the ECG as microvolt T-wave alternans (μM-TWA)[69,70]. μM-TWA can easily progrediate to life threatening arrhythmias and can predict the evolvement of ventricular

fibrillation and sudden cardiac death (SCD)[70-72]. Alternation of the APD and DI exerts repolarization inhomogeneity and transmural heterogeneity within the myocardium[73,74].

The exact mechanism underlying the development of cardiac alternans is not fully clarified. Currently two hypotheses are supposed to explain the mechanism of alternans. According to the restitution hypothesis, alternans are governed by the APD restitution (i.e. APD function depending on the previous DI)[75]. Nolasco and Dahlen claimed that alternans appear when the APD restitution curve is larger than 1[75]. This hypothesis is controversially discussed, and recent studies suggest minor fidelity of the restitution in the prediction of alternans, while they highlight the role of Ca^{2+} handling and enhanced frequency. Ca^{2+} driven hypothesis claims that Ca^{2+} handling imbalance as a response to high heart rate can cause alternans since intracellular Ca^{2+} and membrane potential are tightly coupled[67,76-78].

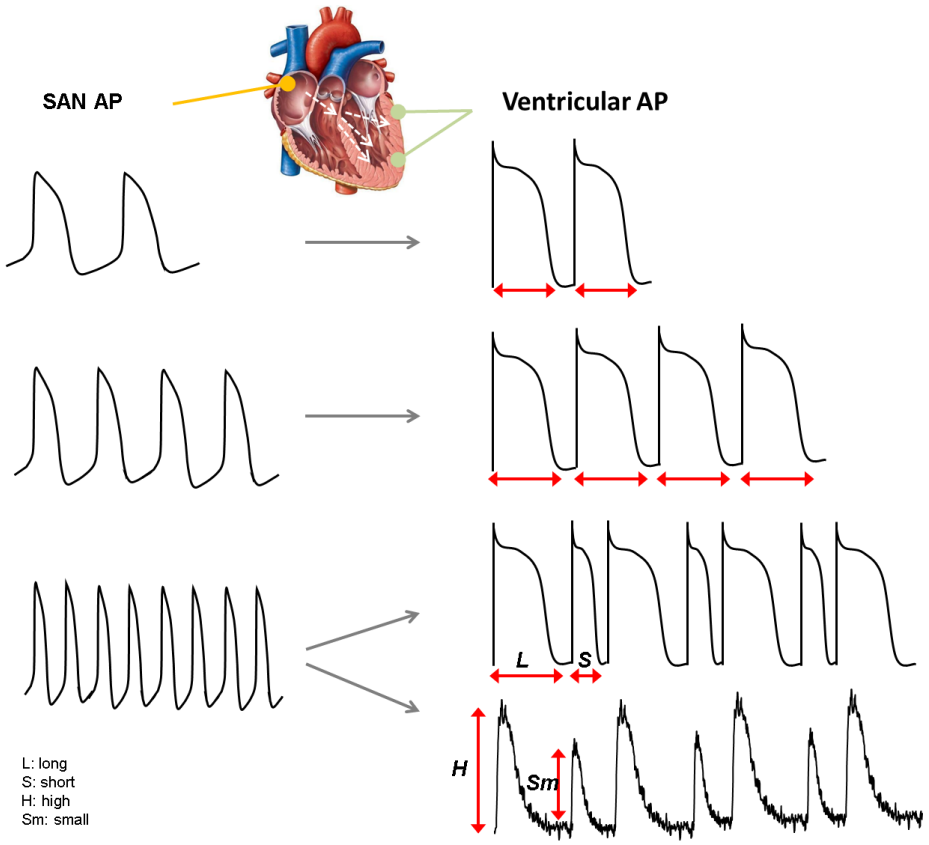

Figure 5: Schematic illustration on how does the SAN frequency may influence the AP morphology of ventricular cells

SAN pacemaking influences the morphology of ventricular APs, since the impulse spreads through the cardiac conduction system and reaches the working myocardium. Enhanced SAN frequency leads to CL shortening via the shortening of the diastolic intervals. As the frequency further increases and reaches a critical threshold, AP alternans occur as beat-to-beat oscillations of APD with parallel alternans of Ca^{2+} transient amplitude. APD alternates with a long-short-long pattern, while transient alternates with high-small-high pattern. The development of alternans implies higher risk for malignant arrhythmias.

2. AIMS

Since the mechanism of SAN pacemaking is not fully clarified, the aims of the present study were the followings:

1.) to investigate the function of the forward NCX current by its direct pharmacological inhibition using the novel, selective inhibitor ORM-10962 and analyse the suggested crosstalk between NCX current and I_f in multicellular level of SAN pacemaking,
2.) to investigate the potential existence and functional role of the reverse NCX current in the SAN pacemaker mechanism,
3.) to investigate the role of $I_{K(Ca)}$ in the SAN pacemaking,
4.) to study the arrhythmogenic consequences of enhanced SAN pacemaking on the function of ventricles (i.e. test the possible role of Ca^{2+} handling and restitution in the development of cardiac alternans).

3. MATERIALS AND METHODS

3.1 Animals

Every experiments were accomplished in compliance with the Guide for the Care and Use of Laboratory Animals (USA NIH publication No 85–23, revised 1996) and were approved by the Csongrád-Csanád County Governmental Office for Food Safety and Animal Health, Hungary (approval No.: XIII/1211/2012).

To study NCX in SAN pacemaking New-Zealand white rabbits of either sex (weighing 1,5-2 kg) were used. The rabbits initially have received iv. injection of 400 IU/kg heparin into the ear vein, then they were sacrificed by concussion in order to avoid the possible cardiodepressant effects of any anaesthetics. The chest was opened and after the quick removal of the heart, it was placed into cold (4°C) solution with the following composition (mM): 135 NaCl, 4.7 KCl, 1.2 KH_2PO_4, 1.2 $MgSO_4$, 1 $CaCl_2$, 10 glucose, 10 HEPES, 20 taurine, 4.4 $NaHCO_3$, 5 Na-pyruvic acid, pH 7.2 with NaOH.

To study the development of cardiac alternans Beagle dogs of either sex (weighing 10-12 kg) were used. The animals were anaesthetized and sacrificed with iv. injection of pentobarbital (60 mg/kg), then the heart was rapidly removed through a right lateral thoracotomy. After the removal of the heart, the atria were removed and both the right and left ventricle were opened. Papillary muscles were excised from the right ventricle, while the left ventricular segment was cannulated from a coronary and placed on a modified Langendorff perfusion system for enzymatic digestion.

3.2 Tissue experiments on SAN

3.2.1 Conventional microelectrode technique on SAN

After the removal of the heart, the atria were cut and the sinoatrial region was excised. Since the sinoatrial tissue had spontaneous activity in every case therefore the visible contractions helped us to cut as small tissue as we could. The preparations were mounted in a custom made plexiglass chamber and were allowed to equilibrate for 45-60 minutes while they were continuously superfused with O_2-CO_2 saturated Locke's solution (containing in mM: NaCl 120, KCl 4, $CaCl_2$ 1.0, $MgCl_2$ 1, $NaHCO_3$ 22, and glucose 11). The pH of this solution was set between 7.35 and 7.4 with a mixture of 95% O_2 and 5% CO_2 at 37 ºC. Since the SAN tissue was contracting on its own, no external stimuli were needed. APs were measured using conventional microelectrode technique. Tip resistance of sharp glass capillary microelectrodes were 10-20 MΩ, filled with 3 M KCl. Microelectrodes were connected to a high-impedance amplifier (Biologic Amplifier, model VF 102). Voltage output from the amplifier was

sampled by an AD converter (NI 6025, Unisip Ltd). Intracellular recordings were displayed by EvokeWave v1.49 software (Unisip Ltd.) and the following parameters were analysed: APDs, CLs, DD, AP amplitude. Control recordings were sampled after the equilibrium period. Intensive efforts were made to maintain the same impalement throughout the whole experiment. When the impalement was moved, an adjustment was attempted. The measurements were only continued if the action potential characteristics of the re-established impalement deviated less than 5% from the previous one.

Beside some limiting factors (i.e. cell-to-cell coupling influence the AP waveform) measuring action potentials on multicellular preparations has several advantages. Firstly, without enzymatic dissociation all of the ion channels could remain intact. Furthermore, the SAN tissue is able to represent the whole heart better, since the atrial cells with more negative resting membrane potential could influence the SAN cells by the electrotonic coupling. It may have a great importance as it is known that I_f increases with parallel decrease in the membrane potential.

3.3 Tissue experiments on ventricular myocardium

3.3.1 Conventional microelectrode technique on canine papillary muscles

Ventricular APs were recorded from the surface of right ventricular papillary muscles using the conventional microelectrode technique. The tissue placement, the external solution, the measuring temperature and the equilibrium period were the same as described in Chapter 3.2.1 on SAN. As ventricular preparations have no spontaneous automaticity, the papillary muscles were paced with constant pulses of 5 ms length at 1 Hz through a pair of bipolar platinum electrodes using an electrostimulator (EXP-ST-A2, Experimetria Ltd). The sharp microelectrodes were similarly filled with KCl, having a tip resistance of 10-20 MΩ and were connected to an amplifier (Biologic Amplifier, model VF 102). Voltage output from the amplifier was sampled with the same AD converter mentioned above (NI 6025, Unisip Ltd). APs were detected by EvokeWave v1.49 software (Unisip Ltd.).

APD alternans were measured by increasing pacing frequency using cycle lengths of 500-300-250-230-210-190-160 ms. 20 consecutive APs were recorded at each pacing frequency. APD differences were analysed between long and short AP pairs within 6 consecutive pulses at 25, 50 and 90% of repolarization ($APD_{25,}$ APD_{50} and APD_{90}, respectively) and the average of these APD differences were defined as APD alternans amplitude.

Conventional S1S2 restitution protocol was also applied on the papillary muscles, when basic cycle length (BCL) was 1000 and 500 ms. Extra delays for S2 AP stimuli ranged from -50 ms

to 1000 ms respective to the baseline APD_{90}. 15 S1 stimuli were applied between the S2 stimuli. DIs refer to the proximity of the extra beat (S2) to the APD_{90} of the basic S1 beat (illustrated on **Figure 20 panel A**).

3.4 Cell experiments on SAN

3.4.1 Single SAN cell isolation

The heart was mounted on a modified, 60 cm high Langendorff column and perfused with oxygenated and prewarmed (37°C) solution mentioned above in Chapter 3.1. After washing out of blood (3–5 min) with normal isolation solution (containing in mM: 135 mM NaCl, 4.7 mM KCl, 1.2 mM KH_2PO_4, 1.2 mM $MgSO_4$, 1 mM $CaCl_2$, 10 mM glucose, 10 mM HEPES, 20 mM taurine, 4.4 mM $NaHCO_3$, 5 mM Na-pyruvic acid, pH 7.2 adjusted with NaOH) the heart was perfused with nominally Ca^{2+}-free solution until the heart stopped beating (approximately 10 min). The digestion was performed by perfusion with the same solution supplemented with 1.8 mg/ml (260 U/ml) collagenase (type II, Worthington) and 33 μM $CaCl_2$. After 14–15 min, the heart was removed from the cannula. The right atrium was cut and the crista terminalis and SAN region were excised and cut into small strips. Strips were placed into enzyme free solution containing 1 mM $CaCl_2$ and equilibrated at 37°C for 10 min. After gentle agitation, the cells were separated by filtering through a nylon mesh. The cells were stored at room temperature.

3.4.2 Measurement of NCX current with ramp protocol

To study the possible role of reverse NCX current in SAN pacemaking two experimental groups were established. One group with active reverse NCX and the other group with suppressed reverse function. In order to achieve the difference between the experimental groups, the applied pipette solution contained 8 mM NaCl (8 mM $[Na^+]_{pip}$ group) and 2 mM NaCl (2 mM $[Na^+]_{pip}$ group), respectively. 8 mM NaCl ensured the approximately physiological Na^+ level of the SAN cells, while in the other group the pipette Na^+ concentration was reduced to 2 mM in order to diminish the reverse mode of the NCX, without completely eliminating the exchanger function. Firstly, NCX current was measured with standard voltage ramp protocol both with 8 mM $[Na^+]_{pip}$ and 2 mM $[Na^+]_{pip.}$ The holding potential was -40 mV, then the membrane was depolarized to 30 mV having a slope of 0.7 V/s. After this, the membrane was hyperpolarized to -70 mV. Reverse and forward mode operation were calculated at different membrane voltage during the downhill phase of the current, i.e. at 25 mV and -60 mV, respectively. The pipette solution contained (in mM): 20

TEACl, 125 CsCl, 5 MgATP, 10 HEPES, and 8 or 2 NaCl, titrated to pH 7.2 with CsOH. The intracellular Ca^{2+} was buffered to ~100 nM (by using a mixture of EGTA and Ca^{2+} calculated by using MaxChelator software) to approximate the normal diastolic Ca^{2+} value. The external solution contained: 135 mM NaCl, 10 mM CsCl, 10 mM TEACl, 0.33 mM NaH_2PO_4, 10 mM glucose, 1 mM $MgCl_2$, 10 mM HEPES, 1 mM $CaCl_2$, 20 μM ouabain, 1 μM nisoldipin, 50 μM lidocain, titrated to pH 7.4.

3.4.3 Measurement of NCX current under SAN AP command

To measure the NCX current under a SAN AP, the spontaneously beating cells were paced using a canonical AP waveform. This AP command was obtained from our previous perforated patch clamp measurements by the average of 10 independent APs. The parameters of the pacing AP were the following: MDP: -57 mV, CL: 410 ms, overshoot: 24 mV, APD: 180 ms, DD slope: 0.124 mV/ms. The extracellular solution contained: 135 mM NaCl, 10 mM CsCl, 10 mM TEACl, 0.33 mM NaH_2PO_4, 10 mM glucose, 1 mM $MgCl_2$, 10 mM HEPES, 1.8 mM $CaCl_2$, 0.2 mM BaCl2, 20 μM ouabain, 1 μM nisoldipine, 50 μM lidocain, 1 μM mibefradil, titrated to pH 7.4. The intracellular solution contained (in mM): 125 CsCl, 20 TEACl, 5 MgATP, 10 HEPES and 10 EGTA titrated to pH 7.2 with CsOH, and 2 or 8 mM NaCl was added respectively.

3.4.4 Measurement of $I_{K(Ca)}$ under SAN AP command

The cells were paced with the previously mentioned canonical SAN AP waveform with the same parameters. To measure the $I_{K(Ca)}$, normal Tyrode's external solution was used (in mM): 144 NaCl, 4 KCl, 0.4 NaH_2PO_4, 0.53 $MgSO_4$, 5.5 glucose, 1.8 $CaCl_2$ and 5 HEPES, titrated to pH 7.4. After the control recording in Tyrode's solution, the external solution was supplemented with 100 nM apamin. $I_{K(Ca)}$ was determined as a difference current (i.e. apamin sensitive current). The pipette solution contained (in mM): 1.15 $MgCl_2$, 10 HEPES, 144 K-gluconate.

3.4.5 AP measurements in single SAN cells

APs were measured using current clamp method of patch clamp by perforated or whole-cell configuration. The membrane potential was recorded using a gap-free acquisition protocol. As always, spontaneously and rhythmically contracting SAN cells were chosen. Perforated patch clamp measurements were performed according to the method Lyashkov et al. described[60]. Normal Tyrode's solution was used as an external solution (see above in Chapter 3.4.4). The pipette solution contained (in mM): 120 K-gluconate, 2.5 MgATP, 2.5 Na_2ATP, 2.5 NaCl, 5

HEPES, 20 KCl, titrated to pH 7.2 with KOH. Pore-forming β-escin (35 μM) was included in the pipette solution to achieve the membrane patch perforation.

In contrast, when whole-cell configuration was used β-escin was omitted from the pipette solution that contained (in mM): 120 K-gluconate, 2.5 K_2ATP, 2.5 MgATP, 5 HEPES, 20 KCl supplemented with 8 mM NaCl or 2 mM NaCl accordingly to 8 mM $[Na^+]_{pip}$ and 2 mM $[Na^+]_{pip}$ groups, titrated to pH 7.2 with KOH.

Membrane voltage was obtained by using an Axoclamp 1-D amplifier (Molecular Devices, Sunnyvale, CA, USA) connected to a Digidata 1440A (Molecular Devices, Sunnyvale, CA, USA) analogue-digital converter. The membrane voltage was also recorded by Clampex 10.0 (Molecular Devices, Sunnyvale, CA, USA).

The analysed parameters of the APs were the following: MDP, TOP, DD slope, APD and CL. MDP is defined as the most negative potential before the AP depolarization. TOP is the voltage measured at the time when the voltage derivative exceeds 0.5 mV/ms. Slope of DD was estimated as the mean voltage derivative of the AP between MDP and TOP. APD is defined as the time interval between TOP and the next MDP. CLs were analysed between the peaks of consecutive APs. The experiments were performed on 37°C.

3.4.6 Ca^{2+} transient measurements in SAN cells

CaTs were measured by optical fluorescent method when the SAN cells were loaded with Fluo-4 AM (5 μM) fluorescent dye. The cell suspension was kept in darkness at room temperature and was loaded with the dye for 20 minutes. Imaging was performed on the stage of an Olympus IX 71 inverted fluorescence microscope. The dye was excited at 480 nm and the emitted fluorescence was detected at 535 nm. Optical signals were sampled at 1 kHz and recorded by a photon counting photomultiplier (Hamamatsu, model H7828). Spontaneously beating cells were chosen, therefore no external pacing was needed to record CaTs. The difference between systolic and diastolic values of the CaT was defined as the CaT amplitude. To obtain maximal fluorescence (F_{max}), the cells were damaged by the patch pipette at the end of the experiment. Ca^{2+} was calibrated using the following formula: $K_d(F-F_{min})/(F_{max}-F)$. The K_d of the Fluo-4 AM was set to 335 nM. The extracellular solution was normal Tyrode's solution (as seen in chapter 3.4.4).

3.5 Cell experiments in ventricular myocytes

3.5.1 Single left ventricular myocyte isolation

The isolation process of left ventricular cardiomyocytes was similar to the isolation of SAN cells described above with a few differences. Only the left ventricular segment was used instead of the whole heart as the whole heart is much larger than the rabbit heart. The segment was perfused first with normal isolation solution (composition seen in Chapter 3.4.1) supplemented with 1 mM $CaCl_2$ for 10 minutes, then it was replaced with Ca^{2+} free isolation solution for another 10 minutes. This was followed by the perfusion with isolation solution containing Collagenase type II (0.66 mg/ml, Worthington) and 33 μM $CaCl_2$. In the 15^{th} minute of the enzymatic digestion protease type XIV (0.12 mg/ml) was added to the solution. CaTs were measured under ventricular AP commands with different extent of APD alternans. The CLs of the applied AP commands were 250 ms to 210 ms. CaT alternans measurement was based on 6 consecutive transients, where the average CaT amplitude was calculated for even and odd beats. The amplitude of a single CaT was analysed as the difference between the peak value and the minimum directly preceding the first analyzed CaT.

3.6 Statistical analysis

Data in this study are expressed as mean ± standard error of means (SEM). Statistical analysis was performed with Student's t-test and ANOVA with Bonferroni *post hoc* test or Tukey *post hoc* test. The results were considered statistically significant when $p < 0.05$.

4. RESULTS

4.1 Investigation of forward NCX function and the NCX-I_f coupling in SAN pacemaking

The role of NCX have been suspected in the coupled clock concept of SAN pacemaking since the NCX mediated inward current is directly translated to membrane potential changes via the operation of forward mode of the exchanger. However, direct pharmacological experiments have not been performed so far because of the lack of selective inhibitor. In the first part of this study, the role of forward NCX and the potential strong cooperation of I_f-NCX were tested with the selective NCX blocker, ORM-10962.

4.1.1 NCX inhibition exerted CL prolongation on SAN tissue

The selectivity of the NCX inhibitor ORM on Ca^{2+}-, Na^{+}- and major K^{+} currents was examined in a previous study showing no effect on other currents than NCX[52]. Since the majority of these experiments were performed in ventricular cardiomyocytes, the effect of ORM on I_f was not investigated[52]. Therefore, the initial step was to test the potential effect of ORM on I_f. As I_f develops at negative membrane potentials, the current was activated by a voltage step protocol by applying hyperpolarizing voltage pulses from a holding potential of -30 mV. The slowly developed current from -30 mV to -120 mV remained unchanged after the application of 1 μM ORM. Since ORM has no effect on other currents contributing to the APs in different heart regions, it is a suitable tool for investigating the role of NCX in the SAN pacemaking (Figure not shown).

Spontaneous automaticity (i.e. spontaneous APs) on SAN tissue was measured by conventional microelectrode technique. 1 μM selective NCX inhibitor ORM slightly but statistically significantly increased the CL (455.6 ± 32 ms vs. 493.0 ± 38 ms; Δ = 8.1 ± 1.8% $p < 0.05$, n = 16/16 hearts, **Figure 6 panel A, B,** and **C**) without any influence on the APD (94.3 ± 6.7 ms vs. 96.7 ± 5.9 ms) or the CL variability (7.6 ± 1.2 ms vs. 8.1 ± 1.3 ms) shown on **Figure 6 panel D** and **F**. The slope of the DD phase was significantly reduced after ORM application (15.7 ± 3.1 mV/s vs. 10.9 ± 2.8 mV/s; n = 14/14; $p < 0.05$, **Figure 6 panel E**). The slope of phase 0 AP depolarization was identical during control conditions and after ORM superfusion (11.2 ± 2.7 V/s vs. 12.5 ± 2.3 V/s, not shown). Solvent control experiments were performed to exclude any effect of DMSO. The preparations maintained the stable frequency when DMSO was applied (440 ± 36.1 ms vs. 445 ± 37.6; n = 4). In the computational SAN

action potential model[79] the degree of NCX current suppression required to obtain equal CL increase as was experimentally measured was found to be 41%.

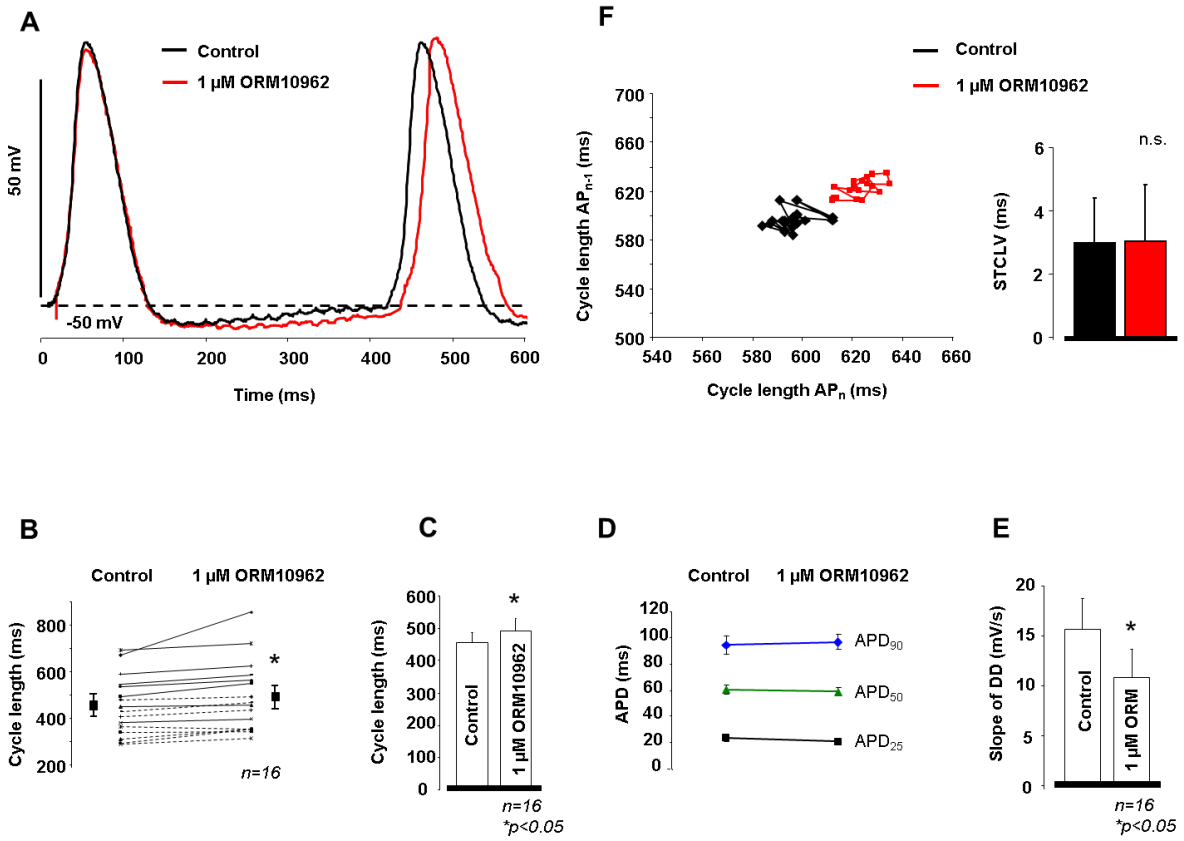

Figure 6: **Effect of selective NCX inhibition in SAN tissue**

Panel A shows representative AP traces in control conditions, then after the application of ORM-10962. As representative traces, individual experiments on **panel B** and bar graphs on **panel C** indicate, the selective NCX inhibitor ORM exerted slight, but statistically significant CL prolongation in SAN tissue. ORM did not change the APD seen on **panel D**, however considerably decreased the slope of DD (**panel E**). Short-term CL variability was calculated by analyzing 30 consecutive AP cycles. Poincaré-plot of CLs and bar graph show that ORM did not alter the CL variability (**panel F**).

4.1.2 NCX inhibition exerted larger CL lengthening effect when I_f was previously impaired

In the next set of experiments, the supposed coupling between I_f and NCX was tested by the subsequent application of the blocking agents (**Figure 7 panel A** and **B**). I_f was inhibited with ivabradine (IVA). The effect of NCX inhibition was significantly larger when I_f was previously inhibited compared with the condition when ivabradine was not applied (8.1 ± 1.88% *versus* 17.1 ± 2.5%; $p < 0.05$, ANOVA, Bonferroni *post hoc* test). A clear, gradual increasing ORM effect was observed on the CL with combined increasing concentration of ivabradine (1 µM ORM effect in the presence of 0 µM IVA: 8.1 ± 1.88%; in the presence of 0.5 µM IVA: 9.6 ± 2.3%; in the presence of 3 µM IVA: 17.1 ± 2.5%, **Figure 7 panel C**). Ivabradine significantly increased the CL both with the concentration of 0.5 and 3 µM ($p <$

0.05, ANOVA, Bonferroni *post hoc* test). Axel Loewe, our cooperation colleague from Karlsruhe University, performed the computational modeling, then we compared the modeling and the experimental results (**Figure 7 panel D**). Using the Yaniv et. al model[79], I_f inhibition was equivalent with 0%-20%-60% block corresponding to 0 µM, 0.5 µM and 3 µM ivabradine (**Figure 7 panel D**). Larger inhibition (~85%) was only set in the model, because the experimental application of 10 µM ivabradine has marked inhibitory effect on I_{Kr}[80] which can also decrease the spontaneous firing rate. The modeling results show a similar tendency as it was seen in the experiments, despite the lack of quantitative match (**Figure 7 panel D**). The same NCX inhibition exerted larger CL prolongation with parallel increase of the I_f inhibition (**Figure 7 panel D**).

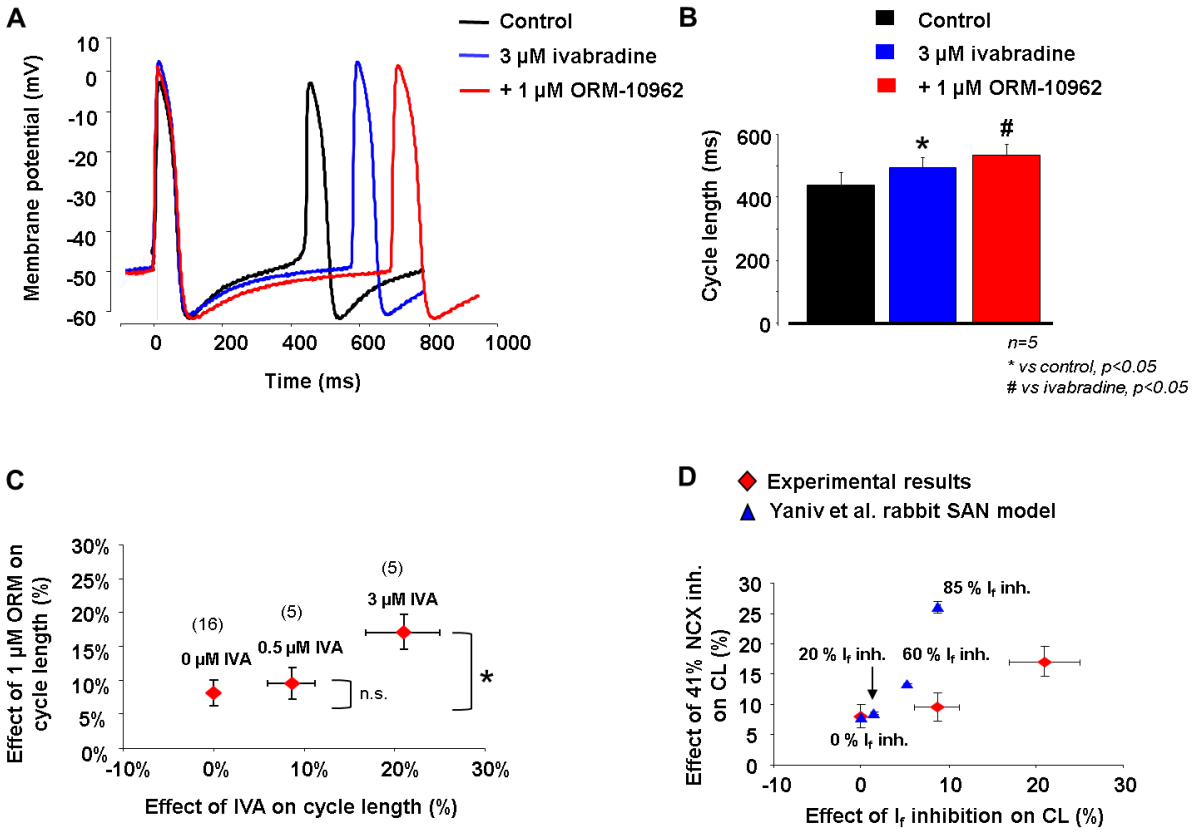

Figure 7: **Effect of combined inhibition of NCX and I_f in SAN tissue**

Panel A shows representative AP traces in control conditions, then after the application of ivabradine, then ORM-10962. As representative traces and bar graphs on **panel B** illustrate, selective NCX inhibitor ORM exerted enhanced CL lengthening effect after ivabradine pretreatment. **Panel C** shows the dose dependent effect of ivabradine on SAN AP CL plotted against the effect of consecutive administration of 1 µM ORM on CL. Without ivabradine, ORM exerted 8% CL lengthening effect (**panel C**). Increasing concentration of ivabradine resulted in increased ORM-induced reduction of firing rate. The numbers in parentheses represent the corresponding n. The experimental results were compared with the Yaniv SAN computational model on **panel D**. 0.5 and 3 µM ivabradine represent 20% and 60% I_f block.. **Panel D** shows the modeling results of combined I_f and NCX block. I_f was inhibited with different degrees and was combined with 41% NCX inhibition. Similarly to the experiments, the effect of NCX inhibition increased as I_f inhibition was enhanced.

4.1.3 Repolarization inhibition induced bradycardia does not facilitate the CL lengthening effect of NCX inhibition

Ivabradine decreased the spontaneous frequency by inhibiting the inward depolarizing I_f (**Figure 7 panel A**). However, bradycardia can be evoked by other mechanisms as well. Therefore, we studied whether repolarization inhibition induced bradycardia influences the effect of NCX inhibition. I_{Kr} was blocked by 100 nM dofetilide (DOF) causing significant CL prolongation (control: 489.3 ± 31 ms → 100 nM dofetilide: 649.1 ± 40.2 ms, **Figure 8 panel A** and **B**). **Panel A** of **Figure 8** shows that the CL prolongation was due to the increase of the APD, without affecting the DI. Subsequent administration of 1 μM ORM resulted in the same effect compared with the individual application of ORM (7.2 ± 1.8% *vs.* 8.1 ± 1.8%, **Figure 8 panel F**). It is very important to highlight that the effect of dofetilide on CL was approximately similar to the effect of 3 μM ivabradine. However, when we observe the AP morphology, a remarkable difference is visible. Dofetilide mediated CL increase was an APD increase induced effect (APD_{90}: 94.4 ± 3 ms *vs.* 187 ± 7.1 ms; $p < 0.05$, n = 7; DI: 338.3 ± 39 ms *vs.* 352.7 ± 44.6 ms, n = 7), while ivabradine caused CL prolongation by influencing only the DI with no change in the APD (**Figure 8 panel C, D** and **E**). NCX inhibition and I_f inhibition both influence the DI by decreasing its slope, while dofetilide does not have any effect on the DD. This could be the reason why the CL lengthening effect of ORM in combination with prior application of dofetilide was not additive.

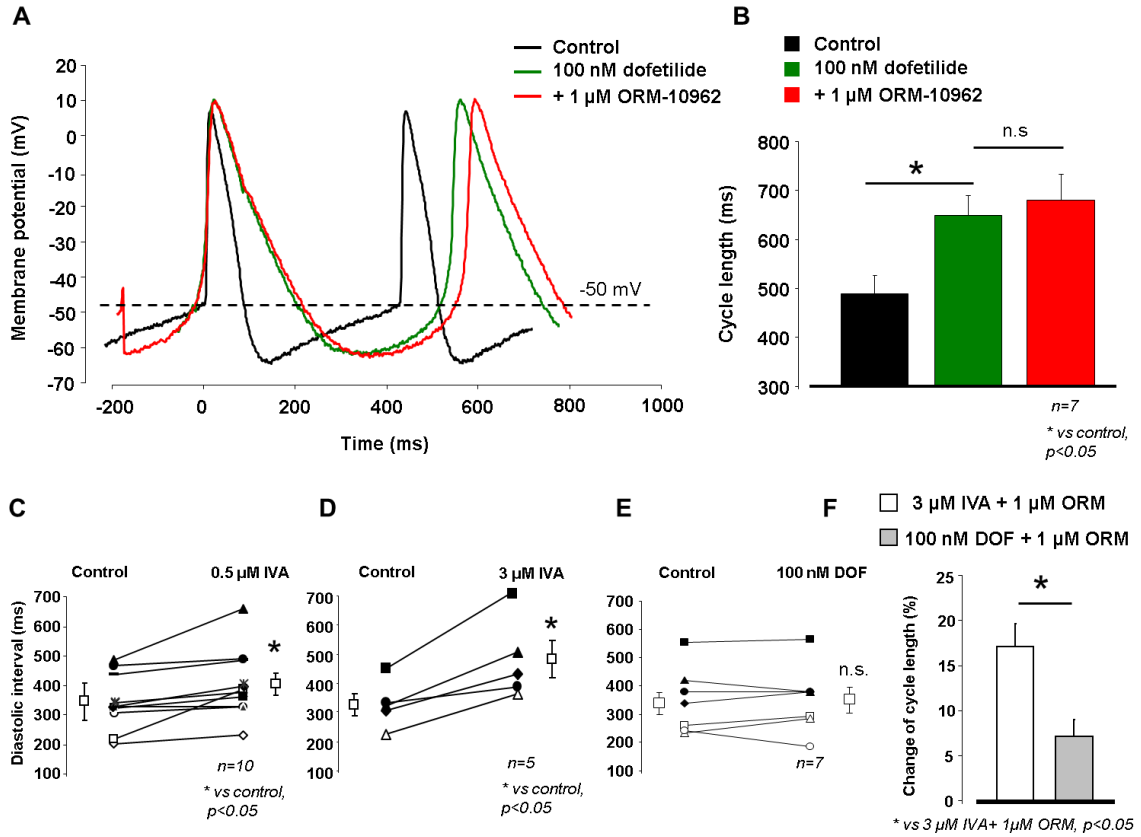

Figure 8: Effect of I_{Kr} inhibition and combined I_{Kr}-NCX inhibition on SAN tissue

Complete block of I_{Kr} by 100 nM dofetilide caused significant CL prolongation (**panel A**). As representative AP traces and bar graphs indicate selective NCX inhibitor ORM did not further enhanced the CL prolongation after the application of dofetilide compared with the individual effect of ORM (**panel A** and **B**). The CL lengthening effect of ivabradine and dofetilide were compared in **panel C, D, E** and **F**. 0.5 and 3 µM ivabradine increased the DI, while dofetilide had no effect on the DI (**panel C, D, E**). The different mechanism could explain that the ORM effect after I_{Kr} inhibition was not additive (**panel F**).

4.1.4 Reduction of $[Ca^{2+}]_i$ increases the CL lengthening effect of I_f inhibition

Results from the previous experiments show that NCX inhibition is larger when I_f is previously attenuated. This suggests a functional coupling between Ca^{2+} handling and I_f and supposes that the effect of I_f inhibition could also have larger effect when NCX is impaired. Therefore, further experiments were performed, and the potential effect of reduction in SR Ca^{2+} release on the effect of ivabradine was tested. After the control recording, 5 µM ryanodine (RYA) was applied to prevent the Ca^{2+} release induced augmentation of the forward NCX current. Ryanodine exerted a significant CL prolongation (437.8 ± 20.3 ms *vs.* 499.8 ± 10.4 ms; $p < 0.05$, n = 6/6, **Figure 9 panel A** and **B**). ORM was subsequently applied and caused a moderate CL increase (**Figure 9 panel A** and **B**). However, when 3 µM ivabradine was added top of the ORM, it markedly and significantly increased the CL of SAN tissue (520.8 ± 29.9 ms *vs.* 726.6 ± 39.8 ms; $p < 0.05$, n = 6/6, **Figure 9 panel B**). **Figure 9 panel C** shows that I_f inhibition resulted in larger CL prolongation in the presence of impaired

Ca^{2+} handling (RYA and ORM application, 42.4 ± 5.7%, $p < 0.05$, Student's T-test) compared to the individual administration of ivabradine.

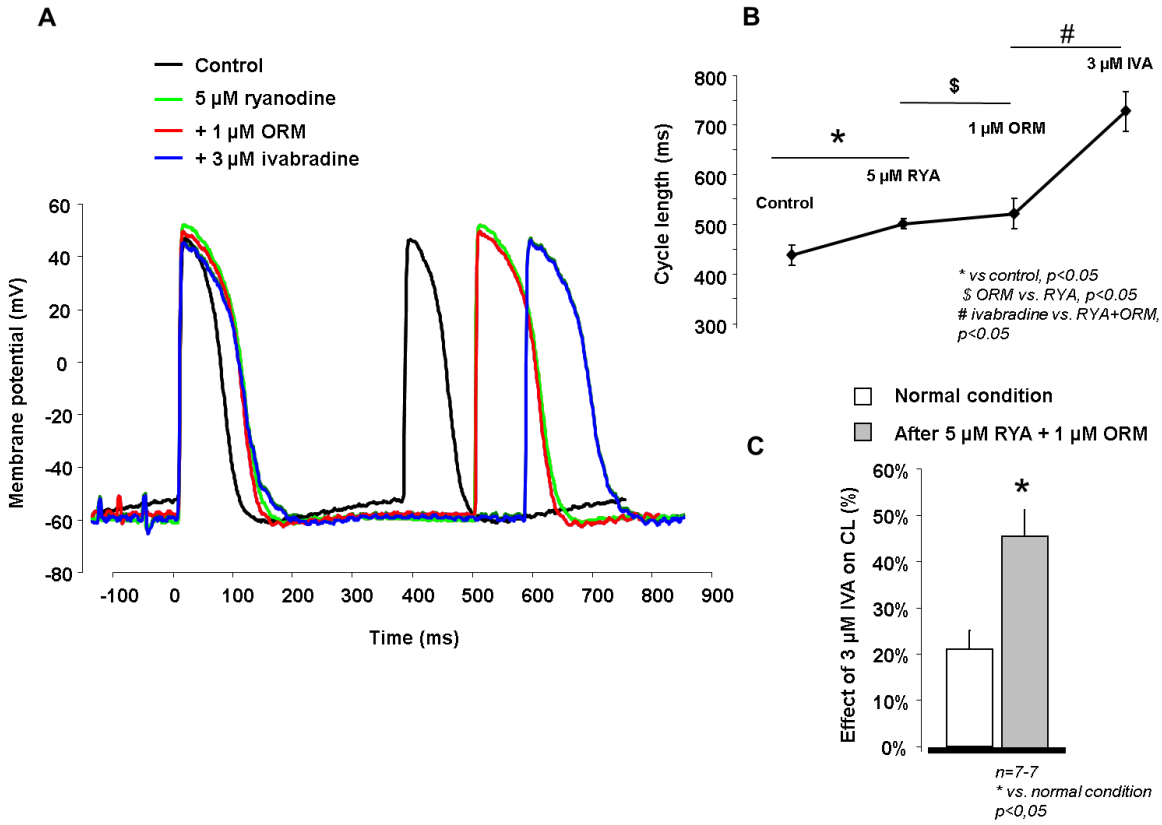

Figure 9: Influence of Ca^{2+} handling suppression with ryanodine and ORM on the effect of I_f reduction

Ca^{2+} handling suppression was achieved by 5 µM ryanodine and 1 µM ORM application. As representative AP traces on **panel A** and graph on **panel B** show, both compound increased the CL of APs. * means ryanodine compared to control, $ means ORM compared to ryanodine, and # means ivabradine compared to ORM. Bar graph of **panel C** depicts that same dose of ivabradine has markedly increased CL lengthening effect when NCX was priorly reduced by concomitant use of ryanodine and ORM compared with the individual effect of ivabradine.

Quite similar approach to the previous one was when reduced $[Ca^{2+}]$ external solution was used. Ca^{2+} concentration was set to 0.9 mM. Reduced extracellular $[Ca^{2+}]$ prolonged the CL which was further lengthened after the application of 3 µM ivabradine (control: 469 ± 39.5 ms → 0.9 mM $[Ca^{2+}]_o$: 515.8 ± 40.8 ms → 3 µM IVA: 777 ± 58.7 ms; $p < 0.05$, n = 6/6 hearts, **Figure 10 panel A** and **B**). Ivabradine has improved CL lengthening effect when extracellular $[Ca^{2+}]$ is low compared with normal extracellular $[Ca^{2+}]$ settings (51.1 ± 5.1% *versus* 20.99 ± 4.1%, $p < 0.05$; Student's t-test, **Figure 10 panel C**).

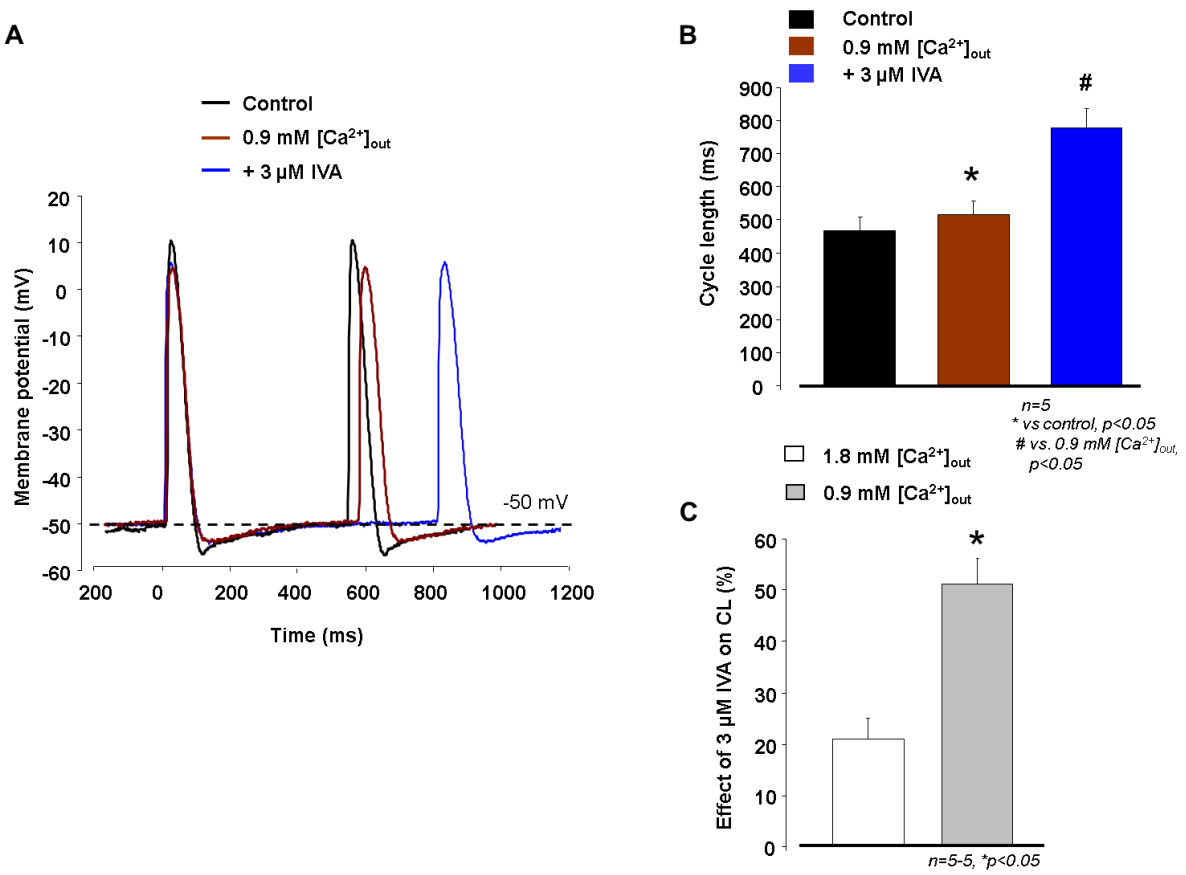

Figure 10: Influence of Ca^{2+} handling suppression with low extracellular Ca^{2+} solution on the effect of I_f reduction

Representative AP traces of **panel A** and bar graph of **panel B** show that the CL lengthening effect of hypocalcaemic (0.9 mM) extracellular solution was marginal, however subsequent application of ivabradine exerted considerable CL prolongation. Comparison of ivabradine effect in the presence of normal Ca^{2+} concentration *vs.* low Ca^{2+} concentration revealed nearly doubled CL lengthening effect of ivabradine in response of Ca^{2+} reduction (**panel C**). * means 0.9 mM $[Ca^{2+}]_{out}$ compared to control, # means ivabradine versus 0.9 mM $[Ca^{2+}]_{out.}$

4.1.5 Subsequent inhibition of NCX and I_f increases the CL variability

Stability and rhythmicity of SAN pacemaking is essential for physiological cardiovascular function. CL variability was assessed by analysing 30 consecutive spontaneous APs and was presented on Poincaré-plots.

Application of 1 µM ORM and 3 µM ivabradine individually decreased the spontaneous frequency without considerably changing the CL variability (**Figure 11 panel A** and **B**). The concomitant application of 5 µM ryanodine and 5 µM ryanodine + 1 µM ORM showed an enhancement in the CL variability, however it was not statistically significant (**Figure 11 panel C** and **D**). In contrast, additional administration of 3 µM ivabradine remarkably and statistically significantly increased the CL variability (**Figure 11 panel C and E**).

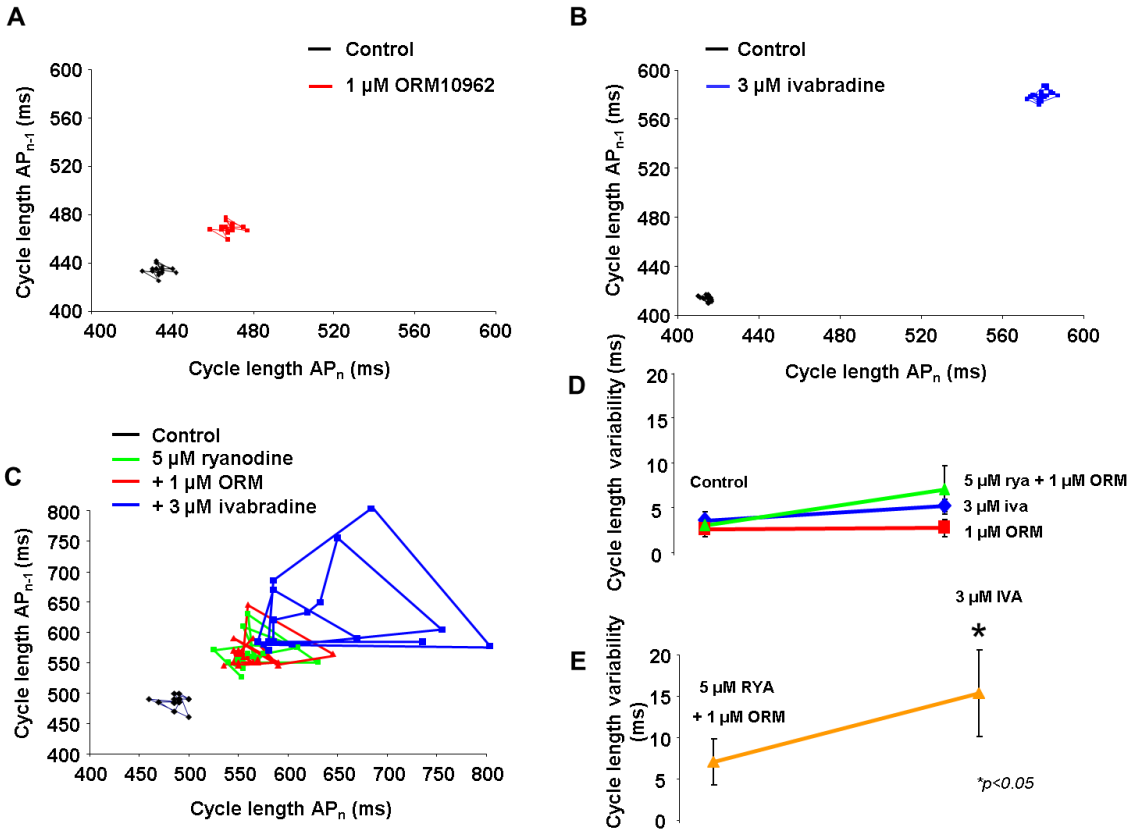

Figure 11: Effect of DD currents inhibition on CL variability

Individual application of ORM (**panel A**) or ivabradine (**panel B**) prolonged the CLs, but did not change the CL variability. Ca^{2+} handling suppression alone also did not influence significantly the CL variability (**panel C** and **D**). In contrast, ivabradine application after the combined use of ryanodine and ORM resulted in considerably increased CL variability as seen with blue on Poincaré plot of **panel C** and on the graph of **panel E**.

4.2 Investigation of reverse NCX function in SAN pacemaking

Our experimental results support the coupled clock hypothesis and the essential role of forward NCX in the clock-like oscillatory system. However, it is well known that the direction of the ionic transport through the NCX is reversible and influenced by several factors. As it was mentioned before, in cardiac research regarding the spontaneous automaticity of SAN the focus was entirely on the forward operation of the NCX. To our best knowledge, there is only one computational study that attributed important role to reverse function[81]. Therefore, in the other part of this study we investigated the potential existence and functional role of the reverse NCX current in the SAN pacemaker mechanism.

4.2.1 Experimental validation of 2 mM and 8 mM $[Na^+]_{pip}$ groups in the measurement of reverse NCX current

To study the possible role of reverse NCX current in SAN pacemaking two experimental groups (2 mM and 8 mM $[Na^+]_{pip}$) were established as described in chapter 3.4.2. Firstly, conventional NCX voltage ramp protocol was used to study the reverse NCX current in 2 mM and 8 mM $[Na^+]_{pip}$ conditions. The effect of the selective NCX inhibitor ORM was also assessed and compared between the different experimental conditions to exclude any Na^+-dependent action of ORM. After an 8-10 minutes incubation period in the bath solution a control current was recorded, then 1 μM ORM and finally 10 mM $NiCl_2$ were applied to dissect the total NCX current (**Figure 12 panel A**). The total NCX current was calculated as a difference current of the control and the $NiCl_2$ insensitive current. As **Figure 12 panel B** indicates no outward (i.e. reverse) NCX current was found in the presence of 2 mM $[Na^+]_{pip,}$ while NCX blockers dissected a notable outward component with 8 mM $[Na^+]_{pip.}$ The measured and the calculated reversal potentials showed a marked difference between the experimental groups. In the 8 mM $[Na^+]_{pip}$ group the reversal potential approximates the calculated value, indicating a thermodynamical room for the activation of the reverse mode function (**Figure 12 panel C**). In contrast, in the 2 mM $[Na^+]_{pip}$ group the measured reversal potential is far from the calculated value, probably because the exact intracellular $[Na^+]$ sensed by the NCX was larger than the pipette concentration (**Figure 12 panel C**). This difference does not influence the conclusion since NCX current was negative from -60 to +30 mV and the experiments were carried out within this range, showing no reverse component with 2 mM $[Na^+]_{pip.}$ Forward NCX current was identical between the groups (**Figure 12 panel B**).

ORM was used to further investigate the NCX current, since it was found to be selective inhibitor of NCX. Prior to this it was important to rule out any possible Na^+-dependent effect of ORM. Calculating the ratio between the total NCX current and the ORM-inhibited fraction, no significant difference was found between the experimental groups (i.e. with different intracellular Na^+ levels; 2 mM forward mode: 63.5±8%, n=6; 8 mM forward mode: 74.5±6%, n=7; ANOVA with Tukey *post hoc* test, **Figure 12 panel D**). ORM effect on the reverse component was not quantified in 2 mM $[Na^+]_{pip}$ group due to the lack of reverse current, while the inhibitory effect on the reverse mode in the presence of 8 mM $[Na]_{pip}$ was: 72.5±5%, n=7.

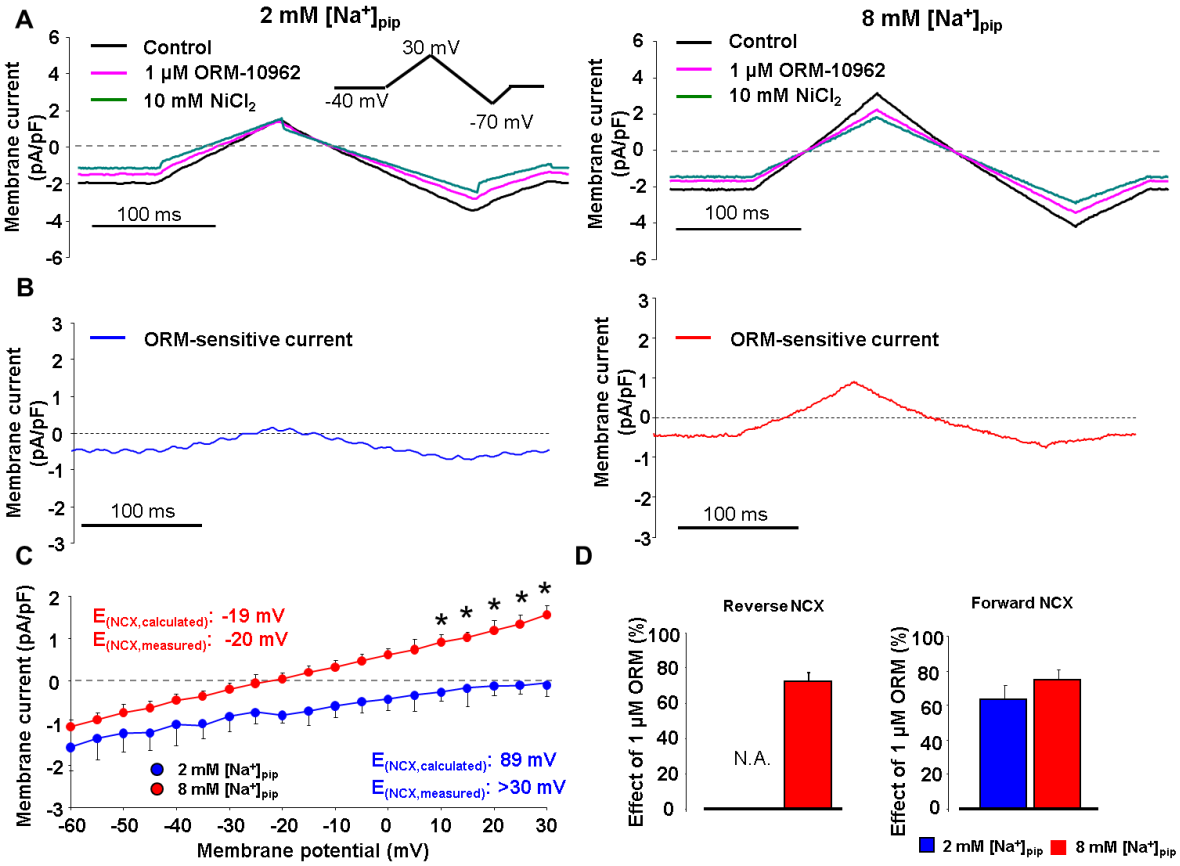

Figure 12: Characterization of the experimental groups (2 mM $[Na]_{pip}$ *vs.* 8 mM $[Na]_{pip}$) and the effect of selective NCX inhibitor ORM in both conditions

Panel A shows representative current traces of control conditions (black), 1 µM ORM-10962 (pink) and 10 mM $NiCl_2$ (green) using conventional voltage ramp protocol. Intracellular Ca^{2+} concentration was set to ~100 nM, Ca^{2+} - and K^+ currents were inhibited. Outward component of NCX was observable only in the presence of 8 mM $[Na^+]_{pip}$ (**panel A**, right side). ORM-sensitive currents obtained from ramp protocol experiments are shown in **panel B**. Reduced intracellular $[Na^+]$ resulted in no reverse NCX component, while ORM dissected a notable reverse NCX current in the presence of 8 mM $[Na]_{pip.}$ Current-voltage characteristics of the $NiCl_2$ sensitive current illustrates the lack of reverse NCX current when 2 mM $[Na^+]_{pip}$ was employed (**panel C**). Possible influence of intracellular $[Na^+]$ on the effect of ORM is shown on bar graphs of **panel D**. ORM similarly inhibits the forward component of NCX irrespective of the intracellular $[Na^+]$ that may exclude Na^+-dependent effect of ORM in further experiments.

Under conventional voltage ramp protocol both ORM and $NiCl_2$ dissected a significant outward current that may reflect an active reverse NCX current in SAN cells which is Na^+-dependent and increases as the membrane potential is getting more positive. Therefore in this study we consider 8 mM $[Na^+]_{pip}$ group as an experimental condition with active reverse mode, and the 2 mM $[Na^+]_{pip}$ group as having suppressed or no reverse NCX activity.

4.2.2 Characterization of NCX current under the SAN AP

Conventional ramp protocol showed a notable reverse NCX current, however that result does not prove the development of reverse NCX current under the SAN AP. In the next set of

experiments a canonical SAN AP waveform was used as a command potential to investigate the NCX current under the entire AP (**Figure 13 panel A**).

Spontaneously contracting cells were chosen and the intracellular Ca^{2+} was buffered by 10 mM EGTA. I_{CaL}, I_{CaT}, K^+-currents, and $I_{Na/K}$ were inhibited during these experiments. In order to fully inhibit the NCX current 10 mM $NiCl_2$ was applied after the control recording (**Figure 13 panel B**). NCX current was gained as a subtracted current from the control current and the current remained after the application of $NiCl_2$. In the presence of 2 mM $[Na^+]_{pip}$ a negligible 0.33±0.3 pC outward current was observed (n=5), while in the presence of 8 mM $[Na^+]_{pip}$ the outward current was significantly larger (2.1±0.3 pC, n=7, $p<0.05$) (**Figure 13 panel C**). This value is almost identical with the prediction of the Maltsev-Lakatta model (2.45 pC)[81]. This experimental condition allows estimating the total carried charges via the reverse NCX, however lacks the Ca^{2+} release that is fundamental driving force of NCX. Therefore, the same protocol was applied on SAN cells with enabled Ca^{2+} release. Aiming to avoid the I_{CaL} suppressing effect of $NiCl_2$, in these experiments ORM was used to assess the reverse NCX current. Similar to the results with $NiCl_2$, an outward component of the NCX current appeared at the beginning of the AP, and it was absent in the 2 mM $[Na^+]_{pip}$ group.

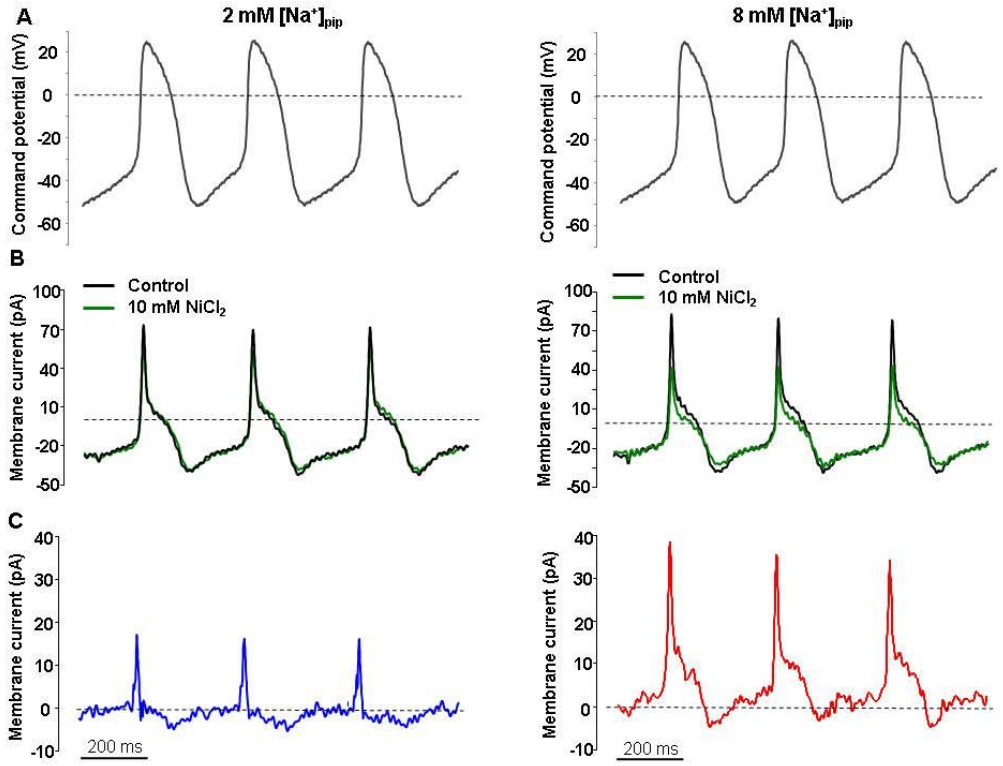

Figure 13: Characterization of the NCX current under a canonical SAN AP command

Command SAN AP is shown on **panel A**. Intracellular Ca^{2+} was buffered with 10 mM EGTA, Ca^{2+}- and K^+ currents were also inhibited. **Panel B** illustrates the NCX current recorded in control conditions (black) and after the application of 10 mM $NiCl_2$ (green). The difference current calculated from the control and $NiCl_2$ currents show a significant outward component of NCX (**panel C**, red) in the presence of 8 mM $[Na^+]_{pip,}$ while it is missing with 2 mM$[Na^+]_{pip}$ (**panel C**, blue).

4.2.3 In the presence of active reverse NCX the CaT is larger

Ca^{2+} influx function of the reverse NCX suggests that the active reverse NCX current could contribute to the Ca^{2+} handling of the SAN cells. CaTs were measured and were compared between the experimental groups. The same AP command was used with unbuffered intracellular Ca^{2+} and nisoldipin was omitted from the external solution (**Figure 14 panel A)**. Diastolic Ca^{2+} level and CaT amplitude were analysed. CaT amplitude was found to be significantly higher with functioning reverse NCX (i.e. 8 mM $[Na^+]_{pip}$) than with no reverse NCX function (2 mM $[Na]_{pip}$: 308±37 nM, n=14 *vs* 8 mM $[Na^+]_{pip}$: 539±52 nM, n=14; $p<0.05$, ANOVA with Tukey *post hoc* test) (**Figure 14 panel B** and **C**). The diastolic Ca^{2+} level showed no difference comparing the groups (2 mM $[Na^+]_{pip}$: 117±14 nM, *vs* 8 mM $[Na^+]_{pip}$: 149±24 nM, n=14-14; $p<0.08$, ANOVA with Tukey *post hoc* test, **Figure 14 panel C**), while the half relaxation time was significantly longer when reverse NCX was active (2 mM $[Na^+]_{pip}$: 112±5 ms *vs.* 8 mM $[Na^+]_{pip}$: 146±9 ms; n=14-14, $p<0.05$; ANOVA with Tukey *post hoc* test, **Figure 14 panel D**).

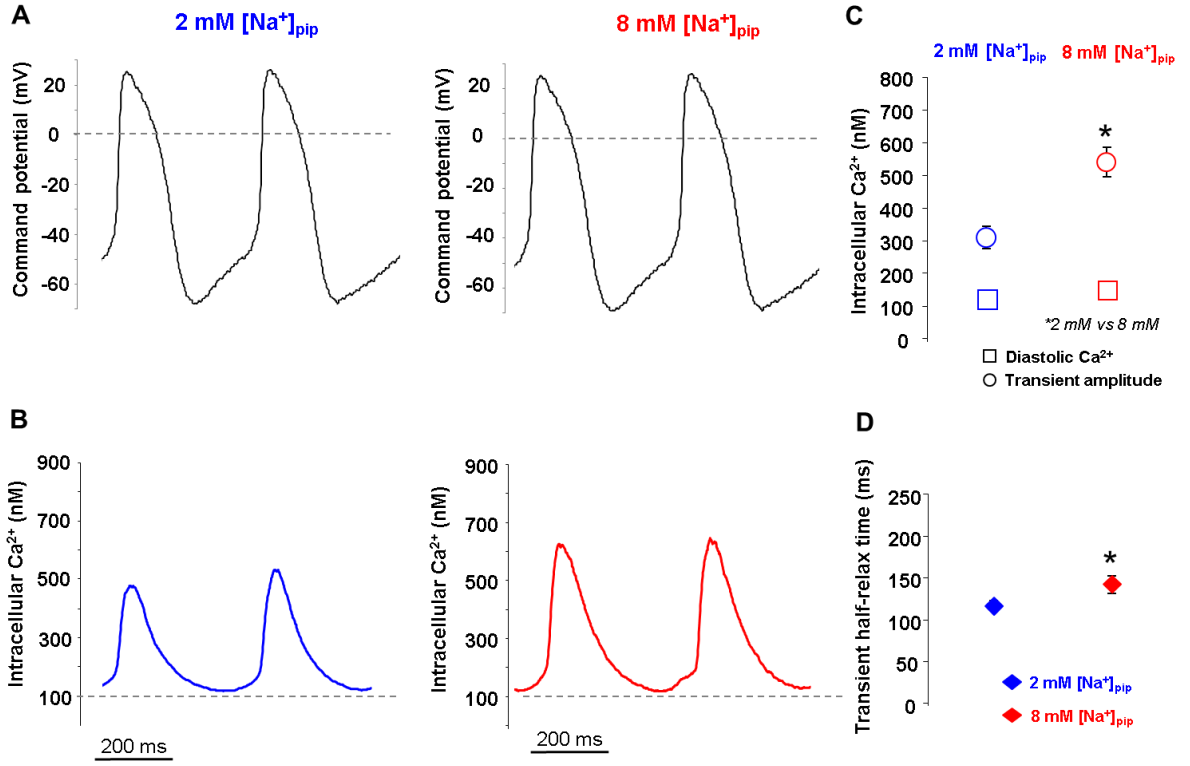

Figure 14: Characterization of the Ca^{2+} transients under a canonical SAN AP command in the presence and absence of reverse NCX current

Intracellular Ca^{2+} was unbuffered to enable free Ca^{2+} movements, while K^+ currents, I_f and Na^+/K^+ ATPase were inhibited. Command SAN AP is shown on **panel A**. Amplitude of CaTs was larger with functioning reverse NCX (i.e. 8 mM $[Na]_{pip}$), while the diastolic Ca^{2+} level remained unchanged (**panel B** and **C**). * on **panel C** refers to the difference of transient amplitudes between 2 and 8 mM $[Na]_{pip.}$ Similarly, the half-relaxation time of CaT was slower with active reverse NCX current (**panel D**, * refers to the half-relaxation time in comparison between 2 and 8 mM $[Na]_{pip}$ groups).

4.2.4 Reverse NCX activity enhances the SR Ca^{2+} content

The larger CaT amplitude found with functioning reverse NCX suggests increased SR Ca^{2+} content. Ca^{2+} content of the SR was measured by rapid administration of 10 mM caffeine. Caffeine is a worldwide used valuable tool to measure the SR Ca^{2+} content as activates the Ca^{2+} release via RyRs and probably also inhibits the reuptake[82]. Prior to caffeine application the steady state Ca^{2+} level of the SR was gained by 10 consecutive AP commands. The AP commands were immediately followed by the rapid caffeine flush under which the membrane potential was constantly kept at -80 mV (**Figure 15 panel A**). Caffeine evoked an inward current and a caffeine induced CaT.

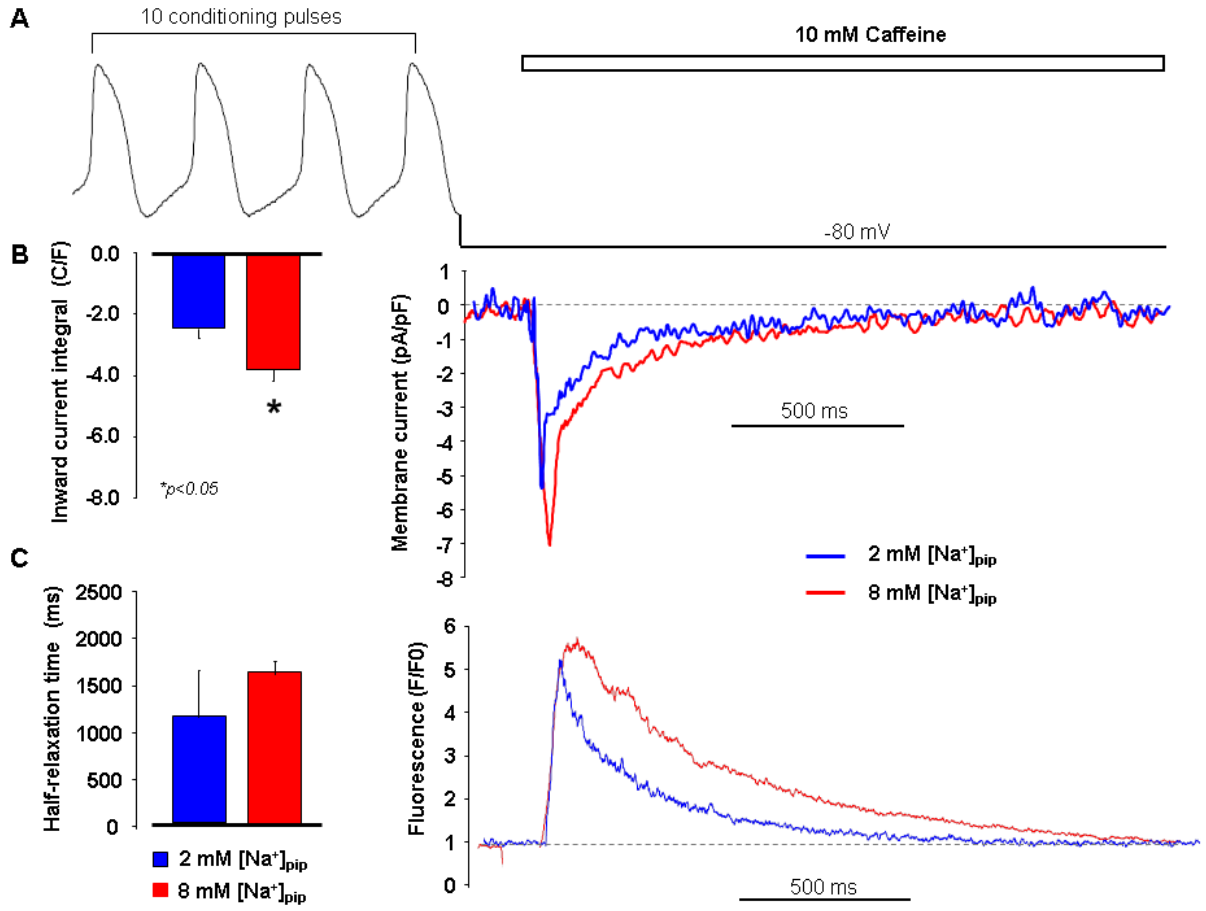

Figure 15: Measurement of SR Ca^{2+} content in the presence and absence of reverse NCX current

10 consecutive conditioning AP pulses were applied to reach the steady-state SR Ca^{2+} content, then the Ca^{2+} stores were emptied by rapid application of 10 mM caffeine (**panel A**). **Panel B** depicts representative caffeine induced inward current, while **panel C** illustrates the parallel measured caffeine induced CaT with 2 mM $[Na^+]_{pip}$ (blue) and 8 mM $[Na^+]_{pip}$ (red). SR Ca^{2+} content was calculated by analysing the inward current integral that was normalized to the cell capacitance. Larger SR Ca^{2+} content was found with active reverse NCX current (8 mM $[Na^+]_{pip}$) (**panel B**). As for the half-relaxation time of caffeine induced CaT, the difference did not reach the significant level (**panel C**).

The SR Ca^{2+} concentration was calculated from the integral of the caffeine induced inward current with normalization to the cell capacitance. Functioning reverse NCX increased the SR

Ca^{2+} content shown in **Figure 15 panel B** (8 mM $[Na^+]_{pip}$: -3.7±0.5 C/F, n=11; 2 mM $[Na^+]_{pip}$: -2.3±0.3 C/F, n=11; $p<0.05$, unpaired t-test). The half-relaxation time of the caffeine induced Ca^{2+} transient showed an increasing tendency with higher intracellular Na^+ level, however did not reach the statistically significant level (8 mM $[Na^+]_{pip}$:1.59±0.18 s, n=17; 2 mM $[Na^+]_{pip}$: 1.2±0.16 s, n=16) (**Figure 15 panel C**).

4.2.5 Active reverse NCX enhances the spontaneous AP firing rate

Since the main role of the SAN operation is setting the actual pacemaker frequency, it is important to study how does the reverse NCX mediated Ca^{2+} influx contribute to the pacemaking. Spontaneous frequency of SAN cells were measured using whole cell patch clamp technique with current clamp mode. Parallel with the APs, CaTs were also detected from the cells. The frequency was calculated by analysing the CLs of 30 consecutive AP. We found higher frequency, i.e. shorter CLs in the presence of active reverse NCX (8 mM $[Na^+]_{pip:}$ 369±15 ms *vs* 2 mM $[Na^+]_{pip}$ 463±38 ms; $p<0.05$, n=8-8) (**Figure 16 panel A** and **B**). The underlying mechanism under the frequency enhancement could be the increased slope of the diastolic depolarization or the shortened APD. Functioning reverse NCX directly and indirectly influences both mechanism, therefore a steeper DD (0.12±0.02 mV/ms *vs* 0.07±0.01 mV/ms; $p<0.05$, n=8-8) and shortened APD (189±3 ms *vs* 232±11 ms; $p<0.05$, n=8-8) were found in the presence of 8 mM $[Na^+]_{pip}$ (**Figure 16 panel C** and **D**). CaT amplitude was larger with 8 mM $[Na^+]_{pip}$ (420±52 nM *vs* 250±22 nM; $p<0.05$, n=8-8) as illustrated on **Figure 16 panel A** and **E**.

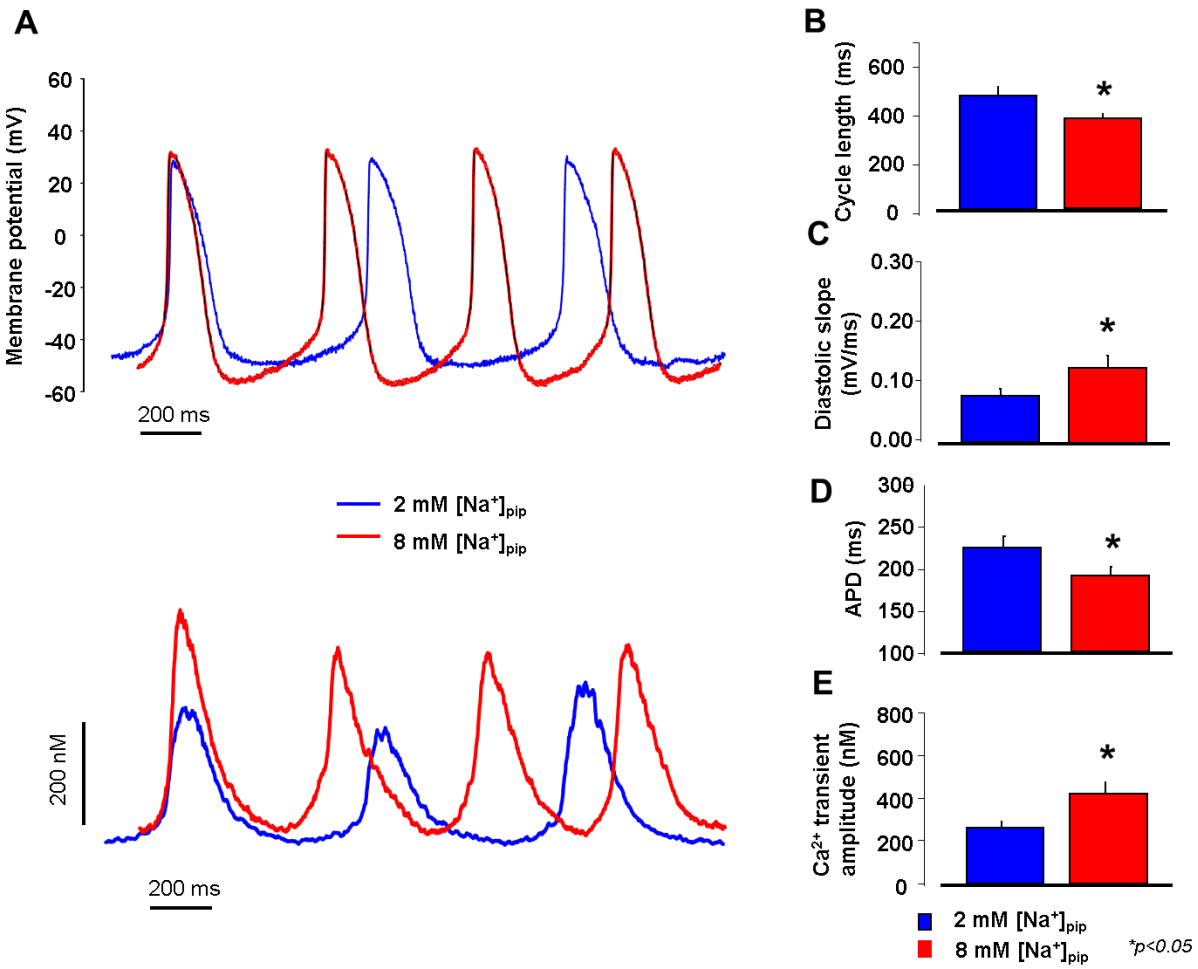

Figure 16: Characterization of spontaneous AP firing rate in SAN cells in the presence and absence of reverse NCX current

APs and parallel CaT were measured by whole-cell configuration of patch clamp technique in current clamp method. Blue traces and blue bar graphs represent suppressed reverse NCX function (i.e. 2 mM $[Na^+]_{pip}$), while active reverse NCX function (i.e. 8 mM $[Na^+]_{pip}$) is marked with red. CLs of APs were shorter (**panel A** and **B**), the DD slope was steeper (**panel A** and **C**), the APD was also shorter (**panel A** and **D**) and CaT amplitude was larger (**panel A** and **E**) in the presence of active reverse NCX.

Another approach was also used to confirm the role of reverse NCX function in the SAN pacemaking. Reverse NCX function was facilitated by the inhibition of Na^+/K^+ ATPase with 1 μM strophantin. The inhibition of the pump enhances the intracellular $[Na^+]$. Strophantin increased the intracellular $[Ca^{2+}]$ by 18.9±6% (n=6) and increased the spontaneous frequency (CL: 433±25 ms *vs* 389±11 ms, $p<0.05$, n=6) with increased DD slope (0.09±0.008 mV/ms *vs* 0.11±0.006 mV/ms, $p<0.05$). Representative APs and bar graphs that indicate the observed changes are depicted on **Figure 17 panel A** and **B**. APD remained unchanged (222±18 ms *vs* 219±10 ms, n=6, **Figure 17 panel B**).

In the next set of experiments, ORM was applied prior to strophantin administration to block the NCX. We assumed that if the reverse NCX is responsible for the Ca^{2+} gain seen with strophantin, in these experiments with ORM the Ca^{2+} increase would be missing. Indeed, no

change in the intracellular Ca^{2+} level was found after strophantin when the NCX was previously blocked. Furthermore, the previously measured AP parameters also remained unchanged (CL: 466±50 ms *vs* 450±26 ms; slope: 0.09±0.01 mV/ms *vs* 0.08±0.01 mV/ms; APD: 236±10 ms *vs* 244±17 ms; n=6, **Figure 17 panel C** and **D**).

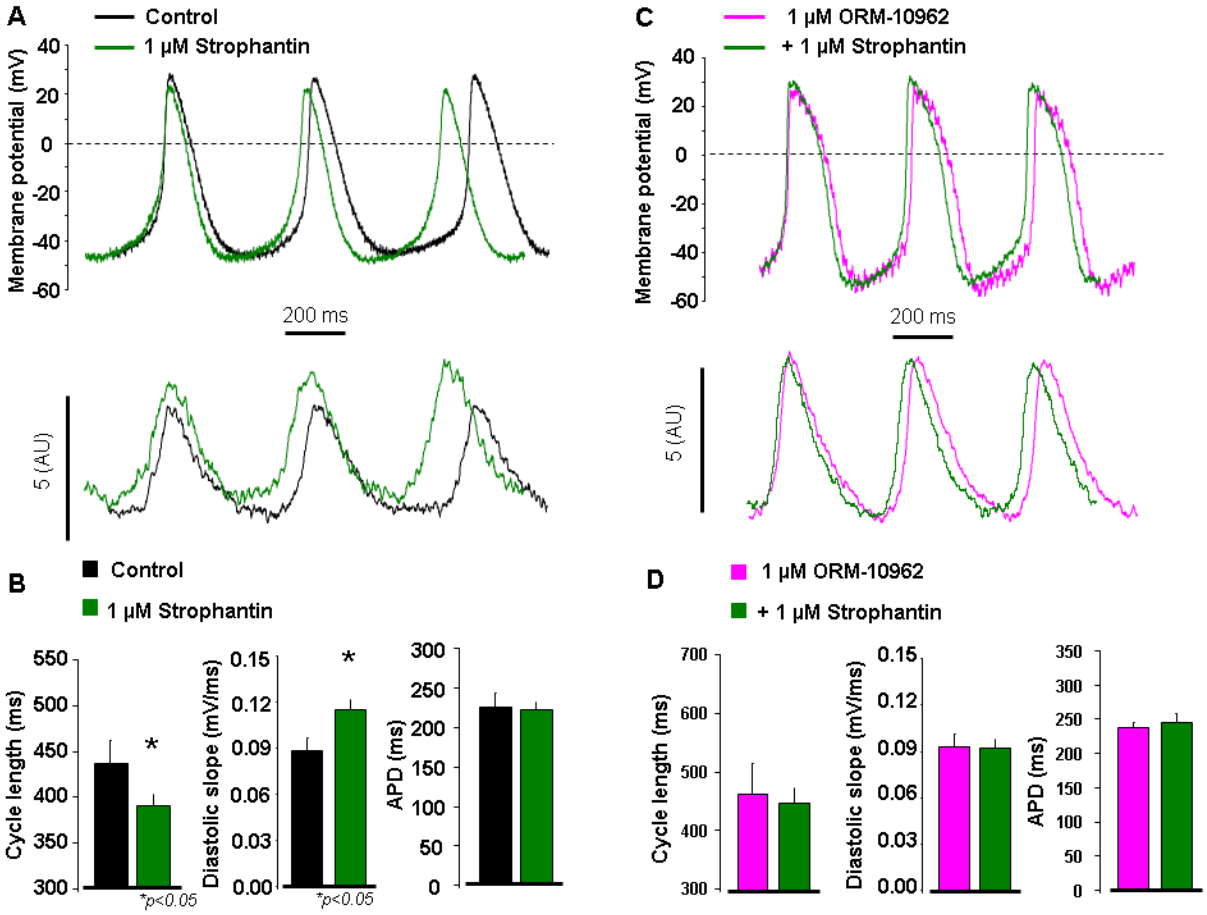

Figure 17: Characterization of spontaneous AP firing rate and CaTs in SAN cells after Na^+/K^+ ATPase inhibition mediated enhancement of reverse NCX

APs and parallel CaTs were measured by perforated patch clamp technique in current clamp method. Na^+/K^+ ATPase block by 1 µM strophantin enhances the reverse NCX current (see the text for detailed mechanism). Strophantin induced AP CL prolongation, DD slope increase and larger CaT amplitude compared to control conditions (**panel A** and **B**). In contrast, when 1 µM ORM was added prior to strophantin (i.e. reverse NCX was inhibited), Na^+/K^+ ATPase block could not change AP parameters and CaT amplitude (**panel C** and **D**).

4.3 $I_{K(Ca)}$ has no role in the spontaneous SAN pacemaking

Spontaneous AP measurements revealed enhanced firing rate with 8 mM $[Na^+]_{pip}$**,** while the APD also shortened. This interesting APD shortening could be a consequence of the higher $[Ca^{2+}]_i$ induced faster I_{CaL} inactivation, or due to an additional repolarizing current activation via possible activation of the small-conductance Ca^{2+}-activated K^+-channels, as was reported in a previous study[83]. Since $I_{K(Ca)}$ carries a functional repolarizing current that depends on the intracellular Ca^{2+} level, it is possible that $I_{K(Ca)}$ also influence the spontaneous frequency. We measured the possible contribution of $I_{K(Ca)}$ in the pacemaking under the previously defined

SAN AP command. Control current was recorded in Tyrode's solution, then 100 nM apamin was added to dissect the apamin sensitive $I_{K(Ca)}$ current (**Figure 18**). Negligible apamin sensitive current was found in normal conditions (**Figure 18**). To further test the assumption, spontaneous APs were measured in this case as well. APs were measured by perforated patch clamp technique. Apamin failed to alter any parameter of the spontaneous APs as seen on **Figure 19** (control → apamin; cycle length: 391 ± 30 ms → 388 ± 33 ms; cycle length variability: 43 ± 10 ms → 41 ± 13 ms; APD: 176 ± 17 ms → 193 ± 25 ms; slope of diastolic depolarization: 0.08 ± 0.01 mV/ms → 0.08 ± 0.01 mV/ms; n = 7). This finding and the negligible current found under the AP support that $I_{K(Ca)}$ has no role in the spontaneous pacemaking.

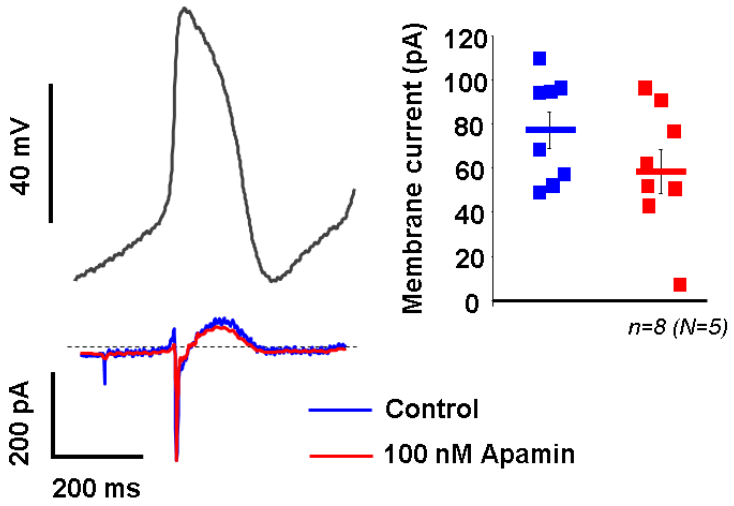

Figure 18: Characterization of apamin sensitive current under canonical SAN AP command

Control current recording (blue trace) was followed by the application of 100 nM apamin (red curve). As representative traces and dot chart also demonstrate, $I_{K(Ca)}$ inhibition did not alter the peak of the total current, claiming negligible $I_{K(Ca)}$ in SAN cells.

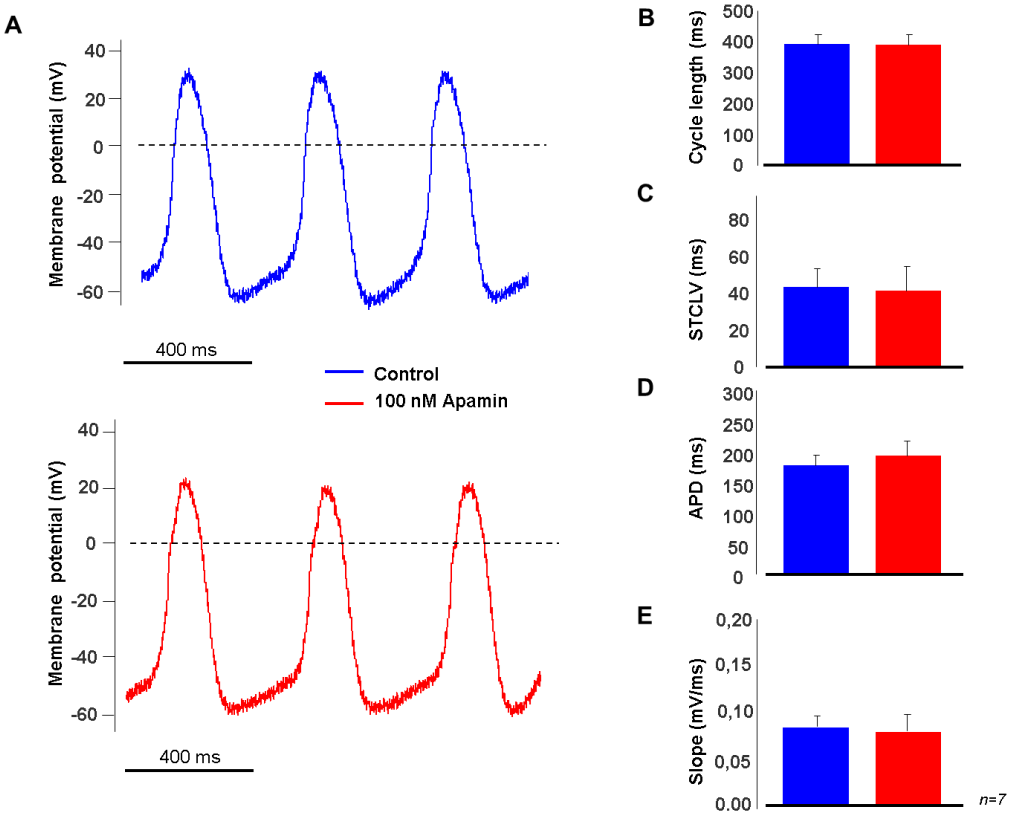

Figure 19: Characterization of spontaneous AP firing rate in SAN cells after $I_{K(Ca)}$ inhibition

Panel A shows control current recording (blue traces) followed by 100 nM apamin application (red traces). Apamin had no change in AP CLs (**panel B**), in CL variability (**panel C**), in APD (**panel D**) and in the slope of DD (**panel E**). *STCLV: short-term cycle length variability, APD: action potential duration*

4.4 Cardiac alternans show a restitution independent nature that is associated with enhanced frequency

APD restitution and AP alternans protocol were measured on intact subendocardial tissue**. Figure 20 panel A** illustrates the used S1S2 restitution protocol. The S1S2 restitution was recorded at both BCL of 1000 and 500 ms, but only the BCL of 1000 ms is presented here on **Figure 20 panel B**. Alternans were observable in all cases (n=20) with clear frequency threshold, i.e. when the pacing length was equal or shorter than 250 ms. Alternans were maintained from the start to the end of the protocol without any decline in the amplitude of APD oscillation. Restitution slopes and corresponding amplitude of APD alternans were compared on **Figure 20**. Our results show that alternans were inducible even if the restitution slope was smaller than 1, and data show mainly weak and in some cases moderate correlations between the restitution slope and alternans amplitude at different repolarization levels of APD (**Figure 20 panel B**). Parallel with the demonstration of negligible role of restitution slope in the development of cardiac alternans, strong correlation was found between CaT and AP alternans amplitude. Stimulus AP command from a CL of 250 to 210

ms was applied to ventricular cardiomyocytes and CaTs were measured (**Figure 21 panel A**). The CaT amplitude oscillations are plotted against the corresponding APD_{90} alternans on **Figure 21 panel B**. A close relationship between APD and CaT amplitude alternans is observable: larger APD alternans were associated with larger CaT amplitude alternans (n=15). Non-alternating AP sequence failed to induce CaT alternans as seen on **Figure 21 panel C**, which finding assumes the possible role of transmembrane ionic currents (e.g. recovery kinetics of I_{CaL}).

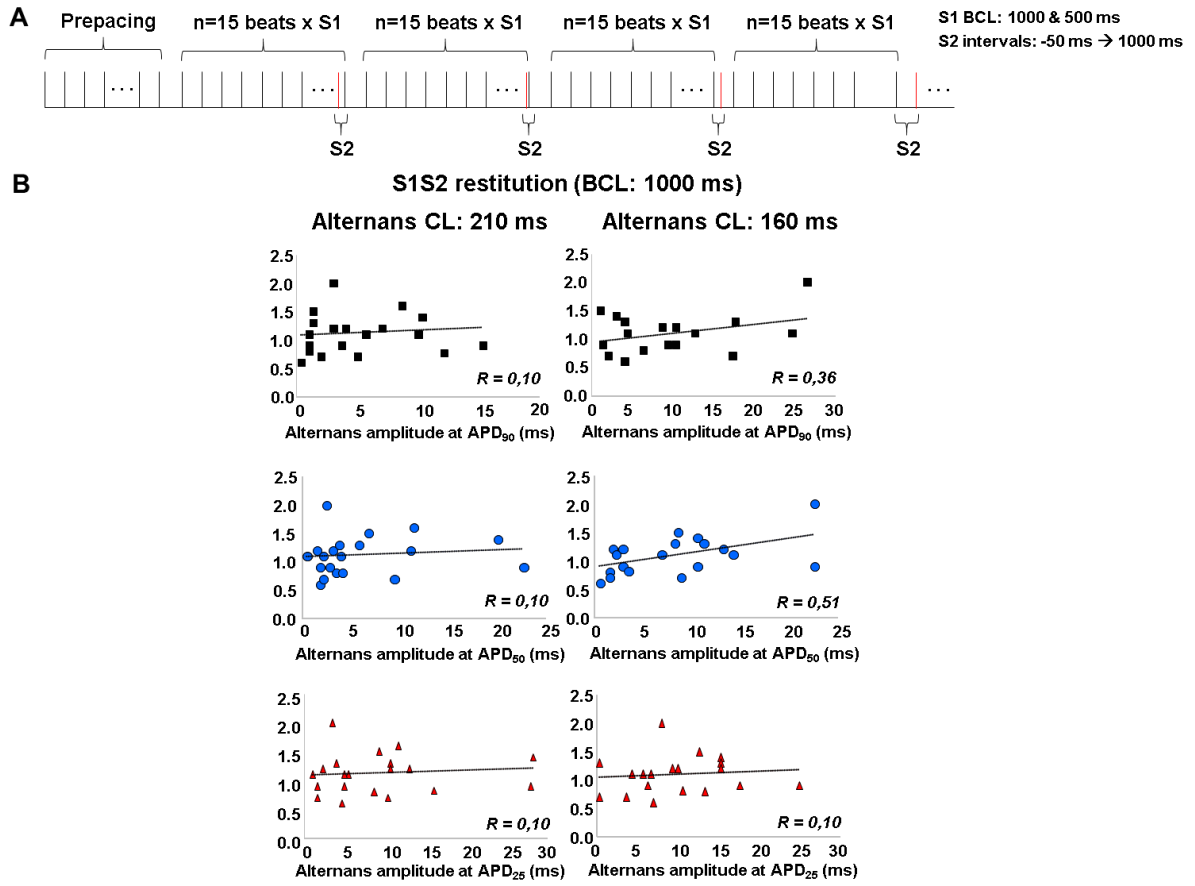

Figure 20: Relationship of AP alternans and standard S1S2 restitution

Panel A depicts the applied S1S2 restitution protocol. The basic cycle length was 1000 ms. **Panel B** illustrates correlation tests between alternans and restitution slopes. APD_{90} is presented in the first row, APD_{50} in the second row, while bottom row demonstrates APD_{25}. It is observable that AP alternans developed even if the slope of restitution was smaller than 1, and data show weak correlations between the variables.

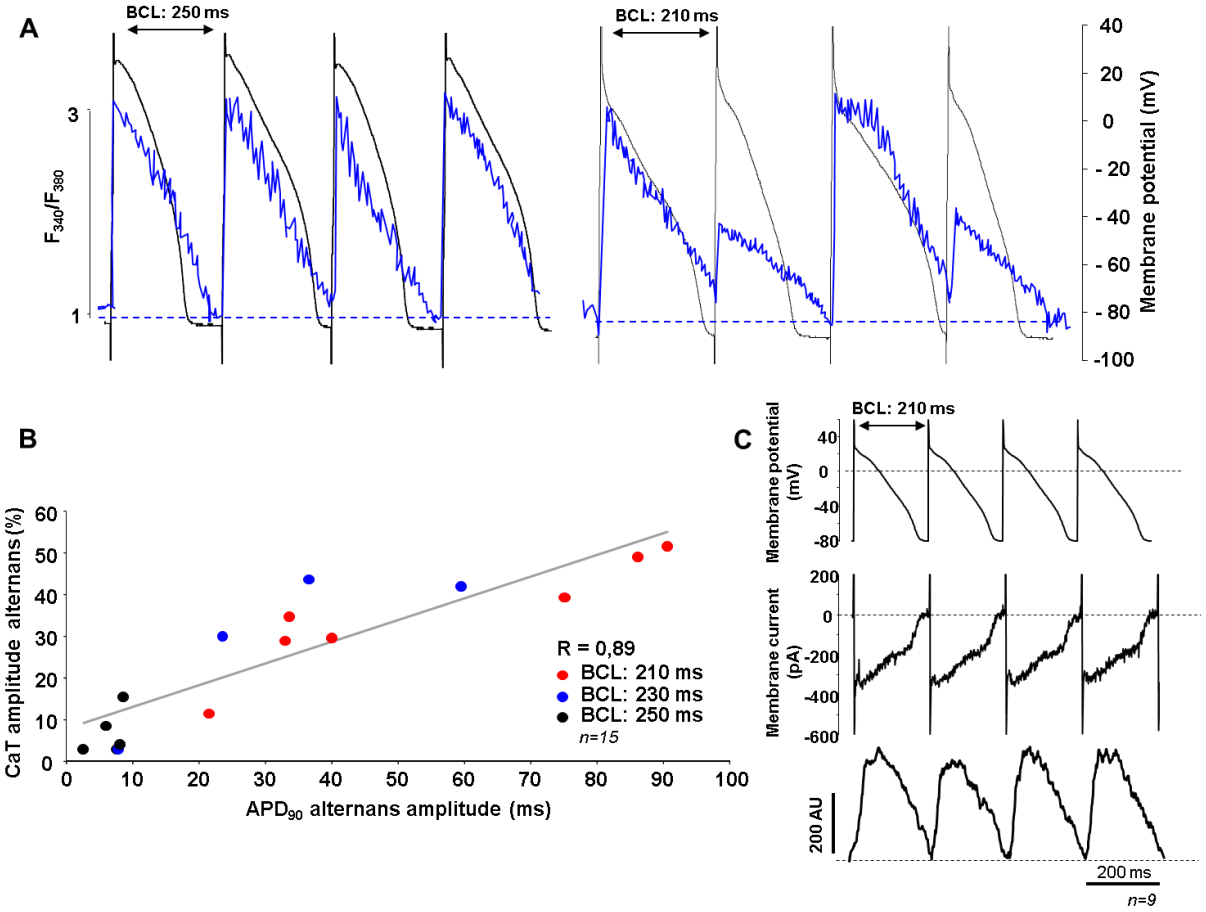

Figure 21: Relationship of action potential alternans and Ca^{2+} transient alternans

Panel A demonstrates parallel measurements of AP and CaT recorded at 250 and 210 ms of basic cycle length. Marginal AP alternation cause minor CaT alternans (left side of **panel A**), however remarkable CaT alternans are present when AP alternans are enhanced (right side of **panel A**). This linear association between AP alternans and CaT alternans is presented in **panel B**. **Panel C** shows that rapid pacing non alternating AP sequence failed to induce CaT alternans. The membrane currents were identical and the evoked CaTs showed negligible alternans.

5. DISCUSSION

Previous data on the Ca^{2+} dependent molecular mechanisms underlying the spontaneous activity of SAN cells are controversially discussed. Therefore the aim of this study was to investigate the assumed contribution of 1) forward NCX, 2) reverse NCX, 3) $I_{K(Ca)}$ in SAN automaticity and 4) to analyse the rate-dependent consequence of SAN pacemaking on the ventricular AP morphology.

5.1 Forward mode of the NCX has an important role in the spontaneous automaticity forming a strong functional coupling with I_f

A slight, but statistically significant decrease in the spontaneous AP firing rate was found in SAN tissue after selective NCX inhibition by ORM. ORM prolonged the CL by decreasing the steepness of the DD phase. The CL prolongation of ORM is a direct experimental evidence proving the contribution of the inward depolarizing NCX current in the spontaneous rhythm generation. Yaniv et al. showed in cellular level that not only the frequency decrease, but the parallel increase of rhythm variability reports the uncoupling of I_f-NCX cooperation and the destabilization of the DD[84,85]. In our experiments the CL variability did not change and the pacing rate was only slightly reduced, therefore we suggest that individual NCX inhibition does not result considerable uncoupling of I_f-NCX. If we think about that fact that the coupled clock mechanism suggests a crucial role of the NCX current in the SAN pacemaking, one may ask why the NCX inhibition mediated CL prolongation was relatively small. Previously, Gao et al. showed that partial ablation of NCX (~70-80%) using a genetic mouse model has also a moderate slowing effect on the baseline spontaneous frequency[86]. It was found, that even a small contribution of NCX is able to generate enough inward depolarizing current to maintain the normal SAN activity[45]. In line with this, our results indicate that a functional coupling between NCX and I_f is present and is able to compensate for the NCX inhibition mediated reduction of the firing rate. The compensating reserve capacity between the currents could be the underlying cause for the moderate effect of 3 μM or 10 μM ivabradine on CL. Caesium was also unable to terminate the spontaneous AP firing even though it completely blocks the I_f[12]. Voltage dependent block of ivabradine or caesium could be an explanation for this finding[87], or it is also possible that I_f serves as an insulator by protecting the SAN cells from the negative electrical sink of the surrounding atrial cells[88]. However, the functional coupling of I_f and NCX could also contribute to the observed results[20,84]. Functional cooperation of I_f and NCX can create a phenomenon that is similar to

the repolarization reserve in cardiomyocytes[89-92], and it can prevent the SAN cells from notable changes in the spontaneous frequency caused by individual inhibition of NCX or I_f.

In the next set of experiment, the SAN firing rate was decreased by complete block of I_{Kr} that caused a statistically significant CL prolongation by enhancing the APD. In this case, NCX inhibition provided the same effect to the case when ORM was applied individually. The underlying reason could be the I_f dependent compensation of the NCX effect.

Assuming that a strong cooperation exists between NCX and I_f, the "crosstalk" should work vica versa, i.e. the impairment of Ca^{2+} handling properties should affect I_f. In line with previous data[93], joint application of ryanodine and ORM caused ~20% increase in the CLs. Subsequent administration of ivabradine exerted considerably larger CL lengthening effect than in experiments where ivabradine was applied alone.

Similar augmentation of ivabradine effect was found when Ca^{2+} handling was suppressed by application of low extracellular Ca^{2+} solution. These experiments suppose that reduction of intracellular [Ca^{2+}] decreases the function of forward NCX current leading to decreased DD slope. The reduced net current during the DD therefore provides improved effect of I_f inhibition.

Previous studies assumed that I_f-NCX coupling not only set the actual spontaneous firing rate but it may have an important role in the maintenance of the stable rhythm of SAN. Based on this, CL variability could be another suitable indicator of the integrity of the coupling, as a considerable CL increase leads to significant I_f-NCX uncoupling. Our experiments indicated that individual inhibition of NCX or I_f does not upset the rhythmicity of pacemaking. However, when both currents were reduced, besides the remarkable CL prolongation, a perturbation in the spontaneous rhythmicity also appeared resulting from the exhausted capacity of I_f-NCX coupling to depolarize the membrane.

Taking together, I_f and NCX contributes to DD forming a "pacemaker reserve". Similar to the concept of repolarization reserve, individual inhibition of NCX or I_f does not lead to excessive decrease of automaticity because the other, intact current is able to compensate for the effect of inhibition. This crosstalk could increase the robustness of pacemaking by providing a safety margin.

5.2 Reverse mode of the NCX contributes to pacemaking by refilling the Ca^{2+} clock

The transport direction of Na^+/Ca^{2+} exchanger is determined by the actual thermodynamical properties of the cells. Reversal potential of the exchanger (E_{NCX}) is calculated from $E_{NCX}= 3E_{Na}-2E_{Ca}$ equation. When the actual membrane potential is more positive than E_{NCX}, the reverse operation is favored (i.e. Ca^{2+} entry), mostly at the beginning of the AP. However, when membrane potential becomes more negative than E_{NCX}, the direction of the ionic transport changes, and Ca^{2+} efflux is provided by forward operation mode. The presence or absence of reverse NCX in various cell types is defined by the actual thermodynamical driving force. In cardiomyocytes reverse NCX is expected at the initial phase of the AP when the intracellular Ca^{2+} is low and the AP is above 0 mV. Time window for the operation of reverse NCX is short, as the intracellular Ca^{2+} rapidly increases shifting E_{NCX} more positive where forward NCX is favored. Research regarding the SAN pacemaking set the focus on forward NCX function, therefore we did not have any experimental data on the existence of reverse NCX current is SAN cells. The reverse mode activity was suggested by modelling simulations of Lakatta et al., however it was not verified experimentally so far[81].

NCX equilibrium potential (calculated based on our experimental results) suggests a potential development of reverse NCX current in the first 55-65 ms of the AP. In line with this calculation, an outward $NiCl_2$ sensitive current was observed in this time range when intracellular $[Na^+]$ was 8 mM, but no outward current appeared when intracellular $[Na^+]$ was reduced to 2 mM in the pipette. Similar result was obtained when ORM was applied (Figure not shown). This result indicates that a $NiCl_2$- and ORM-sensitive and $[Na^+]_i$ dependent outward current is active during the first part of the SAN AP where the membrane potential is depolarized. This characteristic of the current suggests that reverse NCX exists during the SAN AP.

Since SR serves as the Ca^{2+} clock, SAN pacemaking is considerably depends on the actual Ca^{2+} content of the SR. Therefore, effective refilling of the SR is critical for SAN pacemaking. It is well known that I_{CaL} has essential role in SR refilling, however a functional reverse NCX could also contribute to SR refilling. Larger SR Ca^{2+} content and consequently larger Ca^{2+} transient amplitude was found in the presence of active reverse NCX. It suggests that active reverse mode provides an additional Ca^{2+} influx – supporting the I_{CaL} function – making the SR refilling a redundant mechanism that could improve the robustness of SAN pacemaking. An interesting further question was whether this additional, reverse NCX

mediated Ca^{2+} influx has any role in setting the actual SAN CL. AP measurements with 2 and 8 mM $[Na^+]$ in the pipette solution revealed that in the presence of active reverse mode the CL was shorter and the diastolic slope was steeper.

Interestingly, the APD also shortened in the presence of active reverse exchange. Shortening of the APD could be the result of faster I_{CaL} inactivation induced by the higher intracellular Ca^{2+} concentration or it could be a result of other Ca^{2+} dependent current activation.

Previous study reported CL shortening followed by digoxigenin induced increase in $[Na^+]_i$ with parallel increase of $[Ca^{2+}]_i$[94]. In our experiments, 1 μM strophantin was used to increase $[Na^+]_i$ via the inhibition of Na^+/K^+ ATPase. Rise in intracellular $[Na^+]$ is expected to cause a shift of E_{NCX} towards more negative values where reverse component of NCX is able to increase. Accordingly, higher AP pacing frequency was found in response to Na^+/K^+ ATPase block by strophantin. Our experimental observations strongly suggest that amplification of reverse NCX could further enhance the spontaneous pacemaking. To further verify that reverse NCX is responsible for the frequency enhancement, the exchanger was inhibited by ORM prior to strophantin application. In the presence of NCX block strophantin failed to change the spontaneous firing rate, which could be attributable to the unchanged $[Ca^{2+}]_i$ after strophantin administration in the presence of reverse NCX block. Similar results were found in canine ventricular cardiomyocytes where 1 μM ORM-10103 pretreatment suppressed the strophantin induced spontaneous diastolic Ca^{2+} release[95].

Lakatta et al. model was used to assess the effects of $[Na^+]_i$ changes on several parameters. 2, 4, 6, 8, 10 mM $[Na^+]_i$ concentrations were set to analyse the spontaneous frequency, reverse NCX current, CaT and SR Ca^{2+} content. Increase of $[Na^+]_i$ enhanced the spontaneous automaticity and a gradual increase of reverse NCX current was also detectable. Both the intracellular Ca^{2+} content and SR Ca^{2+} content increased in line with enhanced $[Na^+]_i$. Modelling results further support that reverse NCX mediated Ca^{2+} influx provides an important fraction of total SR Ca^{2+} content, therefore reverse NCX could contribute to fine tuning of the heart rate.

Large body of studies showed that SAN is a functionally and electrophysiologically heterogeneous structure [96-98]. During physiological cardiac activation, the spontaneous AP is generated in the center region of the SAN, and then the AP is conducted through the periphery to crista terminalis[99]. In the central region the cells are smaller compared to those in the peripheral zone and contain fewer myofilaments [98,99]. The AP properties are also different between the central region and transitional- or peripheral region. Previous studies reported intracellular Ca^{2+} handling heterogeneity between the regions as the expression of Ca^{2+}

regulatory proteins also differs [100]. As for the reverse NCX, two important regional differences are present. Starting from the central regions the action potential upstroke becomes larger and the CL shortens as the AP spreads towards to the peripheral zone[96]. These differences could be the consequence of the larger atrial influence and the higher contribution of I_f in the peripheral zone, while different role of I_{CaL} could also affect the AP morphology. Considering our results, it is reasonable that the small upstroke in central pacemaker cells considerably restricts the reverse NCX function, while the distal cells promote increasing amount of reverse NCX contribution. Accordingly, reverse NCX could also contribute to the electrophysiological heterogeneity of SAN as increasing reverse NCX gradient from the central area to the periphery contributes to the observed AP CL shortening in transitional and peripheral SAN cells.

5.3 $I_{(KCa)}$ has no role in the spontaneous automaticity in basal conditions

When 8 mM [Na^+] was used in the patch pipette the SAN APD was shortened. This finding raises the possibility that other Ca^{2+} dependent mechanisms, such as Ca^{2+}-activated K^+-current could contribute to APD shortening. In contrast, we found no apamin sensitive current and in line with this, we failed to observe apamin induced frequency alteration and AP morphology change in SAN cells under normal conditions. Similar results were observed in a recent clinical trial. In a randomized, double-blind, placebo controlled phase I study by Gao et al., forty-seven healthy male volunteers were enrolled and examined after receiving $I_{K(Ca)}$ blocker AP30663 in single ascending dose[101]. No effect of AP30663 was seen on electrocardiographic parameters, such as RR interval, irrespective of the applied dose[101]. This finding is in line with our experimental results claiming negligible apamin sensitive current during the SAN action potential in response to dynamic intracellular Ca^{2+} changes under basal conditions.

5.4 Ventricular alternans are independent from restitution

In our tissue experiments it was found that the APD gradually shortened as pacing frequency increased, and when pacing rate reached a given threshold, APD alternans developed in all cases. At the same time, the development of APD alternans could be induced irrespective of the restitution slope, i.e. alternans appeared when restitution slope was steep or flat. This result indicates negligible role of restitution curve in the prediction of alternans. A close relationship was found between APD and CaT alternans, supporting bidirectional coupling between membrane potential (i.e. action potential) and Ca^{2+} handling: when APD alternans

were larger, CaT alternans were also enhanced. The magnitude of alternans of both variables was larger in the presence of higher pacing frequency.

Our results imply that alternans could be considered as a deleterious consequence of excessive SAN frequency. It is important to note that despite of the fact that alternans are frequency induced, under healthy condition the threshold frequency required for alternans induction is out of the range of physiological heart rate. However, in several diseases such as heart failure, the threshold frequency could be shifted toward lower frequencies[66]. In this case alternans induction can occur via slightly increased heart rate that may cause life threatening arrhythmias[70].

6. CONCLUSION

In conclusion, it was found that I_f-NCX cooperation - in maintaining the diastolic depolarization - as well as the I_{CaL}-reverse NCX cooperation - in refilling the SR - may provide two parallel redundant systems to make the sinoatrial node pacemaking more robust, i.e. fail-safe. SAN pacemaking considerably influences the morphology of the ventricular action potentials and above a given frequency threshold it can induce alternans which are irrespective of restitution.

The main findings of this Ph.D. thesis are the followings:

1.) With the direct pharmacological inhibition of NCX, we provided experimental evidence regarding the role of forward NCX in the spontaneous pacemaking, furthermore, our data also supported a strong coupling between NCX and I_f. Individual inhibition of the currents does not lead to significant frequency changes and does not perturb the rhythmicity and stability of spontaneous automaticity. I_f and NCX may be able to develop a pacemaker reserve capacity, where they can compensate each other's operation ensuring stable pacemaking.

2.) In agreement with previous computational simulations[81] a voltage-, and $[Na^+_i]$ dependent outward current was found during the initial part of the SAN action potential which was sensitive to ORM and $NiCl_2$, indicating that the current is reverse NCX. Reverse NCX mediated Ca^{2+} influx contributes to SR Ca^{2+} refilling and facilitates SAN pacemaking.

3.) Negligible Ca^{2+} activated K^+ current was developed under the SAN action potential, indicating no function of the current in the rhythm generation in normal conditions.

4.) Restitution has no role in the prediction of APD and CaT alternans.

7. ACKNOWLEDGEMENT

This work was carried out at the Department of Pharmacology and Pharmacotherapy, Szent-Györgyi Albert Medical School, University of Szeged. I respectfully thank István Baczkó MD PhD, the present Head of the Department and András Varró MD, PhD, Dsc, the former Head of the Department for ensuring the opportunity to do scientific research in the Department. I am especially grateful for András Varró MD, PhD, Dsc and Gyula Papp MD, PhD, Dsc for their professional help, suggestions and support. I would like to express my thanks to László Dux MD, PhD, Dsc, the Head of the Doctoral School of Multidisciplinary Medical Sciences for allowing me to conduct doctoral studies at the University.

Most importantly, I would like to express my sincere gratitude to my all-time supervisor since undergraduate years, Norbert Nagy PhD. I thank him for introducing me to the field of cardiac electrophysiology and for teaching me the professional skills and critical thinking I need at scientific work. His stimulating enthusiasm, kindness and continuous support guided me through my doctoral studies.

I am also grateful for my closest colleagues and friends at the same time, Zsófia Nagy PhD, Leila Topal PharmD, Gergő Bitay medical student, Alexandra Polyák MD for their help and work throughout the years.

I am thankful to all my colleagues at the Department. I would like to say special thanks to Rea Fritz, Anikó Kőrös, Gábor Girst, Gábor Dobai, Zsolt Tóth, Róbert Motzwickler for their excellent administrative and technical support.

Above all, I would like to express my heart-felt gratitude to my family and friends, especially to my parents, my sister and my fiancé. Without their love, all-time support and encouragement none of this work would indeed have been possible.

8. FUNDING

This work was supported by grants from the National Research Development and Innovation Office (NKFIH PD-125402 (for NN), FK-129117 (for NN), GINOP-2.3.2-15-2016-00006, the LIVE LONGER EFOP-3.6.2-16-2017-00006 project, the János Bolyai Research Scholarship of the Hungarian Academy of Sciences (for NN), the UNKP-18-4-SZTE-76 New National Excellence Program of the Ministry for Innovation and Technology (for NN), the EFOP 3.6.3 VEKOP-16-2017-00009 (for NT), the Hungarian Academy of Sciences and by the Orion Pharma (ORM-10962).

9. REFERENCES

1 Keith, A. & Flack, M. The Form and Nature of the Muscular Connections between the Primary Divisions of the Vertebrate Heart. *Journal of anatomy and physiology* **41**, 172-189 (1907).

2 Boyett, M. R. 'And the beat goes on.' The cardiac conduction system: the wiring system of the heart. *Experimental physiology* **94**, 1035-1049, doi:10.1113/expphysiol.2009.046920 (2009).

3 Weiss, J. N. *et al.* From pulsus to pulseless: the saga of cardiac alternans. *Circulation research* **98**, 1244-1253, doi:10.1161/01.RES.0000224540.97431.f0 (2006).

4 Mangoni, M. E. & Nargeot, J. Genesis and regulation of the heart automaticity. *Physiological reviews* **88**, 919-982, doi:10.1152/physrev.00018.2007 (2008).

5 Noma, A. Ionic mechanisms of the cardiac pacemaker potential. *Japanese heart journal* **37**, 673-682, doi:10.1536/ihj.37.673 (1996).

6 Lakatta, E. G. & DiFrancesco, D. What keeps us ticking: a funny current, a calcium clock, or both? *Journal of molecular and cellular cardiology* **47**, 157-170, doi:10.1016/j.yjmcc.2009.03.022 (2009).

7 Weidmann, S. Effect of current flow on the membrane potential of cardiac muscle. *The Journal of physiology* **115**, 227-236, doi:10.1113/jphysiol.1951.sp004667 (1951).

8 Noble, D. & Tsien, R. W. The kinetics and rectifier properties of the slow potassium current in cardiac Purkinje fibres. *The Journal of physiology* **195**, 185-214, doi:10.1113/jphysiol.1968.sp008454 (1968).

9 Brown, H. F., DiFrancesco, D. & Noble, S. J. How does adrenaline accelerate the heart? *Nature* **280**, 235-236, doi:10.1038/280235a0 (1979).

10 DiFrancesco, D. A new interpretation of the pace-maker current in calf Purkinje fibres. *The Journal of physiology* **314**, 359-376, doi:10.1113/jphysiol.1981.sp013713 (1981).

11 DiFrancesco, D., Ferroni, A., Mazzanti, M. & Tromba, C. Properties of the hyperpolarizing-activated current (if) in cells isolated from the rabbit sino-atrial node. *The Journal of physiology* **377**, 61-88, doi:10.1113/jphysiol.1986.sp016177 (1986).

12 Noma, A., Morad, M. & Irisawa, H. Does the "pacemaker current" generate the diastolic depolarization in the rabbit SA node cells? *Pflugers Archiv : European journal of physiology* **397**, 190-194, doi:10.1007/BF00584356 (1983).

13 Rigg, L. & Terrar, D. A. Possible role of calcium release from the sarcoplasmic reticulum in pacemaking in guinea-pig sino-atrial node. *Experimental physiology* **81**, 877-880, doi:10.1113/expphysiol.1996.sp003983 (1996).

14 Bogdanov, K. Y., Vinogradova, T. M. & Lakatta, E. G. Sinoatrial nodal cell ryanodine receptor and Na(+)-Ca(2+) exchanger: molecular partners in pacemaker regulation. *Circulation research* **88**, 1254-1258, doi:10.1161/hh1201.092095 (2001).

15 Huser, J., Blatter, L. A. & Lipsius, S. L. Intracellular Ca2+ release contributes to automaticity in cat atrial pacemaker cells. *The Journal of physiology* **524 Pt 2**, 415-422, doi:10.1111/j.1469-7793.2000.00415.x (2000).

16 Monfredi, O. *et al.* Beat-to-Beat Variation in Periodicity of Local Calcium Releases Contributes to Intrinsic Variations of Spontaneous Cycle Length in Isolated Single Sinoatrial Node Cells. *PloS one* **8**, e67247, doi:10.1371/journal.pone.0067247 (2013).

17 Maltsev, V. A., Vinogradova, T. M. & Lakatta, E. G. The emergence of a general theory of the initiation and strength of the heartbeat. *Journal of pharmacological sciences* **100**, 338-369, doi:10.1254/jphs.cr0060018 (2006).

18 DiFrancesco, D. & Robinson, R. B. beta-modulation of pacemaker rate: novel mechanism or novel mechanics of an old one? *Circulation research* **90**, E69-69, doi:10.1161/01.res.0000014803.05780.e7 (2002).

19 Lakatta, E. G., Maltsev, V. A., Bogdanov, K. Y., Stern, M. D. & Vinogradova, T. M. Cyclic variation of intracellular calcium: a critical factor for cardiac pacemaker cell dominance. *Circulation research* **92**, e45-50, doi:10.1161/01.res.0000055920.64384.fb (2003).

20 Lakatta, E. G., Maltsev, V. A. & Vinogradova, T. M. A coupled SYSTEM of intracellular Ca2+ clocks and surface membrane voltage clocks controls the timekeeping mechanism of the heart's pacemaker. *Circulation research* **106**, 659-673, doi:10.1161/CIRCRESAHA.109.206078 (2010).

21 Tsutsui, K. *et al.* A coupled-clock system drives the automaticity of human sinoatrial nodal pacemaker cells. *Science signaling* **11**, doi:10.1126/scisignal.aap7608 (2018).

22 Bers, D. M. Cardiac excitation-contraction coupling. *Nature* **415**, 198-205, doi:10.1038/415198a (2002).

23 Eisner, D. A., Choi, H. S., Diaz, M. E., O'Neill, S. C. & Trafford, A. W. Integrative analysis of calcium cycling in cardiac muscle. *Circulation research* **87**, 1087-1094, doi:10.1161/01.res.87.12.1087 (2000).

24 Bers, D. M. Calcium fluxes involved in control of cardiac myocyte contraction. *Circulation research* **87**, 275-281, doi:10.1161/01.res.87.4.275 (2000).

25 Hayashi, T. *et al.* Three-dimensional electron microscopy reveals new details of membrane systems for Ca2+ signaling in the heart. *Journal of cell science* **122**, 1005-1013, doi:10.1242/jcs.028175 (2009).

26 Eisner, D. A., Caldwell, J. L., Kistamas, K. & Trafford, A. W. Calcium and Excitation-Contraction Coupling in the Heart. *Circulation research* **121**, 181-195, doi:10.1161/CIRCRESAHA.117.310230 (2017).

27 Bers, D. M. & Perez-Reyes, E. Ca channels in cardiac myocytes: structure and function in Ca influx and intracellular Ca release. *Cardiovascular research* **42**, 339-360, doi:10.1016/s0008-6363(99)00038-3 (1999).

28 Ono, K. & Iijima, T. Cardiac T-type Ca(2+) channels in the heart. *Journal of molecular and cellular cardiology* **48**, 65-70, doi:10.1016/j.yjmcc.2009.08.021 (2010).

29 Wier, W. G. & Balke, C. W. Ca(2+) release mechanisms, Ca(2+) sparks, and local control of excitation-contraction coupling in normal heart muscle. *Circulation research* **85**, 770-776, doi:10.1161/01.res.85.9.770 (1999).

30 Eisner, D. A. & Lederer, W. J. Na-Ca exchange: stoichiometry and electrogenicity. *The American journal of physiology* **248**, C189-202, doi:10.1152/ajpcell.1985.248.3.C189 (1985).

31 Puglisi, J. L., Bassani, R. A., Bassani, J. W., Amin, J. N. & Bers, D. M. Temperature and relative contributions of Ca transport systems in cardiac myocyte relaxation. *The American journal of physiology* **270**, H1772-1778, doi:10.1152/ajpheart.1996.270.5.H1772 (1996).

32 Pieske, B., Maier, L. S., Bers, D. M. & Hasenfuss, G. Ca2+ handling and sarcoplasmic reticulum Ca2+ content in isolated failing and nonfailing human myocardium. *Circulation research* **85**, 38-46, doi:10.1161/01.res.85.1.38 (1999).

33 Hove-Madsen, L. & Bers, D. M. Sarcoplasmic reticulum Ca2+ uptake and thapsigargin sensitivity in permeabilized rabbit and rat ventricular myocytes. *Circulation research* **73**, 820-828, doi:10.1161/01.res.73.5.820 (1993).

34 Hilgemann, D. W. Numerical approximations of sodium-calcium exchange. *Progress in biophysics and molecular biology* **51**, 1-45, doi:10.1016/0079-6107(88)90009-0 (1988).

35 Bers, D. M. & Ginsburg, K. S. Na:Ca stoichiometry and cytosolic Ca-dependent activation of NCX in intact cardiomyocytes. *Annals of the New York Academy of Sciences* **1099**, 326-338, doi:10.1196/annals.1387.060 (2007).

36 Bridge, J. H., Smolley, J., Spitzer, K. W. & Chin, T. K. Voltage dependence of sodium-calcium exchange and the control of calcium extrusion in the heart. *Annals of the New York Academy of Sciences* **639**, 34-47, doi:10.1111/j.1749-6632.1991.tb17287.x (1991).

37 Noble, D. *et al.* The role of sodium-calcium exchange during the cardiac action potential. *Annals of the New York Academy of Sciences* **639**, 334-353, doi:10.1111/j.1749-6632.1991.tb17323.x (1991).

38 Bers, D. M., Despa, S. & Bossuyt, J. Regulation of Ca2+ and Na+ in normal and failing cardiac myocytes. *Annals of the New York Academy of Sciences* **1080**, 165-177, doi:10.1196/annals.1380.015 (2006).

39 Venetucci, L. A., Trafford, A. W., O'Neill, S. C. & Eisner, D. A. Na/Ca exchange: regulator of intracellular calcium and source of arrhythmias in the heart. *Annals of the New York Academy of Sciences* **1099**, 315-325, doi:10.1196/annals.1387.033 (2007).

40 Brown, H. F., Kimura, J., Noble, D., Noble, S. J. & Taupignon, A. The slow inward current, isi, in the rabbit sino-atrial node investigated by voltage clamp and computer simulation. *Proceedings of the Royal Society of London. Series B, Biological sciences* **222**, 305-328, doi:10.1098/rspb.1984.0066 (1984).

41 Zhou, Z. & Lipsius, S. L. Na(+)-Ca2+ exchange current in latent pacemaker cells isolated from cat right atrium. *The Journal of physiology* **466**, 263-285 (1993).

42 Li, J., Qu, J. & Nathan, R. D. Ionic basis of ryanodine's negative chronotropic effect on pacemaker cells isolated from the sinoatrial node. *The American journal of physiology* **273**, H2481-2489, doi:10.1152/ajpheart.1997.273.5.H2481 (1997).

43 Sanders, L., Rakovic, S., Lowe, M., Mattick, P. A. & Terrar, D. A. Fundamental importance of Na+-Ca2+ exchange for the pacemaking mechanism in guinea-pig sino-atrial node. *The Journal of physiology* **571**, 639-649, doi:10.1113/jphysiol.2005.100305 (2006).

44 Herrmann, S. *et al.* The cardiac sodium-calcium exchanger NCX1 is a key player in the initiation and maintenance of a stable heart rhythm. *Cardiovascular research* **99**, 780-788, doi:10.1093/cvr/cvt154 (2013).

45 Groenke, S. *et al.* Complete atrial-specific knockout of sodium-calcium exchange eliminates sinoatrial node pacemaker activity. *PloS one* **8**, e81633, doi:10.1371/journal.pone.0081633 (2013).

46 Wakabayashi, S. & Goshima, K. Comparison of kinetic characteristics of Na+-Ca2+ exchange in sarcolemma vesicles and cultured cells from chick heart. *Biochimica et biophysica acta* **645**, 311-317, doi:10.1016/0005-2736(81)90202-9 (1981).

47 Trosper, T. L. & Philipson, K. D. Effects of divalent and trivalent cations on Na+-Ca2+ exchange in cardiac sarcolemmal vesicles. *Biochimica et biophysica acta* **731**, 63-68, doi:10.1016/0005-2736(83)90398-x (1983).

48 Birinyi, P. *et al.* Effects of SEA0400 and KB-R7943 on Na+/Ca2+ exchange current and L-type Ca2+ current in canine ventricular cardiomyocytes. *Naunyn-Schmiedeberg's archives of pharmacology* **372**, 63-70, doi:10.1007/s00210-005-1079-x (2005).

49 Matsuda, T. *et al.* SEA0400, a novel and selective inhibitor of the Na+-Ca2+ exchanger, attenuates reperfusion injury in the in vitro and in vivo cerebral ischemic models. *The Journal of pharmacology and experimental therapeutics* **298**, 249-256 (2001).

50 Matsuda, T., Koyama, Y. & Baba, A. Functional proteins involved in regulation of intracellular Ca(2+) for drug development: pharmacology of SEA0400, a specific inhibitor of the Na(+)-Ca(2+) exchanger. *Journal of pharmacological sciences* **97**, 339-343, doi:10.1254/jphs.fmj04007x2 (2005).

51 Jost, N. *et al.* ORM-10103, a novel specific inhibitor of the Na+/Ca2+ exchanger, decreases early and delayed afterdepolarizations in the canine heart. *British journal of pharmacology* **170**, 768-778, doi:10.1111/bph.12228 (2013).

52 Kohajda, Z. *et al.* The Effect of a Novel Highly Selective Inhibitor of the Sodium/Calcium Exchanger (NCX) on Cardiac Arrhythmias in In Vitro and In Vivo Experiments. *PloS one* **11**, e0166041, doi:10.1371/journal.pone.0166041 (2016).

53 Eisner, D. A. & Vaughan-Jones, R. D. Do calcium-activated potassium channels exist in the heart? *Cell calcium* **4**, 371-386, doi:10.1016/0143-4160(83)90015-5 (1983).

54 Xu, Y. *et al.* Molecular identification and functional roles of a Ca(2+)-activated K+ channel in human and mouse hearts. *The Journal of biological chemistry* **278**, 49085-49094, doi:10.1074/jbc.M307508200 (2003).

55 Chua, S. K. *et al.* Small-conductance calcium-activated potassium channel and recurrent ventricular fibrillation in failing rabbit ventricles. *Circulation research* **108**, 971-979, doi:10.1161/CIRCRESAHA.110.238386 (2011).

56 Kirchhoff, J. E., Diness, J. G., Sheykhzade, M., Grunnet, M. & Jespersen, T. Synergistic antiarrhythmic effect of combining inhibition of Ca(2)(+)-activated K(+) (SK) channels and voltage-gated Na(+) channels in an isolated heart model of atrial fibrillation. *Heart rhythm* **12**, 409-418, doi:10.1016/j.hrthm.2014.12.010 (2015).

57 Yin, D. *et al.* Role of apamin-sensitive small conductance calcium-activated potassium currents in long-term cardiac memory in rabbits. *Heart rhythm* **15**, 761-769, doi:10.1016/j.hrthm.2018.01.016 (2018).

58 Nagy, N. *et al.* Does small-conductance calcium-activated potassium channel contribute to cardiac repolarization? *Journal of molecular and cellular cardiology* **47**, 656-663, doi:10.1016/j.yjmcc.2009.07.019 (2009).

59 Strong, P. N. & Brewster, B. S. in *Methods in Neurosciences* Vol. 8 (ed P. Michael Conn) 15-24 (Academic Press, 1992).

60 Lyashkov, A. E., Behar, J., Lakatta, E. G., Yaniv, Y. & Maltsev, V. A. Positive Feedback Mechanisms among Local Ca Releases, NCX, and ICaL Ignite Pacemaker Action Potentials. *Biophysical journal* **114**, 2024, doi:10.1016/j.bpj.2018.03.024 (2018).

61 Hoffman, B. F. & Suckling, E. E. Effect of heart rate on cardiac membrane potentials and the unipolar electrogram. *The American journal of physiology* **179**, 123-130, doi:10.1152/ajplegacy.1954.179.1.123 (1954).

62 Opthof, T. *et al.* Changes in sinus node function in a rabbit model of heart failure with ventricular arrhythmias and sudden death. *Circulation* **101**, 2975-2980, doi:10.1161/01.cir.101.25.2975 (2000).

63 Williams, B. A., Dickenson, D. R. & Beatch, G. N. Kinetics of rate-dependent shortening of action potential duration in guinea-pig ventricle; effects of IK1 and IKr blockade. *British journal of pharmacology* **126**, 1426-1436, doi:10.1038/sj.bjp.0702443 (1999).

64 Li, G. R. *et al.* Transmembrane ICa contributes to rate-dependent changes of action potentials in human ventricular myocytes. *The American journal of physiology* **276**, H98-H106, doi:10.1152/ajpheart.1999.276.1.H98 (1999).

65 Hund, T. J. & Rudy, Y. Rate dependence and regulation of action potential and calcium transient in a canine cardiac ventricular cell model. *Circulation* **110**, 3168-3174, doi:10.1161/01.CIR.0000147231.69595.D3 (2004).

66 Kaufman, E. S., Mackall, J. A., Julka, B., Drabek, C. & Rosenbaum, D. S. Influence of heart rate and sympathetic stimulation on arrhythmogenic T wave alternans. *American journal of physiology. Heart and circulatory physiology* **279**, H1248-1255, doi:10.1152/ajpheart.2000.279.3.H1248 (2000).

67 Saitoh, H., Bailey, J. C. & Surawicz, B. Alternans of action potential duration after abrupt shortening of cycle length: differences between dog Purkinje and ventricular muscle fibers. *Circulation research* **62**, 1027-1040, doi:10.1161/01.res.62.5.1027 (1988).

68 LEWIS, T. NOTES UPON ALTERNATION OF THE HEART. *QJM: An International Journal of Medicine* **os4**, 141-144, doi:10.1093/oxfordjournals.qjmed.a069273 (1911).

69 Cutler, M. J. & Rosenbaum, D. S. Explaining the clinical manifestations of T wave alternans in patients at risk for sudden cardiac death. *Heart rhythm* **6**, S22-28, doi:10.1016/j.hrthm.2008.10.007 (2009).

70 Hekkanen, J. J. *et al.* Increased Beat-to-Beat Variability of T-Wave Heterogeneity Measured From Standard 12-Lead Electrocardiogram Is Associated With Sudden Cardiac Death: A Case-Control Study. *Frontiers in physiology* **11**, 1045, doi:10.3389/fphys.2020.01045 (2020).

71 Narayan, S. M. T-wave alternans and the susceptibility to ventricular arrhythmias. *Journal of the American College of Cardiology* **47**, 269-281, doi:10.1016/j.jacc.2005.08.066 (2006).

72 Rosenbaum, D. S. *et al.* Electrical alternans and vulnerability to ventricular arrhythmias. *The New England journal of medicine* **330**, 235-241, doi:10.1056/NEJM199401273300402 (1994).

73 Pastore, J. M., Girouard, S. D., Laurita, K. R., Akar, F. G. & Rosenbaum, D. S. Mechanism linking T-wave alternans to the genesis of cardiac fibrillation. *Circulation* **99**, 1385-1394, doi:10.1161/01.cir.99.10.1385 (1999).

74 Laurita, K. R., Katra, R., Wible, B., Wan, X. & Koo, M. H. Transmural heterogeneity of calcium handling in canine. *Circulation research* **92**, 668-675, doi:10.1161/01.RES.0000062468.25308.27 (2003).

75 Nolasco, J. B. & Dahlen, R. W. A graphic method for the study of alternation in cardiac action potentials. *J Appl Physiol* **25**, 191-196, doi:10.1152/jappl.1968.25.2.191 (1968).

76 Hirayama, Y., Saitoh, H., Atarashi, H. & Hayakawa, H. Electrical and mechanical alternans in canine myocardium in vivo. Dependence on intracellular calcium cycling. *Circulation* **88**, 2894-2902, doi:10.1161/01.cir.88.6.2894 (1993).

77 Tse, G. *et al.* Cardiac dynamics: Alternans and arrhythmogenesis. *Journal of arrhythmia* **32**, 411-417, doi:10.1016/j.joa.2016.02.009 (2016).

78 Pruvot, E. J., Katra, R. P., Rosenbaum, D. S. & Laurita, K. R. Role of calcium cycling versus restitution in the mechanism of repolarization alternans. *Circulation research* **94**, 1083-1090, doi:10.1161/01.RES.0000125629.72053.95 (2004).

79 Yaniv, Y., Stern, M. D., Lakatta, E. G. & Maltsev, V. A. Mechanisms of beat-to-beat regulation of cardiac pacemaker cell function by Ca(2)(+) cycling dynamics. *Biophysical journal* **105**, 1551-1561, doi:10.1016/j.bpj.2013.08.024 (2013).

80 Koncz, I. *et al.* Electrophysiological effects of ivabradine in dog and human cardiac preparations: potential antiarrhythmic actions. *European journal of pharmacology* **668**, 419-426, doi:10.1016/j.ejphar.2011.07.025 (2011).

81 Maltsev, V. A. & Lakatta, E. G. Numerical models based on a minimal set of sarcolemmal electrogenic proteins and an intracellular Ca(2+) clock generate robust,

flexible, and energy-efficient cardiac pacemaking. *Journal of molecular and cellular cardiology* **59**, 181-195, doi:10.1016/j.yjmcc.2013.03.004 (2013).

82 Reggiani, C. Caffeine as a tool to investigate sarcoplasmic reticulum and intracellular calcium dynamics in human skeletal muscles. *Journal of muscle research and cell motility* **42**, 281-289, doi:10.1007/s10974-020-09574-7 (2021).

83 Torrente, A. G. *et al.* Contribution of small conductance K(+) channels to sinoatrial node pacemaker activity: insights from atrial-specific Na(+) /Ca(2+) exchange knockout mice. *The Journal of physiology* **595**, 3847-3865, doi:10.1113/JP274249 (2017).

84 Yaniv, Y. *et al.* New evidence for coupled clock regulation of the normal automaticity of sinoatrial nodal pacemaker cells: bradycardic effects of ivabradine are linked to suppression of intracellular Ca(2)(+) cycling. *Journal of molecular and cellular cardiology* **62**, 80-89, doi:10.1016/j.yjmcc.2013.04.026 (2013).

85 Yaniv, Y., Lakatta, E. G. & Maltsev, V. A. From two competing oscillators to one coupled-clock pacemaker cell system. *Frontiers in physiology* **6**, 28, doi:10.3389/fphys.2015.00028 (2015).

86 Gao, Z. *et al.* Genetic inhibition of Na+-Ca2+ exchanger current disables fight or flight sinoatrial node activity without affecting resting heart rate. *Circulation research* **112**, 309-317, doi:10.1161/CIRCRESAHA.111.300193 (2013).

87 DiFrancesco, D. Cesium and the pacemaker current. *Journal of cardiovascular electrophysiology* **6**, 1152-1155, doi:10.1111/j.1540-8167.1995.tb00394.x (1995).

88 Morad, M. & Zhang, X. H. Mechanisms of spontaneous pacing: sinoatrial nodal cells, neonatal cardiomyocytes, and human stem cell derived cardiomyocytes. *Canadian journal of physiology and pharmacology* **95**, 1100-1107, doi:10.1139/cjpp-2016-0743 (2017).

89 Roden, D. M. Taking the "idio" out of "idiosyncratic": predicting torsades de pointes. *Pacing and clinical electrophysiology : PACE* **21**, 1029-1034, doi:10.1111/j.1540-8159.1998.tb00148.x (1998).

90 Roden, D. M. Repolarization reserve: a moving target. *Circulation* **118**, 981-982, doi:10.1161/CIRCULATIONAHA.108.798918 (2008).

91 Varro, A. & Baczko, I. Cardiac ventricular repolarization reserve: a principle for understanding drug-related proarrhythmic risk. *British journal of pharmacology* **164**, 14-36, doi:10.1111/j.1476-5381.2011.01367.x (2011).

92 Biliczki, P., Virag, L., Iost, N., Papp, J. G. & Varro, A. Interaction of different potassium channels in cardiac repolarization in dog ventricular preparations: role of repolarization reserve. *British journal of pharmacology* **137**, 361-368, doi:10.1038/sj.bjp.0704881 (2002).

93 Bucchi, A., Baruscotti, M., Robinson, R. B. & DiFrancesco, D. I(f)-dependent modulation of pacemaker rate mediated by cAMP in the presence of ryanodine in rabbit sino-atrial node cells. *Journal of molecular and cellular cardiology* **35**, 905-913, doi:10.1016/s0022-2828(03)00150-0 (2003).

94 Sirenko, S. G. *et al.* Electrochemical Na+ and Ca2+ gradients drive coupled-clock regulation of automaticity of isolated rabbit sinoatrial nodal pacemaker cells. *American journal of physiology. Heart and circulatory physiology* **311**, H251-267, doi:10.1152/ajpheart.00667.2015 (2016).

95 Nagy, N. *et al.* Selective Na(+) /Ca(2+) exchanger inhibition prevents Ca(2+) overload-induced triggered arrhythmias. *British journal of pharmacology* **171**, 5665-5681, doi:10.1111/bph.12867 (2014).

96 Boyett, M. R., Honjo, H. & Kodama, I. The sinoatrial node, a heterogeneous pacemaker structure. *Cardiovascular research* **47**, 658-687, doi:10.1016/s0008-6363(00)00135-8 (2000).

97 Lancaster, M. K., Jones, S. A., Harrison, S. M. & Boyett, M. R. Intracellular Ca2+ and pacemaking within the rabbit sinoatrial node: heterogeneity of role and control. *The Journal of physiology* **556**, 481-494, doi:10.1113/jphysiol.2003.057372 (2004).

98 Masson-Pevet, M. A. *et al.* Pacemaker cell types in the rabbit sinus node: a correlative ultrastructural and electrophysiological study. *Journal of molecular and cellular cardiology* **16**, 53-63, doi:10.1016/s0022-2828(84)80714-2 (1984).

99 Bleeker, W. K., Mackaay, A. J., Masson-Pevet, M., Bouman, L. N. & Becker, A. E. Functional and morphological organization of the rabbit sinus node. *Circulation research* **46**, 11-22, doi:10.1161/01.res.46.1.11 (1980).

100 Musa, H. *et al.* Heterogeneous expression of Ca(2+) handling proteins in rabbit sinoatrial node. *The journal of histochemistry and cytochemistry : official journal of the Histochemistry Society* **50**, 311-324, doi:10.1177/002215540205000303 (2002).

101 Gal, P. *et al.* First Clinical Study with AP30663 - a KCa 2 Channel Inhibitor in Development for Conversion of Atrial Fibrillation. *Clinical and translational science* **13**, 1336-1344, doi:10.1111/cts.12835 (2020).

I.

pharmaceuticals

MDPI

Article

The Inhibition of the Small-Conductance Ca^{2+}-Activated Potassium Channels Decreases the Sinus Node Pacemaking during Beta-Adrenergic Activation

Gergő Bitay [1], Noémi Tóth [1], Szilvia Déri [1], Jozefina Szlovák [1], Zsófia Kohajda [2], András Varró [1,2,3] and Norbert Nagy [1,2,*]

[1] Department of Pharmacology and Pharmacotherapy, Albert Szent-Györgyi Medical School, University of Szeged, 6720 Szeged, Hungary; geribitay@gmail.com (G.B.); toth.noemi@med.u-szeged.hu (N.T.); deri.szilvia@med.u-szeged.hu (S.D.); szlovak.j93@gmail.com (J.S.); varro.andras@med.u-szeged.hu (A.V.)
[2] ELKH-SZTE Research Group of Cardiovascular Pharmacology, Hungarian Academy of Sciences, 6725 Szeged, Hungary; kohajda.zsofia@med.u-szeged.hu
[3] Department of Pharmacology and Pharmacotherapy, Interdisciplinary Excellence Centre, University of Szeged, 6720 Szeged, Hungary
* Correspondence: nagy.norbert@med.u-szeged.hu

Abstract: Sinus pacemaking is based on tight cooperation of intracellular Ca^{2+} handling and surface membrane ion channels. An important player of this synergistic crosstalk could be the small-conductance Ca^{2+}-activated K^+-channel (I_{SK}) that could contribute to the sinoatrial node (SAN) pacemaking driven by the intracellular Ca^{2+} changes under normal conditions and beta-adrenergic activation, however, the exact role is not fully clarified. SK2 channel expression was verified by immunoblot technique in rabbit SAN cells. Ionic currents and action potentials were measured by patch-clamp technique. The ECG R-R intervals were obtained by Langendorff-perfusion method on a rabbit heart. Apamin, a selective inhibitor of SK channels, was used during the experiments. Patch-clamp experiments revealed an apamin-sensitive current. When 100 nM apamin was applied, we found no change in the action potential nor in the ECG R-R interval. In experiments where isoproterenol was employed, apamin increased the cycle length of the SAN action potentials and enhanced the ECG R-R interval. Apamin did not amplify the cycle length variability or ECG R-R interval variability. Our data indicate that I_{SK} has no role under normal condition, however, it moderately contributes to the SAN automaticity under beta-adrenergic activation.

Keywords: SAN pacemaking; small-conductance Ca^{2+}-activated K^+-channels; ISK; heart rate

Citation: Bitay, G.; Tóth, N.; Déri, S.; Szlovák, J.; Kohajda, Z.; Varró, A.; Nagy, N. The Inhibition of the Small-Conductance Ca^{2+}-Activated Potassium Channels Decreases the Sinus Node Pacemaking during Beta-Adrenergic Activation. *Pharmaceuticals* **2022**, *15*, 313. https://doi.org/10.3390/ph15030313

Academic Editors: Gary J. Stephens, Balazs Horvath and Péter P. Nánási

Received: 31 October 2021
Accepted: 1 March 2022
Published: 4 March 2022

1. Introduction

The Ca^{2+}-activated K^+-current was first described in neurons in 1974 [1]. The existence and functional role of the Ca^{2+}-activated K^+-current in the heart was addressed in 1983 and it was concluded that there is no such current in the ventricular myocardium that carries exclusively K^+-ions and is activated by intracellular Ca^{2+} [2]. In 2003, Xu et al. reiterated this issue and described a notable small-conductance Ca^{2+}-activated K^+-current (I_{SK}) in ventricular and atrial myocytes of mice and human [3]. Recently, it was found that I_{SK} has an important role in several diseases and conditions such as atrial fibrillation, heart failure [4–6], cardiac memory [7,8], and J-wave syndrome [9]. Its important role was shown in normal atrial electrophysiology [10], however, no role was found in ventricular myocytes under normal conditions [11].

Considering that I_{SK} is a Ca^{2+}-driven K^+-current, theoretically it could have an important function in sinoatrial node (SAN) automaticity via providing a functional link between the intracellular Ca^{2+} and the repolarization process, especially under beta-adrenergic condition. However, the function of I_{SK} in SAN cells is poorly elucidated. Recently,

Chen et al. and Torrente et al. demonstrated that I_{SK} contributes to the SAN pacemaking in normal rabbit and mouse SAN cells and NCX-knock out cell line [12,13]. In rabbit SAN cells, I_{SK} was even claimed as a key player of the pacemaking mechanism and action potential morphology.

The underlying mechanism of the SAN automaticity, after a long and intense debate, seems to be settled in a concept of the so-called coupled-clock mechanism [14]. It is widely accepted that SAN automaticity is based on the mutual crosstalk of the Ca^{2+}-handling and surface membrane ion channels, where the ensemble of the membrane currents (I_{CaL}, I_{CaT}, I_{Kr}, I_f, I_{NCX}) and the rhythmical Ca^{2+} releases from the sarcoplasmic reticulum (local Ca^{2+} releases, LCR, Ca^{2+}-clock) form a robust, flexible coupled system, where neither part is dominant, and work synergistically [15]. The I_{SK}, if functionally exists, could be a new component of this coupled-clock system.

Pharmacological control of the heart rate is a crucial intervention of the daily clinical practice in several diseases. However, the applied drugs, such as beta1-adrenoreceptor antagonists, funny current inhibitors (ivabradine), or L-type Ca^{2+} channels blockers (verapamil, diltiazem) have several limitations [16,17]. Since I_{SK} is a Ca^{2+}-driven current, its contribution to pacemaking could be augmented under beta-adrenergic activation, but this issue was not previously examined. The aim of this study was to investigate the role of I_{SK} and its pharmacological inhibition under normal conditions as well as during beta-adrenergic activation in rabbit SAN cells and on isolated heart.

2. Results

2.1. Immunoblotting and Confocal Microscopy

SK2 expression was directly detected on isolated sinus node cells. Confocal microscopy on immunostained sinus node cells revealed abundant expression of SK2 channels on the surface membrane (Figure 1A). The SK2 fluorescence intensity does not show difference from the sinus node-specific HCN4 (n = 16 cells/4 animals; p = 0.97; Figure 1B). Colocalization of the SK2 immunofluorescence with WGA Texas-Red fluorescence was then analyzed by Pearson's Correlation Coefficient (PCC) and we found that average PCC values of SK2 (0.82; (0.75–0.86)) were similar with HCN4 (0.82; (0.76–0.89); n = 16 cells/4 animals; p = 0.89; Figure 1C). These data suggest that SK2 is represented in the membrane of sinus node cells as HCN4.

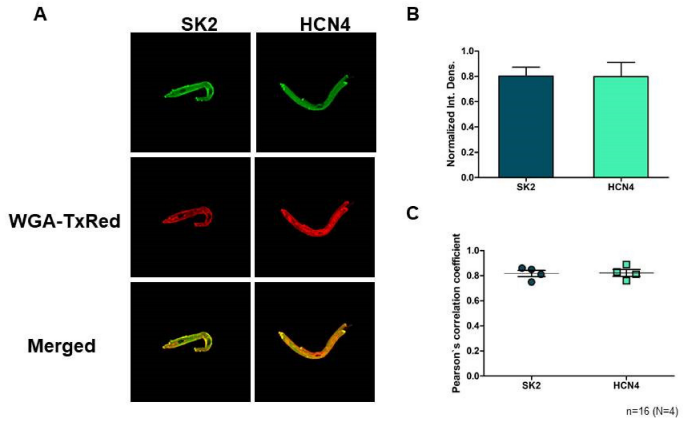

Figure 1. (**A**) shows representative immunofluorescent images of rabbit sinus node cells with SK2 and HCN4 immunolabelling. (**B**) shows the relative expression of SK2 and HCN4. There were no significant changes between the SK2 and HCN4 fluorescence intensity. (**C**) shows fluorescence colocalization analysis. One data point represents one animal. Four cells were evaluated and averaged from each animal. Data are presented as mean ± SEM, applied statistical probe was unpaired Student's t-test ($p \leq 0.05$).

2.2. Measurement of the Apamin-Sensitive Current

In the first set of electrophysiological measurements, we aimed to investigate the potential existence of I_{SK} in SAN cells. In order to address this issue, a selective inhibitor apamin was employed in 100 nM concentration, which fully inhibits all three isoforms of the SK-channels. As SK-channels carry Ca^{2+}-sensitive current, the intracellular Ca^{2+} level was set to 500 nM to activate the channels by using an appropriate mixture of EGTA and $CaCl_2$. Rectangular voltage steps were applied from −80 mV to 50 mV from a holding potential of −60 mV. Application of apamin revealed a time-independent apamin-sensitive current within the membrane potential range of −40 to 50 mV (Figure 2).

For further validation of the current, in the next set of experiments we buffered the intracellular Ca^{2+} with 10 mM BAPTA, and the same voltage protocol was applied (Figure 3). In this case, 100 nM apamin failed to dissect any current fragment from the control current, indicating that no I_{SK} was activated without free intracellular Ca^{2+}.

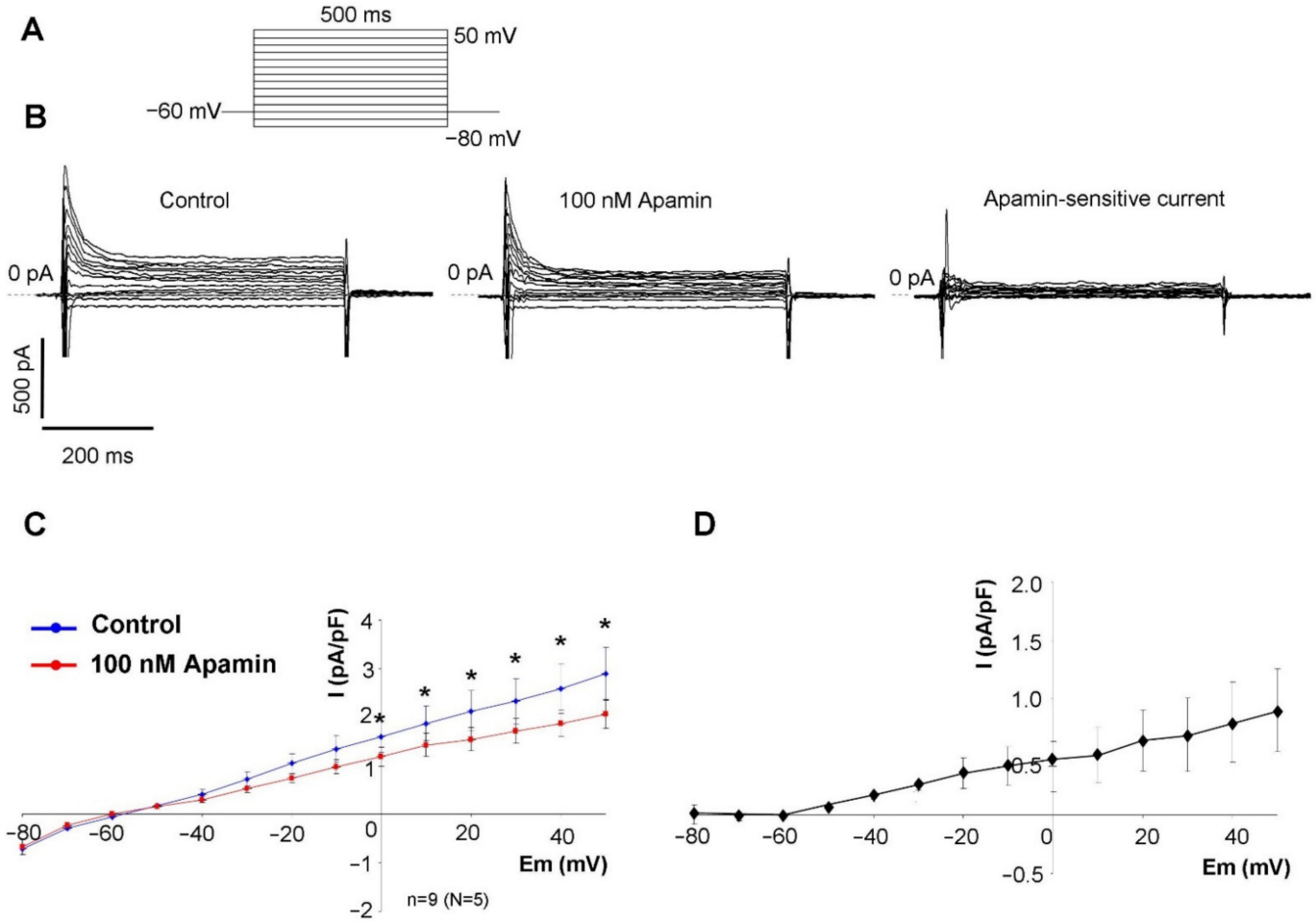

Figure 2. Characterization of the apamin-sensitive current. (**A**) illustrates the applied voltage protocol. (**B**) shows total membrane current under control condition (left curves), after 100 nM apamin application (middle curves), and the apamin sensitive current (right curves). (**C**) shows the current-voltage diagram of the control and apamin-treated currents and (**D**) illustrates the current-voltage relationship of the apamin-sensitive current. Statistical analysis was performed by paired *t*-test ($p < 0.05$).

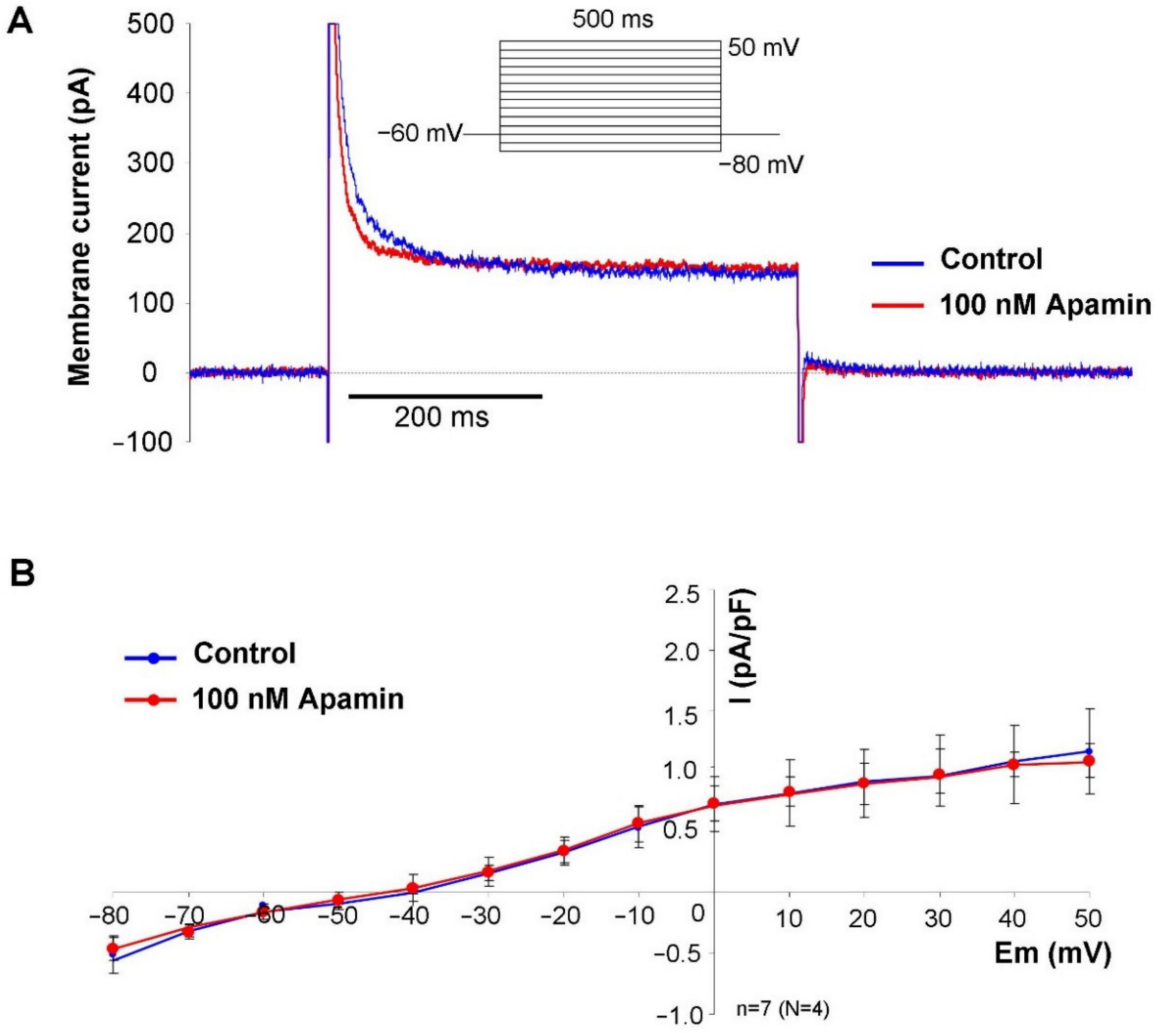

Figure 3. Characterization of the apamin-sensitive current. For further validation, the intracellular solution was heavily buffered with 10 mM BAPTA. Under this condition, the apamin failed to dissect any current from the control recording. (**A**) shows representative current traces under control condition (blue curve) and in the presence of 100 nM apamin (red curve) at 20 mV voltage pulse. (**B**) shows the current-voltage diagram where control and apamin resulted in identical curves. Statistical analysis was performed by paired *t*-test.

The apamin-sensitive current was also determined under a representative SAN action potential waveform, in the absence and in the presence of 200 nM isoproterenol without using Ca^{2+}-chelators in the patch pipette. Figure 4A demonstrates that 200 nM isoproterenol did not change the diastolic Ca^{2+} level (104 ± 30 nM → 131 ± 33 nM; n = 8, N = 6; p = 0.13). The systolic peak was 566 ± 99 nM under control condition and was significantly increased to 732 ± 112 nM after isoproterenol application (n = 8, N = 6; $p < 0.05$). In the absence of isoproterenol, 100 nM apamin failed to significantly alter the peak of the total current (76 ± 8 pA → 59 ± 9 pA; n = 8, N = 5; panel B). In contrast, when 200 nM isoproterenol was applied previously, 100 nM apamin markedly decreased the peak of total current (144 ± 33 pA → 78 ± 15 pA; $p < 0.05$; n = 8, N = 6; panel C). Panel D demonstrates the comparison of apamin-sensitive currents in the absence (black curve) and in the presence of 200 nM isoproterenol (18 ± 6 pA vs 65 ± 20 pA; $p < 0.05$). The average cell capacitance of the current measurements was: 56.7 ± 4 pA/pF (n = 32).

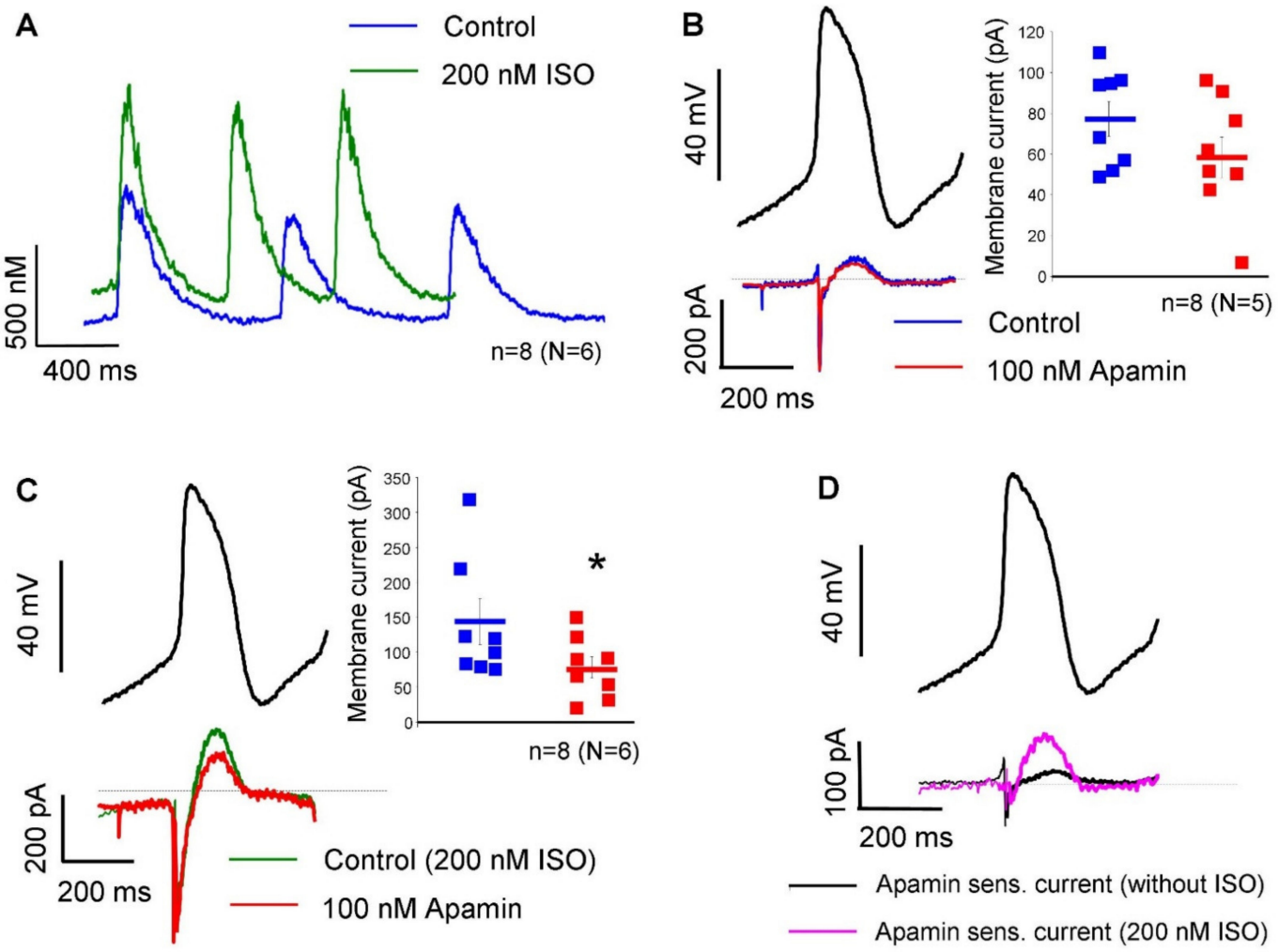

Figure 4. Measurement of apamin-sensitive current under a representative SAN action potential waveform in the absence and in the presence of 200 nM isoproterenol (ISO). (**A**) demonstrates the effect of 200 nM isoproterenol on Ca^{2+} transients. When isoproterenol was omitted, 100 nM apamin (red curve) did not alter the peak of the total current (blue curve, panel (**B**)). In the presence of 200 nM isoproterenol, 100 nM apamin (red curve) decreased the peak current (green curve, panel (**C**)). Representative original traces were determined after subtraction of currents. When 200 nM isoproterenol was employed, the apamin-sensitive current (purple curve) was larger than under normal conditions (black curve, panel (**D**)). Paired and unpaired *t*-tests ($p < 0.05$).

Since the SK-channels are expected to carry a functional current depending on the intracellular Ca^2, they may contribute to the SAN action potential and pacemaking in rabbit-isolated SAN cells. This assumption was investigated in the subsequent experiments.

2.3. The I_{SK} Has No Role in the SAN Pacemaking under Normal Condition

The effect of selective SK-channel inhibition was tested in SAN pacemaking under basal condition (i.e., without beta-adrenergic modulation) by applying 100 nM apamin. Action potentials were measured by perforated patch-clamp technique from spontaneously beating SAN cells. It was found that apamin failed to influence any parameter of the SAN action potential (control → apamin; cycle length: 391 ± 30 → 388 ± 33 ms; cycle length variability: 43 ± 10 → 41 ± 13 ms; APD: 176 ± 17 → 193 ± 25 ms; slope of diastolic depolarization: 0.08 ± 0.01 → 0.08 ± 0.01 ms; $n = 7$, Figure 5).

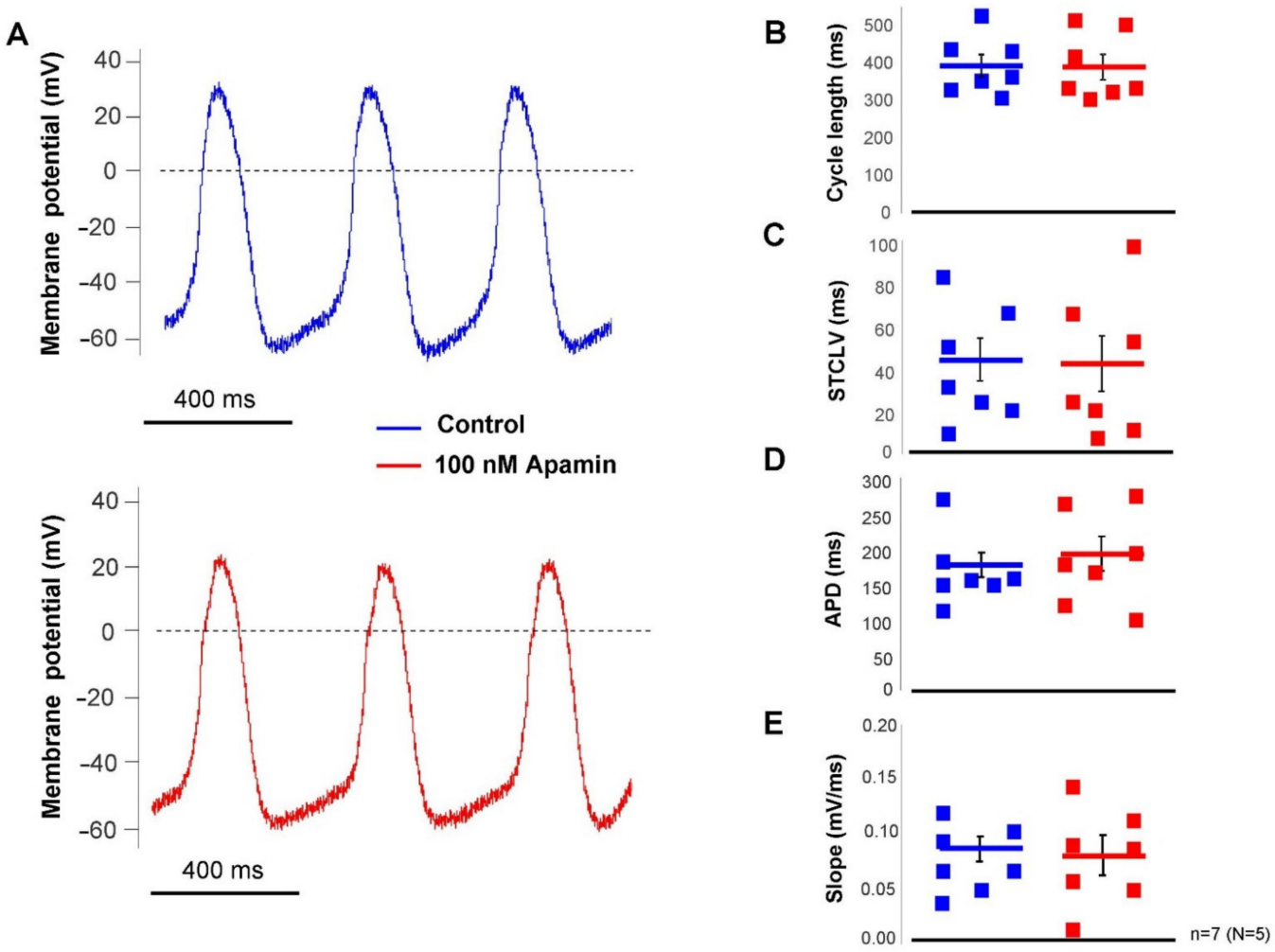

Figure 5. Action potential recordings from isolated SAN cells by perforated patch-clamp technique under normal condition. After control recordings (blue curve), 100 nM apamin was employed (red curve, (**A**). Bar graphs reported identical cycle lengths (**B**), short-term cycle length variability (**C**), APD (**D**), and slope of diastolic depolarization (**E**). Statistical analysis was performed by paired *t*-test.

2.4. I_{SK} Contributes to the SAN Action Potential under Beta-Adrenergic Activation

The failure of apamin to influence SAN pacemaking demonstrated in Figure 5 indicated that the intracellular Ca^{2+} level may not reach an appropriate level to activate a sufficiently large current during the action potential. In this set of experiments, we activated the beta-receptors by the application of 200 nM isoproterenol to enhance the intracellular Ca^{2+} content of the cells. Under this condition (Figure 6), the application of 100 nM apamin significantly lengthened the cycle length ($323 \pm 17 \rightarrow 387 \pm 28$ ms, $p < 0.05$, $n = 7$), without altering the short-term cycle length variability in a statistically significant manner ($26 \pm 6 \rightarrow 40 \pm 11$ ms, $p = 0.21$, $n = 7$), but prolonged the APD ($153 \pm 10 \rightarrow 176 \pm 8$ ms, $p < 0.05$, $n = 7$) and did not alter the slope of diastolic depolarization ($0.11 \pm 0.01 \rightarrow 0.095 \pm 0.01$ mV/ms, $n = 7$). The maximal diastolic potential also did not show change upon apamin application ($-56 \pm 2 \rightarrow 60 \pm 3$ mV, $n = 7$).

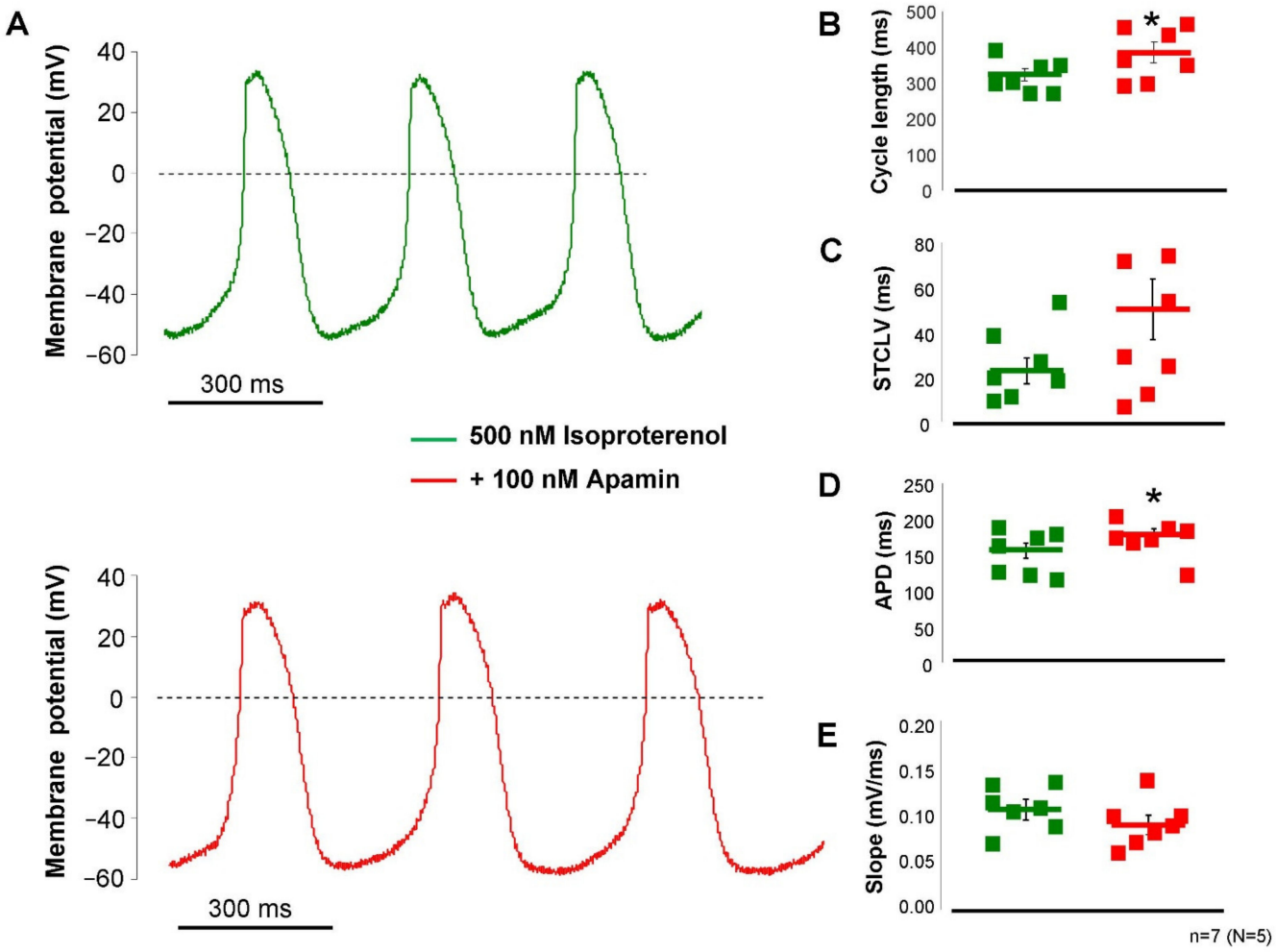

Figure 6. Action potential recordings from isolated SAN cells by perforated patch-clamp technique in the presence of 200 nM isoproterenol. The control recordings were measured in the presence of isoproterenol (green curve), then 100 nM apamin was employed (red curve, (**A**)). Application of apamin increased the cycle length (**B**) without alteration of the short-term cycle length variability (**C**), and increased the APD (**D**) without changing the diastolic depolarization (**E**). Statistical analysis was performed by paired *t*-test ($p < 0.05$).

2.5. Inhibition of the I_{SK} Lengthens the ECG R-R Interval under Beta-Adrenergic Activation

The effect of 100 nM apamin was tested on *ex-vivo* isolated Langendorff-perfused hearts (Figure 7). During measurements, 40 consecutive ECG R-R intervals were measured and the mean R-R intervals and short-term R-R variability were calculated. Under normal conditions (i.e., without beta-adrenergic activation), 100 nM apamin failed to alter both the ECG R-R intervals ($373 \pm 20 \rightarrow 393 \pm 17$ ms, $p = 0.43$, $n = 10$) and the R-R variability ($6.4 \pm 1.2 \rightarrow 6.8 \pm 1.4$ ms, $n = 10$). Parallel with the apamin experiments, a time control group was measured where the vehicle of apamin was applied in order to detect any non-specific or time-dependent changes. No change was found in the ECG R-R interval ($379 \pm 10 \rightarrow 373 \pm 17$ ms, $n = 10$) nor in the R-R variability ($6.9 \pm 1.6 \rightarrow 7.1 \pm 1.6$ ms, $n = 10$).

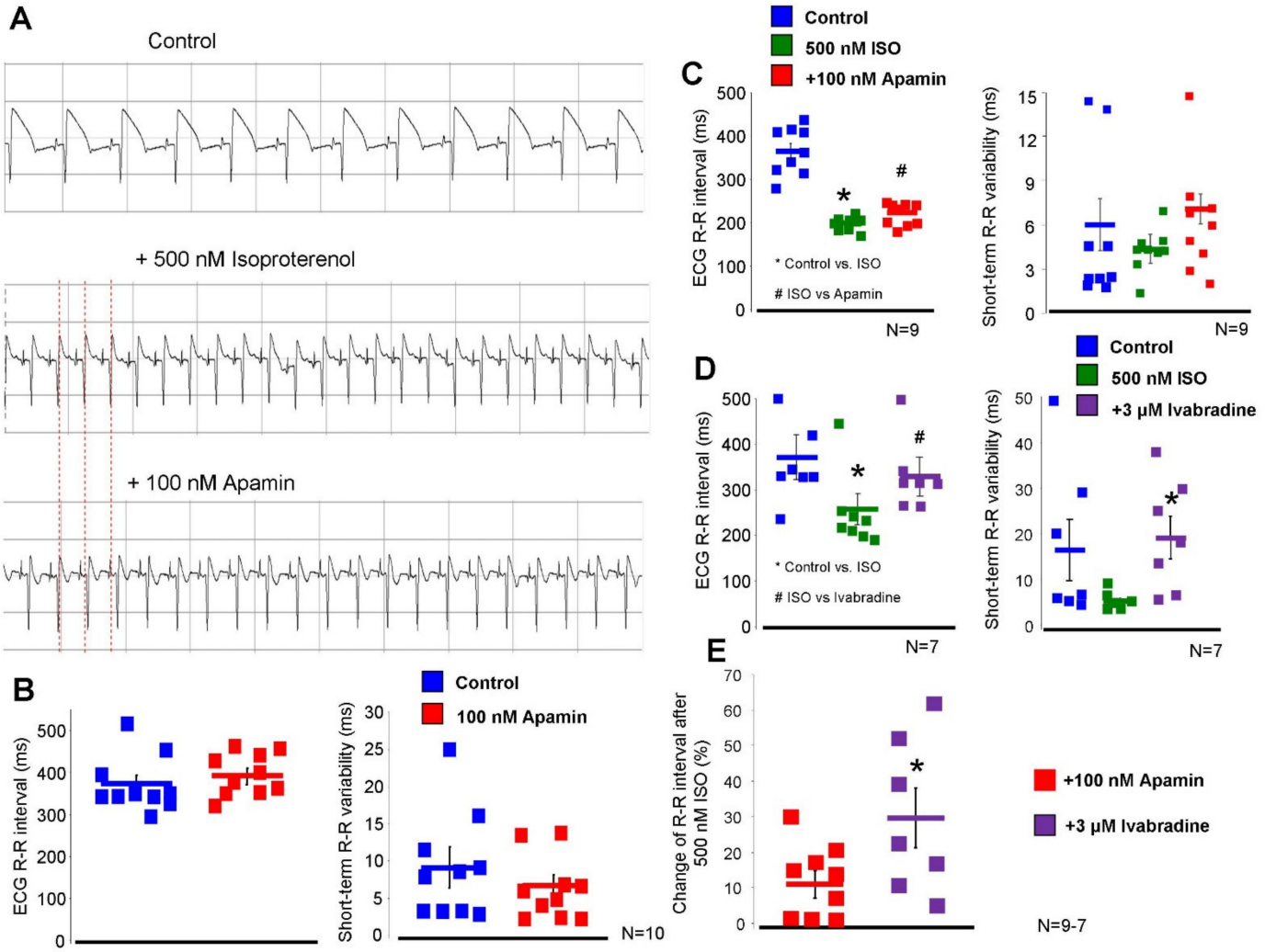

Figure 7. Results of Langendorff-perfused experiments on isolated hearts. (**A**) demonstrates original ECG traces in control condition (upper panel), in the presence of 200 nM isoproterenol (middle panel), and after apamin application (lower panel). Red vertical dashed lines indicate the change of the cycle lengths. (**B**) represents the basal condition (i.e., without application of isoproterenol). The ECG R-R interval (left graph) and the R-R variability (right graph) were unaltered after apamin administration. (**C**) represents apamin application in the presence of 500 nM isoproterenol. 100 nM apamin increased the ECG R-R interval (left graph), however, it did not change the R-R variability (right graph). (**D**) illustrates the effect of 3 µM ivabradine. Ivabradine markedly increases the R-R interval (left graph) and the R-R interval variability (right graph). (**E**) shows the comparison of the effects of apamin and ivabradine on the ECG R-R interval after 200 nM isoproterenol. Statistical analysis was performed by paired *t*-test and repeated measures ANOVA ($p < 0.05$).

In the second set of Langendorff experiments, we aimed to substantially activate the beta-adrenergic receptors in order to enhance the intracellular Ca^{2+} without causing arrhythmogenic events. Our preliminary experiments showed that 500 nM isoproterenol shortens the ECG R-R interval by 44 ± 4%, while arrhythmias were not observed. Under this condition, 100 nM apamin lengthened the ECG R-R interval (364 ± 17 → 200 ± 5 → 223 ± 10 ms, $p < 0.05$, $n = 9$) but did not alter the R-R variability (6.0 ± 1.7 → 4.4 ± 0.6 → 7.1 ± 3.8 ms, $p = 0.41$, $n = 10$). The parallel time control measurements exerted no statistically significant change in these variables upon administration of the vehicle (R-R interval: 370 ± 16 → 223 ± 8 → 231 ± 11 ms, $n = 10$; R-R variability: 8.1 ± 2.1 → 3.0 ± 0.3 → 4.0 ± 0.5 ms, $n = 10$).

In order to compare the magnitude and nature of the apamin effect to a well-known bradycardic agent, the effect of 3 μM ivabradine was examined in the presence of 500 nM isoproterenol. As it was expected, the application of ivabradine lengthened the ECG R-R interval (386 ± 48 → 257 ± 34 → 330 ± 41 ms, $p < 0.05$, $n = 7$), however, it also significantly increased the ECG R-R variability (11.7 ± 4.0 → 6.0 ± 0.7 → 20.0 ± 5 ms, $n = 7$).

3. Discussion

In this study we analyzed the possible role of the small-conductance Ca^{2+}-activated K^+-current under basal condition and during beta-adrenergic stimulation. Previous studies reported the functional role of SK-channels in SAN pacemaking without adrenergic stimulation. In contrast, in this study we failed to demonstrate a significant effect of SK-inhibition under normal condition, unless beta adrenergic stimulation was applied.

We do not know the discrepancy of the difference between our and the study of Chen at al. [12], but differences in the intracellular Ca^{2+} level cannot be ruled out between the two studies. Further investigations are necessary to resolve this issue.

The most important findings of this paper are: (i) the SK2-channels are expressed in rabbit SAN sarcolemma. (ii) The I_{SK} has no role in SAN pacemaking with basal intracellular Ca^{2+} level. (iii) Beta-adrenergic stimulation activates the I_{SK} and its inhibition causes moderate decrease in spontaneous automaticity via APD lengthening without increasing the cycle length variability.

3.1. The SK Channels Are Expressed in Rabbit SAN Myocytes

A previous paper demonstrated the expression of SK-channel in mice myocytes [13], however, based on our best knowledge this is the first data regarding the expression of SK2 in rabbit SAN cells, which is emphasized by the fact that the vast majority of SAN data are obtained from rabbit cells. Since a previous study indicated that the selective SK-channel inhibitor apamin exerts the highest sensitivity toward SK2 [18], the expression of SK2 isoform was elucidated in this study. Our experiments showed that the SK2 isoform is expressed in the surface membrane of rabbit SAN myocytes.

3.2. The Apamin-Sensitive Current Is Present in SAN Cells

SK-channels can be divided into three major subgroups: SK1 channels are encoded by KCNN1, SK2-channel encoded by KCNN2, and SK3 encoded by KCNN3 gene. Apamin, a polypeptide blocker of the I_{SK} isolated from bee venom, selectively blocks the current with isoform-dependent effectivity [19]. SK1 channels have the lowest sensitivity (IC_{50}~10 nM); the SK3 is moderately sensitive (IC_{50}~1 nM); and SK2 exerts the highest sensitivity (IC_{50}~40 pM) [19]. This indicates that the applied 100 nM apamin in this study is far above the IC_{50}-values of any channel subtypes, therefore, complete SK-channel block is expected in our experiments.

The SK-channels are suggested to be voltage-independent ion channels, activated by the rise of intracellular Ca^{2+} concentration, and carrying repolarizing K-currents [3]. Previous studies suggested that inward rectification of the SK-channels is caused by voltage-dependent block of intracellular divalent ions, however, a later study identified an intrinsic mechanism of channels causing inward rectification, which is independent of divalent ions [20].

Our patch clamp experiments revealed apamin-sensitive current in the voltage range between −40 to +40 mV when the intracellular Ca^{2+} was buffered to 500 nM. The half-maximal Ca^{2+} concentration for channel activation was reported as 300 nM [21], therefore, this Ca^{2+} concentration is suggested to cause nearly maximal current activation. When intracellular Ca^{2+} was buffered to 500 nM, the apamin-sensitive difference current was monotonously enhanced as the voltage was increased from −60 to + 40 mV. The current-voltage characteristic of the apamin-sensitive current both in terms of absolute current values and voltage-dependence was found to be similar to those that were illustrated in a previous study [13]. This current-voltage characteristic of the I_{SK} may imply that notable

current could be expected above −20 mV, which corresponds to the main repolarization, at the same time it is plausible that marginal current is activated during the maximal diastolic potential. It is underpinned by the fact that modelling and experimental results indicate that intracellular Ca^{2+} level is the highest during early repolarization and considerable decays during the terminal phase of the repolarization [22,23]. Therefore, neither the membrane potential nor the intracellular Ca^{2+} favour I_{SK} activation at the maximal diastolic potential. In line with this, we did not find change in the maximal diastolic potential and any secondary change in the diastolic depolarization. As a negative control, highly buffered cells were used to demonstrate the Ca^{2+} sensitivity of the apamin-sensitive current. In contrast to high depolarization (i.e., +40 mV), apamin-sensitive current was not detected in the absence of free intracellular Ca^{2+}.

For further validation, we analyzed the effect of apamin under a representative SAN action potential waveform without Ca^{2+} chelators in the patch pipette. In contrast to experiments with buffered Ca^{2+}, we found negligible apamin-sensitive current under normal conditions in the presence of dynamic Ca^{2+} changes. Ca^{2+} transient measurements indicated that systolic peak of intracellular Ca^{2+} was barely larger than 500 nM and declined fast, which may induce small I_{SK}. In contrast, when 200 nM isoproterenol was employed, intracellular Ca^{2+} was increased and apamin-sensitive current was considerably larger.

3.3. I_{SK} Has No Role in Sinus-Node Pacemaking under Normal Conditions but Its Inhibition Lengthens APD during Beta-Adrenergic Activation

Under normal conditions, apamin-induced AP alteration was not observed, which is in contrast to a previous report where ~18% cycle length increase was observed after apamin application under normal conditions in mouse SAN cells [13]. This extent of effect is comparable to the effect of I_f inhibition by ivabradine under normal conditions [24]. Similarly, apamin also failed to alter the ECG R-R interval in Langendorff-perfused hearts in our study without adrenergic stimulation. A recent clinical study also reported similar results. Forty-seven healthy male volunteers were examined during AP30663 (I_{SK} inhibitor) administration. AP30663 did not influence the R-R interval, regardless of the applied dose [25]. These results are in line with experiments demonstrating marginal apamin-sensitive current during the action potential in response to dynamic Ca^{2+} changes, under normal conditions.

Activation of the β-adrenoreceptors induces the adenylate-cyclase via stimulatory G-proteins, leading to increased intracellular cyclic AMP (cAMP) level. The elevated cAMP then increases the protein-kinase A level, which phosphorylates the L-type Ca^{2+} channels. The L-type Ca^{2+} channel-phosphorylation increases the Ca^{2+} influx, thus causing a net gain of the intracellular Ca^{2+}. The elevated intracellular Ca^{2+} also increases the CaM/CaMKII axis, which is involved in several Ca^{2+}-dependent processes [26–28]. Experiments demonstrated in Figure 4C,D suggest that the increased intracellular Ca^{2+} increases the current density of the apamin-sensitive current, where inhibition could influence the sinus-node pacemaking. In order to address this issue, the beta-receptor agonist, isoproterenol, was employed.

Application of apamin in the presence of beta-receptor activation caused a ~20% increase in the cycle length, while the slope of the diastolic depolarization was not changed. This result implies that the increase of cycle length after I_{SK} inhibition was attributable to the increased APD, but the diastolic depolarization was not changed. This effect could be attributable to: (i) the current-voltage diagram and apamin-sensitive current during the canonical action potential suggest marginal or no current in the voltage range of diastolic depolarization and (ii) the intracellular Ca^{2+} level is considerably decreased during the diastolic depolarization. In agreement with this result, the ECG R-R intervals of Langendorff-perfused hearts were increased by 12% after apamin administration when beta-receptors were activated.

3.4. I_{SK} inhibition Does Not Increase Cycle Length Variability

The rhythmicity of spontaneous action potential and ECG R-R interval was characterized by the short-term cycle length variability (in the case of action potentials) and short-term R-R variability (in the case of ECG measurements). The coupled-clock hypothesis claims that cycle length variability is an important indicator of the coupling between the Ca^{2+}-clock and the surface membrane ion channels: When the synchronization between the two clocks is strong, the variability is low. Any intervention disrupting the Ca^{2+}-clock and/or the membrane clock attenuates the coupling and leads to increased cycle length and cycle length variability [29]. In this study, neither the cellular measurements nor the isolated heart experiments show a significant increase in the cycle length variability after apamin administration. This result suggests that I_{SK} may not be involved in the ionic mechanism that directly governs the pacemaker mechanism. However, it may also imply that inhibition of I_{SK} under beta-adrenergic activation could be considered a safe intervention to decrease the heart rate.

The effect of apamin was compared to the effect of ivabradine, and it was found that the ECG R-R interval-increasing effect of apamin was 1/3 of the ivabradine (~12 vs. ~30%). This result implies that the significance of I_{SK} in controlling the heart rate is markedly smaller than the I_f; this probably provides extra repolarizing current during beta-adrenergic stimulation, which may increase the flexibility of pacemaking. In contrast, ivabradine also significantly augmented the cycle length variability since I_f is a principal component of the coupled-clock mechanism.

4. Materials and Methods

4.1. Animals

New Zealand white rabbits from both genders weighing 2.0–2.5 kg were used for experiments obtained from a licensed supplier (Innovo Ltd., Budapest, Hungary).

4.2. Cell Isolation

Isolated single SAN cells were obtained by enzymatic dissociation. Rabbits were sacrificed by concussion after intravenous administration of 400 IU/kg heparin. The heart was rapidly removed and placed into a solution containing in mM: 135 NaCl, 4.7 KCl, 1.2 KH_2PO_4, 1.2 $MgSO_4$, 10 HEPES, 4.4 $NaHCO_3$, 10 glucose, and 1.8 $CaCl_2$ (titrated to pH 7.2 with NaOH). The heart was mounted on a cc. 60 cm high modified Langendorff column and was perfused with oxygenated solution at 37 °C. In the initial period, the blood was washed out (3–5 min) from the heart, then it was continuously perfused with nominally Ca^{2+}-free solution until the heart ceased contractions (cca. 10 min). The enzymatic dissociation was performed by using 1.8 mg/mL (260 U/mL) collagenase (type II, Worthington) and 33 μM $CaCl_2$ in the perfusate. After 13–14 min, the heart was taken off the cannula. The right atrium of the heart was cut and the SAN region was excised and cut into small pieces. The strips were placed into enzyme free isolation solution containing 1 mM $CaCl_2$ and equilibrated at 37 °C for 15 min. The cells were separated by filtering through a mesh and were stored at room temperature.

4.3. SK2 Immunocytochemistry

Rabbit sinus node cells were isolated from the sinus-node, then were fixed on glass coverslips with acetone. The cell membrane was labelled Wheat Germ Agglutinin Texas Red-X Conjugate (WGA-TxRed) (ThermoFischer, Waltham, MA, USA; 1:500). After membrane labelling, the samples were blocked for 1 h with PBST (PBS with 0.01% Tween) containing 2.5% BSA at room temperature. SK2 and HCN4 were labelled with anti-KCa2.2 (SK2) (Alomone, Jerusalem, Israel; 1:50) and anti-HCN4 (Alomone; 1:50) primary antibody overnight at 4 °C. Next day, the cells were incubated with Goat anti-Guinea Pig IgG Alexa Fluor 488 secondary antibody (ThermoFischer; 1:500) for 1 h at room temperature. Fluorescent images were captured by an LSM 880 (Zeiss, Oberkochen, Germany) laser scanning

confocal microscope. Images were quantitatively analyzed by ImageJ software. Control samples were incubated with secondary antibody only (No Primary Control).

4.4. Measurement of Apamin-Sensitive Current

The isolated SAN cells were placed in a low volume chamber (RC47FSLP, Warner Instruments, Hamden, CT, USA). Five minutes were allowed for the cells to settle and adhere, and the solution was continuously superfused by a peristaltic pump (C.P.78012-45, Ismatec, Zurich, Switzerland). Patch-pipettes were created from borosilicate glass capillaries using a P-97 microelectrode puller (Sutter Instruments, Novato, CA, USA), having a tip resistance between 1.5–2.5 MΩ. Ionic currents were recorded by using Axopatch 200B amplifier (Molecular Devices, Sunnyvale, CA, USA). Membrane currents were digitalized by Digidata 1550B (Molecular Devices, Sunnyvale, CA, USA) with 250 kHz under software control (pClamp 10.0, Molecular Devices, Sunnyvale, CA, USA). The temperature of the measurements was kept at 37 °C by using TC-344B temperature controller (Warner Instruments, USA).

Apamin-sensitive current was measured by rectangular voltage pulses, or by representative SAN action potential waveform. Rectangular voltage steps before and after 100 nM apamin application were employed from a holding potential of −60 mV. The membrane was depolarized to 50 mV for 500 ms by using 10 mV voltage steps. The internal solution contained (in mM): KCl 40, K_2ATP 5, HEPES 10, $MgCl_2$ 5, and GTP 0.1 and was titrated to pH 7.2 by using KOH. The free Ca^{2+} concentration in the pipette solution was set to 500 nM by using an appropriate mixture of EGTA and $CaCl_2$ (calculated by the Maxchelator software). In experiments where the intracellular Ca^{2+} was highly buffered, we used 10 mM BAPTA without applying $CaCl_2$ in the pipette. The composition of the external solution was (in mM): NaCl 144, NaH_2PO_4 0.4, KCl 4, $MgSO_4$ 0.53, $CaCl_2$ 1.8, HEPES 5, glucose 5.5, titrated to pH 7.4 with NaOH.

In another set of experiments, the cells were paced using a canonical AP waveform by the average of 10 independent action potentials from previously recorded perforated patch clamp experiments. The parameters of this representative AP waveform were: cycle length: 410 ms, AP duration: 180 ms, maximal diastolic potential: −57 mV, overshoot: 24 mV, and diastolic depolarization slope: 0.124 mV/ms. Two experimental groups were established. In the first group, the current was recorded first in normal Tyrode's solution (as previously described) as the control current, then 100 nM apamin was applied. In the other experimental group, the solutions were supplemented with 200 nM isoproterenol to enhance the intracellular Ca^{2+} of the SAN cells. Apamin-sensitive current was determined as a difference current. The pipette solution was as previously described without chelators.

4.5. Measurement of Ca^{2+} Transients

Ca^{2+} transients were measured from spontaneously active isolated SAN cells. Cells were loaded with Fluo-4 AM (5 μM) fluorescent dye. The isolated cells were kept in darkness at room temperature and were loaded with the dye for 20 min. Fluorescence measurements were performed on the stage of an Olympus IX 71 inverted fluorescence microscope. The dye was excited at 480 nm and the emitted fluorescence was detected at 535 nm. Optical signals were sampled at 1 kHz and recorded by a photon counting photomultiplier (Hamamatsu, model H7828; Hamamatsu Photonics Deutschland GmbH, Herrsching am Ammersee, Germany). Optical signal was converted to voltage using photon-voltage converter (Ionoptix, Westwood, MA, USA) and analyzed by pClamp 10.0 (Molecular Devices, Sunnyvale, CA, USA). Spontaneously and rhythmically contracting cells were chosen, therefore, no external pacing was needed to record Ca^{2+} transients. Amplitudes of the measured Ca^{2+} transients were calculated as differences between systolic and diastolic values. To obtain maximal fluorescence (Fmax), the cells were damaged by a patch pipette at the end of the experiment. Ca^{2+} was calibrated using the following formula: Kd(F-Fmin)/(Fmax-F). The Kd of the Fluo-4 AM was set to 335 nM. The extracellular solution was normal Tyrode's solution as was previously described.

4.6. Action Potential Measurements from Single Cells by Current Clamp Configuration

Action potentials were measured from spontaneously beating sinus-node cells by using the perforated patch-clamp technique as was described in a previous study [30]. Normal Tyrode's solution was applied, containing (in mM): 144 NaCl, 0.4 NaH_2PO_4, 4 KCl, 0.53 $MgSO_4$, 1.8 $CaCl_2$, 5.5 glucose, and 5 HEPES, titrated to pH 7.4 with NaOH. The microelectrodes were filled with a solution that contained (in mM): 120 K-gluconate, 2.5 NaCl, 2.5 MgATP, 2.5 Na_2ATP, 5 HEPES, 20 KCl, titrated to pH 7.2 with KOH. 35 μM β-escin was employed in the pipette solution to achieve the membrane patch perforation.

The parameters of the APs were calculated as follows:

(a) Maximum diastolic potential (MDP) was defined as the most negative potential before the next AP depolarization.
(b) Take off potential (TOP) was calculated as the voltage measured at the time when the voltage derivative exceeded 0.5 mV/ms.
(c) The slope of diastolic depolarization was defined as the mean voltage derivative of the AP between MDP and take off potential.
(d) Action potential duration (APD) was obtained as the time interval between TOP and the next MDP.
(e) Cycle length was calculated between the peaks of two consecutive APs.
(f) All experiments in this study were carried out at 37 °C.

4.7. Langendorff-Perfusion Measurements on Isolated Hearts

ECG of isolated rabbit hearts were obtained in Langendorff-perfused hearts as described before [31]. Rabbits were sacrificed by concussion after 400 IU heparin were injected intravenously. The excised hearts were mounted by the aorta on a Langendorff-apparatus and retrogradely perfused with modified Krebs-Henseleit bicarbonate buffer (KHB) at a constant pressure (80 Hgmm). The KHB solution contained (in mM): NaHCO3 25; KCl 4.3; NaCl 118.5; MgSO4 1.2; KH2PO4 1.2; glucose 10; CaCl2 1.8, having a pH of 7.4 ± 0.05 when gassed with 95% O_2 + 5% CO_2.

The electrical activity as electrocardiogram (ECG) was obtained by the three lead custom-made electrodes and signal amplifier (Experimetria Ltd., Budapest, Hungary). Signal processing and analysis was carried out using HaemoSys (Experimetria Ltd., Budapest, Hungary).

4.8. Statistics

Normal distribution of the data was verified by using Shapiro–Wilk test. Statistical significance ($p < 0.05$) was assessed using Student's *t*-test and repeated measures ANOVA depending on the experiment. Data are presented as means ±S.E.M.

5. Conclusions

Our results indicate that I_{SK} has no or very limited role in SAN pacemaking under basal condition, however, it may contribute to the repolarization under beta-adrenergic activation. Selective inhibition of I_{SK} induces a moderate cycle length increase, with the latter effect being attributed to the lengthening of APD. Further in-vitro and in-vivo studies are required to estimate the possible therapeutic potential of I_{SK} inhibition as a supportive heart-rate-reducing agent.

Author Contributions: Conceptualization, N.N. and A.V.; methodology, N.N.; investigation, G.B., N.T., S.D., J.S. and Z.K.; resources, N.N. and A.V.; data curation, G.B., N.T. and N.N.; writing—original draft preparation, N.N.; writing—review and editing, N.T. and A.V.; visualization, N.N.; funding acquisition, N.T., A.V. and N.N. All authors have read and agreed to the published version of the manuscript.

Funding: This research was funded by the National Research Development and Innovation Office (FK-129117 to N.N.) and the Ministry for Innovation and Technology (ÚNKP-21-3-SZTE-106 to N.T.).

Institutional Review Board Statement: All experiments were conducted in compliance with the Guide for the Care and Use of Laboratory Animals (USA NIH publication No 85-23, revised 1996) and conformed to Directive 2010/63/EU of the European Parliament. The protocols were approved by the Review Board of the Department of Animal Health and Food Control of the Ministry of Agriculture and Rural Development, Hungary (XIII./1211/2012).

Informed Consent Statement: Not applicable.

Data Availability Statement: Data is contained within the article.

Conflicts of Interest: The authors declare no conflict of interest. The funders had no role in the design of the study; in the collection, analyses, or interpretation of data; in the writing of the manuscript, or in the decision to publish the results.

References

1. Meech, R.W.; Standen, N.B. Calcium-mediated potassium activation in Helix neurones. *J. Physiol.* **1974**, *237*, 43–44.
2. Eisner, D.A.; Vaughan-Jones, R.D. Do calcium-activated potassium channels exist in the heart? *Cell Calcium* **1983**, *4*, 371–863. [CrossRef]
3. Xu, Y.; Tuteja, D.; Zhang, Z.; Xu, D.; Zhang, Y.; Rodriguez, J.; Nie, L.; Tuxson, H.R.; Young, J.N.; Glatter, K.A.; et al. Molecular identification and functional roles of a Ca$^{(2+)}$-activated K$^+$ channel in human and mouse hearts. *J. Biol. Chem.* **2003**, *278*, 49085–49094. [CrossRef]
4. Chua, S.K.; Chang, P.C.; Maruyama, M.; Turker, I.; Shinohara, T.; Shen, M.J.; Chen, Z.; Shen, C.; Rubart-von der Lohe, M.; Lopshire, J.C.; et al. Small-conductance calcium-activated potassium channel and recurrent ventricular fibrillation in failing rabbit ventricles. *Circ. Res.* **2011**, *108*, 971–979. [CrossRef] [PubMed]
5. Kirchhoff, J.E.; Diness, J.G.; Sheykhzade, M.; Grunnet, M.; Jespersen, T. Synergistic antiarrhythmic effect of combining inhibition of Ca^{2+}-activated K$^+$ (SK) channels and voltage-gated Na$^+$ channels in an isolated heart model of atrial fibrillation. *Heart Rhythm* **2015**, *12*, 409–418. [CrossRef]
6. Nattel, S. Calcium-activated potassium current: A novel ion channel candidate in atrial fibrillation. *J. Physiol.* **2009**, *587*, 1385–1386. [CrossRef] [PubMed]
7. Yin, D.; Chen, M.; Yang, N.; Wu, A.Z.; Xu, D.; Tsai, W.C.; Yuan, Y.; Tian, Z.; Chan, Y.H.; Shen, C.; et al. Role of apamin-sensitive small conductance calcium-activated potassium currents in long-term cardiac memory in rabbits. *Heart Rhythm* **2018**, *15*, 761–769. [CrossRef] [PubMed]
8. Chan, Y.H.; Tsai, W.C.; Ko, J.S.; Yin, D.; Chang, P.C.; Rubart, M.; Weiss, J.N.; Everett, T.H.t.; Lin, S.F.; Chen, P.S. Small-Conductance Calcium-Activated Potassium Current Is Activated During Hypokalemia and Masks Short-Term Cardiac Memory Induced by Ventricular Pacing. *Circulation* **2015**, *132*, 1377–1386. [CrossRef] [PubMed]
9. Chen, M.; Xu, D.Z.; Wu, A.Z.; Guo, S.; Wan, J.; Yin, D.; Lin, S.F.; Chen, Z.; Rubart-von der Lohe, M.; Everett, T.H.t.; et al. Concomitant SK current activation and sodium current inhibition cause J wave syndrome. *JCI Insight* **2018**, *3*, e122329. [CrossRef] [PubMed]
10. Skibsbye, L.; Poulet, C.; Diness, J.G.; Bentzen, B.H.; Yuan, L.; Kappert, U.; Matschke, K.; Wettwer, E.; Ravens, U.; Grunnet, M.; et al. Small-conductance calcium-activated potassium (SK) channels contribute to action potential repolarization in human atria. *Cardiovasc. Res.* **2014**, *103*, 156–167. [CrossRef]
11. Nagy, N.; Szuts, V.; Horváth, Z.; Seprényi, G.; Farkas, A.S.; Acsai, K.; Prorok, J.; Bitay, M.; Kun, A.; Pataricza, J.; et al. Does small-conductance calcium-activated potassium channel contribute to cardiac repolarization? *J. Mol. Cell. Cardiol.* **2009**, *47*, 656–663. [CrossRef]
12. Chen, W.T.; Chen, Y.C.; Lu, Y.Y.; Kao, Y.H.; Huang, J.H.; Lin, Y.K.; Chen, S.A.; Chen, Y.J. Apamin modulates electrophysiological characteristics of the pulmonary vein and the Sinoatrial Node. *Eur. J. Clin. Investig.* **2013**, *43*, 957–963. [CrossRef] [PubMed]
13. Torrente, A.G.; Zhang, R.; Wang, H.; Zaini, A.; Kim, B.; Yue, X.; Philipson, K.D.; Goldhaber, J.I. Contribution of small conductance K$^+$ channels to sinoatrial node pacemaker activity: Insights from atrial-specific Na$^+$/Ca^{2+} exchange knockout mice. *J. Physiol.* **2017**, *595*, 3847–3865. [CrossRef] [PubMed]
14. Kohajda, Z.; Loewe, A.; Toth, N.; Varro, A.; Nagy, N. The Cardiac Pacemaker Story-Fundamental Role of the Na$^+$/Ca^{2+} Exchanger in Spontaneous Automaticity. *Front. Pharmacol.* **2020**, *11*, 516. [CrossRef] [PubMed]
15. Lakatta, E.G.; Maltsev, V.A.; Vinogradova, T.M. A coupled SYSTEM of intracellular Ca2+ clocks and surface membrane voltage clocks controls the timekeeping mechanism of the heart's pacemaker. *Circ. Res.* **2010**, *106*, 659–673. [CrossRef]
16. Komajda, M.; Isnard, R.; Cohen-Solal, A.; Metra, M.; Pieske, B.; Ponikowski, P.; Voors, A.A.; Dominjon, F.; Henon-Goburdhun, C.; Pannaux, M.; et al. Effect of ivabradine in patients with heart failure with preserved ejection fraction: The EDIFY randomized placebo-controlled trial. *Eur. J. Heart Fail.* **2017**, *19*, 1495–1503. [CrossRef]
17. DeWitt, C.R.; Waksman, J.C. Pharmacology, pathophysiology and management of calcium channel blocker and beta-blocker toxicity. *Toxicol. Rev.* **2004**, *23*, 223–238. [CrossRef] [PubMed]
18. Adelman, J.P.; Maylie, J.; Sah, P. Small-conductance Ca^{2+}-activated K$^+$ channels: Form and function. *Annu. Rev. Physiol.* **2012**, *74*, 245–269. [CrossRef] [PubMed]

19. Lamy, C.; Goodchild, S.J.; Weatherall, K.L.; Jane, D.E.; Liégeois, J.F.; Seutin, V.; Marrion, N.V. Allosteric block of $K_{Ca}2$ channels by apamin. *J. Biol. Chem.* **2010**, *285*, 27067–27077. [CrossRef] [PubMed]
20. Li, W.; Aldrich, R.W. Electrostatic influences of charged inner pore residues on the conductance and gating of small conductance Ca^{2+} activated K^+ channels. *Proc. Natl. Acad. Sci. USA* **2011**, *108*, 5946–5953. [CrossRef] [PubMed]
21. Xia, X.M.; Fakler, B.; Rivard, A.; Wayman, G.; Johnson-Pais, T.; Keen, J.E.; Ishii, T.; Hirschberg, B.; Bond, C.T.; Lutsenko, S.; et al. Mechanism of calcium gating in small-conductance calcium-activated potassium channels. *Nature* **1998**, *395*, 503–507. [CrossRef]
22. Kohajda, Z.; Toth, N.; Szlovak, J.; Loewe, A.; Bitay, G.; Gazdag, P.; Prorok, J.; Jost, N.; Levijoki, J.; Pollesello, P.; et al. Novel Na^+/Ca^{2+} Exchanger Inhibitor ORM-10962 Supports Coupled Function of Funny-Current and Na^+/Ca^{2+} Exchanger in Pacemaking of Rabbit Sinus Node Tissue. *Front. Pharmacol.* **2019**, *10*, 1632. [CrossRef] [PubMed]
23. Tsutsui, K.; Monfredi, O.J.; Sirenko-Tagirova, S.G.; Maltseva, L.A.; Bychkov, R.; Kim, M.S.; Ziman, B.D.; Tarasov, K.V.; Tarasova, Y.S.; Zhang, J.; et al. A coupled-clock system drives the automaticity of human sinoatrial nodal pacemaker cells. *Sci. Signal.* **2018**, *11*, eaap7608. [CrossRef] [PubMed]
24. Du, X.-J.; Feng, X.; Gao, X.-M.; Tan, T.P.; Kiriazis, H.; Dart, A.M. I(f) channel inhibitor ivabradine lowers heart rate in mice with enhanced sympathoadrenergic activities. *Br. J. Pharmacol.* **2004**, *142*, 107–112. [CrossRef] [PubMed]
25. Gal, P.; Klaassen, E.S.; Bergmann, K.R.; Saghari, M.; Burggraaf, J.; Kemme, M.J.B.; Sylvest, C.; Sørensen, U.; Bentzen, B.H.; Grunnet, M.; et al. First Clinical Study with AP30663—A $K_{Ca}2$ Channel Inhibitor in Development for Conversion of Atrial Fibrillation. *Clin. Transl. Sci.* **2020**, *13*, 1336–1344. [CrossRef]
26. Vinogradova, T.M.; Bogdanov, K.Y.; Lakatta, E.G. beta-Adrenergic stimulation modulates ryanodine receptor Ca^{2+} release during diastolic depolarization to accelerate pacemaker activity in rabbit sinoatrial nodal cells. *Circ. Res.* **2002**, *90*, 73–79. [CrossRef] [PubMed]
27. Bucchi, A.; Baruscotti, M.; Robinson, R.B.; DiFrancesco, D. Modulation of rate by autonomic agonists in SAN cells involves changes in diastolic depolarization and the pacemaker current. *J. Mol. Cell. Cardiol.* **2007**, *43*, 39–48. [CrossRef] [PubMed]
28. Bucchi, A.; Baruscotti, M.; DiFrancesco, D. Current-dependent block of rabbit sino-atrial node I(f) channels by ivabradine. *J. Gen. Physiol.* **2002**, *120*, 1–13. [CrossRef] [PubMed]
29. Yaniv, Y.; Sirenko, S.; Ziman, B.D.; Spurgeon, H.A.; Maltsev, V.A.; Lakatta, E.G. New evidence for coupled clock regulation of the normal automaticity of sinoatrial nodal pacemaker cells: Bradycardic effects of ivabradine are linked to suppression of intracellular Ca^{2+} cycling. *J. Mol. Cell. Cardiol.* **2013**, *62*, 80–89. [CrossRef] [PubMed]
30. Lyashkov, A.E.; Behar, J.; Lakatta, E.G.; Yaniv, Y.; Maltsev, V.A. Positive Feedback Mechanisms among Local Ca Releases, NCX, and I(CaL) Ignite Pacemaker Action Potentials. *Biophys. J.* **2018**, *114*, 1176–1189. [CrossRef] [PubMed]
31. Szepesi, J.; Acsai, K.; Sebok, Z.; Prorok, J.; Pollesello, P.; Levijoki, J.; Papp, J.G.; Varro, A.; Toth, A. Comparison of the efficiency of Na^+/Ca^{2+} exchanger or Na^+/H^+ exchanger inhibition and their combination in reducing coronary reperfusion-induced arrhythmias. *J. Physiol. Pharmacol.* **2015**, *66*, 215–226. [PubMed]

II.

scientific reports

Check for updates

OPEN

The development of L-type Ca^{2+} current mediated alternans does not depend on the restitution slope in canine ventricular myocardium

Noémi Tóth[1], Jozefina Szlovák[1], Zsófia Kohajda[2], Gergő Bitay[1], Roland Veress[3], Balázs Horváth[3,4], Julius Gy. Papp[1,2], András Varró[1,2,5] & Norbert Nagy[1,2]✉

Cardiac alternans have crucial importance in the onset of ventricular fibrillation. The early explanation for alternans development was the voltage-driven mechanism, where the action potential (AP) restitution steepness was considered as crucial determining factor. Recent results suggest that restitution slope is an inadequate predictor for alternans development, but several studies still claim the role of membrane potential as underlying mechanism of alternans. These controversial data indicate that the relationship of restitution and alternans development is not completely understood. APs were measured by conventional microelectrode technique from canine right ventricular papillary muscles. Ionic currents combined with fluorescent measurements were recorded by patch-clamp technique. APs combined with fluorescent measurements were monitored by sharp microelectrodes. Rapid pacing evoked restitution-independent AP duration (APD) alternans. When non-alternating AP voltage command was used, Ca^{2+}_i-transient (CaT) alternans were not observed. When alternating rectangular voltage pulses were applied, CaT alternans were proportional to I_{CaL} amplitude alternans. Selective I_{CaL} inhibition did not influence the fast phase of APD restitution. In this study we found that I_{CaL} has minor contribution in shaping the fast phase of restitution curve suggesting that I_{CaL}—if it plays important role in the alternans mechanism—could be an additional factor that attenuates the reliability of APD restitution slope to predict alternans.

Cardiac alternans refer to a regular beat-to-beat oscillation of the ECG T-waves caused by parallel alternans of the AP and the CaT at the cellular level[1,2]. It is generally accepted that alternans are associated with arrhythmogenesis and were identified as a suitable predictor of sudden cardiac death[3,4]. Large body of evidence demonstrated that cardiac alternans are complex phenomenon, where mutual crosstalk of the membrane potential changes and alterations of the intracellular Ca^{2+} play a key role in the development of alternans (for review[5–7]). At the same time, it is uncertain whether the AP or the intracellular Ca^{2+} initialize and govern alternans.

Regarding the underlying mechanism of alternans, two major concepts have been emerged: voltage-driven and Ca^{2+}-driven alternans. Growing body of recent evidence indicate the importance of Ca^{2+} handling in the development of alternans. *Ca^{2+}-driven alternans* were originally suggested to develop as a result of release-reuptake mismatch following steep dependence of sarcoplasmic reticulum (SR) release on loading[7,8], and later the refractory state of the ryanodine receptor was assumed as the underlying mechanism[9]. Third possibility is the refractoriness of the Ca^{2+} cycling proteins that arises from the combination of steep load-release relationship, and refractoriness of the SR release[10]. Recent evidence indicates the '3R-theory' that claims the alternans rises via an instability caused by interactions between three critical properties: randomness of Ca^{2+} sparks, recruitment of Ca^{2+} sparks by neighboring Ca^{2+} release units (CRU), and refractoriness of CRUs[11,12]. An important milestone of the Ca^{2+}-driven hypothesis was several reports demonstrating that CaT alternans can be evoked in the presence of non-alternating AP sequence[13–16].

[1]Department of Pharmacology and Pharmacotherapy, Faculty of Medicine, University of Szeged, Dóm tér 12, P.O. Box 427, 6720 Szeged, Hungary. [2]ELKH-SZTE Research Group of Cardiovascular Pharmacology, Szeged, Hungary. [3]Department of Physiology, Faculty of Medicine, University of Debrecen, Debrecen, Hungary. [4]Faculty of Pharmacy, University of Debrecen, Debrecen, Hungary. [5]Department of Pharmacology and Pharmacotherapy, Interdisciplinary Excellence Centre, University of Szeged, Szeged, Hungary. ✉email: nagy.norbert@med.u-szeged.hu

The concept of *voltage-driven alternans* represents an early explanation for the underlying mechanism of alternans development. A general view is that the voltage-driven alternans are governed by the restitution slope, i.e. alternans are expected to develop when the slope of AP duration-diastolic interval (APD-DI) function is larger than 1[17]. This means that restitution-hypothesis—which was originally proposed by Nolasco and Dahlen[17]—represents an ultimate underlying factor of the voltage-driven alternans[1,5,7].

The restitution hypothesis was challenged by several laboratories[1,18], at the same time there are experimental and modeling papers claiming important role of membrane voltage in the development of alternans[19–22]. This discrepancy suggests that the relationship of restitution and alternans is not completely understood and requires further investigations.

Methods

Ethical statement. All experiments were conducted in compliance with the *Guide for the Care and Use of Laboratory Animals* (USA NIH publication No 85-23, revised 1996) and conformed to Directive 2010/63/EU of the European Parliament. The protocols were approved by the Review Board of the Department of Animal Health and Food Control of the Ministry of Agriculture and Rural Development, Hungary (XIII./1211/2012). Animal studies were carried out in compliance of ARRIVE guidelines.

Determination of the action potential parameters in canine multicellular papillary muscle. Beagle dogs (obtained from a licensed supplier, licence number: XXXV./2018) from both sex weighing 10–15 kg were used for conventional microelectrode experiments. The animals were anesthetized and sacrificed with pentobarbital (60 mg/kg iv), then the heart was removed through a right lateral thoracotomy.

APs were recorded at 37 °C from the surface of right ventricular papillary muscles using conventional microelectrode technique. For measuring tissue APs similar protocol was applied as described earlier with minor modifications[23,24]. Briefly, the preparations were mounted in a custom made Plexiglas chamber, allowing continuous super-fusion with Locke's solution (130 mM NaCl, 21.5 mM $NaHCO_3$, 4.5 mM KCl, 12 mM glucose, 0.4 mM $MgCl_2$, 1.8 mM $CaCl_2$, ph 7.35 ± 0.05) and stimulated with constant pulses of 5 ms duration at a rate of 1 Hz through a pair of bipolar platinum electrodes using an electro-stimulator (EX-ST-A2, Experimetria Ltd). Sharp microelectrodes with tip resistance of 10–20 MΩ, when filled with 3 M KCl, were connected to an amplifier (Biologic Amplifier, model VF 102). Voltage output from the amplifier was sampled using an AD converter (NI 6025, Unisip Ltd). APs were monitored and evaluated by using Evokewave v1.49 (Unisip Ltd).

APD alternans protocol. APD alternans were measured by rapid pacing using cycle lengths of 250-230-210-190-160 ms. 20 consecutive stimuli were used at each frequency. APD differences were calculated between long and short AP pairs along at least 6 consecutive pulses at 25, 50 and 90% of repolarization ($APD_{25,}$ APD_{50} and APD_{90}, respectively) and were averaged providing APD alternans amplitude.

Conventional S1S2 restitution protocol. The basic cycle length (BCL) was 1000 and 500 ms. Extra delays for S2 stimuli ranged from − 50 to 1000 ms related to the baseline APD_{90}. 15 consecutive stimuli were applied (S1) between all S2 stimuli. Diastolic intervals (DI) refer to the proximity of S2 stimuli (extra beat) to the APD_{90} of the basic beat evoked by S1.

Dynamic restitution protocol. Following a pre-pacing at 1 Hz, the basic cycle length was gradually decreased from 1000 to 500 ms by 100 ms steps, from 500 to 300 ms by 50 ms steps. When the cycle length reached the 250 ms the action potential started to alternate and the AP alternation was constantly maintained from 250 to 160 ms. In this cycle length interval, we applied the previously described cycle length pattern for alternans. During these measurements the APD_{90} was plotted against the preceding diastolic interval at each cycle length.

Previous study reported that standard S1S2 restitution method is not suitable tool to predict alternans since the slope in most cases < 1[25]. However, we observed restitution slopes larger and smaller than 1 in approximately 50–50% of our experiments, providing an average value of 1.12 ± 0.1 (BCL: 1000 ms; n = 20) and 1.08 ± 0.1 (BCL: 500 ms; n = 20). Therefore, we considered standard S1S2 restitution protocol as an appropriate tool to assess restitution slope.

Voltage-clamp measurements combined with fluorescent recordings. The isolation of canine left ventricular cardiomyocytes of Beagle dogs' hearts was performed as described previously[26]. In brief, cardiac myocytes were isolated from the left ventricle, containing an arterial branch through which the segment was perfused on a Langendorff apparatus with solutions in the following sequence: normal isolation solution (containing in mM: 135 mM NaCl, 4.7 mM KCl, 1.2 mM KH_2PO_4, 1.2 mM $MgSO_4$, 1 mM $CaCl_2$, 10 mM Glucose, 10 mM HEPES, 20 mM taurine, 4.4 mM $NaHCO_3$, 5 mM Na-pyruvic acid, pH 7.2 adjusted with NaOH) for 10 min, Ca^{2+}-free isolation solution for 10 min and isolation solution containing collagenase (Worthington type II, 0.66 mg/mL) and 33 µM $CaCl_2$. To the final perfusion solution protease (type XIV, 0.12 mg/mL) was added at the 15th minutes for digestion. The isolated cardiomyocytes were loaded with Fluo-4-AM (1–2 µM, Molecular Probes, USA; AM is the membrane permeable acetoxymethyl ester conjugated form of the dye) for 20 min at room temperature in dark. The loaded cells were placed in a low volume imaging chamber (RC47FSLP, Warner Instruments, USA), and the cells were then continuously perfused with normal Tyrode solution at 37 °C (1 mL/min). Data acquisition and analysis were performed using Axon Digidata 1550B System (Molecular Devices, Sunnyvale, CA, USA). Parallel with the current measurements, the fluorescent recordings were performed on a stage of an inverted fluorescent microscope (IX71, Olympus, Japan) and the signal was recorded by a photomul-

tiplier module (H7828, Hamamatsu, Japan), sampled at 1 kHz. Data acquisition and analysis were (both current and Ca^{2+} transient) performed using the pClamp 11.0 software (Molecular Devices, Sunnyvale, CA, USA).

Calcium alternans were based on six consecutive CaTs, where the average CaT amplitude was computed for even and odd beats. The amplitude of a single CaT was estimated as the difference between the peak and the minimum directly preceding the first analyzed CaT (i.e., it is the CaT upstroke amplitude).

Parallel measurement of AP and CaT with current clamp technique. Single cell AP measurements were performed as described previously[27]. Rod-shaped viable ventricular cardiomyocytes, showing clear striation, were placed in a 1 ml volume experimental chamber mounted on the stage of an inverted microscope (Nikon Diaphot 300; Nikon Co., Tokyo, Japan). After sedimentation, cardiomyocytes were continuously superfused with at 37 °C Tyrode solution at a rate of 1–2 mL/min. Cells were impaled with 3 M KCl filled conventional borosilicate microelectrodes having tip resistances between 20 and 40 MΩ, connected to the input of a Multiclamp 700A amplifier (Molecular Devices, Sunnyvale, CA, USA). Action potentials (AP) were elicited through these intracellular electrodes by applying 2 ms wide rectangular current pulses having amplitudes of twice the diastolic threshold. The membrane potential signal was digitalized at 50 kHz using Digidata 1440A A/D card, recorded with pClamp 10 software (both from Molecular Devices) and stored for later analysis. APs were recorded at pacing cycle lengths of 1000, 500, 300, 250, 230, 210 ms in this respective order. Cardiomyocytes were loaded with 5 μM Fura-2 AM for 30 min at room temperature in a Pluronic F-127 containing Tyrode solution. 25 mg Pluronic F-127 was dissolved in 1 mL DMSO and this solvent was used to make a Fura-2 AM stock solution of 1 mM. After loading, the cells were washed twice with Tyrode solution, and were allowed to rest for 30 min at room temperature to de-esterify the dye, and then they were stored at 15 °C before the experiments. Fluorescence was measured using an alternating dual beam excitation fluorescence photometry setup (RatioMaster; Photon Technology International, New Brunswick, NJ, USA) coupled to the inverted microscope. Fluorescence signals of Ca^{2+}-bound and Ca^{2+}-free Fura-2 dye were detected at excitation wavelengths of 340 nm (F_{340}) and 380 nm (F_{380}), respectively. Emitted photons were detected at 510 nm with an R1527P photomultiplier tube (Hamamatsu Photonics K.K., Hamamatsu, Japan). This signal was digitalized at 200 Hz using the FelixGX software (Photon Technology International) and stored for offline analysis. Background fluorescence was measured by moving the cell out of the field of view, and it was subtracted from total fluorescence in order to obtain fluorescence originating exclusively from the preparation. Fluorescence ratio of F_{340}/F_{380} was used to assess intracellular Ca^{2+} transients (CaT). The CaT was recorded in parallel with AP and CL.

Measurement of I_{CaL}. The L-type calcium current (I_{CaL}) was recorded in HEPES-buffered Tyrode's solution, supplemented with 3 mM 4-aminopyridine under perforated patch (Fig. 2) or whole-cell configuration (Fig. 3).

To obtain *I_{CaL} current and alternans* (Fig. 3), 3 separated voltage protocols were used. In all protocols, the current was activated by voltage steps to 0 mV after a 25 ms long prepulse at − 40 mV. The voltage protocols differed in the length of consecutive voltage pulses used to evoke I_{CaL}: (1) 140/80 ms (2) 180/40 ms (3) 200/20 ms. The holding potential was − 80 mV, the basic cycle length was 220 ms in all cases. The cells were loaded with Fluo-4-AM fluorescent dye, and the experiments were performed by perforated patch technique with a pipette solution containing (in mM): 120 K-gluconate, 2.5 NaCl, 2.5 MgATP, 2.5 Na_2ATP, 5 HEPES, 20 KCl, titrated to pH 7.2 with KOH. During perforated patch-clamp experiments 50 μM β-escin was added to the pipette solution. I_{CaL} current measurements with buffered $Ca^{2+}{}_i$ (10 mM EGTA) were performed with whole cell configuration with pipette solution containing (in mM): 125 CsCl, 20 TEACl, 5 MgATP, 10 HEPES, 10 NaCl titrated to 7.2 with CsOH.

Recovery characteristic of I_{CaL} was obtained by activation of the I_{CaL} current by rectangular pulses from a holding potential of − 80 mV to 0 mV for 400 ms. Subsequently interpulse intervals were used from 25 to 500 ms before the second rectangular pulse that was identical with the initial pulse. The I_{CaL} recovery was calculated by comparing the initial I_{CaL} peaks evoked by the initial pulse with I_{CaL} pulse elicited by the second pulse, and were plotted against the corresponding interpulse intervals. During these experiments the Ca^{2+} handling was intact. The cells were loaded with Fluo-4-AM fluorescent dye, and experiments were performed by whole-cell patch-clamp technique.

All chemicals were purchased from Sigma (USA). All experiments were carried out at 37 °C.

Statistics. Normal distribution of the data was verified by using Shapiro–Wilk test. Statistical significance ($p < 0.05$) was assessed using Student's t-test. Data are presented as mean ± S.E.M.

Results

Action potential alternans and restitution measurements in intact subendocardial right ventricular papillary muscle. In the first set of experiments APD restitution (S1S2 protocol) and APD alternans protocol were measured and compared from the same intact subendocardial tissue (right ventricular papillary muscle). Figure 1 represents the summary of 20 experiments (from 11 dogs) of control S1S2 restitution—alternans experiments. Figure 1a illustrates the applied S1S2 restitution protocol. The S1S2 restitution was recorded at BCL of 1000 then 500 ms. The APD alternans amplitude was defined from at least 6 consecutive, regular short-long APs at APD_{90}, APD_{50} and APD_{25} as APD difference. Alternans could be evoked in all cases ($n = 20$) with clear threshold, i.e. when the pacing length became equal or shorter than 250 ms (action potential waveforms can be seen in Supplementary Fig. S1). When AP alternans developed, they were maintained during the entire pacing protocol without any decline in the magnitude of APD oscillation.

Figure 1b represents comparisons between restitution slopes and the corresponding magnitude of APD alternans. Left side of the panel represents S1S2 restitutions at BCL of 500 ms, right side illustrates restitutions at 1000 ms (restitution was analyzed at APD_{90} level). Alternans measured at 210 ms cycle length (odd columns) and

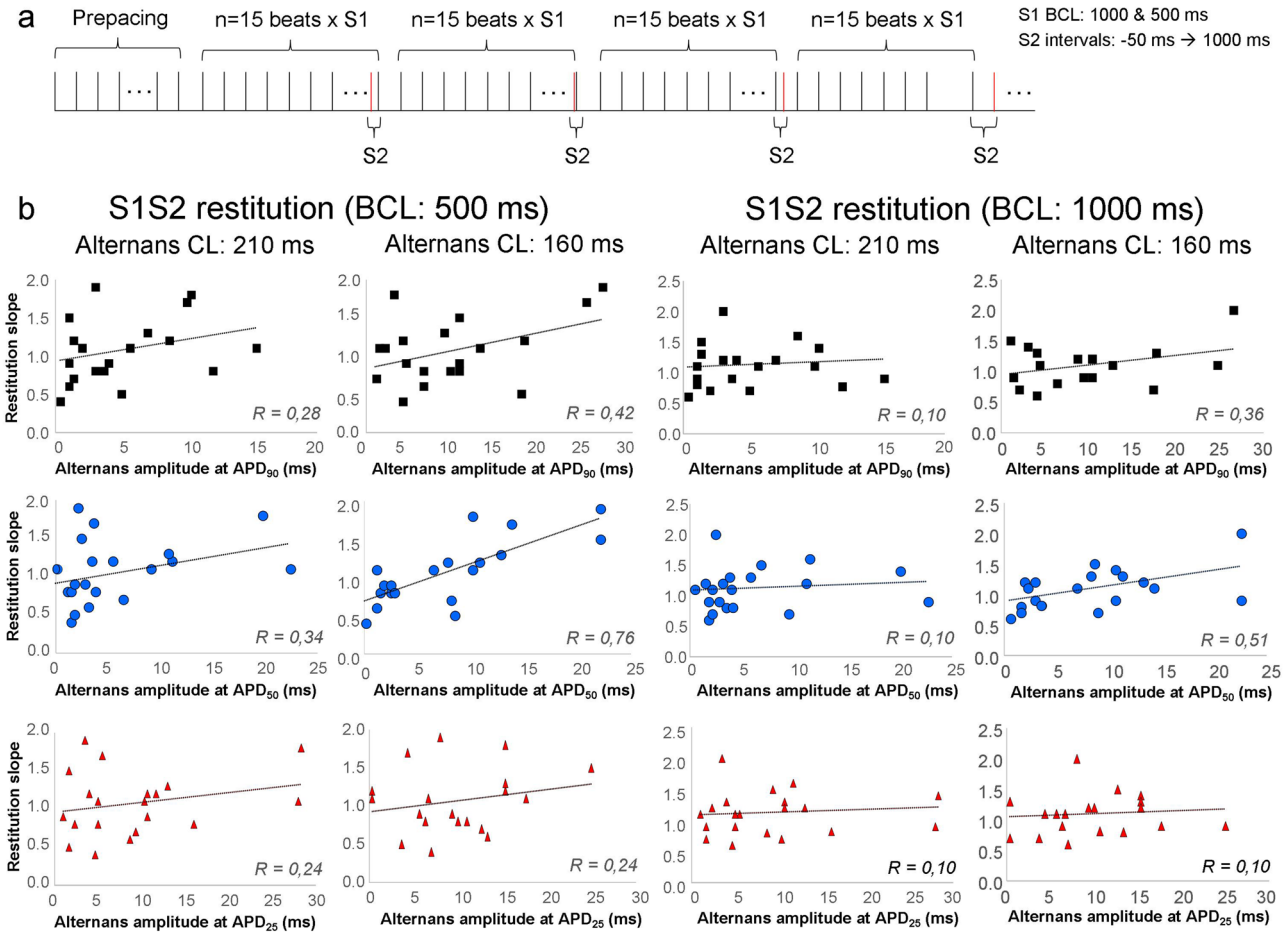

Figure 1. Relationship between action potential alternans and S1S2 restitution. **(a)** Illustrates the applied protocol for S1S2 restitution. The basic cycle length for restitution was 1000 and 500 ms. The diastolic intervals increased from − 50 to 1000 ms (relative to APD_{90}) and the slope of APD_{90} restitution was calculated at both 500 and 1000 ms BCLs. After the restitution protocols, alternans were measured from a cycle length of 250 ms to 160 ms. The magnitude of alternans was measured at APD_{90}, APD_{50}, and APD_{25}. **(b)** Demonstrates correlation tests between S1S2 restitution slope and alternans. The left 6 panels show S1S2 restitutions at BCL of 500 ms, in the right 6 panels the BCL was 1000 ms. The first row demonstrates alternans at APD_{90} level, middle row at APD_{50}, bottom row at APD_{25}. Our results indicate that alternans developed even if the restitution slope was smaller than 1, furthermore, data show mainly weak and in some cases moderate correlations between variables.

160 ms (even columns) were highlighted. The first row represents alternans amplitudes measured at APD_{90} level, middle row shows alternans recorded at APD_{50} level, and bottom row illustrates alternans at 25% of repolarization. Our results indicate that alternans developed even if the restitution slope was smaller than 1, furthermore, data show mainly weak and in some cases moderate correlations between variables.

We also analyzed the S1S2 restitutions at APD_{50} and APD_{25} and these values were plotted against the corresponding alternans magnitude. Weak or moderate correlations were found (Supplementary Fig. S2).

Figure 2 demonstrates comparisons of restitution slopes obtained from dynamic restitution and alternans amplitude. Figure 2a depicts the applied dynamic restitution protocol: the pacing cycle length was gradually decreased. At cycle length of 250 ms the APD started to alternate.

Functions of restitution slope—alternans amplitude are illustrated in Fig. 2b. Left column represents alternans at cycle length of 210 ms, right column represents the same at cycle length of 160 ms. The first row shows alternans amplitudes measured at APD_{90} level, middle row represents alternans recorded at APD_{50} level, and bottom row illustrates alternans at 25% of repolarization. Similarly to the S1S2 restitution, we found that alternans developed even if the slope was smaller than 1, and data exerted weak or no correlations between restitution slope and alternans.

The temporal relationship of alternans and restitution slopes was further illustrated in Supplementary Fig. S3. It can be observable that alternans could be evoked at slower pacing cycle lengths (i.e. 250 ms) where the corresponding restitution curves were slow, indicating that alternans can be evoked even if the restitution slope is smaller than 1 (Supplementary Fig. S3).

Non-alternating AP sequence failed to elicit CaT alternans. In order to further address the relationship between AP and CaT alternans, current clamp experiments by using sharp microelectrodes were performed

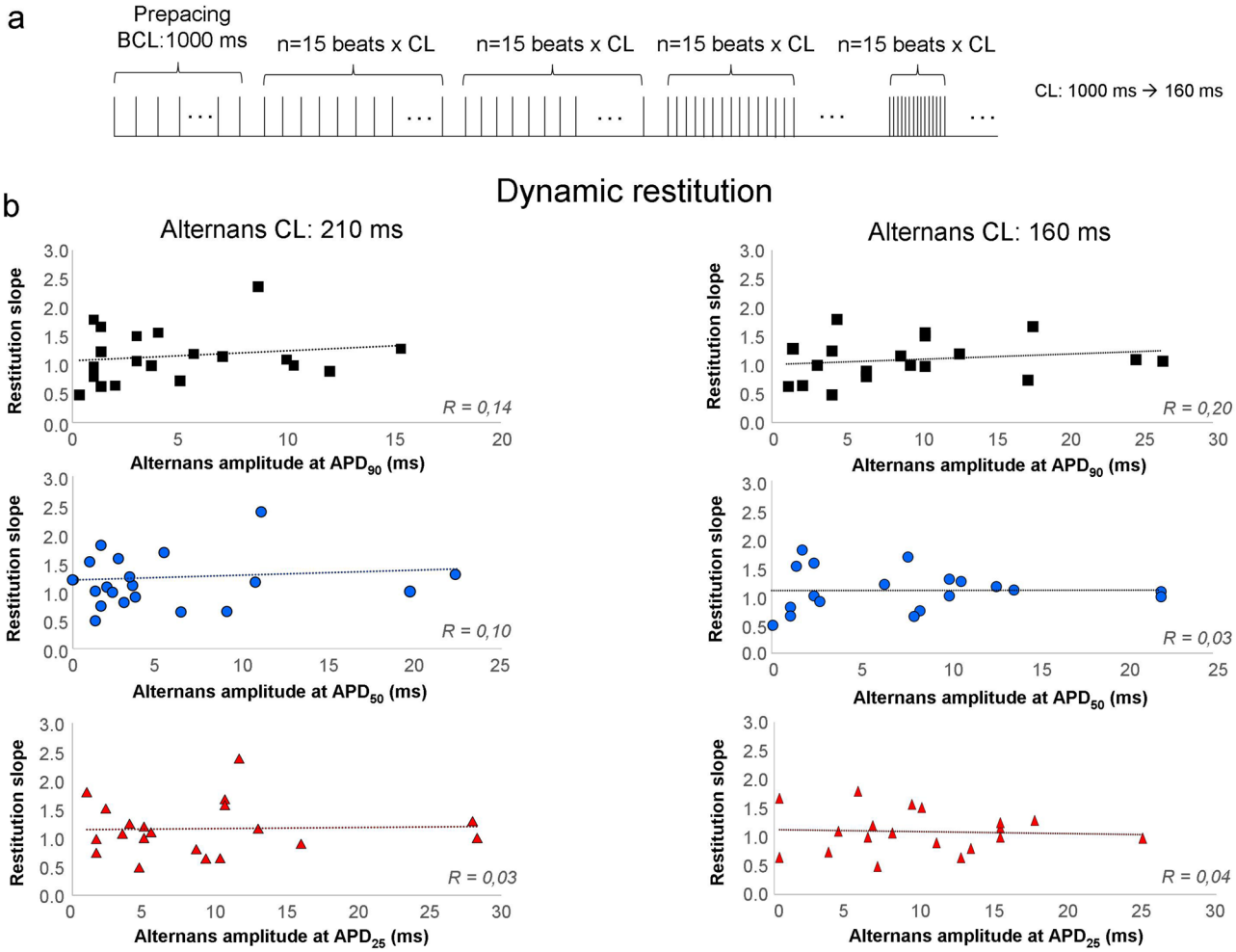

Figure 2. Relationship between action potential alternans and dynamic restitution. **(a)** Illustrates the applied protocol for dynamic restitution. The basic cycle length for restitution was progressively decreased from 1000 to 160 ms. When BCL was 250 ms or shorter the action potential started to alternate. APD_{90} was plotted against the preceding diastolic interval in both long and short AP during alternans. **(b)** The slope of APD_{90} restitution was calculated and was plotted against the magnitude of alternans. The first row demonstrates alternans at APD_{90} level, middle row at APD_{50}, bottom row at APD_{25}. Similarly to the S1S2 restitution, we found that alternans developed even if the slope was smaller than 1, and data exerted weak or no correlations between restitution slope and alternans.

in single cells (Fig. 3a). Stimulus pattern from a cycle length of 250 to 210 ms was applied. The CaT amplitude oscillations were plotted against the corresponding APD_{90} difference (Fig. 3b) within the range of 250–210 ms stimulus cycle length. A close relationship between APD and CaT amplitude alternans was found: larger APD alternans were associated with larger CaT amplitude alternans (n = 15).

In order to elucidate the initiator mechanism of alternans, a non-alternating AP sequence having a BCL of 210 ms was applied under voltage-clamp mode (Fig. 3c upper panel). During measurements, the ionic currents (Fig. 3c middle panel) and CaT (Fig. 3c lower panel) were monitored. The experiments were performed by perforated patch-clamp method to preserve the intracellular milieu. Here we found that the inward ionic currents (other currents were inhibited, see Methods) as well as CaT exerted (6.7 ± 2.2%, n = 9) negligible alternans. These results suggest that in our experiments the action potential alternans are required for CaT alternans.

I_{CaL} kinetics during alternating voltage pulses. Among transmembrane ionic currents I_{CaL} could be the most obvious candidate that may have important role in the alternans mechanism. As a trigger of the Ca^{2+} release it can directly influence the magnitude of the actual Ca^{2+} transient, and its kinetic is strongly influenced by the membrane potential.

In order to address the contribution of I_{CaL} in alternans, we applied 3 alternating voltage pulse protocols to produce different extent of I_{CaL} alternans due to alternans of the recovery time (Fig. 4a). The measurements were performed by using perforated patch clamp method. The magnitude of corresponding CaT amplitude alternans was analyzed and compared to the I_{CaL} amplitude alternans. The BCL of all protocols was 220 ms in all cases (see description in the "Methods" section).

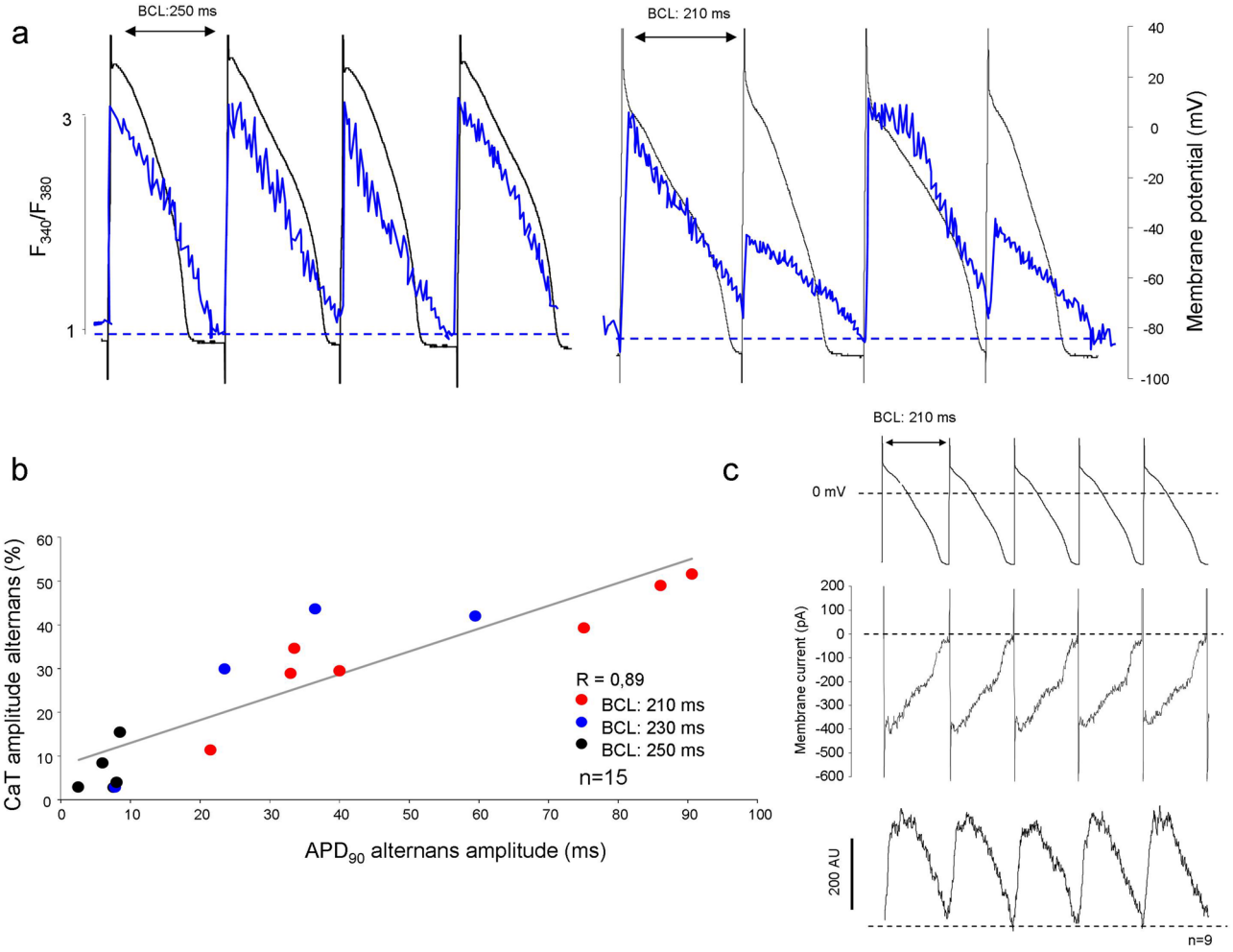

Figure 3. Relationship between APD and CaT amplitude alternans. **(a)** Illustrates simultaneous measurements of AP and CaT recorded at 250, 230 and 210 ms of BCL. At the left side a moderate AP alternans (black) coupled with marginal alternans of the CaT (blue curve), measured at 250 ms. **(a)** Right side illustrates marked AP alternans (black) associated with pronounced CaT alternans (blue) monitored at 210 ms. **(b)** Illustrates the APD_{90} alternans amplitude plotted against the extent of CaT alternans defined as CaT peak alternans ratio, at various BCLs. The grey line represents the linear regression of the points. **(c)** Depicts rapid pacing by non-alternating membrane potential, (upper curve) failed to induce CaT alternans under perforated patch-clamp condition. Parallel measured membrane current (middle curve) and CaT (lower curve) traces at a basic cycle length of 210 ms are shown. The evoked membrane currents were identical, and the evoked CaTs exerted negligible alternans.

In these experiments a close correlation between I_{CaL} amplitude alternans and corresponding CaT amplitude alternans was found (Fig. 4d). It implies that CaT alternans were marginal when I_{CaL} alternans were small even though the high pacing frequency. Thus, these results are in agreement with the observed failure of the high pacing rate to produce alternans (Fig. 3c) and the close relationship between APD and CaT alternans demonstrated in Fig. 3a,b.

The Ca^{2+} release channel recovery is also sensitive to membrane potential oscillations[9]. Therefore, there is a possibility that an alternating Ca^{2+} release controlled by ryanodine recovery could also directly contribute to the observed I_{CaL} alternans. In order to assess this issue, whole cell patch clamp experiments were devised where 10 mM EGTA was employed to buffer Ca^{2+}_i (Supplementary Fig. S4). In the absence of Ca^{2+} release the average of I_{CaL} alternans did not differ from those that were measured in the presence of intact Ca^{2+} handling (presented in Fig. 4) indicating major role of membrane potential in the development of I_{CaL} alternans (140 ms—EGTA-free: 7.3 ± 1.2% *vs* EGTA: 6.5 ± 1.3%. 180 ms—EGTA-free: 25.7 ± 6% *vs* EGTA: 21.3 + 3%. 200 ms—EGTA-free: 41.4 + 4% *vs* EGTA: 45.5 ± 7%. n(EGTA-free) = 9, n(EGTA) = 6)).

Recovery of the I_{CaL}. A further important question is the behavior of I_{CaL} during the fast phase of the restitution curve. This issue was investigated by whole-cell patch clamp omitting Ca^{2+} buffer from the pipette solution (Fig. 5). The description of the recovery protocol can be found in the Methods section. We found that during the first 30 ms of the DI, where the APD restitution is the fastest, the I_{CaL} recovers only 20.7 ± 2.4%

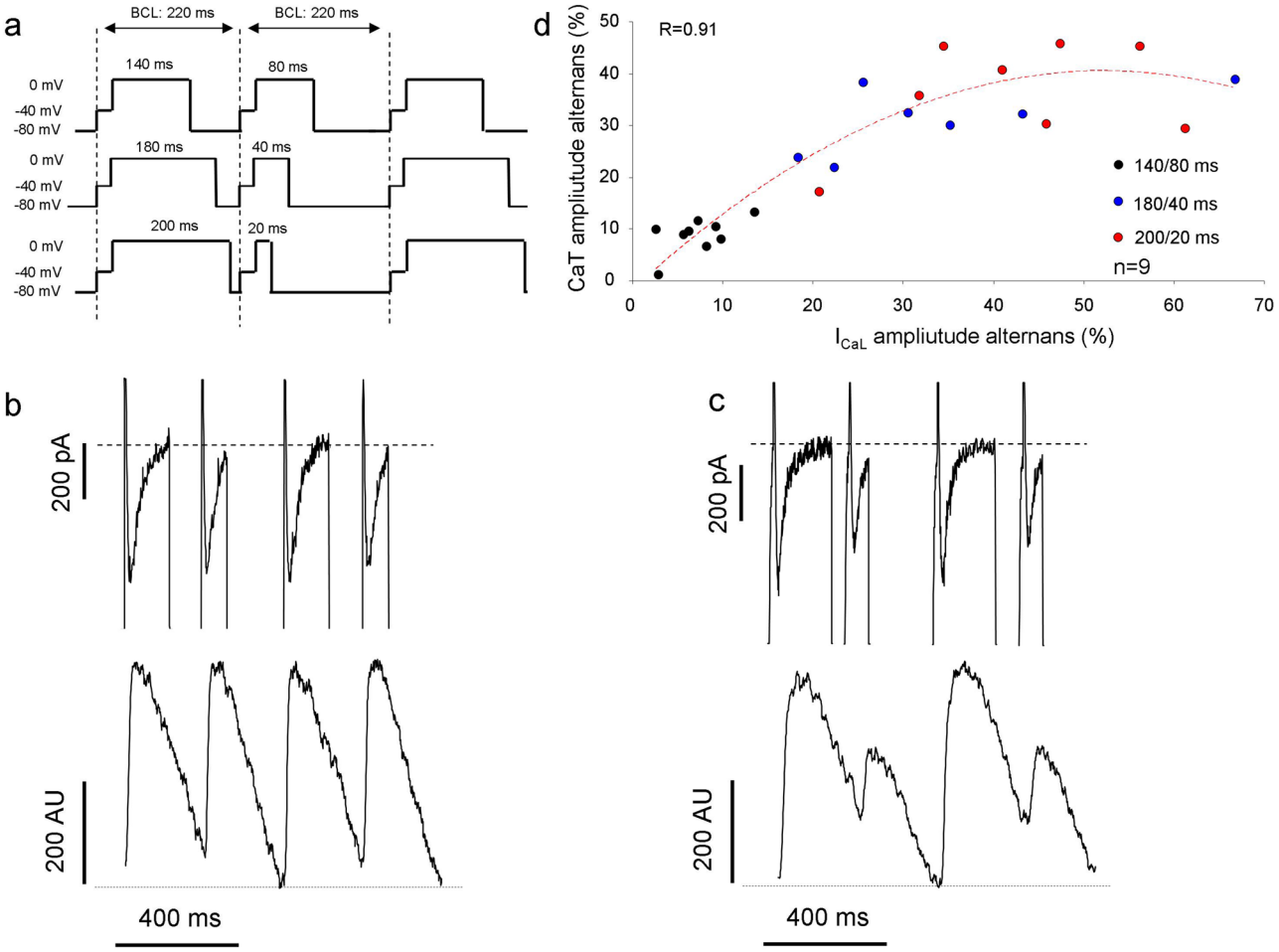

Figure 4. The role of I_{CaL} alternans in ignition of CaT alternans. I_{CaL} were evoked by 3 subsequently applied alternating voltage clamp pulses, having a basic cycle length of 220 ms in all cases **(a)**. **(b)** Illustrates a membrane current and CaT measurement evoked by a 140/80 ms voltage protocol. The I_{CaL} peaks as well as the corresponding CaT did not show notable alternans. **(c)** Represents alternating I_{CaL} and CaT during application of 180/40 ms protocol. **(d)** Illustrates a close relationship when the peak I_{CaL} alternans were plotted against the corresponding CaT amplitude alternans. The black circles represent experiments evoked by 140/180 ms protocol, the blue circles demonstrate measurements under 180/40 ms protocol, while red circles indicates recordings during 200/20 protocol.

(n = 11) providing relatively small (0.6 ± 0.08 pA/pF, n = 11) current (Fig. 5b,c). These results indicate that I_{CaL} has restricted contribution to the initial, rapid phase of restitution.

I_{CaL} inhibition suppresses alternans without influencing the initial phase of restitution. In order to further investigate the role of I_{CaL} in the restitution, action potential measurements were performed in multicellular tissue. 1 μM nisoldipine was employed to inhibit selectively the I_{CaL} (Fig. 6). At first, the restitution protocol was applied at 500 ms of BCL then the alternans protocol was used from 250 to 190 ms BCLs. Administration of 1 μM nisoldipine suppressed the APD_{90} alternans at 250 ms of BCL (7.5 ± 1.2 ms *vs* 3.8 ± 0.8 ms; $p < 0.05$, n = 7, not shown in the figure). The APD_{25} alternans were reduced at 250 ms (14.7 ± 4.6 ms *vs* 4.4 ± 0.9 ms; $p < 0.05$, n = 7/7 hearts), at 230 ms (13 ± 3.1 ms *vs* 3.1 ± 1 ms; $p < 0.05$, n = 7), and at 210 ms (10.8 ± 2.6 ms *vs* 4.7 ± 0.7 ms; $p < 0.05$, n = 7, Fig. 6a,b). We found that 1 μM nisoldipine significantly shortened the baseline APD_{90} (187 ± 5 ms *vs* 159 ± 5 ms; $p < 0.05$, n = 7, bar graphs). In contrast, I_{CaL} inhibition failed to change the initial phase of the restitution steepness but changed it at DIs larger than 60 ms (Fig. 6b,c). Dynamic restitution was calculated from the APD alternans protocol and the effect of nisoldipine was investigated on the restitution slope. It was found that 1 μM nisoldipine does not alter the dynamic restitution slope (1.31 ± 0.1 *vs* 1.2 ± 0.1; n = 7; Figure not shown).

Discussion

The major findings of this study are the followings: (1) in tissue AP measurements, the development of AP alternans could be evoked irrespective of the restitution slope, suggesting a minor fidelity of restitution curve in prediction of alternans. (2) In our experiments, CaT alternans were not observed in the absence of I_{CaL} alternans (3) I_{CaL} has little influence on the early phase of APD restitution curve.

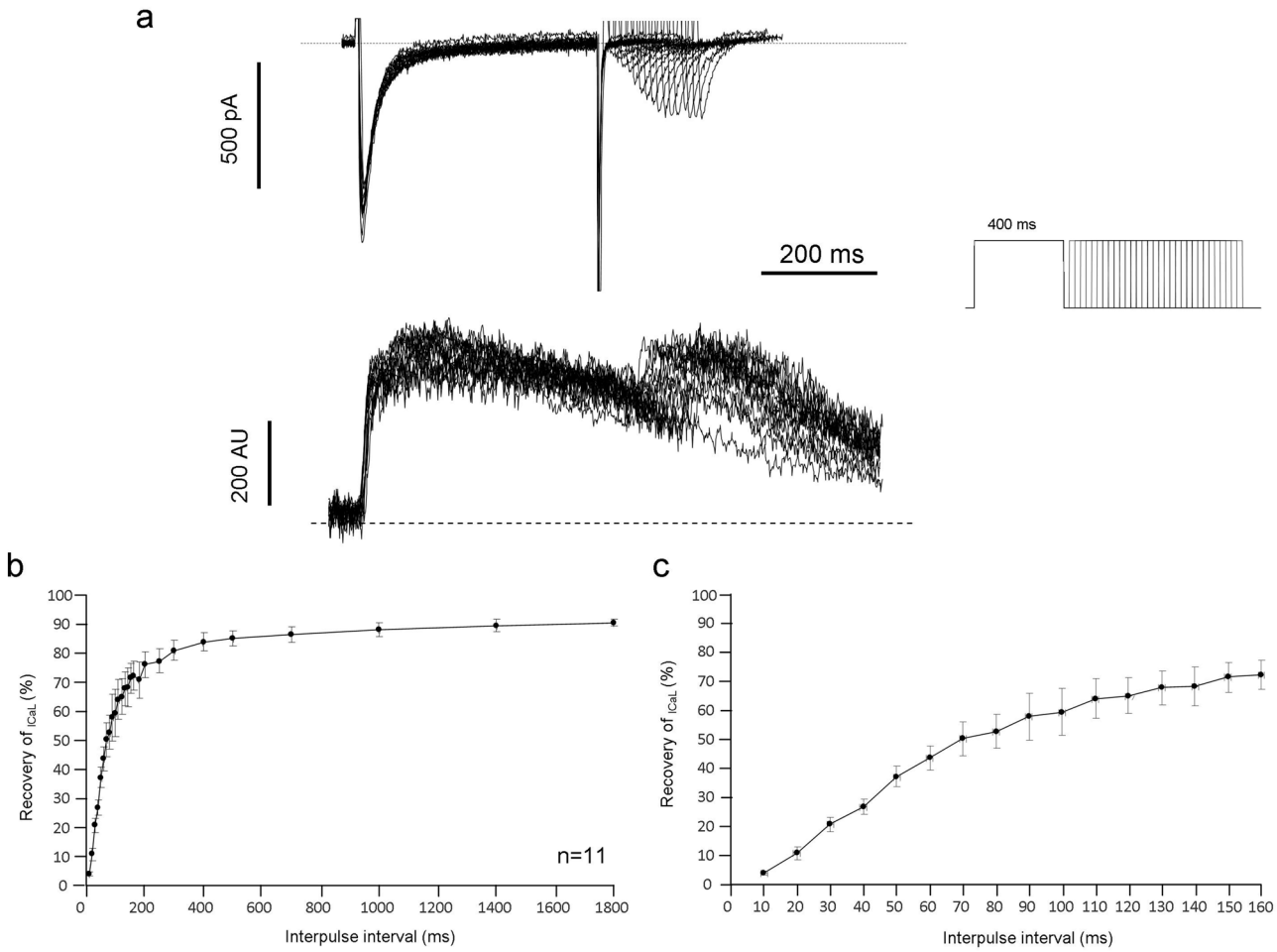

Figure 5. Analysis of the I_{CaL} recovery in the presence of unbuffered Ca^{2+} handling. **(a)** (upper traces) demonstrates original representative current traces of recovery kinetics of the $I_{CaL,}$ Inset shows the applied voltage protocol. The lower panel demonstrates the parallel Ca^{2+} releases. The **(b)** depicts the extent of I_{CaL} recovery plotted against the respective diastolic intervals, while **(c)** highlights the first 160 ms of the I_{CaL} recovery.

Has any role of restitution in the alternans development? The general view is that membrane voltage-driven alternans are determined by a single parameter: APD restitution[5]. The restitution quantifies the relationship between APD and preceding DI. The major factors governing APD restitution are recovery from inactivation of the inward currents and deactivation of outward currents, as well as Ca^{2+} cycling also affects restitution through Ca^{2+} dependent currents[28]. Our results, similar to those that were reported in other previous studies[1,18], do not support previous assumption by Nolasco and Dahlen suggesting that the steepness of restitution reflects the susceptibility of alternans[17]. The restitution hypothesis claims that alternans will occur when the restitution slope is larger than 1. In our tissue AP measurements, the restitution steepness did not influence the *development* of alternans (i.e. could be triggered regardless of the restitution steepness), rather the basic cycle length: alternans occurred in all cases (20/20 experiments) when the BCL was 250 ms or shorter. In our experiments, alternans *occurred* even if the restitution steepness (S1S2 or dynamic) was smaller than 1, however, the *extent* of alternans was weakly/moderately connected to restitution steepness. These results suggest that restitution steepness may have little fidelity in prediction of development of cardiac alternans. At the same time, it is important to note that several transmembrane ionic currents having potential role in alternans development do not contribute to the rapid restitution phase equally[29].

The idea that alternans may have a restitution-independent cause has been recognized by Wu and Patwardhan. Using a feedback-based pacing protocol where diastolic intervals were selected explicitly and independently of APDs it was possible to investigate whether alternans occur when diastolic intervals preceding each AP do not change[30]. It was shown that identical diastolic intervals were also followed by APD alternans claiming that diastolic interval dependent restitution may not be directly linked to alternans development[30].

Do CaT alternans require action potential alternans? Our current clamp experiments (Fig. 3) revealed a close relationship between APD and CaT alternans. This correlation implies that membrane potential

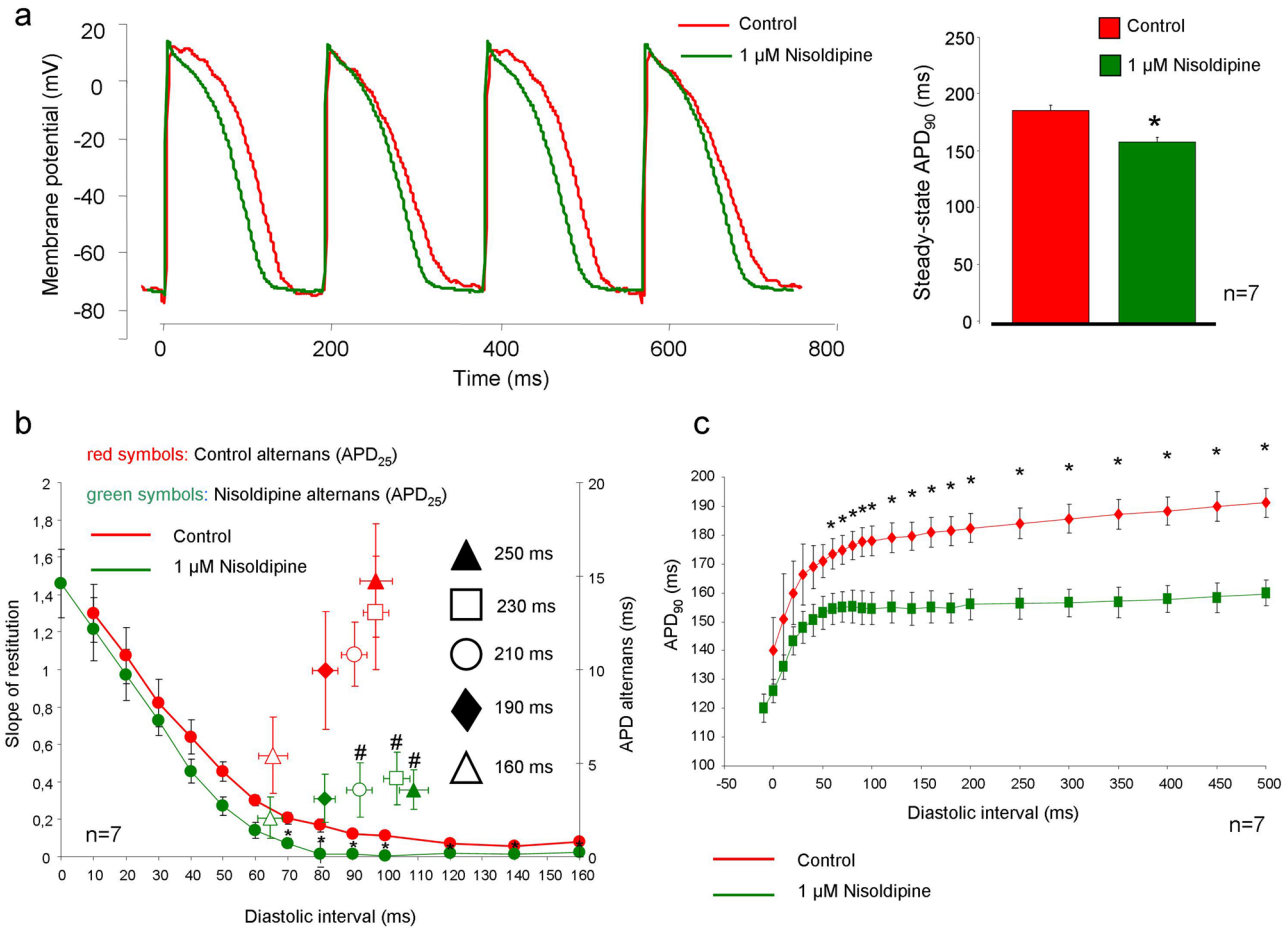

Figure 6. Effect of 1 μM nisoldipine on APD alternans and restitution curve measured on multicellular tissue. **(a)** Illustrates representative original traces in control (red curve) and in the presence of 1 μM nisoldipine (green curve). Nisoldipine reduced the steady-state APD_{90} (bar graphs) measured at 500 ms BCL. **(b)** Represents a comparison between nisoldipine effect on restitution steepness (left y-axis) and on APD_{25} alternans (right y-axis) at a BCL of 500 ms. The nisoldipine reduced the slope of the restitution (green *versus* red curves) only in a slow phase, at DIs larger than 70 ms (significance marked with *). The APD_{25} alternans were significantly reduced at 250, 230, and 210 ms (green versus red symbols, significance marked with #). **(c)** Depicts APD_{90} restitution under control (red curve) and in the presence of 1 μM nisoldipine (green curve) at a BCL of 500 ms. However, the APD_{90} shortening after nisoldipine administration is clear, we can observe that the steepness of the curve primarily reduced at the slow phase.

or Ca^{2+} could be a potential driver of the alternans, however when membrane potential did not alternate the beat-to-beat CaT remained also unaltered.

A bidirectional coupling exists between AP and Ca^{2+}-handling, and I_{CaL} is a major determinant of both actual APD and Ca^{2+}-transients. When the $Ca^{2+}{}_i$ alternates, it significantly alters the APD via the balance of I_{CaL} and I_{NCX} causing positive or negative Ca^{2+} to Vm coupling[31].

Several voltage-clamp studies reported that notable Ca^{2+} transient alternans were observed in the presence of non-alternating AP sequence[13–16]. These results were interpreted as the alternans were arose directly from the Ca^{2+} handling dynamics and not only the passive response of the beat-to-beat alternans of the AP[13]. In contrast, the data of this study indicate that membrane potential (i.e. AP alternans) is required for the development of CaT alternans in our experiments, and may support the important role of I_{CaL} and the bidirectional coupling between AP and Ca^{2+} handling in the development of alternans.

I_{CaL} fluctuation is able to ignite CaT alternans. Previous results are controversial regarding the role of I_{CaL} in APD alternans initiation: the incomplete time-dependent recovery of I_{CaL} was found to cause alternans in several studies[8,21,32,33]. In a computer modelling study of ischaemic myocytes, alternans have been proposed to appear due to the interplay of I_{CaL} and potassium transient outward currents[34]. In our previous study we found that selective Na^+/Ca^{2+} exchanger inhibition decreased alternans without influencing the restitution slope while indirectly inhibits I_{CaL}[35].

In contrast, several papers found in both atrial and ventricular myocytes that alternans can occur while peak I_{CaL} remained unchanged from beat to beat[14–16,36,37]. Additionally, numerous papers demonstrated mechanical and CaT alternans in the absence of AP alternans[2,13,14,16,37].

In our experiments we found that oscillation of the I_{CaL} recovery time (that is often developed during alternans) is able to induce I_{CaL} peak fluctuation—as was expected, and the relationship between I_{CaL} and CaT amplitude alternans was closely coupled (Fig. 4). In line with previous results demonstrated in Fig. 3, the high pacing rate per se was insufficient again to induce CaT alternans, since when I_{CaL} alternans were small the corresponding CaT alternans were also restricted. The magnitude of I_{CaL} alternans was not altered even if the $Ca^{2+}{}_i$ was buffered (Supplementary Fig. S4) indicating the membrane potential origin of the I_{CaL} fluctuations.

At the same time, it is important to note that AP morphology and alternans influence the SR Ca^{2+} content and the efficiency of the excitation–contraction coupling[21]. Therefore, the actual SR Ca^{2+} content—together with I_{CaL}—may have important contribution to the development of alternans[15], however, this was out of the scope of this study.

Does I_{CaL} contribute to alternans development in a restitution independent manner? Since previous experiment showed that I_{CaL} can induce CaT alternans via alterations of the recovery period (i.e. voltage-dependent manner) the relationship of I_{CaL} with the restitution slope was investigated. Several papers reported that I_{CaL} is an important contributor of the restitution slope[38–40].

In order to address this question the I_{CaL} kinetics was investigated under different recovery intervals. Our current measurement in the presence of unbuffered intracellular solution revealed that under short diastolic intervals—that corresponds to the fast phase of restitution—the recovered fraction of the I_{CaL} is relatively low (Fig. 5). Similarly, our tissue AP experiments with 1 μM nisoldipine (Fig. 6) demonstrated that selective I_{CaL} inhibition does not influence the fast phase of the restitution curve. This fact, in line with previous report[41], may indicate that I_{CaL} has a minor role in shaping the fast phase of the restitution, presumably because highly incomplete recovery allows small I_{CaL} during short diastolic intervals. Furthermore, according to previous study[42], the failure of nisoldipine to change restitution steepness could be also attributable to the relatively small effect on the baseline APD (~ 20%). Previous paper also reported no change in the time constant of electrical restitution of human ventricle after application of 1 μM nisoldipine in human[29]. At the same time, in line with our results, a numerical simulation demonstrated that I_{CaL} suppression reduces alternans[32].

Previous studies reported that I_{CaL} blocker verapamil flattened the restitution curve[38,39], however it is known that it also inhibits the I_{Kr} in submicromolar level[43,44] that was not taken into account in those studies. I_{Kr} suppression was reported to flatten restitution[42], while in contrast, dihydropyridines did not inhibit the I_{Kr}[43,44]. Therefore, verapamil could not be considered as a suitable tool to assess the role of I_{CaL} in restitution, and its additional I_{Kr} suppressing effect makes the data interpretation difficult.

Possible role of cardiac memory. Cardiac memory is a term introduced by Rosenbaum et al.[45]. The short term cardiac memory reflects the effect of pacing "history" on the APD, therefore, the relationship of alternans and APD restitution is complicated by the possible presence of the short-term cardiac memory. In our measurements the S1S2 restitutions measured at different BCLs and dynamic restitutions are different (Supplementary Fig. S3), indicating the presence of memory in the system. Several studies claimed that the presence of cardiac memory decreases the reliability of the restitution in prediction of alternans[46,47]. Therefore in our experiments the cardiac memory could be also an important contributor that reduces the coupling between alternans and restitution slope.

Conclusion

In this study we found that I_{CaL} has minor contribution in shaping the fast phase of restitution curve. This suggest that I_{CaL}—if it contributes to the mechanism of alternans—could be an additional factor that attenuates the reliability of APD restitution slope to predict alternans.

Since I_{CaL} can induce alternans in voltage-dependent manner (i.e. by the change of the recovery period) it could contribute to the development of a voltage-driven alternans that are largely independent of restitution.

Limitations

The alternans-restitution comparison was investigated in endocardial tissue therefore it does not represent the whole heart. Other cell layers, such as midmyocardial cells or Purkinje fibers may exert different behavior.

Received: 26 February 2021; Accepted: 23 July 2021
Published online: 17 August 2021

References

1. Pruvot, E. J., Katra, R. P., Rosenbaum, D. S. & Laurita, K. R. Role of calcium cycling versus restitution in the mechanism of repolarization alternans. *Circ. Res.* **94**, 1083–1090. https://doi.org/10.1161/01.res.0000125629.72053.95 (2004).
2. Wan, X., Laurita, K. R., Pruvot, E. J. & Rosenbaum, D. S. Molecular correlates of repolarization alternans in cardiac myocytes. *J. Mol. Cell. Cardiol.* **39**, 419–428. https://doi.org/10.1016/j.yjmcc.2005.06.004 (2005).
3. Ikeda, T. *et al.* T-wave alternans as a predictor for sudden cardiac death after myocardial infarction. *Am. J. Cardiol.* **89**, 79–82. https://doi.org/10.1016/s0002-9149(01)02171-3 (2002).
4. Rosenbaum, D. S. *et al.* Electrical alternans and vulnerability to ventricular arrhythmias. *N. Engl. J. Med.* **330**, 235–241. https://doi.org/10.1056/nejm199401273300402 (1994).
5. Edwards, J. N. & Blatter, L. A. Cardiac alternans and intracellular calcium cycling. *Clin. Exp. Pharmacol. Physiol.* **41**, 524–532. https://doi.org/10.1111/1440-1681.12231 (2014).
6. Qu, Z., Nivala, M. & Weiss, J. N. Calcium alternans in cardiac myocytes: Order from disorder. *J. Mol. Cell. Cardiol.* **58**, 100–109. https://doi.org/10.1016/j.yjmcc.2012.10.007 (2013).

7. Weiss, J. N. *et al.* From pulsus to pulseless: The saga of cardiac alternans. *Circ. Res.* **98**, 1244–1253. https://doi.org/10.1161/01.RES.0000224540.97431.f0 (2006).
8. Shiferaw, Y., Watanabe, M. A., Garfinkel, A., Weiss, J. N. & Karma, A. Model of intracellular calcium cycling in ventricular myocytes. *Biophys. J.* **85**, 3666–3686. https://doi.org/10.1016/s0006-3495(03)74784-5 (2003).
9. Picht, E., DeSantiago, J., Blatter, L. A. & Bers, D. M. Cardiac alternans do not rely on diastolic sarcoplasmic reticulum calcium content fluctuations. *Circ. Res.* **99**, 740–748. https://doi.org/10.1161/01.res.0000244002.88813.91 (2006).
10. Livshitz, L. M. & Rudy, Y. Regulation of Ca2+ and electrical alternans in cardiac myocytes: Role of CAMKII and repolarizing currents. *Am. J. Physiol. Heart Circ. Physiol.* **292**, H2854–H2866. https://doi.org/10.1152/ajpheart.01347.2006 (2007).
11. Cui, X. *et al.* Period-doubling bifurcation in an array of coupled stochastically excitable elements subjected to global periodic forcing. *Phys. Rev. Lett.* **103**, 044102. https://doi.org/10.1103/PhysRevLett.103.044102 (2009).
12. Rovetti, R., Cui, X., Garfinkel, A., Weiss, J. N. & Qu, Z. Spark-induced sparks as a mechanism of intracellular calcium alternans in cardiac myocytes. *Circ. Res.* **106**, 1582–1591. https://doi.org/10.1161/circresaha.109.213975 (2010).
13. Chudin, E., Goldhaber, J., Garfinkel, A., Weiss, J. & Kogan, B. Intracellular Ca(2+) dynamics and the stability of ventricular tachycardia. *Biophys. J.* **77**, 2930–2941. https://doi.org/10.1016/s0006-3495(99)77126-2 (1999).
14. Díaz, M. E., Eisner, D. A. & O'Neill, S. C. Depressed ryanodine receptor activity increases variability and duration of the systolic Ca2+ transient in rat ventricular myocytes. *Circ. Res.* **91**, 585–593. https://doi.org/10.1161/01.res.0000035527.53514.c2 (2002).
15. Díaz, M. E., O'Neill, S. C. & Eisner, D. A. Sarcoplasmic reticulum calcium content fluctuation is the key to cardiac alternans. *Circ. Res.* **94**, 650–656. https://doi.org/10.1161/01.res.0000119923.64774.72 (2004).
16. Hüser, J. *et al.* Functional coupling between glycolysis and excitation-contraction coupling underlies alternans in cat heart cells. *J. Physiol.* **524**(Pt 3), 795–806. https://doi.org/10.1111/j.1469-7793.2000.00795.x (2000).
17. Nolasco, J. B. & Dahlen, R. W. A graphic method for the study of alternation in cardiac action potentials. *J. Appl. Physiol.* **25**, 191–196. https://doi.org/10.1152/jappl.1968.25.2.191 (1968).
18. Goldhaber, J. I. *et al.* Action potential duration restitution and alternans in rabbit ventricular myocytes: The key role of intracellular calcium cycling. *Circ. Res.* **96**, 459–466. https://doi.org/10.1161/01.res.0000156891.66893.83 (2005).
19. Jordan, P. N. & Christini, D. J. Action potential morphology influences intracellular calcium handling stability and the occurrence of alternans. *Biophys. J.* **90**, 672–680. https://doi.org/10.1529/biophysj.105.071340 (2006).
20. Jordan, P. N. & Christini, D. J. Characterizing the contribution of voltage- and calcium-dependent coupling to action potential stability: Implications for repolarization alternans. *Am. J. Physiol.-Heart Circ. Physiol.* **293**, H2109–H2118. https://doi.org/10.1152/ajpheart.00609.2007 (2007).
21. Kanaporis, G. & Blatter, L. A. Membrane potential determines calcium alternans through modulation of SR Ca(2+) load and L-type Ca(2+) current. *J. Mol. Cell. Cardiol.* **105**, 49–58. https://doi.org/10.1016/j.yjmcc.2017.02.004 (2017).
22. Shiferaw, Y., Sato, D. & Karma, A. Coupled dynamics of voltage and calcium in paced cardiac cells. *Phys. Rev. E Stat. Nonlinear Soft Matter Phys.* **71**, 021903. https://doi.org/10.1103/PhysRevE.71.021903 (2005).
23. Jost, N. *et al.* ORM-10103, a novel specific inhibitor of the Na+/Ca2+ exchanger, decreases early and delayed afterdepolarizations in the canine heart. *Br. J. Pharmacol.* **170**, 768–778. https://doi.org/10.1111/bph.12228 (2013).
24. Kohajda, Z. *et al.* The effect of a novel highly selective inhibitor of the sodium/calcium exchanger (NCX) on cardiac arrhythmias in in vitro and in vivo experiments. *PLoS ONE* **11**, e0166041. https://doi.org/10.1371/journal.pone.0166041 (2016).
25. Koller, M. L., Riccio, M. L. & Gilmour, R. F. Jr. Dynamic restitution of action potential duration during electrical alternans and ventricular fibrillation. *Am. J. Physiol.* **275**, H1635–H1642. https://doi.org/10.1152/ajpheart.1998.275.5.H1635 (1998).
26. Kormos, A. *et al.* Efficacy of selective NCX inhibition by ORM-10103 during simulated ischemia/reperfusion. *Eur. J. Pharmacol.* **740**, 539–551. https://doi.org/10.1016/j.ejphar.2014.06.033 (2014).
27. Horváth, B. *et al.* Frequency-dependent effects of omecamtiv mecarbil on cell shortening of isolated canine ventricular cardiomyocytes. *Naunyn Schmiedebergs Arch. Pharmacol.* **390**, 1239–1246. https://doi.org/10.1007/s00210-017-1422-z (2017).
28. Nagy, N. *et al.* Role of Ca^2+-sensitive K+ currents in controlling ventricular repolarization: Possible implications for future antiarrhytmic drug therapy. *Curr. Med. Chem.* **18**, 3622–3639. https://doi.org/10.2174/092986711796642463 (2011).
29. Árpádffy-Lovas, T. *et al.* Electrical restitution and its modifications by antiarrhythmic drugs in undiseased human ventricular muscle. *Front. Pharmacol.* **11**, 479. https://doi.org/10.3389/fphar.2020.00479 (2020).
30. Wu, R. & Patwardhan, A. Mechanism of repolarization alternans has restitution of action potential duration dependent and independent components. *J. Cardiovasc. Electrophysiol.* **17**, 87–93. https://doi.org/10.1111/j.1540-8167.2005.00319.x (2006).
31. Wan, X. *et al.* New experimental evidence for mechanism of arrhythmogenic membrane potential alternans based on balance of electrogenic I(NCX)/I(Ca) currents. *Heart Rhythm* **9**, 1698–1705. https://doi.org/10.1016/j.hrthm.2012.06.031 (2012).
32. Fox, J. J., McHarg, J. L. & Gilmour, R. F. Ionic mechanism of electrical alternans. *Am. J. Physiol.* **282**, H516–H530. https://doi.org/10.1152/ajpheart.00612.2001 (2002).
33. Li, Y., Díaz, M. E., Eisner, D. A. & O'Neill, S. The effects of membrane potential, SR Ca2+ content and RyR responsiveness on systolic Ca2+ alternans in rat ventricular myocytes. *J. Physiol.* **587**, 1283–1292. https://doi.org/10.1113/jphysiol.2008.164368 (2009).
34. Hopenfeld, B. Mechanism for action potential alternans: the interplay between L-type calcium current and transient outward current. *Heart Rhythm* **3**, 345–352. https://doi.org/10.1016/j.hrthm.2005.11.016 (2006).
35. Szlovák, J. *et al.* Blockade of sodium-calcium exchanger via ORM-10962 attenuates cardiac alternans. *J. Mol. Cell. Cardiol.* **153**, 111–122. https://doi.org/10.1016/j.yjmcc.2020.12.015 (2021).
36. Belevych, A. E. *et al.* Redox modification of ryanodine receptors underlies calcium alternans in a canine model of sudden cardiac death. *Cardiovasc. Res.* **84**, 387–395. https://doi.org/10.1093/cvr/cvp246 (2009).
37. Shkryl, V. M., Maxwell, J. T., Domeier, T. L. & Blatter, L. A. Refractoriness of sarcoplasmic reticulum Ca2+ release determines Ca2+ alternans in atrial myocytes. *Am. J. Physiol.* **302**, H2310–H2320. https://doi.org/10.1152/ajpheart.00079.2012 (2012).
38. Riccio, M. L., Koller, M. L. & Gilmour, R. F. Jr. Electrical restitution and spatiotemporal organization during ventricular fibrillation. *Circ. Res.* **84**, 955–963. https://doi.org/10.1161/01.res.84.8.955 (1999).
39. Wu, T. J., Lin, S. F., Weiss, J. N., Ting, C. T. & Chen, P. S. Two types of ventricular fibrillation in isolated rabbit hearts: Importance of excitability and action potential duration restitution. *Circulation* **106**, 1859–1866. https://doi.org/10.1161/01.cir.0000031334.49170.fb (2002).
40. Tse, G. *et al.* Cardiac dynamics: Alternans and arrhythmogenesis. *J. Arrhythmia* **32**, 411–417. https://doi.org/10.1016/j.joa.2016.02.009 (2016).
41. Kobayashi, Y., Peters, W., Khan, S. S., Mandel, W. J. & Karagueuzian, H. S. Cellular mechanisms of differential action potential duration restitution in canine ventricular muscle cells during single versus double premature stimuli. *Circulation* **86**, 955–967. https://doi.org/10.1161/01.cir.86.3.955 (1992).
42. Shattock, M. J. *et al.* Restitution slope is principally determined by steady-state action potential duration. *Cardiovasc. Res.* **113**, 817–828. https://doi.org/10.1093/cvr/cvx063 (2017).
43. Chouabe, C., Drici, M. D., Romey, G. & Barhanin, J. Effects of calcium channel blockers on cloned cardiac K+ channels IKr and IKs. *Therapie* **55**, 195–202 (2000).
44. Zhang, S., Zhou, Z., Gong, Q., Makielski, J. C. & January, C. T. Mechanism of block and identification of the verapamil binding domain to HERG potassium channels. *Circ. Res.* **84**, 989–998. https://doi.org/10.1161/01.res.84.9.989 (1999).
45. Rosenbaum, M. B., Blanco, H. H., Elizari, M. V., Lázzari, J. O. & Davidenko, J. M. Electrotonic modulation of the T wave and cardiac memory. *Am. J. Cardiol.* **50**, 213–222. https://doi.org/10.1016/0002-9149(82)90169-2 (1982).

46. Kalb, S. S. *et al.* The restitution portrait: A new method for investigating rate-dependent restitution. *J. Cardiovasc. Electrophysiol.* **15**, 698–709. https://doi.org/10.1046/j.1540-8167.2004.03550.x (2004).
47. Tolkacheva, E. G., Schaeffer, D. G., Gauthier, D. J. & Krassowska, W. Condition for alternans and stability of the 1:1 response pattern in a "memory" model of paced cardiac dynamics. *Phys. Rev. E Stat. Nonlinear Soft Matter Phys.* **67**, 031904. https://doi.org/10.1103/PhysRevE.67.031904 (2003).

Acknowledgements

This work was supported by grants from the National Research Development and Innovation Office FK-129117, the János Bolyai Research Scholarship of the Hungarian Academy of Sciences, GINOP-2.3.2-15-2016-00006, the Ministry of Human Capacities Hungary (20391-3/2018/FEKUSTRAT and EFOP-3.6.2-16-2017-0006) and the Ministry for Innovation and Technology (ÚNKP-20-5-SZTE-165, ÚNKP-20-3-SZTE-126). SZTE Open Access Found 5358.

Author contributions

N.T. performed experiments, data analysis and contributed writing the manuscript. J.S., Z.K., G.B., R.V. and B.H. performed experiments. J.G.Y.P. contributed in data interpretation. A.V. contributed in data interpretation and ensured financial support of the study. NN contributed to conception of the study, visualization, writing the manuscript and ensured financial support of the study. All authors reviewed the manuscript.

Competing interests

The authors declare no competing interests.

Additional information

Supplementary Information The online version contains supplementary material available at https://doi.org/10.1038/s41598-021-95299-7.

Correspondence and requests for materials should be addressed to N.N.

Reprints and permissions information is available at www.nature.com/reprints.

Publisher's note Springer Nature remains neutral with regard to jurisdictional claims in published maps and institutional affiliations.

III.

frontiers in Pharmacology

ORIGINAL RESEARCH
published: 29 January 2020
doi: 10.3389/fphar.2019.01632

Novel Na^+/Ca^{2+} Exchanger Inhibitor ORM-10962 Supports Coupled Function of Funny-Current and Na^+/Ca^{2+} Exchanger in Pacemaking of Rabbit Sinus Node Tissue

Zsófia Kohajda[1,2†], Noémi Tóth[2†], Jozefina Szlovák[2], Axel Loewe[3], Gergő Bitay[2], Péter Gazdag[2], János Prorok[2], Norbert Jost[1,2], Jouko Levijoki[4], Piero Pollesello[4], Julius Gy. Papp[1,2], András Varró[1,2] and Norbert Nagy[1,2]*

[1] MTA-SZTE Research Group of Cardiovascular Pharmacology, Hungarian Academy of Sciences, Szeged, Hungary, [2] Department of Pharmacology and Pharmacotherapy, Faculty of Medicine, University of Szeged, Szeged, Hungary, [3] Institute of Biomedical Engineering, Karlsruhe Institute of Technology (KIT), Karlsruhe, Germany, [4] Orion Pharma, Espoo, Finland

OPEN ACCESS

Edited by:
Esther Pueyo,
University of Zaragoza, Spain

Reviewed by:
Yael Yaniv,
Technion Israel Institute of Technology, Israel
Oliver Monfredi,
University of Virginia, United States
Thomas Hund,
The Ohio State University, United States

***Correspondence:**
András Varró
varro.andras@med.u-szeged.hu

[†]These authors have contributed equally to this work

Specialty section:
This article was submitted to Cardiovascular and Smooth Muscle Pharmacology, a section of the journal Frontiers in Pharmacology

Received: 03 July 2019
Accepted: 13 December 2019
Published: 29 January 2020

Citation:
Kohajda Z, Tóth N, Szlovák J, Loewe A, Bitay G, Gazdag P, Prorok J, Jost N, Levijoki J, Pollesello P, Papp JG, Varró A and Nagy N (2020) Novel Na^+/Ca^{2+} Exchanger Inhibitor ORM-10962 Supports Coupled Function of Funny-Current and Na^+/Ca^{2+} Exchanger in Pacemaking of Rabbit Sinus Node Tissue. Front. Pharmacol. 10:1632. doi: 10.3389/fphar.2019.01632

Background and Purpose: The exact mechanism of spontaneous pacemaking is not fully understood. Recent results suggest tight cooperation between intracellular Ca^{2+} handling and sarcolemmal ion channels. An important player of this crosstalk is the Na^+/Ca^{2+} exchanger (NCX), however, direct pharmacological evidence was unavailable so far because of the lack of a selective inhibitor. We investigated the role of the NCX current in pacemaking and analyzed the functional consequences of the I_f-NCX coupling by applying the novel selective NCX inhibitor ORM-10962 on the sinus node (SAN).

Experimental Approach: Currents were measured by patch-clamp, Ca^{2+}-transients were monitored by fluorescent optical method in rabbit SAN cells. Action potentials (AP) were recorded from rabbit SAN tissue preparations. Mechanistic computational data were obtained using the Yaniv *et al*. SAN model.

Key Results: ORM-10962 (ORM) marginally reduced the SAN pacemaking cycle length with a marked increase in the diastolic Ca^{2+} level as well as the transient amplitude. The bradycardic effect of NCX inhibition was augmented when the funny-current (I_f) was previously inhibited and *vice versa,* the effect of I_f was augmented when the Ca^{2+} handling was suppressed.

Conclusion and Implications: We confirmed the contribution of the NCX current to cardiac pacemaking using a novel NCX inhibitor. Our experimental and modeling data support a close cooperation between I_f and NCX providing an important functional consequence: these currents together establish a strong depolarization capacity providing important safety factor for stable pacemaking. Thus, after individual inhibition of I_f or NCX, excessive bradycardia or instability cannot be expected because each of these currents may compensate for the reduction of the other providing safe and rhythmic SAN pacemaking.

Keywords: Na^+/Ca^{2+} exchanger, funny-current, ORM-10962, pacemaking, sinus-node

INTRODUCTION

Computational modeling as well as experimental results established previously that the normal pacemaker function is not only regulated by the hyperpolarization-activated funny current (I_f) (DiFrancesco, 1981) but is also regulated by the intracellular Ca^{2+} handling (Lakatta and DiFrancesco, 2009; Yaniv et al., 2013a; Yaniv et al., 2015; Sirenko et al., 2016). Lakatta and co-workers suggested that the sinus node (SAN) cells operate by a rhythmic clock-like oscillator system where the sarcoplasmic reticulum serves as a Ca^{2+}-clock, which rhythmically discharges diastolic local Ca^{2+} releases (LCRs), and activates the forward (inward) Na^+/Ca^{2+} exchanger (NCX) current to accelerate the diastolic depolarization and facilitates the membrane-clock (M-clock) (Yaniv et al., 2015). Recent experimental results further suggest that these clocks work tightly coupled since the M-clock regulates the Ca^{2+} influx and efflux while the NCX also regulates the diastolic depolarization forming a coupled-clock system. Therefore, NCX may have crucial importance in the clock-like oscillator system since the NCX-mediated inward current is directly translated to membrane potential changes *via* the operation of forward mode of the exchanger. This hypothesis was repeatedly challenged and the pivotal role of Ca^{2+} clock was questioned by other authors (Noble et al., 2010; Himeno et al., 2011; DiFrancesco and Noble, 2012).

As early as 1983, Irishawa and Morad showed in elegant experiments that full inhibition of I_f current by caesium did not significantly influence SAN spontaneous activity arguing for mechanisms other than I_f (Noma et al., 1983). On the other hand, other studies suggest a fundamental role of the exchanger in normal automaticity. A low-sodium bath solution inhibited spontaneous action potentials (AP) firing in guinea-pig SAN cells *via* suppressing normal function of NCX (Sanders et al., 2006). Other studies reported that depletion of SR store by application of ryanodine markedly disturbed the normal pacemaker activity in rabbit SAN cells (Bogdanov et al., 2001). Mouse genetic models revealed that partial atrial NCX1 knock out (≈90%) caused severe bradycardia and other rhythm disorders (Herrmann et al., 2013), while complete atrial NCX knock-out completely suppressed the atrial depolarization exerting ventricular escape rhythm on the ECG (Groenke et al., 2013). The application of KB-R7943, a non-selective NCX inhibitor, also suppressed spontaneous beating in guinea-pig SAN cells (Sanders et al., 2006) however it has also marked effect on the Ca^{2+}-currents. The supposed crucial role of NCX in the normal pacemaker function of SAN could not be directly investigated experimentally so far due to the lack of a selective NCX inhibitor. Recently, two novel NCX inhibitors were synthesized: ORM-10103 and ORM-10962, both showing improved selectivity without influencing I_{CaL} function (Jost et al., 2013; Kohajda et al., 2016; Oravecz et al., 2017).

Abbreviations: AP, action potential; APD, action potential duration; CL, cycle length; CLV, cycle length variability; DD, diastolic depolarization; DI, diastolic interval; DOF, dofetilide; NCX, sodium-calcium exchanger; I_f, funny-current; IVA, ivabradine; ORM, ORM-10962; RYA, ryanodine; SAN, sinoatrial-node.

In this study we confirmed the contributing role of NCX to spontaneous pacemaking by its direct pharmacological inhibition *via* the novel, selective inhibitor ORM-10962. Our data suggest that a strong crosstalk between I_f and NCX also exists in multicellular level, which was described and discussed by the Lakatta group earlier in single cell level (Yaniv et al., 2015). In addition, however, extending these earlier findings, we show that the effect of individual I_f and NCX inhibition is minimal whereas a combined inhibition acts synergistically, providing an important safety margin for secure spontaneous activity of the SAN.

MATERIALS AND METHODS

Ethical Statement

All experiments were conducted in compliance with the *Guide for the Care and Use of Laboratory Animals* (USA NIH publication No 85-23, revised 1996) and conformed to Directive 2010/63/EU of the European Parliament. The protocols were approved by the Review Board of the Department of Animal Health and Food Control of the Ministry of Agriculture and Rural Development, Hungary (XIII./1211/2012).

Animals

The measurements were performed in right atrial tissue obtained from young New-Zealand white rabbits from both genders weighing 2.0–2.5 kg.

Voltage-Clamp Measurements

Cell Preparations

For measuring I_f pacemaker current, we isolated single cells from the SAN region of rabbit heart by enzymatic dissociation. The animals were sacrificed by concussion after receiving 400 IU/kg heparin intravenously. The chest was opened and the heart was quickly removed and placed into cold (4°C) solution with the following composition (mM): NaCl 135, KCl 4.7, KH_2PO_4 1.2, $MgSO_4$ 1.2, 4-(2-hydroxyethyl)-1-piperazineethanesulfonic acid (HEPES) 10, $NaHCO_3$ 4.4, glucose 10, $CaCl_2$ 1.8, (pH 7.2 with NaOH). The heart was mounted on a modified, 60 cm high Langendorff column and perfused with oxygenated and prewarmed (37°C) solution mentioned above. After washing out of blood (3–5 min) the heart was perfused with nominally Ca-free solution until the heart stopped beating (approx. 3–4 min). The digestion was performed by perfusion with the same solution supplemented with 1.8 mg/ml (260 U/ml) collagenase (type II, Worthington). After 10–12 min, the heart was removed from the cannula. The right atrium was cut and the crista terminalis and SAN region were excised and cut into small strips. Strips were placed into enzyme free solution containing 1 mM $CaCl_2$ and equilibrated at 37°C for 10 min. After 10 min with gentle agitation, the cells were separated by filtering through a nylon mesh. Sedimentation was used for harvesting cells. The supernatant was removed and replaced by HEPES-buffered Tyrode's solution. The cells were stored at room temperature in the Tyrode's solution.

Measurement of Pacemaker Current (Funny Current)

For the measurement of the I_f current, the method of Verkerk et al. (2009) was adapted and applied. The current was recorded in HEPES-buffered Tyrode's solution while the composition of the pipette solution was the following (in mM): KOH 110, KCl 40, K_2ATP 5, $MgCl_2$ 5, EGTA 5, HEPES 10, and GTP 0.1 (pH was adjusted to 7.2 by aspartic acid). The current was activated by hyperpolarizing voltage pulses to −120 mV from a holding potential of −30 mV. The pacemaker current was identified as ivabradine (IVA) sensitive current. The experiments were performed at 37°C.

Fluorescent Optical Measurements

Isolated, spontaneously beating SAN cells were used for measurements. Ca^{2+} transients were measured by Fluo-4 AM fluorescent dye. Isolated cells were loaded with 5 μM dye for 20 min in room temperature in dark. Loaded cells were mounted in a low volume imaging chamber (RC47FSLP, Warner Instruments) and continuously superfused with normal Tyrode solution. Fluorescence measurements were performed on the stage of an Olympus IX 71 inverted fluorescence microscope. The dye was excited at 480 nm and the emitted fluorescence was detected at 535 nm. Optical signals were sampled at 1 kHz and recorded by a photon counting photomultiplier module (Hamamatsu, model H7828). Amplitudes of the Ca^{2+} transients were calculated as differences between systolic and diastolic values. To measure Ca^{2+} changes the cells were damaged by a patch pipette at the end of the experiment to obtain maximal fluorescence (F_{max}). Ca^{2+} was calibrated using the following formula: $K_d(F-F_{min})/(F_{max}-F)$. K_d of the Fluo-4 AM was 335 nM.

Action Potential Measurements With Standard Microelectrode Technique

We have chosen multicellular preparations for action potential measurements for three reasons: 1) all of the ion channels remained intact (current density, kinetics) because of the lack of enzymatic dissociation, thus providing more precise estimates of the ratio between the currents, 2) since the SAN cells are surrounded with atrial cells having a more negative resting membrane potential, the electrotonic coupling may intimately influence the SAN cells. It may have great importance since the I_f current markedly increases as the membrane potential drops to more negative values (Morad and Zhang, 2017), (3) the action potential frequency was very stable with a cycle-length variability lower than 5 ms.

SAN regions obtained from right atria were mounted in a tissue chamber superfused with oxygenated Locke's solution at 37°C. A conventional microelectrode technique was performed as previously described (Kormos et al., 2014; Kohajda et al., 2016; Oravecz et al., 2017). In the case of SAN, the action potentials were empirically found in the right atrium. SAN action potentials were verified by the maximum upstroke speed, which had to be lower than 15 V/s, the resting membrane potential (>−60 mV), and a clear diastolic depolarization (DD). Efforts were made to maintain the same impalement throughout each experiment. If impalement became dislodged, however, electrode adjustment was attempted and, if the action potential characteristics of the re-established impalement deviated by less than 5% from those of the previous measurement, the experiment was continued. When this 5% limit was exceeded, the experiment was terminated and all data were excluded from the analyses.

Action potential durations were measured at 90, 50, and 25% of repolarization. The maximal diastolic potential was defined as the most negative potential reached during the repolarization. The take off potential is the most negative point of the AP upstroke. DD was defined as the interval between the maximal diastolic potential and take off potential. The DD slope was calculated as $\Delta V_m/\Delta t$ between these points. The cycle length was calculated as the peak-to-peak interval between two consecutive APs. The phase 0 depolarization velocity was defined as the maximum of the first derivative of the AP during the upstroke.

Modeling

To complement the experiments, we performed mechanistic computational modeling using the Yaniv *et al*. model of rabbit SAN cells (Yaniv et al., 2013b). The differential equations of the model were solved using a forward Euler scheme. Simulation results were analyzed when the system had converged to a cyclic steady-state.

Statistical Analysis

All data are expressed as mean ± standard error (SEM). Statistical analysis was performed with Student's *t*-test and ANOVA with Bonferroni *post-hoc* test. The results were considered statistically significant when $p < 0.05$. In the case of action potential experiments, all recordings were obtained from different hearts.

Materials

With the exception of ORM-10962 (ORM) (from Orion Pharma, Espoo, Finland), and Fluo-4 AM (Thermo Fisher Scientific, Waltham, MA, USA), all chemicals were purchased from Sigma-Aldrich Fine Chemicals (St. Louis, MO, USA). ORM was dissolved in dimethyl-sulfoxide (DMSO) to obtain a 1 mM stock solution. This stock solution was diluted to reach the desired final concentration (DMSO concentration not exceeding 0.1%) in the bath.

RESULTS

ORM-10962 Has No Effect on Funny Current

Figure 1 shows the measurement of I_f in isolated SAN cells by applying the whole cell configuration of the patch clamp method. The selectivity of ORM on Na^+-, Ca^{2+}-, and major K^+ currents was tested in a previous study from our laboratory (Kohajda et al., 2016). However, its potential effect on the I_f current was not investigated in that previous study. As **Figures 1A**, **C** show a slowly developed current at negative hyperpolarizing membrane potential (from −30 to −120 mV), which was not altered by application of 1 μM ORM (**Figure 1B**). In contrast, it was markedly inhibited by 10 μM IVA (69.3 ± 3.4%), a well known inhibitor of I_f.

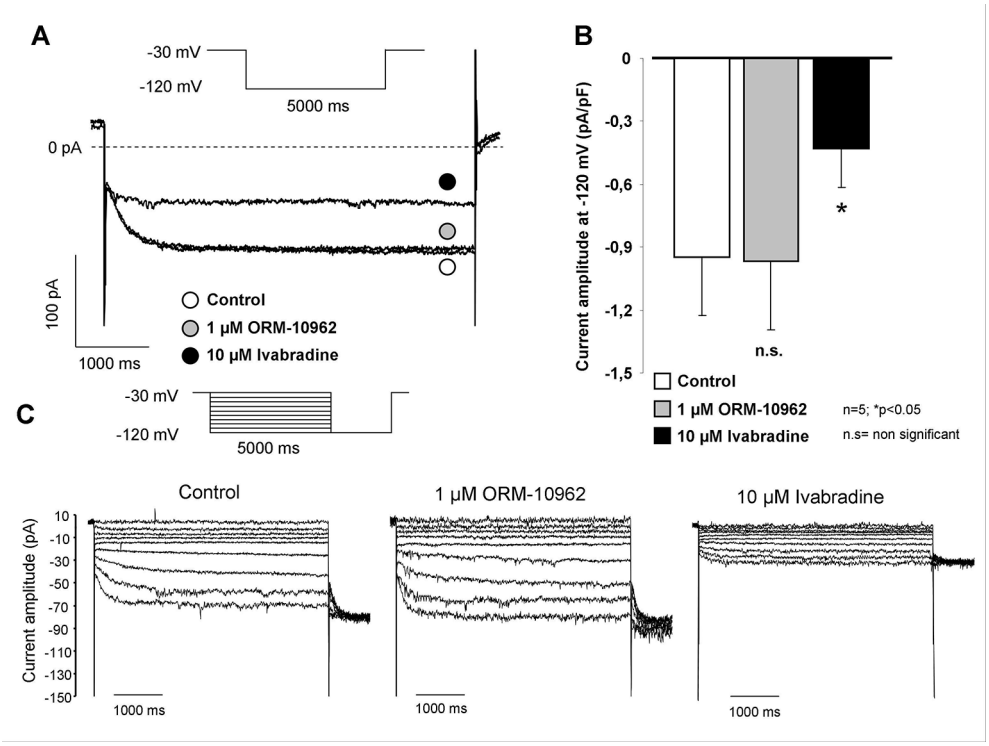

FIGURE 1 | Investigation of the possible effect of ORM-10962 (ORM) on funny current (I_f) in isolated sinus node (SAN) cells. The hyperpolarization activated I_f was elicited by 5,000 ms long rectangle pulse potentials to –120 mV from a holding potential of –30 mV. As representative current traces indicate, the current amplitude after ORM application (gray circle) was identical with the control (open circle). The considerable effect of 10 μM ivabradine (IVA) verified that the elicited current was indeed I_f **(A**, **B)**. Original traces in panel **(C)** represent the absence of ORM effects on current-voltage relationship of I_f by applying hyperpolarization pulses from –120 mV to –30 mV with 10 mV increments.

Na^+/Ca^{2+} Exchanger Inhibition Exerted Moderate Bradycardic Effect on Sinus Node Tissue

Figure 2 summarizes the effect of selective NCX inhibition by ORM on the spontaneous automaticity in SAN. Following application of 1 μM ORM a moderate but significant lengthening effect on the CL was observed (455.6 ± 32 ms *vs.* 493.0 ± 38 ms; Δ = 8.1 ± 1.8% $p < 0.05$, n = 16/16 hearts; **Figures 2A**–**C**) without any influence on the action potential duration (APD) (94.3 ± 6.7 ms *vs.* 96.7 ± 5.9 ms; **Figure 2D**). The slope of the diastolic depolarization phase was significantly reduced after ORM application (15.7 ± 3.1 mV/s *vs.* 10.9 ± 2.8 mV/s; n = 14/14; $p < 0.05$ **Figure 2E**) while the CL variability remained unchanged (7.6 ± 1.2 ms *vs.* 8.1 ± 1.3 ms; **Figure 2F**). The slope of phase 0 AP depolarization was identical during control and ORM experiments (11.2 ± 2.7 V/s *vs.* 12.5 ± 2.3 V/s). The preparations maintained the stable frequency in the time control experiments when DMSO was applied (440 ± 36.1 ms *vs.* 445 ± 37.6; n = 4). In the computational SAN action potential model (Yaniv et al., 2013b), we identified the degree of NCX current suppression required to obtain a similar CL increase as was experimentally measured. Forty-one percent of NCX inhibition was required to obtain 8% CL increase which was equal with the CL change observed experimentally (**Figure 2G**).

Na^+/Ca^{2+} Exchanger Inhibition Slightly Increased the Diastolic Ca^{2+} Level in Isolated Sinus Node Cells

The diastolic Ca^{2+} level increased in isolated SAN cells after ORM treatment (70 ± 11 nM *vs.* 130 ± 24 nM; $p < 0.05$, n = 10; **Figures 3A**, **B**), the effect was similar than was predicted by the Yaniv et al. SAN model (**Figure 3D**). In contrast to the model prediction, we found considerable increase in the transient amplitude (312 ± 37 nM *vs.* 568 ± 85 nM; $p < 0.05$, n = 10 **Figure 3C**), which was nearly doubled (82.1 ± 22%) in response to ORM application compared to the control value.

The Concomitant Application of Ivabradine and ORM-10962 Revealed Coupled Frequency Control Between Funny Current and Na^+/Ca^{2+} Exchanger Measured in Sinus Node Tissue

In the next set of experiments, IVA and ORM were subsequently applied to study a possible coupling between I_f and NCX.

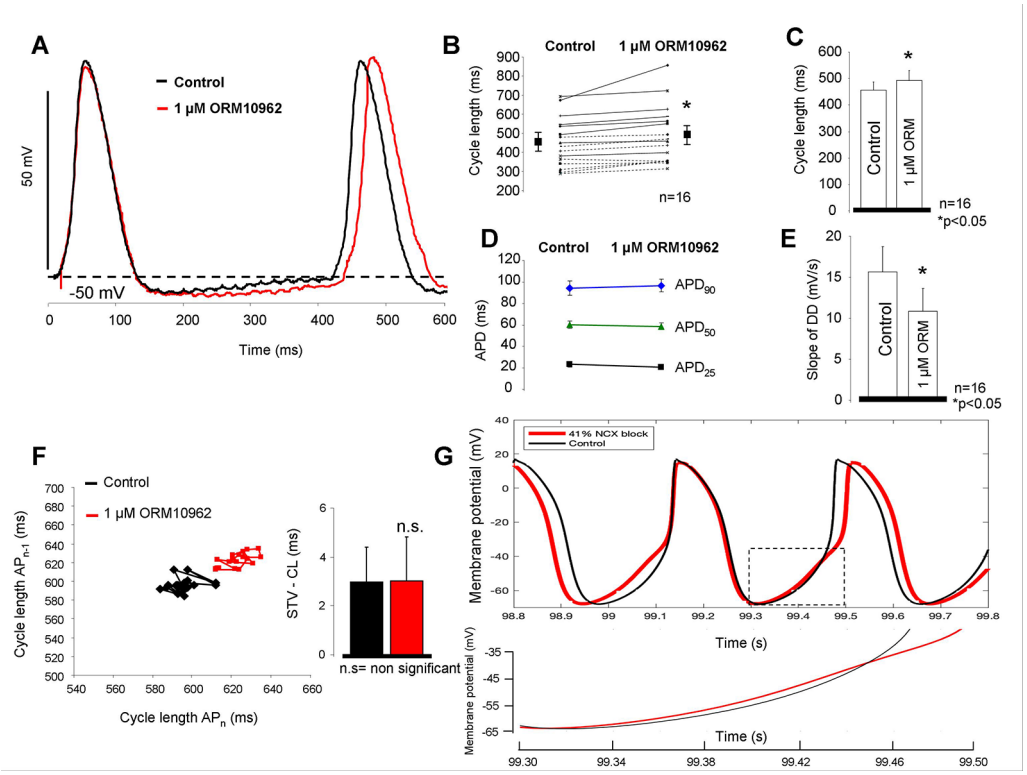

FIGURE 2 | Estimation of the effect of selective Na+/Ca2+ exchanger (NCX) inhibition on sinus node (SAN) tissue. As representative action potential traces **(A)** as well as individual experiments **(B)** and bar graphs **(C)** indicate, application of 1 μM ORM-10962 (ORM) exerted a slight but statistically significant bradycardic effect on SAN tissue. The action potential duration (APD) did not change during the experiment **(D)**, however the slope of the spontaneous depolarization was considerably decreased **(E)**. 30 consecutive cycles were analyzed to estimate the pacing rate variability. Poincaré-plot and bar graphs depict that ORM did not alter the short-term cycle length (CL) variability **(F)**. The Yaniv SAN cell model predicts 41% NCX inhibition to meet with the observed bradycardic effect of 1 μM ORM. The inset illustrates the reduced slope during late diastolic depolarization (DD) when 41% NCX inhibition was applied (red curve) **(G)**.

The effect of 1 μM ORM was substantially larger when I_f was previously inhibited (**Figures 4A**, **B**). Ca^{2+} transient measurements from spontaneously contracting SAN cells showed identical amplitudes (327 ± 23 nM *vs.* 337 ± 42 nM; n = 12) as well as diastolic Ca^{2+} levels (89 ± 22 nM *vs.* 85 ± 13 nM; n = 12) between control and 3 μM IVA (**Figure 4C**). A clear, gradual increase of ORM effect on the CL was observed with combined increasing concentration of IVA (1 μM ORM effect in the presence of 0 μM IVA: 8.1 ± 1.88%; in the presence of 0.5 μM IVA: 9.6 ± 2.3%; in the presence of 3 μM IVA: 17.1 ± 2.5%; **Figure 4D**). The ORM effect in the presence of 0.5 μM IVA did not differ significantly from the control, where 0 μM IVA was applied (8.1 ± 1.88% *versus* 9.6 ± 2.3%). In contrast, ORM effect was significantly larger on the CL in the presence of 3 μM IVA, compared with the control where IVA was not applied (8.1 ± 1.88% *versus* 17.1 ± 2.5%; $p < 0.05$, ANOVA, Bonferroni *post hoc* test). IVA significantly increased the CL both in 0.5 and in 3 μM concentrations ($p < 0.05$, ANOVA, Bonferroni *post hoc* test). In **Figure 4E**, we compare modeling and experimental results. In the Yaniv et al. model, based on a previous study (Bois et al., 1996), I_f inhibition was varied between 0%/20%/60% block (corresponding to 0, 0.5, and 3 μM IVA). Larger, 85% inhibition was only set in the model, since experimental application of 10 μM IVA is not feasible because of the marked I_{Kr} inhibition which can also reduce automaticity. The NCX inhibition was 41% in all cases. As **Figure 4E** shows, the modeling results do not match the experiments quantitatively, however they show a similar tendency (when I_f block increases, the same NCX inhibition causes larger CL prolongation) with markedly steeper correlation.

Figure 4F shows original modeling traces in the presence of 20% (left panel), 60% (middle panel), and 85% (right panel) I_f inhibition when NCX inhibition was 41% in all cases. The action potential modeling demonstrates an increased CL prolongation effect of NCX inhibition as I_f suppression becomes stronger, however, in contrast to the model prediction the steepness of NCX inhibition-induced CL increase was considerable flatter during experiments.

I_{Kr} Inhibition-Induced Bradycardia Did Not Facilitate the Effect of Selective Na^+/Ca^{2+} Exchanger Inhibition on Cycle Length in Sinus Node Tissue

We investigated how bradycardia induced by a mechanism which does not directly involve the inward depolarizing

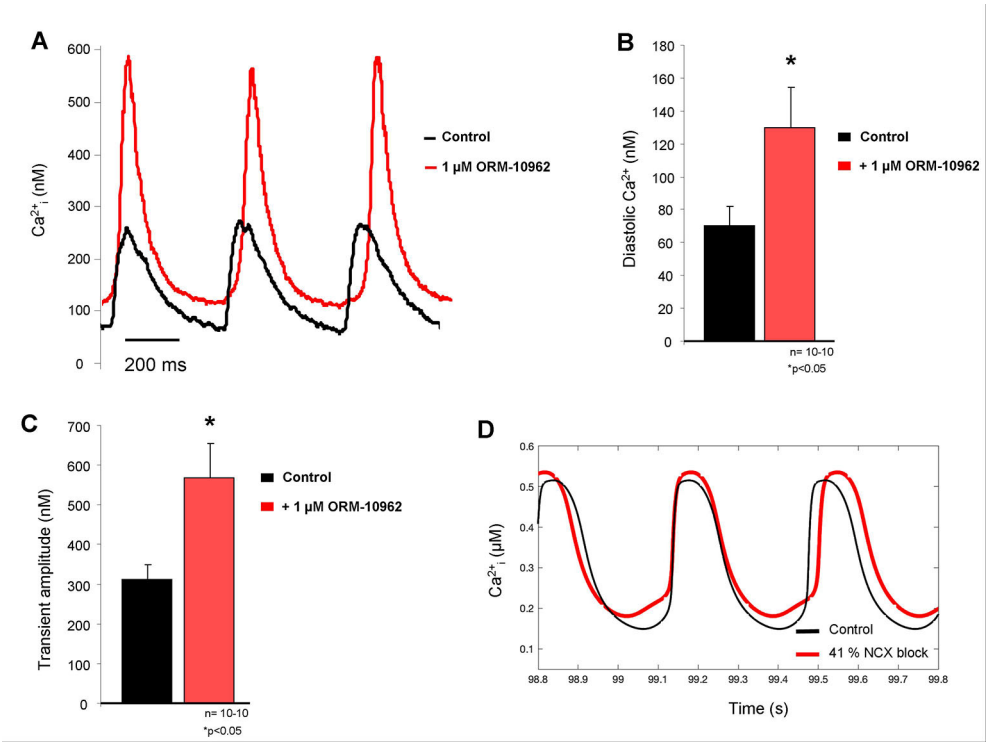

FIGURE 3 | (A) Representative Ca^{2+} transient traces from spontaneously contracting isolated sinus node (SAN) cells under control conditions (black trace) and after 1 µM ORM-10962 (ORM) application (red trace). As original fluorescent data as well as bar graphs indicate, a slight but significant increase of the diastolic Ca^{2+} level **(B)** with increased transient amplitude **(C)** was observed. In line with experimental data, the Yaniv SAN cell model predicted similar diastolic Ca^{2+} gain after 41% Na+/Ca2+ exchanger (NCX) inhibition **(D)**, however the increase of transient amplitude is much more pronounced during the experimental results.

currents (I_f and NCX) would influence the effect of NCX inhibition. Full I_{Kr} block induced by 100 nM dofetilide (DOF) markedly increased the CL of SAN AP (control: 489.3 ± 31 ms → 100 nM dofetilide: 649.1 ± 40.2 ms). This degree of increase of CL was due to the lengthening of APD without changing the DI. The subsequent application of 1 µM ORM exerted a similar effect (1 µM ORM-10962: 679.6 ± 52.6 ms; n = 7/7 hearts; **Figures 5A**, **B**), compared with results obtained after individual administration presented in **Figure 2** (7.2 ± 1.8% *vs.* 8.1 ± 1.8%, **Figure 5F**). It is important that the effect of DOF on CL was nearly similar to 3 µM IVA (32.9 ± 6.7% *vs.* 20.9 ± 4.1%). However, the major difference was that the DOF-mediated increase in CL was practically entirely an APD increase-induced effect (APD_{90}: 94.4 ± 3 ms *vs.* 187 ± 7.1 ms; $p < 0.05$, n = 7; diastolic interval (DI): 338.3 ± 39 ms *vs.* 352.7 ± 44.6 ms, n = 7) while the IVA influenced only the DI without affecting the APD_{90} (**Figures 5C–E**). In contrast, both NCX inhibition by ORM and I_f inhibition by IVA increased the CL due to lengthening of the time of the DI by decreasing its slope. When ORM was applied in combination with DOF the increase of the CL was not additive.

Suppression of Ca^{2+} Increases the Effect of I_f Inhibition on Cycle Length in Sinus Node Tissue

In the next set of experiments, we investigated the potential effect of suppression of SR Ca^{2+} release on the effect of IVA (**Figure 6A**). The aim was to minimize the depolarizing activity of the Ca^{2+} release-induced augmentation of the forward NCX by application of 5 µM ryanodine (RYA) after the control recording. This caused a significant CL prolongation (437.8 ± 20.3 ms *vs.* 499.8 ± 10.4 ms; $p < 0.05$, n = 6/6). The subsequently applied 1 µM ORM-10962 marginally but statistically significantly increased the CL (499.8 ± 10.4 ms *vs.* 520.8 ± 29.9 ms; $p < 0.05$; n = 6/6). However, further 3 µM IVA markedly and significantly augmented the CL of the SAN preparations (520.8 ± 29.9 ms *vs.* 726.6 ± 39.8 ms; $p < 0.05$, n = 6/6; **Figure 6B**). In the **Figure 6C** we compared the IVA effects under normal condition (i.e., in the absence of any other inhibitors—20.9 ± 4.1%) and in the presence of RYA+ORM. As bar graphs in **Figure 6C** show, the IVA exerted markedly larger CL prolongation in the presence of RYA+ORM (42.4 ± 5.7%, $p < 0.05$, Student's T-test).

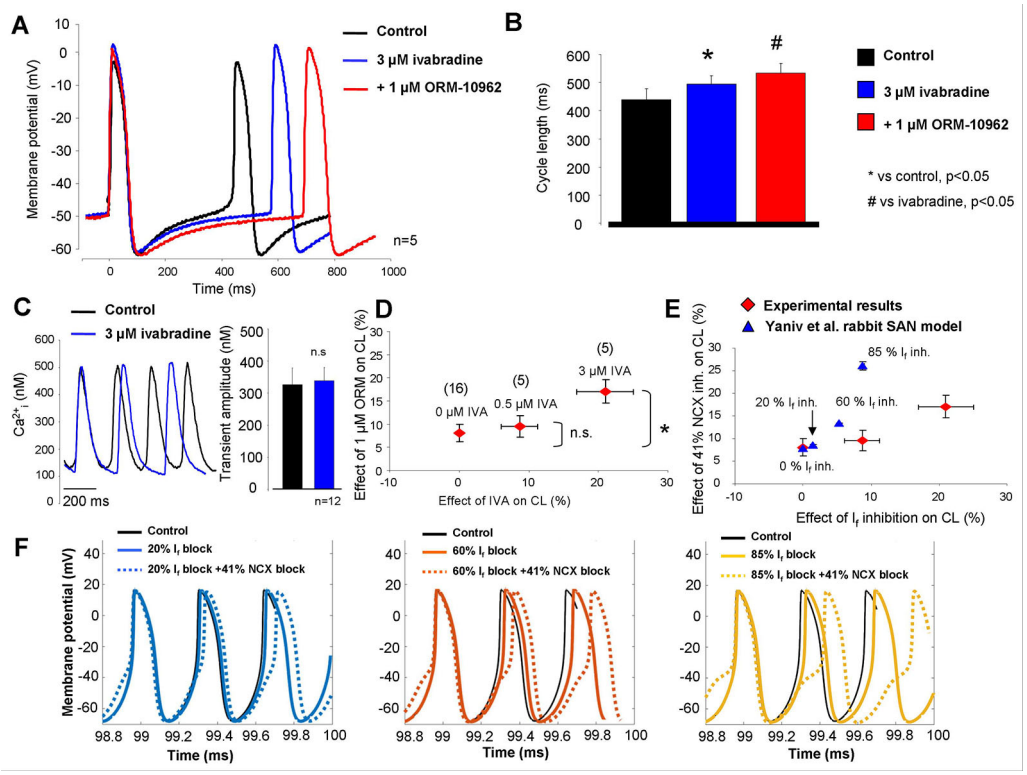

FIGURE 4 | Combined inhibition of Na+/Ca2+ exchanger (NCX) and I_f in sinus node (SAN). As original SAN action potentials and bar graphs report **(A, B)**, 1 µM ORM-10962 (ORM) (red trace) exerted an increased effect after 0.3 µM ivabradine (IVA) pretreatment (blue trace). Panel **(C)** represent Ca^{2+} transients measured from isolated SAN cells under control condition (black trace) and in the presence of 3 µM IVA (blue trace). We found identical Ca^{2+} levels as a result of IVA treatment. In panel **(D)**, the dose dependent effect of IVA (abscissa) on SAN cycle length (CL) was plotted against the effect of consecutive application of 1 µM ORM on CL (ordinate). As was previously described in **Figures 2A–C**, 1 µM ORM has ≈8% effect without IVA. In the presence of 0.5 and 3 µM IVA, the ORM-induced reduction of pacing rate was gradually increased. The numbers in parentheses indicate the corresponding n. The experimental results (red) are compared with the Yaniv SAN cell model (blue) in panel **(E)**. Based on a previous study, 0.5 and 3 µM IVA were represented by 20 and 60% funny current (I_f) inhibition in the presence of constant 41% NCX inhibition. Panel **(F)** represents the modeling results of combined I_f-NCX block. In the three panels, I_f was inhibited by varying degrees (straight lines) and combined with 41% NCX inhibition (dotted lines) yielding an increasing NCX inhibition effect on CL as I_f inhibition increases.

Decrease of $[Ca^{2+}]_O$ Increases the Effect of Funny Current Inhibition on Cycle Length in Sinus Node Tissue

We further tested the coupling between Ca^{2+} handling and I_f on CL control. Reduced $[Ca^{2+}]_o$ (0.9 mM) external solution was selected to achieve this goal since in this concentration, the CL was only slightly reduced (10.3 ± 3.7%). We found that the reduced extracellular Ca^{2+} slightly increased the CL which was further increased after application of 3 µM IVA (control: 469 ± 39.5 ms → 0.9 mM $[Ca^{2+}]_o$: 515.8 ± 40.8 ms → 3 µM IVA: 777 ± 58.7 ms; $p < 0.05$, n = 6/6 hearts, **Figures 7A, B**). We compared again the effects of IVA on the CL under normal condition (i.e., 1.8 $[Ca^{2+}]_o$) and in the presence of low external Ca^{2+} (0.9 mM $[Ca^{2+}]_o$). As bar graphs in **Figure 7C** demonstrates the IVA has markedly improved effect when extracellular Ca^{2+} is low compared with normal Ca^{2+} settings (51.1 ± 5.1% *versus* 20.99 ± 4.1%, $p < 0.05$; Student's t-test). **Figure 7D** represents Ca^{2+} transient measurements from spontaneously contracting isolated cells. We can observe that the application of 0.9 mM $[Ca^{2+}]_o$ significantly decreased the transient amplitude (295 ± 52 nM *vs.* 185 ± 32 nM; $p < 0.05$, n = 8) which may reflect decreased Ca^{2+} influx, SR Ca^{2+} release which may decrease the NCX current and thus attenuate the compensating capacity of NCX. The diastolic Ca^{2+} also significantly decreased (127 ± 33 *vs.* 64 ± 10 nM; $p < 0.05$, n = 8). We addressed this question by using mechanistic modeling (Yaniv et al., 2013b). Left column of **Figure 7E** represents action potentials (upper traces), NCX and I_f current kinetics (middle traces), and global Ca^{2+} transients (lower traces) under normal condition. Upon application of 0.9 mM $[Ca^{2+}]_o$ (right column) the CL slightly reduced, the integral of NCX current under the late phase of DD decreased while the magnitude of I_f current did not changed. The amplitude of the global transient decreased in similar extent as was obtained from SAN cell experiments.

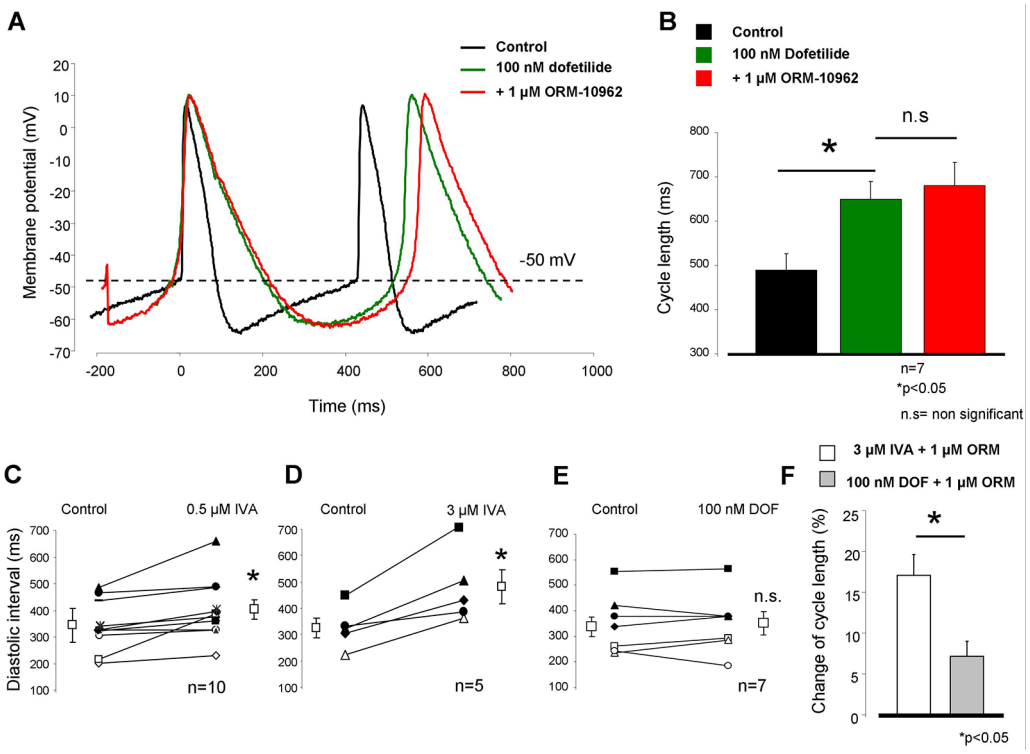

FIGURE 5 | Sinus node (SAN) frequency was decreased by complete I_{Kr} inhibition by 100 nM dofetilide administration. The control cycle length (CL) (black trace) largely increased after dofetilide (green trace). However, the effect of 1 µM ORM-10962 (ORM) did not change compared with the individual effect (red trace, panels **A, B, F)**. The main difference between ivabradine (IVA) and dofetilide (DOF)-induced bradycardia is that 0.5 and 3 µM IVA markedly increased the diastolic interval **(C**, **D)**, which remained unchanged in the case of I_{Kr} inhibition by DOF **(E)**.

Concomitant Inhibition of Na^+/Ca^{2+} Exchanger and Funny Current Increases the Cycle Length Variability in Sinus Node Tissue

The short term CL variability (CLV) was calculated by the analysis of CLs of N = 30 consecutive action potentials by applying the following formula:

$$\mathrm{STV} = \Sigma(\mathrm{CL;i+1} - \mathrm{CL;i}) / \left(n_{beats} x \sqrt{2}\right).$$

One micrometer of ORM-10962 and 3 µM IVA individually prolong the CL without considerable influence on the CL variability (see the area covered in **Figures 8A, B**). The subsequent application of 5 µM RYA (**Figure 8C**, green line) and 5 µM RYA + 1 µM ORM-10962 (**Figure 8C**, red line) showed a tendency to increase the CL variability, however it proved not to be statistically significant. In contrast, additionally adding 3 µM IVA markedly and statistically significantly enhanced the variability parallel with the CL increase, when the Ca^{2+} release and NCX activity were suppressed (**Figure 8C**, blue line). As **Figures 8D**, **E** show, the CL variability exerts similar results as the CL measurements: individual inhibition of NCX (2.53 ± 0.8 ms *vs.* 2.71 ± 0.9 ms; n = 16/16; red line) and I_f (3.6 ± 0.9 ms *vs.* 5.19 ± 0.7 ms; n = 5/5; blue line) or Ca^{2+} handling suppression (3.03 ± 0.87 ms *vs.* 7.0 ± 2.73 ms, n = 7/7; green line) do not alter significantly the CLV while the variability was largely increased if IVA was administrated in the presence of reduced Ca^{2+} cycling activity (7.0 ± 2.73 ms *vs.* 15.29 ± 5.6 ms; orange line).

DISCUSSION

The aim of this study was to verify and estimate the possible contribution of NCX function in SAN automaticity by direct selective pharmacological inhibition. Furthermore, we evaluated the functional consequences of the previously mentioned (Yaniv et al., 2015) I_f-NCX coupling in multicellular tissue level. In this study, we provided evidence for the first time regarding the essential role of NCX in spontaneous automaticity of the SAN by selective pharmacological inhibition. In addition, we described its functional interaction with I_f. This interaction between the DD currents is based on the following experimental results: i) 3 µM IVA has moderate effects on CL (~21%) and CLV (Δ ~ 2 ms), ii) 1 µM ORM has marginal effects on CL (~8%) and no change on CLV, iii) Ca^{2+} cycling suppression by 1 µM ORM + 5 µM RYA has moderate effects on CL (~19%) and CLV (Δ ~ 4 ms), iv) increasing I_f inhibition augments the effect of a

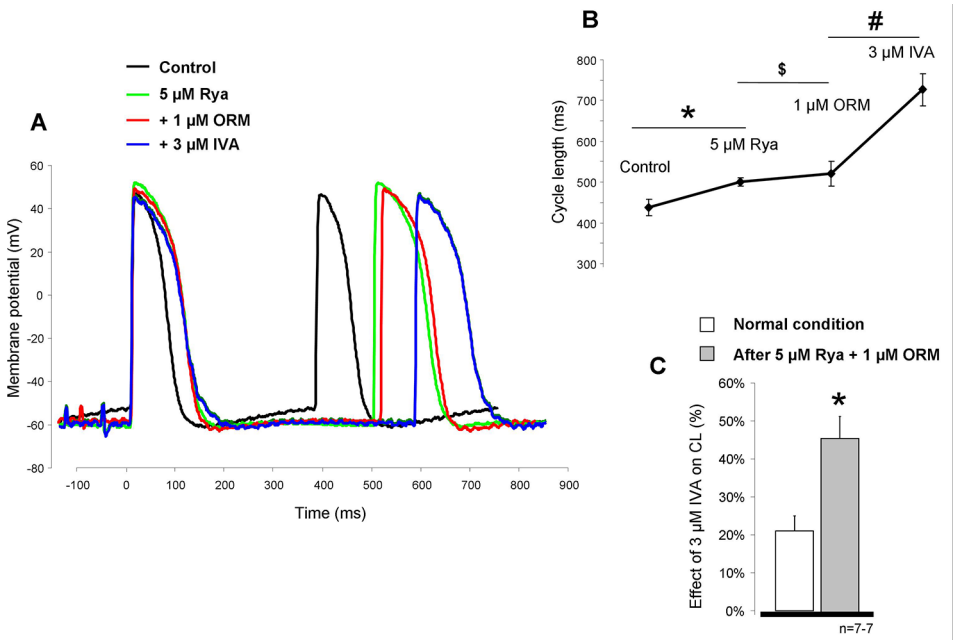

FIGURE 6 | The potential influence of Ca^{2+} handling suppression by 5 μM ryanodine (RYA) (green line) and 1 μM ORM-10962 (red line) on the effect of funny current (I_f) reduction was investigated. As representative curves panel **(A)** and diagram panel **(B)** report, both drugs increased the cycle length (CL) of the action potential. Statistical analysis was achieved by ANOVA. * means RYA compared to control, $ means ORM-10962 (ORM) compared to RYA, and # means ivabradine (IVA) compared to ORM. Comparison of the effect of 3 μM IVA on the CL under normal condition (i.e., without any other inhibitors) and after 5 μM RYA + 1μM ORM shows that the same dose of IVA has markedly increased effect when the contribution of Na+/Ca2+ exchanger (NCX) is reduced by concomitant application of RYA and ORM panel **(C)**.

fixed ORM dose (1 μM) on CL (~ 8 to 17%), v) the effect of 3 uM IVA is enhanced when Ca^{2+} cycling was previously suppressed (from ~ 20 to 42%).

ORM-10962 Does Not Inhibit the Funny Current

The effectiveness and selectivity of ORM-10962, a novel, potent NCX inhibitor was investigated in detail in our previous studies (Kohajda et al., 2016; Oravecz et al., 2017). In these studies, it was shown that ORM inhibited both forward and reverse mode NCX with an IC_{50} values of 55 and 67 nM without changing the I_{Ca}, I_{Na}, I_{K1}, I_{Kr}, I_{Ks}, I_{to}, and $I_{Na}/_K$ pump currents even at high (1 μM) concentrations. However, the I_f current was not investigated. The present study demonstrates that 1 μM ORM did not influence I_f (**Figure 1**) in the presence of high Ca^{2+} buffering, which means that ORM is a suitable tool for the evaluation of NCX in SAN automaticity, however the indirect effects related with ORM-induced Ca^{2+} elevation (without Ca^{2+} buffering) may influence the I_f indirectly (Mattick et al., 2007).

Na^+/Ca^{2+} Exchanger Inhibition Slightly Decreases Sinus Node Firing Rate

We found slight, but statistically significant reduction in the spontaneous firing rate in SAN tissue which is the consequence of the reduced rate of the DD (**Figure 2**). This result is a direct evidence and verification for the contribution of the inward NCX in rhythm generation. Previous studies (Yaniv et al., 2013a; Yaniv et al., 2015) reported that not only the increase of CL, but the parallel increase of pacing variability reports the uncoupling of the I_f-NCX and the destabilization of the DD. Since in our experiments the CL slightly increased while the pacing rate variability did not change, we conclude that the individual NCX inhibition did not cause considerable uncoupling of I_f-NCX.

The rate of forward NCX inhibition by using 1 μM ORM was estimated to ≈90% by applying conventional ramp protocol in the presence of ≈160 nM $[Ca^{2+}]_i$ in canine ventricular myocytes in our previous study (Kohajda et al., 2016). The actual ratio of inhibited NCX which corresponds with the observed CL changes was calculated to 41% by using the Yaniv SAN cell model (Yaniv et al., 2013b). It is important to note, that in our previous study (Oravecz et al., 2017) we have demonstrated that the extent of NCX inhibition (*via* ORM-10962) is decreased when the intracellular Ca^{2+} is intact (i.e., in the presence of Ca^{2+} transient). The underlying mechanism could be asymmetrical block between two modes, autoregulation of the $Ca^{2+}{}_i$ or by preserved inducibility of forward NCX by elevated $Ca^{2+}{}_i$.

Na^+/Ca^{2+} Exchanger Inhibition Markedly Increases the $Ca^{2+}{}_i$ Level

The selective NCX inhibition caused similar diastolic Ca^{2+} changes compared to the Yaniv model predicted, however, in

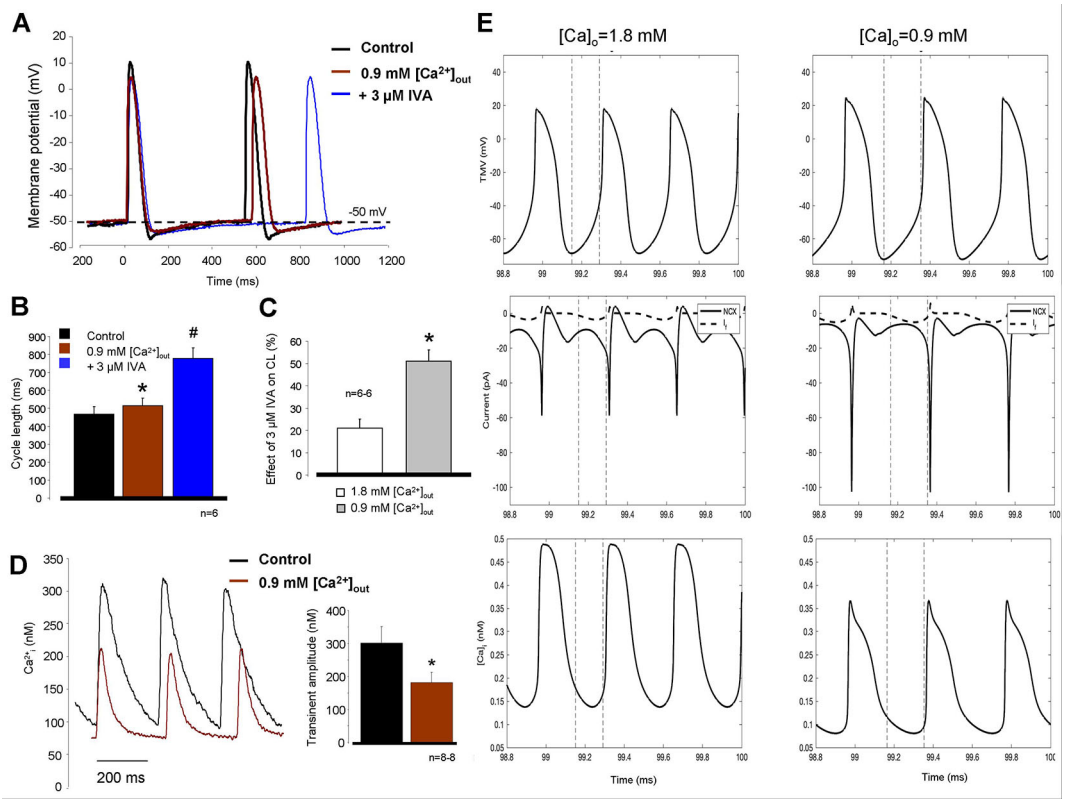

FIGURE 7 | Decreased extracellular Ca^{2+} solution (0.9 mM) was used to suppress the intracellular Ca^{2+} cycling and therefore Na+/Ca2+ exchanger (NCX). The effect of hypocalcemic solution on the cycle length (CL) was marginal (**A, B**, brown trace) however the subsequently applied 3 μM ivabradine (IVA) (blue trace) caused considerable prolongation in the CL. Comparison of the IVA effect in the presence of normal (1.8 mM—white column) *versus* low (0.9 mM—gray column) $CaCl_2$ on panel **(C)** demonstrates nearly doubled effect of IVA on the CL in response of Ca^{2+} reduction **(C)**. * means 0.9 mM $[Ca^{2+}]_o$ compared to control, # means IVA *versus* 0.9 mM $[Ca^{2+}]_o$. Original traces measured from isolated sinus node (SAN) cells in panel **(D)** demonstrate that 0.9 mM $[Ca^{2+}]_o$ (brown trace) significantly decreased the transient amplitude without significant action on diastolic Ca^{2+} levels. **(E)** Modeling simulation of action potentials (upper traces), NCX currents (middle traces, solid lines), I_f currents (middle traces, dashed lines), and global Ca^{2+} transients (lower traces) in the present of normal (1.8 mM), external Ca^{2+} (left column), and 0.9 mM $[Ca^{2+}]_o$ (right column). The results indicate decreased transient amplitude coupled with smaller NCX current in the late diastolic depolarization (DD) with maintained I_f current magnitude in the presence of 0.9 mM $[Ca^{2+}]_o$.

contrast with modeling, we found markedly increased Ca^{2+} transient amplitude which is generally expected after decreased rate of Ca^{2+} extrusion (**Figure 3**). The observed quantitative discrepancy between experiments and modeling may indicate that the extent of NCX inhibition in the experiments could be larger than 41%.

We can speculate that the increasing intracellular Ca^{2+} is known to facilitate the inactivation of the L-type Ca^{2+} current as a part of the autoregulation (Eisner et al., 1998; Eisner et al., 2000). The gain of the $[Ca^{2+}]_i$ may indirectly shortens the CL which means two parallel, counteracting effect of selective NCX inhibition: the inhibition of the inward NCX current may reduce the actual frequency by suppressing its contribution in the DD, however it is partially compensated for the CL abbreviating effect of increased $[Ca^{2+}]_i$. Furthermore, the I_f may also contribute in the limitation of the ORM effect: i) a theoretical possibility exists that ORM-induced Ca^{2+} elevation may increase the I_f, however this was ruled out by a previous work (Zaza et al., 1991). ii) It was reported that SAN myocytes express Ca^{2+}-activated adenylate cyclase isoform, which might raise cAMP (and I_f) in response to NCX blockade (Mattick et al., 2007).

The Moderate Bradycardic Effect of Na^+/Ca^{2+} Exchanger Inhibition May Be Explained by Funny Current-Na^+/Ca^{2+} Exchanger Coupling

However, one may speculate after considering the crucial role of NCX in the coupled-clock theory, why the NCX inhibition-induced "bradycardia" exerted a relatively low influence. Using genetic mouse models Gao *et al.* claimed that partial ablation of NCX (≈70–80%) using an αMHC-inducible "Cre" transgenic line, has also a slight effect on the baseline spontaneous AP firing frequency (Gao et al., 2013). In line with this, it was found that even a small NCX fraction is able to generate sufficient inward current to provide appropriate depolarization current which is

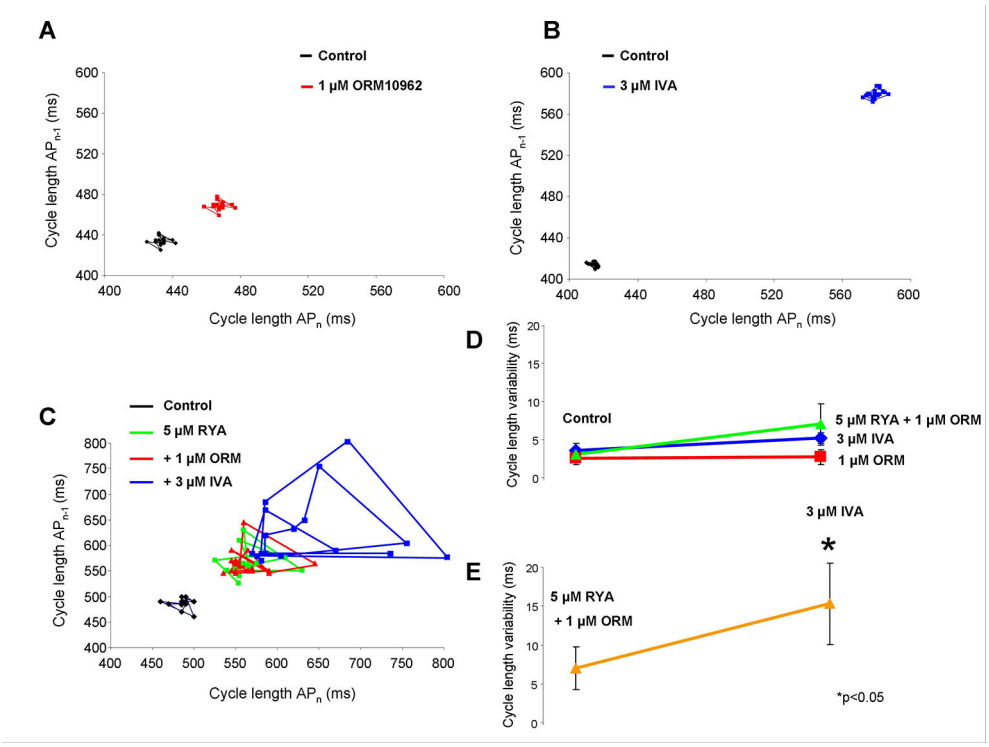

FIGURE 8 | The effect of suppression of diastolic depolarization (DD) currents [Na+/Ca2+ exchanger (NCX) and I_f] on short time cycle length (CL) variability. When 1 μM ORM-10962 panel **(A)** or 3 μM ivabradine (IVA) panel **(B)** were applied, the variability did not change significantly. Instead, the CL was prolonged. Comparison of the effect of 1 μM ORM-10962 (ORM) (red line), 5 μM ryanodine (RYA) (blue line), and 5 μM RYA + 1 μM ORM (green line) on the CL variability shows that these compound do not change the variability significantly panel **(D)**. In contrast IVA administration after the application of RYA+ORM caused considerably increased variability panel **(E)** as the Poincaré-plot (panel **C,** blue line) shows.

able to maintain normal SAN cell activity (Groenke et al., 2013). Our and these previous results highlight the possibility that a functional coupling between I_f and NCX represents a potency to compensate for the NCX inhibition-induced reduction of the pacing frequency.

In accordance with this theory our and previous results indicate a relatively moderate effect of IVA on the CL when it is administrated at 3 μM (**Figure 4A**) or at 10 μM (Yaniv et al., 2012). At the same time, caesium was unable to stop SAN beating even though it has a large effect on I_f (Noma et al., 1983). These inconsistent results can be explained by the voltage-dependent block of IVA or caesium (DiFrancesco, 1995), or by proposing an insulator function of the I_f to protect the SAN cells from the strong negative electrical sink of the connected atrial tissue (Morad and Zhang, 2017). However, a functional coupling between I_f and NCX (Bois et al., 1996; Lakatta et al., 2010; Yaniv et al., 2013a) providing redundant pacemaking systems could also explain—or at least contribute to—the observed results. This phenomenon, which could be very similar to the repolarization reserve (Biliczki et al., 2002; Herrmann et al., 2007; Lengyel et al., 2007; Nagy et al., 2009), may be also able to reduce the effects of the individual inhibition of NCX or I_f explaining the relatively small extent of IVA or NCX effects.

Indeed, we found that the effect of 1 μM ORM gradually increased as the rate of I_f block was enhanced (**Figure 4**). In line with this, the Yaniv model provided similar but steeper tendency, when we represented the 0.5, 1, and 3 μM IVA doses by 20, 60, and 80% I_f block based on previous results (Bois et al., 1996). While 10 μM IVA was not used experimentally due to selectivity problems, 85% I_f inhibition could be computed in the Yaniv model. The detailed modeling results are depicted in **Figures 4E, F**. Consistent with experimental results, the effect of 41% NCX inhibition on CL is increased as I_f inhibition becomes stronger. However, the modeling predicts a much steeper increase in the CL in the presence of enhancing I_f block. The underlying mechanism of this discrepancy could be the markedly higher Ca^{2+} increase measured during experiments which could limit the bradycardic effect of NCX inhibition. A previous study reported a decreased SR Ca^{2+} content after I_f inhibition by IVA (Yaniv et al., 2013a) demonstrating an indirect suppression of NCX during I_f inhibition. Our Ca^{2+} measurements (**Figure 4C**) indicate unchanged Ca^{2+} release after application of IVA, which may indicate that the underlying mechanism of increased ORM effect may be rather related with the increased sensitivity of DD when it is already inhibited by the I_f block.

I_{Kr} Inhibition Mediated Bradycardia Does Not Alter the Effect of Na^+/Ca^{2+} Exchanger Inhibition

It is possible to decelerate spontaneous frequency without major direct influence on I_f or NCX. The SAN rate was reduced by 100% I_{Kr} block (**Figure 5**) in which the developed decrease in the firing rate was mainly achieved by APD prolongation without or minimal change in diastolic interval—instead of I_f block, which markedly increases the diastolic interval without effect on APD. This also means that despite the bradycardia, I_f is intact during these experiments. In line with this, NCX inhibition provided a similar effect to the one which was experienced when NCX was inhibited individually in **Figure 2**. This observation could be explained by an I_f dependent compensation of NCX reduction. At the same time it also means that the mechanism of the bradycardia is important regarding the effect of NCX inhibition. It seems possible that I_f mediated bradycardia and concomitant increase in diastolic interval may be important in the I_f-NCX interaction.

Suppression of Ca^{2+}_i Augments the Effect of Funny Current Inhibition

Assuming that a mutual interaction between I_f and NCX exists, this crosstalk should work in the opposite direction as well, i.e., a disturbance in the Ca^{2+} cycling should affect I_f. The suppression of the Ca^{2+} handling by the subsequent application of ryanodine and ORM together caused ≈20% increase in the CL in line with previous results (Bucchi et al., 2003). Under this condition, the effect of 3 μM IVA was considerably larger compared with normal settings (≈45% *vs.* 20%, see **Figure 6C**). In line with this, we found similar augmentation of IVA effect (21% *vs.* 51%) when Ca^{2+} handling was suppressed by low extracellular Ca^{2+} (**Figure 7**). Experimental as well as modeling simulations suppose that the Ca^{2+} handling and thus the NCX current suppression decreases the flux of the depolarizing NCX current, increases the length of DD, thus, the suppressed net current underlying the DD provides improved effect for I_f inhibition.

Funny Current-Na^+/Ca^{2+} Exchanger Coupling Controls Cycle Length Variability

Previous studies (Yaniv et al., 2013a; Yaniv et al., 2015) reported that the I_f-NCX coupling not only controls the current CL but it may have a crucial role in maintaining the normal rhythm of the SAN. Therefore, the increase of the CL variability could be a further indicator of the integrity of I_f-NCX axis appearing after a considerable CL increase reporting significant I_f-NCX uncoupling. Our results support this assumption indicating that after individual inhibition of I_f or NCX, not only the excessive CL increase is restricted but the SAN rhythm is also maintained. However, when both of I_f and NCX are suppressed, besides the marked CL increase, a perturbation in the rhythm also appeared indicating the exhausted capacity of the I_f-NCX to depolarize the membrane during the DD (**Figure 8**). Since we could not reach complete inhibition of I_f and NCX in our experiments, we cannot estimate precisely the relative importance of these currents in the normal SAN rhythm. However, it seems possible that these currents contribute in the "depolarization reserve" (Herrmann et al., 2007) not only to the control of the current CL but also to the maintenance of the normal pacing rhythm as a consequence of the strong depolarizing of the I_f-NCX crosstalk.

Proposed Mechanism

We suggest that the observed NCX-I_f interplay is the consequence of the increased susceptibility of DD to any intervention when the DD was previously inhibited by another compound (Rocchetti et al., 2000; Zaza and Lombardi, 2001; Monfredi et al., 2014). This means that the bradycardic effect of NCX inhibition is larger when I_f was previously inhibited (independently from the Ca^{2+} handling). *Vice versa*, when the NCX was previously suppressed (as a consequence of reduced Ca^{2+} release) the decreased DD current density is more sensitive to changes, which increases the bradycardic effect of IVA.

CONCLUSION

In the present study, we provide direct pharmacological evidence regarding the role of NCX in pacemaker mechanism by its selective inhibition with the novel, highly selective compound ORM-10962. We found that individual inhibitions of NCX or I_f cause only moderate bradycardia and rhythm disturbance. However, combined suppression of these currents acted synergistically and supports the hypothesis of mutual crosstalk between NCX and I_f in SAN even in multicellular tissue having important functional consequences. This means that individual inhibition of DD currents may have moderated effect on CL and variability under normal conditions because the underlying currents may be able to compensate each other. This important crosstalk may provide a considerable safety margin for SAN pacemaking.

STUDY LIMITATIONS

Our study has three important limitations. 1) The action potentials measured in our experiments do not represent the characteristics of the core SAN cells. These cells are much more "follower" cells, having AP waveforms largely influenced by the cell-to-cell coupling. 2) The applied inhibitors (IVA, ORM, RYA) are not able to cause complete block of ion channels in the applied concentrations. Therefore, the described phenomena indicate only partial effects and not able to estimate the absolute contribution of NCX during the DD. 3) Since our aim was to explore ion current cooperation, our results represent ion channel function independent from the autonomic nervous system. The activation of the sympathetic or parasympathetic nervous system—or modulation of the β_1/M_2 receptors—intimately changes the cAMP, PKA, CaMKII levels which have effects on the DD currents, therefore the discussed I_f-NCX coupling cannot be directly extrapolated to *in vivo* systems. The ion current crosstalk characterization during intact autonomic control requires further experiments.

DATA AVAILABILITY STATEMENT

All datasets generated for this study are included in the article/supplementary material.

ETHICS STATEMENT

The animal study was reviewed and approved by Munkahelyi Állatkísérleti Bizottság (MÁB).

AUTHOR CONTRIBUTIONS

ZK performed ion current measurements and data analysis. NT performed fluorescent optical measurements, action potential measurements and data analysis. JS performed ion current measurements and data analysis. AL performed the computational modeling and data analysis, contributed to conception of the study as well as manuscript preparation and funding for the computational study. PG performed ion current measurements, GB and JP performed action potential measurements. NJ organized the database and ensured the financial support of the study. JL and PP contributed to the development of ORM-10962. JGYP contributed to manuscript preparation, AV and NN ensured the financial support of the study, contributed conception and design of the study, data analysis and visualization, and manuscript preparation. All authors contributed to manuscript revision, read and approved the submitted version.

FUNDING

This work was supported by grants from the National Research Development and Innovation Office (NKFIH PD-125402 (for NN), FK-129117 (for NN), GINOP-2.3.2-15-2016-00006, the LIVE LONGER EFOP-3.6.2-16-2017-00006 project, the János Bolyai Research Scholarship of the Hungarian Academy of Sciences (for NN), the UNKP-18-4-SZTE-76 New National Excellence Program of the Ministry for Innovation and Technology (for NN), the EFOP 3.6.3 VEKOP-16-2017-00009 (for NT), the Hungarian Academy of Sciences and by the Orion Pharma (ORM-10962).

ACKNOWLEDGMENTS

We are grateful to Prof. Dr. David Eisner (University of Manchester, UK) for his help and suggestions for the manuscript. We gratefully acknowledge financial support by the Deutsche Forschungsgemeinschaft (DFG, German Research Foundation) – Project-ID 258734477 – SFB 1173 (to AL). The publication of this study was supported by the University of Szeged Open Access Fund (4309).

REFERENCES

Biliczki, P., Virag, L., Iost, N., Papp, J. G., and Varro, A. (2002). Interaction of different potassium channels in cardiac repolarization in dog ventricular preparations: role of repolarization reserve. *Br. J. Pharmacol.* 137 (3), 361–368. doi: 10.1038/sj.bjp.0704881

Bogdanov, K. Y., Vinogradova, T. M., and Lakatta, E. G. (2001). Sinoatrial nodal cell ryanodine receptor and $Na(^{+})$-$Ca(^{2+})$ exchanger: molecular partners in pacemaker regulation. *Circ. Res.* 88 (12), 1254–1258. doi: 10.1161/hh1201.092095

Bois, P., Bescond, J., Renaudon, B., and Lenfant, J. (1996). Mode of action of bradycardic agent, S 16257, on ionic currents of rabbit sinoatrial node cells. *Br. J. Pharmacol.* 118 (4), 1051–1057. doi: 10.1111/j.1476-5381.1996.tb15505.x

Bucchi, A., Baruscotti, M., Robinson, R. B., and DiFrancesco, D. (2003). I(f)-dependent modulation of pacemaker rate mediated by cAMP in the presence of ryanodine in rabbit sino-atrial node cells. *J. Mol. Cell Cardiol.* 35 (8), 905–913. doi: 10.1016/s0022-2828(03)00150-0

DiFrancesco, D., and Noble, D. (2012). The funny current has a major pacemaking role in the sinus node. *Heart Rhythm.* 9 (2), 299–301. doi: 10.1016/j.hrthm.2011.09.021

DiFrancesco, D. (1981). A new interpretation of the pace-maker current in calf Purkinje fibres. *J. Physiol.* 314, 359–376. doi: 10.1113/JPHYSIOL.1981.SP013713

DiFrancesco, D. (1995). Cesium and the pacemaker current. *J. Cardiovasc. Electrophysiol.* 6 (12), 1152–1155.

Eisner, D. A., Trafford, A. W., Diaz, M. E., Overend, C. L., and O'Neill, S. C. (1998). The control of Ca release from the cardiac sarcoplasmic reticulum: regulation versus autoregulation. *Cardiovasc. Res.* 38 (3), 589–604. doi: 10.1016/s6363(98)00062-5

Eisner, D. A., Choi, H. S., Diaz, M. E., O'Neill, S. C., and Trafford, A. W. (2000). Integrative analysis of calcium cycling in cardiac muscle. *Circ. Res.* 87 (12), 1087–1094. doi: 10.1161/01.res.87.12.1087

Gao, Z., Rasmussen, T. P., Li, Y., Kutschke, W., Koval, O. M., Wu, Y., et al. (2013). Genetic inhibition of Na^{+}-Ca^{2+} exchanger current disables fight or flight sinoatrial node activity without affecting resting heart rate. *Circ. Res.* 112 (2), 309–317. doi: 10.1161/CIRCRESAHA.111.300193

Groenke, S., Larson, E. D., Alber, S., Zhang, R., Lamp, S. T., Ren, X., et al. (2013). Complete atrial-specific knockout of sodium-calcium exchange eliminates sinoatrial node pacemaker activity. *PloS One* 8 (11), e81633. doi: 10.1371/journal.pone.0081633

Herrmann, S., Stieber, J., Stockl, G., Hofmann, F., and Ludwig, A. (2007). HCN4 provides a 'depolarization reserve' and is not required for heart rate acceleration in mice. *EMBO J.* 26 (21), 4423–4432. doi: 10.1038/sj.emboj.7601868

Herrmann, S., Lipp, P., Wiesen, K., Stieber, J., Nguyen, H., Kaiser, E., et al. (2013). The cardiac sodium-calcium exchanger NCX1 is a key player in the initiation and maintenance of a stable heart rhythm. *Cardiovasc. Res.* 99 (4), 780–788. doi: 10.1093/cvr/cvt154

Himeno, Y., Toyoda, F., Satoh, H., Amano, A., Cha, C. Y., Matsuura, H., et al. (2011). Minor contribution of cytosolic Ca2+ transients to the pacemaker rhythm in guinea pig sinoatrial node cells. *Am. J. Physiol. Heart Circ. Physiol.* 300 (1), H251–H261. doi: 10.1152/ajpheart.00764.2010

Jost, N., Nagy, N., Corici, C., Kohajda, Z., Horvath, A., Acsai, K., et al. (2013). ORM-10103, a novel specific inhibitor of the Na+/Ca2+ exchanger, decreases early and delayed afterdepolarizations in the canine heart. *Br. J. Pharmacol.* 170 (4), 768–778. doi: 10.1111/bph.12228

Kohajda, Z., Farkas-Morvay, N., Jost, N., Nagy, N., Geramipour, A., Horvath, A., et al. (2016). The effect of a novel highly selective inhibitor of the Sodium/Calcium exchanger (NCX) on cardiac arrhythmias in In Vitro and In Vivo experiments. *PloS One* 11 (11), e0166041. doi: 10.1371/journal.pone.0166041

Kormos, A., Nagy, N., Acsai, K., Vaczi, K., Agoston, S., Pollesello, P., et al. (2014). Efficacy of selective NCX inhibition by ORM-10103 during simulated ischemia/reperfusion. *Eur. J. Pharmacol.* 740, 539–551. doi: 10.1016/j.ejphar.2014.06.033

Lakatta, E. G., and DiFrancesco, D. (2009). What keeps us ticking: a funny current, a calcium clock, or both? *J. Mol. Cell Cardiol.* 47 (2), 157–170. doi: 10.1016/j.yjmcc.2009.03.022

Lakatta, E. G., Maltsev, V. A., and Vinogradova, T. M. (2010). A coupled system of intracellular Ca^{2+} clocks and surface membrane voltage clocks controls the timekeeping mechanism of the heart's pacemaker. *Circ. Res.* 106 (4), 659–673. doi: 10.1161/CIRCRESAHA.109.206078

Lengyel, C., Varro, A., Tabori, K., Papp, J. G., and Baczko, I. (2007). Combined pharmacological block of I(Kr) and I(Ks) increases short-term QT interval variability and provokes torsades de pointes. *Br. J. Pharmacol.* 151 (7), 941–951. doi: 10.1038/sj.bjp.0707297

Mattick, P., Parrington, J., Odia, E., Simpson, A., Collins, T., and Terrar, D. (2007). Ca^{2+}-stimulated adenylyl cyclase isoform AC1 is preferentially expressed in guinea-pig sino-atrial node cells and modulates the I(f) pacemaker current. *J.7 Physiol.* 582 (Pt 3), 1195–1203. doi: 10.1113/jphysiol.2007.133439

Monfredi, O., Lyashkov, A. E., Johnsen, A. B., Inada, S., Schneider, H., Wang, R., et al. (2014). Biophysical characterization of the underappreciated and important relationship between heart rate variability and heart rate. *Hypertension* 64 (6), 1334–1343. doi: 10.1161/HYPERTENSIONAHA.114.03782

Morad, M., and Zhang, X. H. (2017). Mechanisms of spontaneous pacing: sinoatrial nodal cells, neonatal cardiomyocytes, and human stem cell derived cardiomyocytes. *Can. J. Physiol. Pharmacol.* 95 (10), 1100–1107. doi: 10.1139/cjpp-2016-0743

Nagy, N., Szuts, V., Horvath, Z., Seprenyi, G., Farkas, A. S., Acsai, K., et al. (2009). Does small-conductance calcium-activated potassium channel contribute to cardiac repolarization? *J. Mol. Cell Cardiol.* 47 (5), 656–663. doi: 10.1016/j.yjmcc.2009.07.019

Noble, D., Noble, P. J., and Fink, M. (2010). Competing oscillators in cardiac pacemaking: historical background. *Circ. Res.* 106 (12), 1791–1797. doi: 10.1161/CIRCRESAHA.110.218875

Noma, A., Morad, M., and Irisawa, H. (1983). Does the "pacemaker current" generate the diastolic depolarization in the rabbit SA node cells? *Pflugers Arch.* 397 (3), 190–194. doi: 10.1007/bf00584356

Oravecz, K., Kormos, A., Gruber, A., Marton, Z., Kohajda, Z., Mirzaei, L., et al. (2017). Inotropic effect of NCX inhibition depends on the relative activity of the reverse NCX assessed by a novel inhibitor ORM-10962 on canine ventricular myocytes. *Eur. J. Pharmacol.* 818, 278–286. doi: 10.1016/j.ejphar.2017.10.039

Rocchetti, M., Malfatto, G., Lombardi, F., and Zaza, A. (2000). Role of the input/output relation of sinoatrial myocytes in cholinergic modulation of heart rate variability. *J. Cardiovasc. Electrophysiol.* 11 (5), 522–530. doi: 10.1111/j.1540-8167.2000.tb00005.x

Sanders, L., Rakovic, S., Lowe, M., Mattick, P. A., and Terrar, D. A. (2006). Fundamental importance of Na+-Ca2+ exchange for the pacemaking mechanism in guinea-pig sino-atrial node. *J. Physiol.* 571 (Pt 3), 639–649. doi: 10.1113/jphysiol.2005.100305

Sirenko, S. G., Maltsev, V. A., Yaniv, Y., Bychkov, R., Yaeger, D., Vinogradova, T., et al. (2016). Electrochemical Na+ and Ca2+ gradients drive coupled-clock regulation of automaticity of isolated rabbit sinoatrial nodal pacemaker cells. *Am. J. Physiol. Heart Circ. Physiol.* 311 (1), H251–H267. doi: 10.1152/ajpheart.00667.2015

Verkerk, A. O., den Ruijter, H. M., Bourier, J., Boukens, B. J., Brouwer, I. A., Wilders, R., et al. (2009). Dietary fish oil reduces pacemaker current and heart rate in rabbit. *Heart Rhythm.* 6 (10), 1485–1492. doi: 10.1016/j.hrthm.2009.07.024

Yaniv, Y., Maltsev, V. A., Ziman, B. D., Spurgeon, H. A., and Lakatta, E. G. (2012). The "funny" current (I(f)) inhibition by ivabradine at membrane potentials encompassing spontaneous depolarization in pacemaker cells. *Molecules* 17 (7), 8241–8254.

Yaniv, Y., Sirenko, S., Ziman, B. D., Spurgeon, H. A., Maltsev, V. A., and Lakatta, E. G. (2013a). New evidence for coupled clock regulation of the normal automaticity of sinoatrial nodal pacemaker cells: bradycardic effects of ivabradine are linked to suppression of intracellular Ca(2)(+) cycling. *J. Mol. Cell Cardiol.* 62, 80–89. doi: 10.1016/j.yjmcc.2013.04.026

Yaniv, Y., Stern, M. D., Lakatta, E. G., and Maltsev, V. A. (2013b). Mechanisms of beat-to-beat regulation of cardiac pacemaker cell function by Ca(2)(+) cycling dynamics. *Biophys. J.* 105 (7), 1551–1561. doi: 10.1016/j.bpj.2013.08.024

Yaniv, Y., Lakatta, E. G., and Maltsev, V. A. (2015). From two competing oscillators to one coupled-clock pacemaker cell system. *Front. Physiol.* 6, 28. doi: 10.3389/fphys.2015.00028

Zaza, A., and Lombardi, F. (2001). Autonomic indexes based on the analysis of heart rate variability: a view from the sinus node. *Cardiovasc. Res.* 50 (3), 434–442. doi: 10.1016/s0008-6363(01)00240-1

Zaza, A., Maccaferri, G., Mangoni, M., and DiFrancesco, D. (1991). Intracellular calcium does not directly modulate cardiac pacemaker (if) channels. *Pflugers Arch.* 419 (6), 662–664. doi: 10.1007/BF00370312

Conflict of Interest: PP and JL are employed by Orion Pharma, which has been involved in the development of ORM-10962.

The remaining authors declare that the research was conducted in the absence of any commercial or financial relationships that could be construed as a potential conflict of interest.

Szegedi Tudományegyetem
Farmakológiai és Farmakoterápiai Intézet
Igazgató: Dr. Bazkó István M.D., Ph.D.
Dóm tér 12. 6720 Szeged
Tel.: +36.62.545-682
Fax: +36.62.545-680
e-mail: baczko.istvan@med.u-szeged.hu

NYILATKOZAT

Alulírott, Dr. Nagy Norbert levelező szerző nyilatkozom, hogy az alábbi közleményben:

Zsófia Kohajda, Noémi Tóth, Jozefina Szlovák, Axel Loewe, Gergő Bitay, Péter Gazag, János Prorok, Norbert Jost, Jouko Levijoki, Piero Pollesello, Julius Gy. Papp, András Varró, Norbert Nagy

Novel NCX Inhibitor ORM-10962 Supports Coupled Function of Funny-current and Na+/Ca2+ Exchanger in Pacemaking of Rabbit Sinus Node Tissue

Front. Pharmacol. 2019

Dr. Tóth Noémi „*Ca^{2+} dependent regulation of sinoatrial node pacemaking*" című tézisében a 2. és a 4-8 ábrához tartozó kísérleteket használta fel. Ezek az eredmények későbbi PhD disszertációkban már nem kerülnek bemutatásra.

Továbbá nyilatkozom, hogy Szlovák Jozefina „*The role of Na+/Ca2+ exchanger in development of cardiac alternans*" című disszertációban ugyanezen közlemény 3. ábrájához tartozó kísérleteket használta fel, amely Dr. Tóth Noémi disszertációjában, illetve későbbi disszertációkban sem szerepel, illetve nem fog szerepelni.

.....

Dr. Nagy Norbert
Tudományos munkatárs
SZTE ÁOK Farmakológiai és Farmakoterápiai Intézet

Szeged, 2022. március 30.

Szegedi Tudományegyetem
Farmakológiai és Farmakoterápiai Intézet
Igazgató: Dr. Bazkó István M.D., Ph.D.
Dóm tér 12. 6720 Szeged
Tel.: +36.62.545-682
Fax: +36.62.545-680
e-mail: baczko.istvan@med.u-szeged.hu

NYILATKOZAT

Alulírott, Dr. Nagy Norbert levelező szerző nyilatkozom, hogy az alábbi közleményben:

Gergő Bitay, Noémi Tóth, Szilvia Déri, Jozefina Szlovák, Zsófia Kohajda, András Varró, Norbert Nagy

The Inhibition of the Small-Conductance Ca2+-Activated Potassium Channels Decreases the Sinus Node Pacemaking during Beta-Adrenergic Activation

Pharmaceuticals, 2022

Dr. Tóth Noémi „Ca^{2+} *dependent regulation of sinoatrial node pacemaking* " című tézisében 4.B és 5. ábrához tartozó kísérleteket használta fel. Ezek az eredmények későbbi PhD disszertációkban nem kerülnek felhasználásra.

.....

Dr. Nagy Norbert
Tudományos munkatárs
SZTE ÁOK Farmakológiai és Farmakoterápiai Intézet

Szeged, 2022. március 30.

Szegedi Tudományegyetem
Farmakológiai és Farmakoterápiai Intézet
Igazgató: Dr. Bazkó István M.D., Ph.D.
Dóm tér 12. 6720 Szeged
Tel.: +36.62.545-682
Fax: +36.62.545-680
e-mail: baczko.istvan@med.u-szeged.hu

NYILATKOZAT

Alulírott, Dr. Nagy Norbert levelező szerző nyilatkozom, hogy az alábbi közleményben:

Tóth N, Szlovák J, Kohajda Z, Bitay G, Veress R, Horváth B, Papp JG, Varró A, Nagy N.

The development of L-type Ca2+ current mediated alternans does not depend on the restitution slope in canine ventricular myocardium.

Sci Rep. 2021 Aug 17;11(1):16652.

Dr. Tóth Noémi „*Ca^{2+} dependent regulation of sinoatrial node pacemaking* " című tézisében az 1. és 3. ábrához tartozó kísérleteket használta fel. Ezek az eredmények későbbi PhD disszertációkban nem kerülnek felhasználásra.

.....

Dr. Nagy Norbert
Tudományos munkatárs
SZTE ÁOK Farmakológiai és Farmakoterápiai Intézet

Szeged, 2022. március 30.